Double-Skin Facade

Modelling and Experimental Investigations of Thermal Performance

Kalyanova, Olena

Publication date:
2008

Document Version
Publisher's PDF, also known as Version of record

Double-Skin Facade – Modelling and Experimental Investigations of Thermal Performance

PhD Thesis by Olena Kalyanova

AALBORG UNIVERSITY

Double-Skin Facade – Modelling and Experimental Investigations of Thermal Performance

Olena Kalyanova

AALBORG UNIVERSITY

Department of Civil Engineering

Aalborg University
Department of Civil Engineering
Group of Architectural Engineering

Double-Skin Facade – Modelling and Experimental Investigations of Thermal Performance

by

Olena Kalyanova

SCIENTIFIC PUBLICATIONS AT THE DEPARTMENT OF CIVIL ENGINEERING

Technical Reports are published for timely dissemination of research results and scientific work carried out at the Department of Civil Engineering (DCE) at Aalborg University. This medium allows publication of more detailed explanations and results than typically allowed in scientific journals.

Technical Memoranda are produced to enable the preliminary dissemination of scientific work by the personnel of the DCE where such release is deemed to be appropriate. Documents of this kind may be incomplete or temporary versions of papers—or part of continuing work. This should be kept in mind when references are given to publications of this kind.

Contract Reports are produced to report scientific work carried out under contract. Publications of this kind contain confidential matter and are reserved for the sponsors and the DCE. Therefore, Contract Reports are generally not available for public circulation.

Lecture Notes contain material produced by the lecturers at the DCE for educational purposes. This may be scientific notes, lecture books, example problems or manuals for laboratory work, or computer programs developed at the DCE.

Theses are monograms or collections of papers published to report the scientific work carried out at the DCE to obtain a degree as either PhD or Doctor of Technology. The thesis is publicly available after the defence of the degree.

Latest News is published to enable rapid communication of information about scientific work carried out at the DCE. This includes the status of research projects, developments in the laboratories, information about collaborative work and recent research results.

Aalborg University
Department of Civil Engineering
Sohngaardsholmsvej 57,
DK-9000 Aalborg, Denmark

Printed in Aalborg at Aalborg University

PREFACE

This thesis is submitted in accordance with conditions for attaining the Ph.D. degree. The thesis will be defended by a public lecture on September 4th, 2008 at the Department of Civil Engineering, Aalborg University.

This work was financially supported by the Danish Technical Research Council (Grant 2058-03-0100) and a part of this work was carried out within the International Energy Agency (IEA), Task 34/43: Testing and validation of building energy simulation tools.

This work has been supervised by Professor Per Heiselberg whom I wish to thank for his guidance, and useful advices during my work.

I would also like to thank my colleagues Carl Erik Hyldgaard and Rasmus Lund Jensen, who spent a lot of their time and effort to establish and refine the test facility, for the enthusiastic field support during the tests and experiments and to Torben Christiansen for his help with experimental set-up and technical assistance.

I wish to thank to all those people who participated in work within subtask E in Annex 34/43 by running their programs, for their help and support during this work:

Clemens Felsmann	Technical University of Dresden (TUD) Germany
Paul Strachan	Energy Systems Research Unit (ESRU) Dept. of Mechanical Eng. University of Strathclyde Glasgow Scotland
Aad Wijsman	VABI Software BV Netherlands
Harris Poirazis Bengt Hellström	Division of Energy and Building Design Department of Architecture and Built Environment Lund Institute of Technology (LTH) Sweden

Also, I would like to thank to Tine S. Larsen, Bente Jul Kjaergaard Bodil Jensen and Tove Jensen for their support during these years and, finally, to my family and friends for their strong patience and support.

Olena Kalyanova
July 2008

ABSTRACT

Double-Skin Facades (DSF) are gaining popularity that, in fact, appears to be independent from sturdy critics of the concept in the past years. DSF buildings are being built in Europe and worldwide, DSF concept is being taught at schools of architecture and fully glazed office buildings are being favored by companies and their employees.

To bring the reduction of energy use in these buildings application of suitable tools and methods is necessary to achieve successful design solutions.

Earlier work on the topic of DSF modelling was examined from various publications. As a result, the main difficulties experienced by scientists when attempting to model DSF thermal and energy performance were examined. In addition, the lack of experimental studies and empirical validation of models was realized, many numerical models have not been empirically validated and most of them require an expert knowledge to perform the simulations.

To fill in the gap of lacking experimental data a range of measurements was carried out in an outdoor, double-skin façade full-scale test facility 'The Cube'. As a result, three complete sets of experimental data were composed. These are available for external air curtain, transparent insulation and preheating operation modes of DSF cavity. The data sets include measurements of naturally induced air flow, temperature gradients, velocity profiles, climate data, etc.

Two data sets were used for further empirical validation of building simulation software for DSF modelling within IEA Annex 34/43, subtask E "Double-Skin Facade". The results of empirical validation are discussed in this work.

Discussion and analysis of experimental results is carried out. It has lead to hypothesis of recirculation flow phenomenon in the DSF cavity. Finally, a suggestion of a new numerical model is developed to account for recirculation flow appearance in the DSF cavity. The model is based on a simple mass balance between the boundary layer flow and the main flow in the cavity.

CONTENTS

NOMENCLATURE

Roman symbols

A	area	[m^2]
A	solar radiation factor	[-]
C	undefined coefficient	[-]
C	flow coefficient	[-]
D_h	hydraulic diameter	[m]
D_t	difference between predicted and measured value at hour t	
F	view factor between surfaces	[-]
G	irradiation	[W/m^2]
H_j	height of the opening 'j'	[m]
Ho	height of the neutral plan	[m]
I_s	global solar radiation	[W/m^2]
J	radiosity	[W/m^2]
K	von Karman's constant	[-]
L	characteristic length	[m]
M	volume flow in boundary layer per 1 meter of surface width	[$m^3/(s\ m)$]
M_t	measured value at hour t	
P	pressure	[Pa]
Q	heat flow	[W]
Q_m	energy transport with enthalpy flow	[W]
T	temperature	[K]
U	U-value of construction	[W/m^2K]
V	wind speed	[m/s]
V	fluid velocity	[m/s]
V	volume flow	[m^3/h]
V_*	friction velocity	[m/s]
V^*_{min}	minimum area averaged velocity	[m/s]
V_{10}	reference wind speed at the height 10m	[m/s]
X_t	predicted value at hour t	

c_D	discharge coefficient	[-]
c_p	pressure coefficient	[-]
c_p	specific heat at constant pressure	[J/kgK]
c_t	buoyancy force coefficient	[-]

c_v	wind force coefficient	[-]
d	width of cavity	[m]
e	dissipated energy, between two points	[W/kg]
f	function	
g	gravitational acceleration	[m/s^2]
g	window g-value	[-]
h	height above the ground	[m]
h_o	roughness height	[m]
i	incident solar radiation	[W/m^2]
k	transmittance coefficient for solar radiation	[-]
k	terrain constant	[-]
k	thermal conductivity of the fluid	[W/mK]
k	coefficient which equals Gr_l/Re_l^2	
l	characteristic length	[m]
m	mass flow rate	[kg/s]
n	exponent	[-]
n	number of openings	[-]
n	total number of hours	[-]
n	number of layers in numerical model	[-]
p	pressure	[Pa]
q	heat flux	[W/m^2]
t	temperature	[^{o}C]
t_{film}	film temperature	[^{o}C]
t_s	surface temperature	[^{o}C]
v	velocity	[m/s]
v_1	velocity in the boundary layer	[m/s]
v_x	maximum velocity in boundary layer	[m/s]
x	horizontal distance	[m]
y	vertical distance	[m]

Greek symbols

α	convective heat transfer coefficient	[W/m^{2}K]
α	heat transfer coefficient	[W/m^{2}K]
α	incident angle	[deg]
α	terrain constant	[-]
α	longwave radiation absorptance property of surface	[-]
β	coefficient of volumetric expansion	[1/K]
Δ	difference	
δ	wind boundary layer	[ft]
δ	thickness of boundary layer	[m]
δ	standard error	
ε	longwave radiation emittance property of surface	[-]
η	dimensionless distance	[-]
φ	temperature coefficient	[-]
λ	friction factor	[-]
λ	thermal conductivity of the material	[W/(m^{o}C)]
μ	dynamic viscosity	[N s/m^2]
ρ	fluid density	[kg/m^3]
ρ	longwave radiation reflectance property of surface	[-]
σ	Stefan-Boltzmann constant ($s = 5.67 \times 10^{-8}$)	[W/(m^2 K^4)]
τ	solar transmission	[-]
τ	longwave radiation transmittance property of surface	[-]
υ	kinematic viscosity	[m^2/s]
ξ	local loss factor	[-]

Subscripts

10	subscript for reference wind velocity at the height 10m
I,II,III,IV,V,VI	subscripts for velocity profile measurements in the cavity
*	subscript for friction velocity
∞	fluid
all	subscript for complete set of experimental data
b	buoyancy
bot	bottom opening
c	concuction
c,ei,ie,o	zones in numerical model
conv	convection
D	subscript for discharge coefficient
dim	dimensionless
e	exterior/external
ee	external surface of external window
ei	external surface of inner window
fan	subscript for air temperature in experiment room measured with solver coated, shielded and ventilated thermocouple
film	subscript for film temperature
h	subscript for hydraulic diameter
i	interior/internal
i	surface index
i, j	Zone number in numerical model
ie	internal surface of outer window pane
ii	internal surface of inner window
j	opening number
L,H,D_h	characteristic length, where H - cavity height, L- cavity width, D_h -hydraulic diameter
LW	long wave radiation
met	meteorological station
o	external (outdoor)
o	subscript for roughness height
p	subscript for pressure coefficient
p	sucscript for specific heat at constant pressure
ref	subscript for reference wind speed
s	shaft
s	subscript for global solar radiation
s	surface
sm	subscript for mean value of global solar radiation for a certain time interval
sol	solar
t	transmitted (subscript for transmitted incident solar radiation
t	subscript for buoyancy force coefficient
t	hour number
top	top opening
tot	total
v	subscript for wind force coefficient
w	wind

Abbreviations

MIN	Minimum
MAX	Maximum
MEAN	Average
DT	Difference
DT95	Difference 5%
DT5	Difference 95%

MEANDT	Average Difference
ABMEANDT	Absolute Average Difference
RSQMEANDT	Root Mean Square Difference
STDERR	Standard Error
RNP	Recirculation Neutral Plane
S,B,O,I,H,L	abbreviations for definition of windows in DSF. Where 1,2,3 - define section of DSF Example: *SOH3 – Small Outer window, located Higher than the middle plane in the DSF section 3.* *BIL2– Large (Big) Inner window, located Lower than the middle plane in the DSF section 2.*

Dimensionless numbers

Re	Reynolds number
Gr	Grashof number
Ra	Rayleigh number
Pr	Prandtl number

Chapter 1

INTRODUCTION TO DOUBLE-SKIN FACADE

In this Chapter 1, general information about Double-Skin Facade (DSF) and its functioning modes will be given. Some important features of DSF performance, positive and negative aspects of its application and, finally, the main reasons for application of double-skin facades will be explained.

A short overview of physical processes in DSF is prepared to point out differences between the processes in DSF and conventional buildings. At last, the aim of this work will be introduced.

1.1 DOUBLE-SKIN FACADE

1.1.1 GENERAL

Facade construction, which consists of two layers of fenestration, separated by an air gap is usually called a Double-Skin Facade (DSF), as illustrated in Figure 1-1. In most of cases, the air is allowed to enter the DSF cavity trough the openings in the internal or external skin and then it is expelled to the outdoors or to the adjacent room. It is more than common to install shading device in the air gap between the skins, which can actually contribute to DSF performance by increasing the stack effect in the gap and at the same time it is being protected from wind and dust.

In the literature, one can meet unexpectedly different terminology used with regard to double-skin facade. This is mainly due to manifold functions that a double-skin facade can serve in a building.

DSF systems are very flexible, as their primary operation strategy is to adapt to any rapid variations in weather conditions. This is possible to achieve by change in the DSF operation mode or by any other adjustments, possible in the control strategy. This can for example be a change of opening degree, raised or lowered roller blinds or other shading devices, change in the air flow rate in the cavity, etc. Each time when these changes are applied the performance of the DSF will also change. It is also illustrated in the Figure 1-1, that there are many different combinations for the air passage in the DSF cavity that can be established.

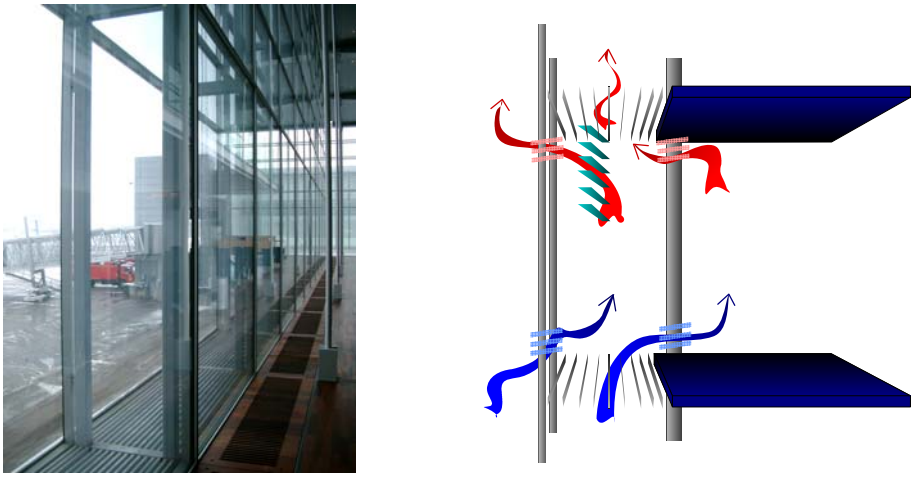

Figure 1-1. Photo and illustration of a Double-Skin Facade.

1.1.2 HISTORY OF DSF

The earliest citation of the double glazed facades belongs to Jean-Baptiste Jobard "at *that time (1849) director of the Industrial Museum in Brussels, described an early version of mechanically ventilated multiple-skin facade. He mentions how in winter hot air should be circulated between two glazings, while in summer it should be cold air*", (Saelens, 2002).

Prior to the Industrial Museum in Brussels, double windows were designed in 1762, for the Winter Palace in Sankt-Petersburg for the air conditioning purposes (Magnus Bredsdorff, 2007).

The further development of DSF in literature is mainly referred to the beginning of 20th century; the authors of the website www.battlemccarthy.demon.co.uk have also found an early example of double-skin facade, made by American botanist Edward Morse. Who "*developed what might be the first working multiple wall*". His observations of warming up process of the dark curtains and so the air behind the window has brought him in 1882 to build a solar wall.

The first real example of the double-skin facade installed in a real building (1903) is known from Richard Steiff who has designed a toy factory for his father, in Giengen, Germany. The double skin curtain wall was installed with consideration of the strong winds, cold weather in the area and intention to maximize the day lightning. "*The building was a success and two additions were built in 1904 and 1908 with the same double skin system...*" (www.buildingenvelopes.org).

In next to no time, in 1904, the Post Office Savings Bank in Vienna, Austria was built, designed by Otto Wagner, as a winner of the design competition (www.buildingenvelopes.org). The building "*has a double skin skylight in the main banking hall... And it is still in use by the same owner*".

Further history of DSF brings on the list many architects with their creations of success and failure. Great modernist le Corbusier, has spent lots of effort on his projects working through the theory, but the advanced practical results were obtained in USA, by Libbey Owens Ford in 1935. Rare examples of the DSF with almost no progress appeared later in history (www. battlemccarthy.demon.co.uk; buildingenvelopes.org)

Examples of present success of implementation of DSF are available in the literature, and on the web.

1.1.3 CLASSIFICATION OF DSF

Almost any new researcher in the field of DSF brings his new classification of DSF. The most simple and common classification offered in the Ph.D work of Saelens, 2002, by:

- the origin and destination of air (internal, external or hybrid)
- the driving force in the DSF (natural, mechanical, hybrid)
- the facade's compartmentalisation (window/box-facade, shaft facade, corridor facade)
- the hybrid schema

Another classification was suggested by authors Arons & Glicksman (Arons & Glicksman, 2001), according to:

- combination and positioning of glazing (single/double)
- height of the building (normally stands for facade's compartmentalization)
- cavity thickness (thin/thick)

Some of authors combine origin of air flow with the type of driving force in the cavity (Nolte & Pasquay, 1997):

- naturally ventilated wall (the cavity is naturally ventilated from/to the outside by buoyancy/wind)
- active wall (the return air from the room is extracted through the cavity and then redirected to the ventilation system)
- interactive wall (the skin is mechanically ventilated from/to the outside)

Definition of more extensive classification for DSF systems can become an impossible assignment, as refer to Arons & Glicksman (2001): "*...each new building is a departure from the previous one... no two facades are the same, and they differ enough that they tend to fill in the spaces between distinctly different schemas*".

It is common to build DSF as a part of the complete building's system. Variable designs of facades (constructional part), different approaches for their operation (origin of the air and driving forces) and, finally, different building systems they are involved with, result in that any DSF differ from the other one and only general identities can be considered. Therefore, some authors think that only one really characterising classification would be appropriate: the name of the building it belongs to (Arons & Glicksman, 2001).

.

Further in this report, a classification of double-skin facades according to the origin and the destination of the air will be used (Loncour et al.,2004),

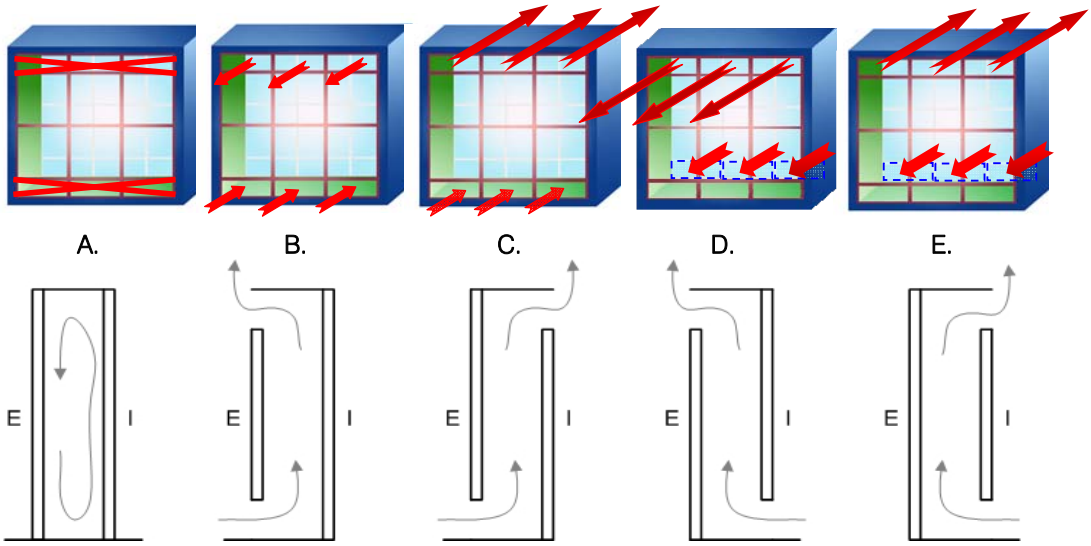

Figure 1-2. Classification of DSF according to the origin and destination of air in the cavity (Loncour et al., 2004).

A. Transparent insulation mode (Buffer zone). In this mode, all of the openings in the DSF cavity are sealed, so there is no exchange of the air with interior or exterior. This functioning mode is normally used in the cold seasons to increase the thermal insulation and radiant temperature in the room adjacent to the DSF.

B. External air curtain mode. In this mode, air enters the cavity at the bottom and comes from the outside. In most of the cases, the air is heated due to the solar radiation captured by the glazing system and/or shading device installed in the cavity. Then, the air is expelled to the outside at the top of the cavity together with the surplus solar heat gains. The air flow in that mode is driven by the buoyancy and wind.

C. Preheating mode (Air supply). In this mode facade openings at the bottom of the cavity are open to the outside and the top openings open to the interior. The air flow is normally driven by mechanical system in the building. This mode is normally used in intermediate seasons when the solar radiation is strong, while the outdoor air temperature is low.

D. Exhaust mode (Air exhaust). In this functioning mode the openings of the DSF cavity are open at the top to the exterior and at the bottom to the interior. Then the stack effect in the cavity is used to enhance the exhaust of the air from the building.

E. Internal air curtain. Openings at the top and bottom of the cavity are open to the interior. This mode is normally used in the cooler seasons together with the heat recovery unit.

1.1.4 WHY DSF?

Glass as a mysterious substance has always been attractive and intriguing for human beings; it has always been a symbol of power, money and prestige. Nowadays, nations are driven by business, customers' aspiration and reputation, which are represented by aesthetic and psychological desire of transparent glazed facades and steel constructions; it is "*rich, modern expression of form and function.*" Customers wish to present an image of environmental stewardship look to the facade as a means of communicating this image (Lee, et al. 2002).

Nowadays, when humanity becomes more conscious about the energy use and emission of carbon dioxide to the atmosphere, the architects and engineers work on the fashionable image of building same time attempt to reduce terrifying energy consumption by application of highly glazed facades (Lee, et al. 2002).

At the same time, *"…there is a growing tendency among the architects to use large areas of glass, often with the aim of contributing to a better view and daylight. Users also welcome the view to the outside and, finally, many companies prefer the distinctive image of themselves that a glazed office building can provide"* (Poirazis, 2008).

As an alternative to highly glazed conventional buildings, the DSF solutions are then being proposed. And, although the application of the DSF buildings is not proven to be energy efficient, and these solutions are being sturdy criticized by many parties, the double-skin facade buildings are being built. Projects with the DSF are favored for the areas with dense traffic or other noisy activities: beside the highways or crowded city-centers.

1.1.5 DSF FEATURES

Compared to a conventional glazed building, DSF can function as a barrier for solar radiation or it can preheat the ventilation air; DSF can reduce the penetration of noise (i.e. traffic) from the outside; it can improve perception of comfort (increased surface temperature of the glazing); it allows for application of night cooling and at the same time it is burglary safe; in some cases, it gives better possibility for fire escape and fire protection; it provides better protection of shading devices and allows to open windows on the top floors in a multistory building.

The main reasons for application of double facades in Europe are found between:

- the aesthetic desire
- the desire of transparency (psychological desire)
- the desire to improve indoor climate (increase of daylight). Improvement of the daylight conditions are normally seen due to comparison with the traditional facade with limited glazing area

It is also seen that the energy performance of double-facades is not one of the reasons for their application. This is because of different opinions regarding the energy performance of the DSF, which are very contradictory and vary from very optimistic and promising future for DSF to the negative rejection.

According to Klaus Daniels: "*... it is worth considering whether they (DSFs) should be marketed solely on the basis of energy savings or whether other essential aspects argue for their use*" (Li, 2001). Actually, besides the aesthetic features, Double-Skin facades can be advertised for many other beneficial features. These, however, are followed with some essential disadvantages.

There are advantages that customers find very attractive and most of the scientists have agreed with:

- transparent image
- improvement of aesthetical appearance, contact with the environment
- improvement of occupants productivity
- reduced infiltration compared with the conventional facades
- burglary save night cooling

However, there are more significant, but uncertain features of DSF considered, most of them are closely connected to energy savings and tend to lessen the environmental impact of building:

- preheating of inlet air in winter time
- heat removal in summer time
- raise of radial temperature in winter, thus the improvement of comfort
- improved use of natural ventilation, night cooling
- contribute to passive energy use
- possible increase of day lightning
- relief from the outside noise
- fire protection

K. Gertis has summarised all advantages and disadvantages of double facades (*Table 1-1*). In this work, the author has also stated that for any positive DSF feature can be found at least one reasonable negative aspect, such as:

- high risk of unacceptable performance
- high cleaning and operating costs
- additional servicing and inspection costs
- colossal maintenance costs
- possibly fire unsafe

Only in a case of an accurate design, good quality construction, well-informed occupants and service personal the DSF can attain a high magnitude of claimed advantages with minor disadvantages.

In order to assess positive and negative sides of DSF, it is often performed by comparative analyses of DSF system with an equivalent conventional single skin facade. Looking for the equivalent is a difficult task, as only reconstructed to DSF buildings can be fairly identified as equivalent. For that reason, the comparisons are carried out using the thermal building simulation tools.

	Pro DSF arguments	Con DSF arguments
Acoustics	Gives better acoustical insulation against exterior noise	DSF has to be opened for ventilation and this will decrease the acoustical insulation of the air gap and will increase the acoustical transmission
Heating energy in the winter	DSF saves heating energy, because solar energy is captured in a collector	Most of the buildings that we looked at have high internal heat loads and heating energy savings is not an issue
Cooling energy in the summer	Summer Heat can be ventilated away through the DSF air gap	In a DSF air gap, we have strong heating in the summer, which will make the building behind the DSF very hot
Room climates for ventilation	DSF increases the climatic comfort in the room because of natural ventilation	With DSF, you can only achieve a comfortable climate in the room by using a mechanical HVAC system and the DSF air gap facilitates the transfer of odours
Solar shading	DSF has the ability to apply a shading system that is protected from the outside in the air gap	A shading system can just be applied inside the building without using the DSF air space
Operable windows	DSF allows the user to open windows even on very high buildings	With hardware, where you limit the amount you can open the window, you can use operable single facade windows in a skyscraper or very high building as well
Pressure needed to close interior doors in a building	On the windward side of tall buildings, DSF reduces the static pressure in the interior, which can result in less pressure needed to close interior doors compared to naturally ventilated	If you use ventilated storm windows in the openings of punched-hole facade to break the wind, you can also reduce the static pressure
Lightning	DSF enables the installation of light redirecting elements	Light redirecting is also possible with a punched-hole facade. The extra glazing layer in DSF actually reduces the amount of day light entering the building
Fire	With horizontal and vertical compartments, fire spread can be prevented in the air gap	The exterior glazing layer reduces the ability for smoke ventilation and the air gap increases the risk of fire spreading between floors or rooms
Condensation	With enough ventilation the DSF air space can be kept free from condensation	The inner surface of the outer pane – it is inevitable that there will be condensation and therefore you need frequent cleaning
Cost	DSF lowers the operation costs of the building because of energy costs	DSF has extremely high investment costs and they increase the amount of operational cost because, for example, the cleaning of four glass surfaces

Table 1-1. Pro and Con arguments for DSF application acc. to K. Gertis, (1999).

1.1.6 PHYSICS OF THE DSF. THEORY

The advantages of the DSF concept compared to the conventional buildings are often expressed in the DSF intelligence and optimal response to the climatic conditions.

Explanations similar to following are frequently used in literature in order to in simple terms describe the DSF performance:

> *In the day time, the air in the double-skin facade cavity is heated by sun and then supplied to the occupants, beneficially using the solar gains (preheating mode). In a hot summer day, the air is expelled to the outdoors, removing the surplus solar heat gains. In this case the DSF functions as a transparent shading device (external air curtain mode). In the cold season, the heated air is captured in the cavity and the DSF functions as a transparent insulation or thermal buffer.*

Some terms, such as: “air heated by sun”, “transparent insulation”, “transparent shading”, etc. do not clearly express the actual physical processes in the DSF:

- *Air heated by sun*, meaning: solar radiation that is absorbed by the glazing and/or shading device is only then transferred to air by convection.
- *Transparent insulation*, meaning: increased air temperature in the cavity, which results in the smaller temperature differences between the occupied zone and the cavity air and in, consequently, smaller heat loss. Also, the longwave radiation heat exchange between the surfaces in the occupied zone and the window is reduced due to the higher temperature of inner pane of the window.
- *Transparent shading, air curtain*, meaning: solar radiation is partly absorbed by glazing and/or shading device, before entering the occupied zone. Absorbed solar radiation is then removed from the cavity by air. Thus, the DSF works as a barrier for solar gains.

The fact that the DSF concept is very complex, by now, is well recognized among the architects and engineers. However, it is rare when one can meet a detailed, but clear explanation of why it is difficult to deal with DSF in practice. In view of that, a simple summary of the main processes in the DSF physics is included in the following section 1.1.6.1 .

1.1.6.1 What is special in the DSF physics?

It is difficult to predict the performance of the DSF-building, as well as the performance of many other buildings. After all, what makes the DSF-building more difficult to design? Why does the rule of thumb apply in the conventional building, but never work for the DSF building? And finally, why can the smallest detail in DSF calculation lead to extreme consequences in energy use?

Conventionally our buildings are built as a static system that is not designed to coexist with the surrounding climate. In the last decade, the situation has begun to change: the buildings are designed to take the advantages of the local weather conditions. The DSF-idea is not new and it can be easily spotted in the history of building architecture, however the DSF-concept is relatively young and belongs to the dynamic building systems, which act in unison with the weather variation during the year.

The performance of the DSF-building is like the behaviour of a chameleon that changes colour, to be in balance with the colour palette of the surroundings. Similar in literature, the skins of the double-skin facade are compared to the human skin: pores of the human skin open in a hot summer day to keep our body in thermal balance and comfort. The openings of the DSF open too, to maintain the comfort environment in the building.

The DSF-buildings are extremely dynamic, especially, if the cavity is naturally ventilated. DSF continuously adjusts its performance not only to the solar radiation intensity, but also to the highly fluctuating natural driving forces. Due to the extreme dynamics of the system, the changes happen rapidly and they cannot be smoothed in time. Consequently, any error in calculations will be, in a full scale, experienced by the occupants.

In a DSF-building the great part of the heat transfer happens through the DSF construction and, for that reason, it is extremely important to be able to predict its performance. The main difference between the DSF and a conventional window is that in case of DSF it is difficult to estimate what part of solar heat gains will penetrate through the DSF into the adjacent zone and what part of solar gains will be captured by the cavity air, especially if the cavity is naturally ventilated.

1. The solar position, in relation to the glazing panes of the DSF, changes continuously. At the same time the amount of solar radiation received on the DSF surface vary with the cloud cover, solar intensity, etc. Furthermore, the optical properties and thus the amount of absorbed, reflected and transmitted solar radiation by the DSF glazing depend both on solar position and on solar radiation intensity.

In the simulations made for the conventional buildings, it is normally enough to consider the g-value (solar heat gain coefficient), which combines the transmitted solar radiation with a part of solar radiation that was absorbed by the glazing panes and then transferred to a zone mainly by convection and longwave radiation exchange. However, this is an unacceptable simplification when considering the DSF, since the concept is built on the fact that the major part of solar radiation absorbed in the panes is then transferred to the *cavity air* and not to the zone adjacent to DSF.

Moreover, in a ventilated cavity the actual g-value will change significantly simultaneously with the changes in the air flow magnitude, air temperature and flow regime. And, finally, the actual g-value will also vary by height of the DSF due to the significant temperature gradient that normally exists in a DSF cavity, especially with application of shading device.

Next, the solar radiation absorbed by glazing is transferred to the surrounding mainly by longwave radiation exchange and convection.

2. Estimation of longwave radiation exchange in the DSF-building as well as in a conventional building requires detailed view factor calculations. However, in presence of error, the consequences will be less notable in the conventional building, due to the smaller deviation between the surface temperatures of the constructions, while in the DSF-building the surface temperature of a shading device or inner window pane can be rather high and can result in additional heat gains to occupied zone when it is highly undesired.

3. Dealing with the convective heat transfer is a particular difficult exercise. Choice of expressions for convective heat transfer coefficient is always a topic for discussion. Nevertheless, the convective heat transfer in the DSF cavity is more difficult than ever to assess. The convective heat exchange is defined by the thermal conditions, flow rate and flow regime, which are subjected to the rapid changes, especially in a naturally ventilated cavity. This leads to the circumstances when more than one expression might be needed and the building simulation tool should be able to handle the change in the flow regime and thus in the convective heat transfer.

Meanwhile, the mass flow rate in the naturally ventilated DSF cavity is driven by buoyancy and wind.

4. The air entering the DSF is heated up/cooled down due to the convective heat transfer at the DSF surfaces and shading device, then the air raises up/falls down, due to the buoyant forces. The strength of the buoyancy strongly depends on the air temperature and thus on the convective heat transfer at the surfaces. The higher temperature - the better strength has the buoyancy force.

At the same time the increase of air temperature in the cavity increases the buoyancy force and the air change rate in the cavity. Consequently, the temperature of the surfaces and cavity air drops. Next, the air change rate in the cavity drops, the surface temperatures and the air temperature starts to increase leading to increase of the flow rate, etc… In this way, the DSF functions as a self-

regulating vent, switching between the magnitudes of the mass flow rates and temperatures (Saelens, 2002).

The increase of the air temperature in the DSF tells about the amount of additional gains that will be supplied to the adjacent zone together with the heated fresh air in preheating mode. It also tells about the amount of surplus solar gains that will be removed from the system with the heated air in external air curtain mode. In both cases the higher the air temperature when leaving the DSF cavity – the higher efficiency it has. This explains why the concept is focused to catch the greatest part of solar radiation in the DSF cavity.

5. The other component of the driving forces is the wind force; its principle is explained in section 5.5.2 . The main characteristic of the wind forces is their random and extremely fluctuating nature. Still now, the wind phenomenon is difficult to simulate or estimate and this obstructs the development and application of the natural ventilation principles. The same is applicable for the naturally ventilated double-skin facade, where the driving forces (wind and buoyancy) may counteract or act together, determining the mass flow rate in the cavity.

The close interrelation between convective heat transfer and random air change rate in the cavity makes it complex to assess the air temperature in the DSF cavity and thus the amount of solar gains that will be transported away with the cavity air or transported to ventilate the adjacent zone. This is further complicated with the recirculating flow phenomena that arise in the cavity when the boundary layer flows are strong. This is explained in detail in section 6.2.1 .

Looking upon each physical process that the building simulation should be able to deal with when modelling a DSF, it is apparent that in every aspect the DSF is more sophisticated and complex to deal with compared to a conventional building.

1.2 AIM OF THIS WORK

The design, dimensioning and the application of DSF are exceptionally responsible tasks, as in case of poor design, the DSF will lead to an increased energy use (mainly for cooling) and inferior indoor climate. In the meantime, it is not enough to use standard tools for design of conventional buildings when dimensioning the DSF, as it requires detailed analysis of the results from the dynamic simulations.

As explained in section 1.1.6 , DSF-buildings are extremely dynamic, especially if the cavity is naturally ventilated. Due to the extreme dynamics of the system, the changes happen very rapidly and they can rarely be smoothed in time. As a result, any shortcomings in the design will result in increased energy use and increased temperature fluctuations in the occupied zone. It is then crucial to find a tool suitable for the simulations of the DSF energy and thermal performance.

In the literature, one of the main problems reported regarding DSF modelling and simulations is the absence of experimental data (Gertis 1999, Saelens 2002). Most of the experimental studies with DSF are available for short time intervals and rarely include measurements of the mass flow rate in the naturally ventilated cavities. Also, as pointed by K. Gertis (Gertis, 1999), in many cases the experimental conditions are poorly described and therefore cannot be used for validation purposes.

Most of the mathematical models have not been validated against empirical data and, often, an expert knowledge is required to perform the simulations. Consequently, the degree of confidence in the simulated results becomes low. There is a lack of systematic literature or guidelines on how to model DSF and what are the most suitable tools to use, most of this is caused by the lack of empirical validations.

Perhaps there is no tool at all, able to deal with the transient and complex air flow in a ventilated double skin facade cavity. As pointed out by H. Manz and Th.Frank:*"…the thermal design of buildings with the DSF type of envelope remains a challenging task. As, yet, no single software tool can accommodate all of the following three modelling levels: optics of layer sequence, thermodynamics and fluid dynamics of DSF and building energy system"* (Manz and Frank, 2005).

Still, DSF solutions are being proposed and built, resulting in poor indoor climate and unnecessary energy use. It is therefore critical to expand the knowledge about modelling tools and principles for DSF buildings available in the field. After all, building simulation tools must be empirically validated to confirm their applicability for the task of DSF simulations.

First of all, the experimental data should be gathered, it must be accurate and well explained for application in empirical validation of software. The experimental data should be complete and must include measurements of the boundary conditions, mass flow rate in the cavity.

With intentions for simulation a double-skin facade, first it is necessary to investigate the challenges faced by different researches when attempting to model double-skin facade performance and their solutions for these challenges.

In order to do that, a literature study of the modelling approaches and tools available for DSF-solutions is carried out in Chapter 2. The experimental studies (Chapter 3) are anticipated to fulfil demand for long-term experimental studies of DSF functioning, conducted within the same test facility with the different functioning modes, such as transparent insulation, external air curtain and preheating mode.

To investigate the applicability of various thermal building simulation tools for modelling of DSF, an empirical validation of building simulation software was conducted in the frame of IEA SHC Task 34 /ECBCS Annex 43 "Testing and Validation of Building Energy Simulation Tools". The results

from this work are evaluated upon the experimental work explained in Chapter 3, and summarized in Chapter 4, to illustrate the present possibilities for DSF modelling.

Different scientists have made their suggestions for further steps in research of DSF models. These are reviewed in Chapter 2. According to their suggestions, there are two key areas to be considered:

- Calculation of naturally induced air flow is still limited in many models, as it is sensitive to the input parameters such as pressure difference coefficients, discharge coefficient, vertical wind speed profile, etc.
- Convective heat transfer in a cavity

Collected experimental data for double-skin facade test facility, literature survey of present modelling approaches and finally empirical validation of various thermal building simulation tools, all together, will be used in the discussion of further steps for improvement of DSF models, with focus on topics pointed out in the literature.

Finally, a hypothesis of recirculation flow occurrence in DSF cavity will be developed on the basis of experimental results in Chapter 6 and literature study (Chapter 2). Until now, none of the models accounts for the recirculation flow that is significant for heat transfer and temperature gradients in the cavity. To bring out the potential of this hypothesis it will be further expanded into a suggestion for a numerical model that is anticipated to result in further improvements in modelling and simulation of DSF (Chapter 7).

This model should be able to deal with the recirculation flow phenomenon (Chapter 7) and lead to better predictions of vertical temperature gradients in the cavity and in that way it will result in better estimations of energy performance of DSF.

Chapter 2

LITERATURE REVIEW

This part of the report is based on report Kalyanova et al. (2005), which is also included as a subchapter in report by Poirazis (2006).

Section 2.3 of this report is based on the BBRI report by Flamant et al. (2004).

In the following section an overview of the key studies (since the '90s) performed on DSF is given. The studies include empirical and experimental investigations, modelling and simulation of the double-facade performance. With such a spread of topics for studies, the focus will be set on the modelling approaches and possibilities. The difficulties regarding the modelling process and different techniques will be explained and the discussion will point out their advantages and disadvantages.

2.1 DSF MODELLING APPROACHES

In the late seventies, some remarkable buildings with double-skin facades (DSF) were built and a few inspiring articles appeared. It was the time when the oil crisis emerged and as a result, the DSF projects became attractive and encouraging. In this period, the prevailing literature had an advertising character, typical for the energy efficient technologies. The knowledge was based on rare examples, as the field of science was not formed yet. After a short time, the interest in the double-skin construction was set aside until the '90s. At that time, the DSF was still considered an innovation and the articles were focused on the performance of double facades with the emphasis on their advantages. Later on the lack of criticism became noticeable and the objective discussions began (Gertis, 1999). Dr. Karl Gertis wrote an article, where the advantages and disadvantages of double-skin facades were summarized. Finally, the author concluded: "*…we do not see a reason to be optimistic about DSF*". Nevertheless, there are many studies available with a positive impression supported by investigations and experiments.

2.1.1 APPROACHES FOR DSF MODELLING

Nowadays, building simulation software and developed mathematical models vary in a wide range of complexity. The simplest model is described by a few equations and the most complex one is the CFD model solving the conservation equations for mass, momentum and thermal energy.

According to Champagne, (2002), "*in the HVAC field, there is a need to validate a proposed design to ensure proper performance. One of two methods is typically used: experimental or numerical. Although experimental values are very reliable when performed in a controlled environment, there are several major drawbacks to this approach. It is expensive and time consuming. Computational Fluid Dynamics (CFD) is a numerical approach that is informative while also saving time and money*".

At the same time Hensen, (2002), categorizes building simulation approaches by level of resolution into macroscopic and microscopic. According to the author the macroscopic approaches deal with the whole building systems, indoor and outdoor conditions over some periods, while microscopic approaches use much smaller spatial and time scales. The building simulation software is normally related to the macroscopic approaches, while the CFD has the microscopic technique, which is usually restricted to the steady state condition. The macroscopic (network) method is more suitable for the time series considerations.

Another direction is taken by Djunaedy, et al. (2002), which categorizes the air flow modelling by levels of resolution and complexity as described below:

- *Building energy balance (BEB) models that basically rely on air flow guesstimates*
- *Zonal air flow network (AFN) models that are based on (macroscopic) zone mass balance and inter-zone flow-pressure relationships; typically for a whole building*
- *CFD that is based on energy, mass and momentum conservation in all (minuscule) cells that make up the flow domain; typically a single building zone*

Hensen, et al. (2002), explain that "*although air flow is demonstrably an important aspect of building/plant performance assessment, the sophistication of its treatment in many modelling systems has tended to lag behind the treatment applied to the other important energy flow paths. The principal reason for this would appear to be the inherent computational difficulties and the lack of sufficient data. In recent times more emphasis has been placed on air flow simulation mostly focused on the following two approaches:*

A. Computational fluid dynamics (CFD) in which the conservation equations for mass, momentum and thermal energy are solved for all nodes of a two- or three-dimensional grid inside or around the object under investigation. In theory, the CFD approach is applicable to any thermo-fluid phenomenon. However, in practice, and in the building physics domain in particular, there are

several problematic issues, of which the amount of necessary computing power, the nature of the flow fields and the assessment of the complex, occupant-dependent boundary conditions are the most problematic. This has often led to CFD applications being restricted to steady-state cases or very short simulation periods.

B. The network method, in which a building and the relevant (HVAC) fluid flow systems are treated as a network of nodes representing rooms, parts of rooms and system components, with inter-nodal connections representing the distributed flow paths associated with cracks, doors, pipes, pumps, ducts, fans and the like. The assumption is made that for each type of connection there exists an unambiguous relationship between the flow through the component and the pressure difference across it. Conservation of mass for the flows into and out of each node leads to a set of simultaneous, non-linear equations, which can be integrated over time to characterize the flow domain".

The CFD code is able to perform many tasks that the network modelling will never achieve. However, some of the CFD features are too sophisticated and unnecessary for an early design stage (e.g. the grid distribution of the velocity, temperature, dissipation of energy etc., obtained when the CFD modelling is performed) and, as mentioned above, the CFD modelling is often restricted to the steady state simulations. According to authors, whose works are mentioned in this section, there is a seriously growing experience in CFD modelling in general and in CFD modelling of DSF, but still there is a number of issues which are considered to be problematic in practice (Hensen, et al., 2002; van Dijk and Henk Oversloot, 2003; Ding, et al., 2004; Jaroš, et al., 2002; Chen, 1997):

- Amount of necessary computer power
- Complex flow fields
- Uneven boundary conditions
- Compulsory validation of the results and the difficulties to achieve satisfaction with validations
- Obligatory advanced knowledge for users

2.1.2 NETWORK APPROACH

In a report, written in 1999 by Karl Gertis, the author comments on the lack of information in publications concerning the results of simulations and developed models for DSF. According to the author, the boundary conditions in publications are poorly described and a deficit of experiments is observed (Gertis, 1999). The recent publications are of better quality: results of simulations are often compared to the results of experiments.

The position of Park, et al. (2003), Gertis, (1999), Hensen, et al. (2002), and work of many other researchers indicates that it is very difficult to find a simple model that would describe the DSF performance appropriately. As explained in Hensen, et al. (2002): "…*to predict the performance of a double-skin facade is not a trivial exercise*…*The temperature inside the cavity, the ambient temperature, wind speed, wind direction, transmitted and absorbed solar radiation, angles of incidence – each of which are highly transient – govern the main driving forces*".

Manz and Frank, (2005), point out that: *"the thermal design of buildings with the DSF type of envelope remains a challenging task. As, yet, no single software tool can accommodate all of the following three modelling levels: optics of layer sequence, thermodynamics and fluid dynamics of DSF and building energy system."*

The complexity of the prediction task is the main reason for the long lasting research and application of simplifying techniques. The iterative approach of the network method became the reason to distinguish the three main issues in the DSF modelling:

- Optical element – responsible for the optical properties of the DSF materials
- Heat transfer element– responsible for the heat transfer processes in the DSF
- Flow element – responsible for the motion of the fluid in the DSF

In various network methods these elements are defined differently in terms of nomenclature. In some methods they even stay undefined. The elements (the physical processes behind them) influence each other and, as it has been argued, together they govern the main heat and mass transfer processes in the DSF. Several researchers (Saelens, Faggembauu, van Paassen, Di Maio, Manz and others) suggested the separation of the flow element and the heat transfer element in the predictions, which allows a better accuracy of wind influence predictions and advanced calculations of the convective and radiative heat transfer (Saelens, 2002).

2.1.3 COUPLING OF MODELS

There are many studies which consider all the elements separately (optical element, heat transfer element and flow element), the works described in the published literature are often focused on one or two elements. While, the remaining ones are neglected as non-influencing or very rough approaches are employed to estimate their effect. However, few articles consider all three elements with a relatively equal effort, as will be explained in the following chapters.

There are many reasons to assume that the task of DSF modelling is too complex to be performed only with the pure network method. Some authors (Djunaedy, et al., 2002; Beausoleil-Morrison, 2001; Manz and Frank, 2005) suggest that the CFD and the network methods should be combined. As pointed out by Manz and Frank, (2005): *"…the nodal network approach is not suitable for cases where intra-zone air movement cannot be predicted by a simple flow resistance approach or where the temperature distribution inside the zone is significant. In such cases the limitations of the nodal network model can only be overcome by coupling building energy simulation tool with a CFD code".*

In this way the CFD is involved in some particular problems, such as calculation of local loss and friction factors (Strigner and Janak, 2001) or calculation of the flow regime and convection coefficients. These issues cannot easily be solved by the network approach, However, the network approach is used for the rest of the calculations. In this manner it is possible to combine the benefits from both approaches and to reduce their disadvantages.

At the same time, combining the two different calculation tools results in a number of questions, the most important ones being specified by Djunaedy, et al. (2002). A detailed procedure of coupling CFD and the network approach is explained by Beausoleil-Morrison (2001) and Beausoleil-Morrison, et al. (2001). The authors give an example how the issue of data exchange protocol between CFD and network model can be solved.

According to Hensen, et al. (2002): *"Both CFD and network method can be integrated with building energy simulation. In case of CFD, this is still very much in development, although enormous progress has been made in recent times. Integration of the network method with building energy simulation is much more mature and more commonly used in practice."*

"The reason for this is threefold. First, there is a strong relationship between the nodal networks that represent the air flow regime and the corresponding networks that represent its thermal counterpart. This means that the information demands of the energy conservation formulations can be directly satisfied. Secondly, the technique can be readily applied to combined multizone buildings and multicomponent, multifluid systems. Finally, the number of nodes involved will be considerably less then the required in a CFD approach and so the additional CPU burden is minimized".

A compromise of choices between modelling approaches was suggested by Hensen, et al. (2002): "*The network method is of course much faster but will only provide information about bulk flows. CFD on the other hand will provide details about the nature of the flow field. It depends on the problem at hand, which of these aspects is the more important one*".

Manz and Frank, (2005), describe three types of software tools to be coupled for simulation of double skin facades:

1. Simulation software to model the optical element of DSF
2. CFD simulation code
3. Building energy simulation software

Coupling is performed in three steps where the heat sources in the building constructions are calculated by software able to handle optical difficulties. These heat sources are then transferred as inputs into the CFD tool. The next step is the CFD simulation of temperatures and mass flow in the DSF, and the final step is to use the air flows predicted by the CFD simulations as inputs into the whole building energy simulation program.

Furthermore, it is concluded *"...a three level modelling approach is a feasible design method for whole buildings with double-skin facade if there is a static coupling between CFD and building energy simulation"* (Manz and Frank, 2005).

Beausoleil Morrison, (2001), disagrees with Manz and Frank, (2005): *"…the static coupling between building simulation and CFD is not sufficient: the simulation program must be given the ability to adapt modelling approaches to prevailing conditions".* The details of adaptive coupling of CFD with whole building thermal simulation can be found in the original paper.

There are other papers available on coupling different simulation software with the CFD tool for modelling the DSF, such as:

- Manz, (2004), and Manz, et al. (2004) - the articles include a detailed explanation of coupling a spectral optical model with a CFD model, and recommend this approach for analyzing and optimizing a DSF.
- Djunaedy, et al. (2003), - develop a guideline for selecting a simulation tool of air flow prediction and propose a methodology for the coupling procedure.
- Djunaedy, et al. (2002), - analyze levels of modelling in terms of resolution and complexity. The case of study uses the two level BEB-CFD coupling approach. Some conclusions were obtained, but even more questions arose. Some of the answers are given in the work of Manz and Frank, (2005), Manz, (2004), Beausoleil-Morrison, (2001), and Beausoleil-Morrison, et al. (2001). It is worth mentioning that these authors do not consider the BEB approach, they use the network approach instead.
- Hensen, et al., (2002) - this paper also gives a short overview of the possibilities for the DSF modelling approaches, mainly the CFD and network approach are compared and discussed.
- Beausoleil- Morrison, et al. (2001),- the article explains: *"a building-integrated CFD model comprises six aspects: domain discretisation; a set of equations to represent the conservation of energy and mass, momentum and species; the imposition of boundary conditions; an equation solver; a method to link the CFD, building thermal and network air flow models; and the interpretation of the results"*. These aspects are carefully explained in the paper.
- Beausoleil-Morrison, (2001), - provides the reasons and details for adaptive coupling of CFD with whole-building thermal simulation.

The above sections provide a description of the possibilities in the DSF modelling, general approaches and their application. The benefits and drawbacks of these approaches are highlighted in a very brief form as these have to be confirmed with theory and practice.

2.1.4 PUBLISHED EXPERIMENTS ON DSF

Since the year 2000 publications on DSF modelling and application are more frequently confirmed by experiments. The earlier publications on DSF are criticised for the quality of representing the results of measurements and the documentation of the experimental set-up.

Zölner, et al. (2002): *"Most of the experiments reported in the European literature were conducted at indoor facilities using artificial radiation sources and, in general, small scale test facades."*

Zölner, et al. (2002): *"Only a few cases an attempt was made to predict the increase in air temperature within the gap subjected to ambient conditions and geometry of double skin facade. A broad, but superficial review of the technical aspects to be considered in designing double-skin facades has recently been provided by Oesterle et.al, (1999)".*

Today measurements are more and more often conducted both in real buildings and in full-scale test facilities. Articles which include the experimental data belong to Grabe, (2002), Jaros, et al. (2002), van Dijk and Oversloot, (2003), Gertis, (1999), Li, (2001), Manz, et al., (2003). Performed experiments investigate the specific constructional elements and geometry, i.e. depth and height of the cavity, different shading devices and their thermal mass, location of glazing, the type of glazing, etc. Results of measurements are used for the validation and enhancement of the developed models and for improvements of DSF performance at the design stage.

Faggembauu, et al. (2003), offer results of experiments on DSF under the North European and South European climatic conditions. The Master thesis written by Li (Li, 2001), includes a range of measurements conducted in the test facility in USA, Virginia. Here, the DSF is investigated together with the whole test facility system.

K. Gertis, (1999) cites some of the research made at Stuttgart University, which is based on measurements of air velocity in the DSF, wind velocity, solar heat gains, and air change rate. An experiment made on a basis of the scale model is also conducted. The results of the scale-model experiments are mentioned in van Dijk and Oversloot, (2003).

In the article written by Park, et al. (2003), for instance, the different mathematical approaches are discussed in connection with the variable air flow regimes in the cavity and combined with the whole building system. In articles written by Faggembauu, et al. (2003), and Baker and McEvoy, (2000) forced convection, free convection and convection in a closed cavity are examined. The comparison of the simulation and experimental results show a good correspondence (the measurements are conducted in different climatic zones).

2.2 MODELS FOR DSF

This chapter reports on the available studies and publications made in the field of DSF modelling. The report includes a short overview of some models and difficulties that were faced by authors in their modelling process.

There are a number of models developed with different levels of complexity. These models aim to describe different modes of DSF function. Some of the models are validated in reference to the experimental results. Several models include modelling of shading devices such as Venetian blinds, roller blinds, etc.

The entire chapter is focused on the network approach, since the topic of CFD modelling is very broad and there are many parameters to be discussed in order to be consistent. For that reason, the following section 2.2.1 CFD models is of purely informative character, while all the conclusions are derived for the network model in section 2.2.3 .

2.2.1 CFD MODELS

The most important issues, related to CFD modelling of DSF, which are emphasized in the literature, will be addressed in this section.

The CFD modelling of passive solar space heating is not an easy matter. Jaroš, Charvát, Švorèík and Gorny presented a paper at the Sustainable and Solar Energy Conference in 2001, which deals with critical aspects of these problems, mentions possibilities and drawbacks of some CFD codes in this area and, in several solved cases, presents outcomes which can be obtained by this method.

According to the authors, "*simulation methods are a very useful tool for the optimization of the solar building performance, since they enable to predict performance parameters still in the stage of the design. The CFD simulation has become very popular, because of its capability to model particular details of the temperature fields and air flow patterns. These features are essential just in the case of solar-heated rooms with the intense heat fluxes and natural convection.*

The CFD simulation of the performance of solar air systems can significantly improve their operation parameters and effectiveness. Moreover, new structures or systems can be evaluated still in the stage of their design. However, the applicability of the CFD simulation is still restricted to the relatively simple cases. The simulation of air flow and heat transfer inside the whole building is still difficult due to the computer performance. The capabilities of CFD simulation will grow with the increasing capabilities of hardware and software".

Gan, (2001), presented in an article a numerical method that he had developed for the prediction of thermal transmittance of multiple glazing based on Computational Fluid Dynamics. As he describes "*the predicted thermal resistance of glazing agrees with reference data for double glazing unit. The results confirm that the heat transfer coefficient, thermal resistance and thermal transmittance vary with the width of air space between glazing panes up to about 25 mm. As the width of air space increases, the thermal resistance increases while the thermal transmittance decreases. It is shown that both the convective heat transfer coefficient and thermal transmittance increase linearly with the temperature difference between the hot and cold panes of glass. The effect of the temperature difference across an air space on the convective heat transfer coefficient is significant. For moderate climate conditions the effect of the temperature difference on the thermal transmittance may be considered negligible*". According to the author, "*one of the advantages of the CFD technique over the analytical method is that it can easily be applied to performance evaluation of novel flow devices such as air flow windows*".

Manz presented in 2003 an article concerning the development of a numerical simulation model of heat transfer by natural convection in cavities of facade elements. The study sets out to compare

the results obtained by means of a CFD code with empirical correlations in relation to heat transfer by natural convection in rectangular, gas-filled cavities. It mostly focuses on tall, vertical cavities in building elements such as insulating glazing units, double skin facades, doors, facade integrated solar collectors, transparent insulation panels etc.

In more detail: "*heat transfer by the natural convection of air layers within vertical, rectangular cavities with aspect ratios (A) of 20, 40 and 80 was investigated in relation to applications in building facade elements, such as insulating glazing units, double-skin facades, doors, etc. using a computational fluid dynamics (CFD) code. Boundary conditions were assumed to be isothermal hot and cold wall, and zero heat flux at bottom and top cavity surfaces. Rayleigh numbers were between 1000 and* 10^6*, i.e. flow was either laminar or turbulent, and a conduction, transition or boundary layer regime was applied. The study focuses on overall convective heat flow through the air layer. This study improves the starting position for future applications of the code to more complex cases of facade elements, where less or even no experimental data are available in literature*".

Manz and Simmler, (2003), presented at the "Building Physics" recurrent conference (in Belgium) an experimental and numerical study of a mechanically ventilated glass double facade with integrated shading device. The procedure for modelling glass double facades is described in the article. Optical properties were calculated and a transient 2D computational fluid dynamic model was developed. The computing program used for the CFD simulations was FLOVENT. Simulated results were compared with data derived from an experimental investigation of a mechanically ventilated glass double facade built in an outdoor test facility.

The authors concluded that "*A total solar energy transmittance of 7% means that solar energy absorbed in the facade is removed efficiently by mechanical ventilation. In addition, thermal comfort problems due to infrared radiation between people and the inner pane are unlikely because the pane temperature did not rise more than 6 K above mean room air temperature. However, an overall analysis of the facade concept should take into account that the fans used for mechanical ventilation consume electrical energy.*

It would be still possible to decrease total solar energy transmission, e.g. by increasing the outside solar reflectance of the shading screen (here n = 0.48). In other words, very low values can be obtained in a carefully designed glass double facade with mechanical ventilation in comparison with the total solar energy transmittance values that are often recommended, e.g. < 15%, as in SIA 180 (1999). Furthermore, it was found that

- *air flow pattern depends on boundary conditions, in particular absorbed solar radiation, and can substantially change over 24 hours*
- *air flow pattern can be much more complex than the piston-flows assumed in simple analytical models such as that to be found in ISO/DIS15099 (2001)*
- *detailed analysis of air flow patterns (e.g. recirculation / counter flow), energy flows and temperature distribution is only possible with CFD boundary conditions, e.g. external heat transfer coefficient, have to be carefully set because they can have a substantial effect on results we have to bear in mind that if the shading screen is open or not fully closed, solar energy flow into the room increases substantially (e.g. present case: shading screen closed* $\tau_{sol,tot} = 0.03$*, shading screen open* $\tau_{sol,tot} = 0.28$*)*".

Zöllner, et al. (2002), performed simulations of DSF, supported by experimental results. The wind influence in this model was not taken into account. Attention was paid to the modelling of mixed convection; the experiments were performed in order to validate a theoretical model for steady two-dimensional incompressible turbulent mixed convection flow in transparent channels.

2.2.2 NETWORK MODELS

This section is not an attempt to emphasize the favourable models or to scale them by level of accuracy, but to reveal the basic and more advanced approaches. Regarding validation and accuracy, models are affirmed to be successful and promising, though in some cases models are valid only under some specific conditions defined by the author. When it is necessary to know the uncertainty of model performance and its validation results, then the original article has to be found for the detailed information. Most of the articles include comments on model limitations and circumstances for their validation. Thus, it is up to the reader to estimate whether it is accurate enough for the specific conditions of other configurations.

All models in the following section are sorted by the year of publication and therefore the historical development can be seen as well.

Cho, et al. (1995)

This paper describes an analytical model developed for a window system with Venetian blinds. The analytical model is validated via published results of experimental investigations and then the analytical model has been introduced into the TRNSYS software.

Since the model deals with the window system, there is no air flow through the double-facade cavity and the flow element is not included in the investigations. However, the overall thermal characteristics of the Venetian blinds (the heat absorbed in each slat) are analyzed and the results are incorporated in the model.

The effect of the slat angle is included in the analytical model and described in this paper. First, the overall thermal characteristics of the Venetian blinds are computed, as a function of slat angle and incident angle. There are three cases considered:

- When all of the solar radiation incident on the Venetian blind is transmitted through the slats, without being absorbed
- When a part of solar radiation is reflected and the rest is transmitted
- When all the incident solar radiation is reflected

A table of equations to calculate transmittance, reflectance and absorbance of the Venetian blinds is included in the article with correspondence to the above cases.

When the overall thermal characteristics of the Venetian blinds are computed, then the ray-tracing method is applied to calculate the transmittance, reflectance and absorptance in multiple layers of double-facade (with inside Venetian blinds). Also, the overall transmittance, reflectance, and absorptance of double-facade with inside Venetian blinds are obtained. Finally, the simple heat balance for each layer of glazing and the air layer between the panes is set up and solved.

The external heat transfer coefficient is described by Lockmanhekin, (1975), and it depends on the wind velocity and wind direction. The internal heat transfer coefficient is calculated from the same source as the external one, and it depends on window height and the temperature difference between the internal environment and the glass surface.

The heat transfer coefficient in the DSF cavity (for natural convection) is determined after the empirical relationships specified by the author. The equation for the radiation heat transfer is also specified (see the original paper).

The article includes a detailed schema of the developed model and results of predictions compared with the experimental results.

Tanimoto and Kimura, (1997)

The model is developed for atypical design of DSF. The authors suggest the use of roller blinds instead of the glass pane of the internal window. This fact imposes the modelling procedure and its final output in the direction, which rarely exists in practice. Nevertheless, the methodology used for this type of DSF can be useful for approaching an ordinary model.

In the model the DSF is vertically subdivided into 10 parts, each part consists of the number of nodes for every glass or air layer. The heat balance equations are set up for every discrete node and combined into the matrix. The heat balance includes the heat conduction, convection, absorption of solar radiation and the long wave radiation. According to the authors, *"A numerical solution was made using an implicit type of finite difference method… "* The equations are solved iteratively, while the heat transfer and air flow are considered simultaneously.

There are no extensive studies made either in optics or in convection (type of flow) for the double-facade cavity. The property of heat accumulation in the materials has been included into the heat balance equations, but the heat storage ability of the Venetian blinds is neglected. The absorption of the solar radiation is expressed through the absorption property of the material. The long wave radiation within a cavity space is calculated through the mean temperature of opposite surfaces, thus the linearized radiative heat transfer coefficient and nodal temperatures are used. The long wave radiation with the external and internal environment has not been explained.

The flow network can be defined as the unusual one, as there is an air flow through the roller blinds into the room. The model considers the stack effect and the mechanical ventilation by the exhaust fan. The pressure difference for the stack effect is calculated from the difference in the specific weights of the air.

Todorovic and Maric, (1998)

In this paper the DSF is considered as a single zone where the simple heat balance is set up for two cases, one when the air is captured in the zone (thermal insulation mode) and another one when the air enters the zone from the outside and leaves with a higher temperature (external air curtain mode). The primary idea is to determine the temperatures of all surfaces in DSF and to solve the overall DSF heat balance. The heat balance for the DSF glass panes includes:

- transmitted solar radiation into the space
- radiation (solar radiation absorbed by glass which is then released by means of long wave radiation and convection to the internal and external environments)

The solar radiation absorbed by the opaque part of the internal window and construction is released to the room and to the cavity air by conduction and convection while the long wave radiation heat transmission from the opaque surfaces is neglected.

When the cavity is closed, the average inter-space air temperature in the DSF is determined from the heat balance equation, depending on air circulation in the cavity. In the case of an open cavity the average inter-space air temperature depends on air flow. The authors include results of experimental studies on DSF inter-space air temperature depending on outside air temperature, cloudiness of the sky and facade orientation. Dominating diffuse or direct solar radiation has a different impact on the temperature in the double-facade cavity. It is possible to include these differences by differentiating the outside air temperature in two groups (for cloudy and clear days). The direct solar radiation dominates on clear days and the diffuse radiation on cloudy days. There is no information provided on the convective heat transfer coefficient.

In the literature, the model is regarded as one of the first models, which is focused on predicting the DSF performance. This model belongs to the period when the authors have not yet distinguished the three governing issues (elements) in predicting of the DSF performance. Nevertheless, the authors find it important to count on absorbed solar radiation for the temperature distribution in the cavity space.

Haddad and Elmahdy, (1998)

This article includes information on a simple numerical model and also a discussion of that model. The model is developed on the basis of a program identical to the Vision software tool that includes the hourly weather data file and it is intended to study monthly variation in the thermal performance of a supply air window. The model considers two cases, the conventional triple glazed window and a supply air window. The primary difference between the supply air window and the DSF is the smaller cavity depth of the former. Based on the work of other researches and by considering comparably small gaps for the air path the authors assume that the flow in the gap: "*…is laminar and hydrodynamically fully developed with unequal wall temperatures".* The expressions for the local Nusselt number are integrated in order to obtain the general heat flux at the cavity surfaces. The information on internal and external convective coefficients is unavailable.

Every glass pane is represented by a node and characterized by temperature. The heat balance is set up for each node. The heat balance includes the long wave radiation with internal and external environments, convection and absorption of solar radiation. There is no detailed information provided on absorption of solar radiation, while the total long wave radiosity is calculated as a sum of the emitted energy and reflected part of the incident energy.

The total long wave radiosity and the total heat flux from the surfaces are combined with correlations for the heat transfer coefficient, which are obtained from the Vision software (no more details provided in the article). The problem is then solved by an iterative technique that is based on the Newton's method. The initial guess of the node temperatures is made between the indoor and outdoor temperature.

The mass rate flow is a known value as it is expected to satisfy ventilation requirement.

Di Maio and van Paassen, (2000)

The modelling approach explained in the paper is very similar to the one described by van Paassen and Stec, (2001). It is composed of two main subsystems:

- Ventilation model
- Thermal model

"The ventilation model should calculate the flows through the inlet and cavities, based on the outputs of the thermal model, the stack effect generator, the pressure generator, the wind generator and on the weather data…" The ventilation and thermal models are calculated separately. The Simulink simulation code is used for this model.

The air flow through the cavities (the cavity is separated into two shafts by a shading device) is calculated similarly to the methods explained in the following model (van Paassen and Stec, 2001). Di Maio and van Paassen compute the air flow in cavities from the total pressure difference between the bottom and top opening, which includes buoyancy, wind force and resistances of the grids at each floor. The pressure difference due to wind is calculated following Chandra and Swami, (1994). The pressure difference due to buoyancy forces is calculated following Liddament, (1996).

The DSF facade is vertically subdivided into one storey high partitions. Each layer of the DSF construction is representing a node in the thermal model; thus the temperatures in the DSF are lumped together per storey. The heat balance is set up for each node and includes conduction, convection and radiation. When the air flows are calculated, the output is used to calculate the convective heat transfer coefficients from the following expression (the source is unknown):

Equation 2-1

$$\alpha = (-7.52d + 8.68)v - 0.448d + 0.542$$

α - convective heat transfer coefficient [W/m^{2}K]
v - air velocity in the cavity [m/s]
d - width of cavity [m]

The solar radiation absorbed by glass is calculated by solar radiation factors, which are not defined in the paper. The radiation heat transfer coefficient is undefined as well.

Both the thermal model and the ventilation model are highly interacting. Thus the output from the temperature element is used as an input for the flow element and then the output from the flow element is used again as an input for the temperature element and so forth.

van Paassen and Stec, (2001)

The model has been developed to evaluate the overall energy performance of a DSF and to be simulated with the MATLAB and SIMULINK software. The modelling of blinds is included.

Similarly, to the previously defined elements of DSF physics the authors distinguish three simultaneously interacting models:

- Air flow model
- Thermal model of the DSF
- Thermal model of the building

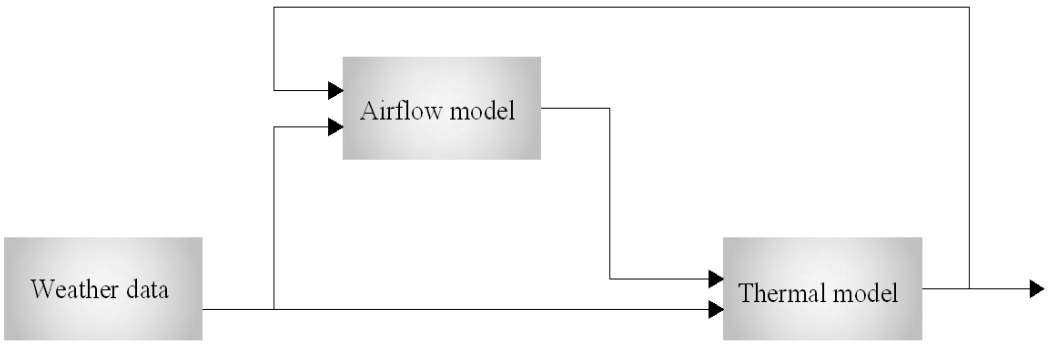

Figure 2-1. Scheme of construction of the simulation model in Matlab (van Paassen and Stec, 2001).

The construction of this model is visualized in Figure 2-1, according to the author: *"the weather data and the first approximation of temperatures in the cavity are used to calculate the differences in pressure and the air flow in the cavities".* The data obtained in the air flow model, together with the weather data, are used to make the next approximation of temperatures and so on.

The article includes clarification of how the air flow and thermal models are organised and solved. The air flow model assumes that the air flow through the DSF is caused by wind and buoyancy forces. There is a significant simplification made: the outside facade window panels are *"installed in such a way, that the openings between the junctions exist. The air goes in and out due to the turbulence of the outside air. The higher the wind velocity, the higher the air flow will be. It is assumed that the turbulence air flow does not change the flow in the cavity. The same amount of outside air enters the cavity through the junction openings and leaves it again after mixing, through the same opening. Consequently, the turbulence air flow only affects the temperature in the cavity because of mixing with the cavity air. To conclude, it is not taken into account in the air flow generator".* By such simplifications, the junctions have a function of openings, located in the DSF of multi-storey buildings. There is also a possibility for the cavity air to enter the room behind the

DSF due to mechanical ventilation in the room. The detailed explanation can be found in the article of Stec and van Paassen, (2003), which describes a similar model by the same authors.

The air flow through the cavity is calculated from the total pressure difference:

Equation 2-2

$$\Delta P_{tot} = \Delta P_b + \Delta P_w$$

ΔP_{tot} - total pressure difference between inlet and outlet opening in the DSF
ΔP_b - buoyancy pressure difference in the DSF
ΔP_w - pressure difference, caused by wind in the DSF

The pressure coefficients are used to calculate the wind-generated pressure difference between the bottom and top openings using the expressions developed by Swami-Chandra (van Paassen and Stec, 2001).

For the thermal model the facade is vertically divided into segments which have a height of one storey. The segment is represented by the nodes in each layer of the DSF (air and material layer) and the heat balance is set up for each node.

The article provides the reference to an expression for determination of convective heat transfer which depends on the air flow and the dimensions in the cavity. The radiant heat transfer coefficient and calculation of optical properties of the DSF are not explained.

A similar model is described in the article of Stec and van Paassen, (2003). Some changes are made to the air flow element, but the main approach is kept the same. This model (Stec and van Paassen, 2003), is developed in order to determine DSF thermal/flow performance and to discover how to combine the DSF with the building systems (HVAC).

Saelens, (2002)

A two-dimensional numerical model for single storey multiple-skin facades with mechanical as well as natural ventilation was developed by Saelens, (2002), and described in his PhD thesis. As the author describes, "*The model is based on a cell centered control volume method. The cavity layers are only vertically subdivided and the temperature of the cavity control volume is represented by a bulk temperature. It is assumed that enthalpy flows only occur in the vertical direction. This restricts the use of the model to multiple-skin facades with roller blinds.*

To estimate the convective heat transfer coefficient, existing relations obtained from experimental research and numerical simulations are implemented. Distinction is made between natural, forced and mixed convection regimes. In most cases, the flow in one storey high multiple-skin can be regarded as a developing flow. For the naturally ventilated as well as the mechanically ventilated multiple-skin facade heat transfer correlations for flow over a single vertical plate are then suggested. During night time and during situations with low solar radiation, uniform wall temperature expressions are used. For all other situations, uniform heat flux correlations are implemented. A limited experimental evaluation of the correlations is presented. The spread on the results, however, shows that obtaining a reliable expression for the heat transfer coefficient is difficult.

The solar radiation absorbed in the different layers depends on the angle of incidence, takes into account multiple reflections and deals with vertical shadowing. The long-wave radiation is calculated by the net-radiation method".

A numerical model developed by D. Saelens also takes into account all three elements. The techniques to describe the heat transfer element, optical element and the flow element are investigated by the author and a reasonable accuracy of the techniques is demonstrated.

The model has been implemented in the energy simulation software TRNSYS and validated with the experimental results. The author has performed a study of the modelling assumptions and has demonstrated that the results of simulation are very sensitive to two issues:

- Whether the angular solar properties are taken into account
- Whether the inlet air temperature is properly described

In the section of conclusions and advice for further research D. Saelens explains that conduction and radiation are relatively well-known issues, but convective heat transfer and modelling of air flow are not. Therefore, the future improvements of the DSF model are required in these fields.

In order to develop the model, the author has implemented existing techniques and relations to describe the air flow and convection phenomena. The air flow through the naturally ventilated cavity is the result of the buoyancy and the wind pressure differences. Some experiments were conducted on the naturally ventilated windows of the Postcheque building. The experimental results have shown mainly the wind driven air flow in the winter season. According to Saelens, in winter it is "*…difficult to find a relationship between the air flow rate and the wind speed or wind direction. In summer, the air flow was mainly caused by thermal buoyancy…It was shown that thermal buoyancy models can predict the air flow through naturally ventilated active envelopes adequately for low wind speeds. For higher wind speeds, simple models fail to predict the complexity of the air flow."*

As a result of comparison between models of low complexity and numerical models Saelens reached a conclusion that: "…not separating radiation and convection in the cavity is an unacceptable simplification. The accuracy of analytical models is determined by the capability to predict the temperature profile." Saelens' numerical model "…performs best because it uses the net-radiation method to calculate the radiation heat exchange and is able to account for shadowing."

Grabe, (2002)

In order to be able to make quick decisions and to avoid fairly complicated CFD tools in DSF modelling, J.V. Grabe developed a software tool, described in the article (Grabe, 2002).

The author distinguishes the temperature and flow functions (similar to the three governing elements in the DSF physics) under steady state conditions. The energy transport equation and the Bernoulli equation are applied as a background and the basic steps of their modifications are later outlined in the paper. The temperature and the flow functions are solved by an iterative process. According to the author, the iteration "*… can be started with an arbitrary value for the mass flow and sensible values for the heat transfer coefficients*", "*…the resulting mass flow density caused by the buoyancy can be calculated and used as an improved value for the temperature function. Within the time step, the heat transfer coefficients should be newly determined.*"

The algorithm does not include the air exchange between the cavity and a room.

The temperature function
The temperature function is described by the energy transport equation. The authors do not consider the molecular heat transport within the cavity air. They also assume that the net heat flow in and out of the gap takes place only in x-direction (for three-dimensional coordinate system). Besides, it is considered that the convective heat transfer exists as the net heat flow in y-direction and there are no single heat sources.

There is a shading device (blinds) installed and it separates the cavity into two shafts. Since the heat transfer coefficients may vary due to different air temperatures and air velocities in the shafts, the convective coefficients for each shaft are treated separately. The Michejew's approach (Elsner, et al., 1992/1993; Elsner, et al., 1993) has been used for calculations of convective heat transfer coefficients, averaged for the height of the DSF. Normally, this approach is used for free convection flows on vertical planes.

The radiative heat exchange between surfaces is approximated by a radiative heat exchange factor (for two infinite parallel planes), which is also averaged over the height of the DSF (the details can be found in the original article).

The author provides references for calculation of the heat exchange with the ambient air.

The absorbed solar radiation is calculated from the solar intensity and absorption properties of the material. Absorbed solar energy equals the total heat flow in the cavity. As a result, the author transforms the above equation into the set of energy balance equations for all surfaces.

The flow function
"For the motion of the air only, buoyancy forces are taken into account". The author starts with the Bernoulli equation, which is transformed as:

Equation 2-3

$$\frac{p_o}{\rho_o} = \frac{p_s}{\rho_s} + \frac{v_s^2}{2} + e$$

p_o - external pressure, Pa
p_s - pressure in the shaft, mean value over height, Pa
ρ_o - external air density, kg/m^3
ρ_s - air density in the shaft, mean value over height, kg/m^3
v_s - velocity in the shaft, mean value over height, m/s
e - dissipated energy, between two points, W/kg

"With the buoyancy driven natural ventilation it is very common thing, to determine the dissipated energy in a similar way to the determination of the turbulence losses of pipes", which are normally expressed through the flow resistance coefficients. In the article, the method to interpret the dissipation energy into the form of resistance coefficients is demonstrated. In addition, the author suggests the use of different resistances for the different types of losses. The local velocities at the resistances are determined from the continuity equation as described in detail in the article.

Since the flow motion in the shaft is driven by buoyancy forces, and the dissipation of energy expressed through the resistance coefficients, the author describes the mean air shaft velocity as:

Equation 2-4

$$v_s = \sqrt{2\left(\frac{\rho_o - \rho_s}{\rho_s} gh - e\right)}$$

p_s - pressure in the shaft, mean value over height, Pa
ρ_o - external air density, kg/m^3
ρ_s - air density in the shaft, mean value over height, kg/m^3
w_s - velocity in the shaft, mean value over height, m/s
e - dissipated energy, between two points, W/kg

Later on, the author finalizes the equation of the mean air shaft velocity, as can be seen in the article.

Balocco, (2002)

The article represents a numerical model for simulation of the energy performance of ventilated facades. In the paper the facade is represented as a Trombe wall with the air intake and extract from and to the outside. The facade is vertically divided into segments, which are the control volumes in the model. The steady state energy and mass balances are applied to each control volume. As a result a set of equations is obtained, where each equation represents the heat balance for the surface or the air mass in the cavity. The model is based on finite element method and implemented into the computer program "ventilcam". The model is solved iteratively, for each control volume, "*different surface and air mass temperatures are calculated. The mass flow rate is calculated as overall natural draught*".

The air velocity in the DSF is expressed as for a solar chimney, based on mass and energy balance:

Equation 2-5

$$v^2 = 2gh\frac{(t\ /t_o - 1)}{(\lambda h / D_h + 0.25)}$$

v - mean air velocity in the cavity, m/s
g - acceleration of gravity, m/s^2
h - height of the cavity, m
t - temperature of the air mass in the cavity, °C
t_o - external air temperature, °C
λ - friction factor
D_h - equivalent diameter, m

The friction factor of pressure losses is found by the Moody expression (Holman, 1991) as a function of Reynolds number. The external convection heat transfer coefficient is calculated by expressions available in the literature developed by Holman or Warren (Holman, 1991; Warren, et al., 1998).

The internal convection coefficient is calculated for the turbulent flow following Warren, et al. (1998). There are no details provided on the radiative and convective heat exchange in the double facade.

Faggembauu, et al. (2003)

The code described in the paper is designed for the simulation of conventional and ventilated facades (DSF). According to the article: *"the discrete equations are obtained from the continuous governing equations using the finite volume method. The building skin is assumed to be divided into a number of independent facades and each facade is in turn divided into a number of zones (approximately 1 m high), which are only coupled due to presence of the air channel. One-dimensional discretisation is used for the air channel and for each of the zones (orthogonally to the facade). This approach is between a one-dimensional and a two-dimensional model".*

The article includes a chapter with a detailed explanation of the internal and external boundary conditions and weather data sets to be used. A standard data set, which is introduced in the code, consists of monthly averaged daily integrated values of global horizontal solar radiation, maximum and minimum temperatures, wind velocities with directions, and humidity of the air.

External surface
There are references to methods for calculation of diffuse or total solar radiation. The ambient temperature distribution is described by a sinusoidal function between the minimal and maximal values. The long wave radiation heat exchange of the external surface with the sky is determined after Berdahl and Martin's expression (Duffie and Beckman, 1991). The radiation exchange with the ground is calculated depending on the view factor between the ground and facade (the

ground is assumed to be adiabatic with a certain reflectivity). The convective heat transfer coefficient is calculated as a function of the wind velocity by application of the empirical expressions developed by Rohsenow, et al. (1985).

Internal surface (facing the room)
"Regarding to the indoor conditions it is assumed that a single constant indoor air and walls temperature exists to evaluate the convective and radiative heat transfers respectively". For the calculation of indoor convective heat transfer coefficients the natural convection is assumed and the empirical equations of Mills, (1992), are employed.

The authors carefully describe the studies of:

- Conduction in each glass layer
- Natural convection between glass layers
- Thermal radiation between glass layers
- Solar radiation
- Air channel heat transfer and fluid flow, depending on governing flow conditions:
    - *"Forced convection: a known air flow rate is imposed.*
    - *Natural convection: the flow rate is driven by the temperature difference between the air and the channel walls".* Time dependent flow rate.
    - Closed channel: recalculating natural convection flow.
- Global model algorithm

The DSF is modelled as a vertical transient algorithm. The governing equations (mass, momentum, energy conservation) are solved by the finite volume method. When the air flow is known (mechanical ventilation), then the step-by-step algorithm is applied to find the temperature, pressure and velocity. The heat transfer coefficients are determined from the empirical equations for the Nusselt number which is defined for the developing and turbulent flow. The approach for calculation of Nusselt number is specified in the article. The authors are aware of possible inaccuracy caused by the expressions used to calculate the heat transfer coefficient; however, they argue that: "*these are the best expressions attested to in published literature…"*

In the case of natural ventilation only the buoyancy forces are included in the model, while the wind forces are neglected. It is assumed that the pressure at the outlet opening in the DSF is a function of the inlet velocity and the density differences at inlet and outlet. The equation is solved iteratively.

The details of the global algorithm and the solution process can be found in the article.

van Dijk and Oversloot, (2003)

The paper highlights the main features of WIS software for simulation of thermal and optical properties of a solar shading device installed in the DSF construction. The algorithms in WIS are based on international standards ISO DIS 15099. According to the authors: *"WIS also contains advanced calculation routines for those components or conditions where no standards are available yet or current standards do not apply".* As explained in the article *"one of the unique elements in the software tool is the combination of glazing and shading devices with the option of free or forced air circulation between the components"* in the sealed cavity space.

First, the modelling of the shading devices is discussed and the main difficulties are identified. There are two cases explained with the sealed cavity space: one with the air motion induced by fan and another induced by natural (buoyancy) forces. The sensitivity of the transmitted solar radiation through the window with blinds and sensitivity of solar radiation on the angle of incidence are investigated by means of the mentioned software.

The DSF is modelled by WIS and CFD tools; some of the results are compared.

Park, et al. (2003)

The authors of this model aimed to develop an occupant responsive optimal control for DSF. The model includes blinds and it is prepared for transient simulations. As described in the article, there are four processes which are involved in the DSF performance:

- Direct, diffuse and reflected solar radiation
- Long wave radiation between surfaces
- Convective heat transfer
- Air movements through the DSF

From the above is seen that the authors recognize the governing elements of the DSF physics, similar to the other models and research.

The temperature distribution over the height of the DSF is assumed to be constant. In the modelling of the convection processes there are six unknown convective coefficients defined: the external and internal heat transfer coefficient, the coefficient in the air layer of the double glazing, at the external and internal window inside the cavity and at the surface of the open slats of the shading device (blinds), as depicted in the Figure 2-2. These coefficients are estimated from literature. The references are specified in the article.

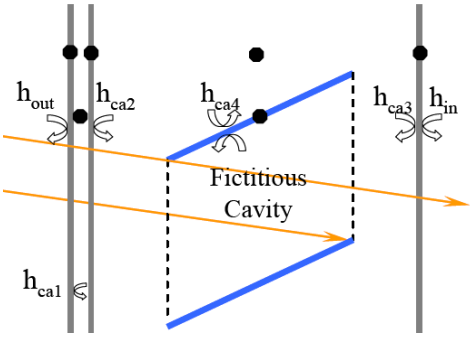

Figure 2-2. Heat transfer coefficients, Park, et al. (2003).

According to the authors: *"In mathematical formulating the direct, diffuse and reflected solar radiation and long wave radiation between surfaces the theoretical model suggested by Rheault, et.al (1989)".*

The model deals with ten different flow regimes, which are depicted in Figure 2-3.

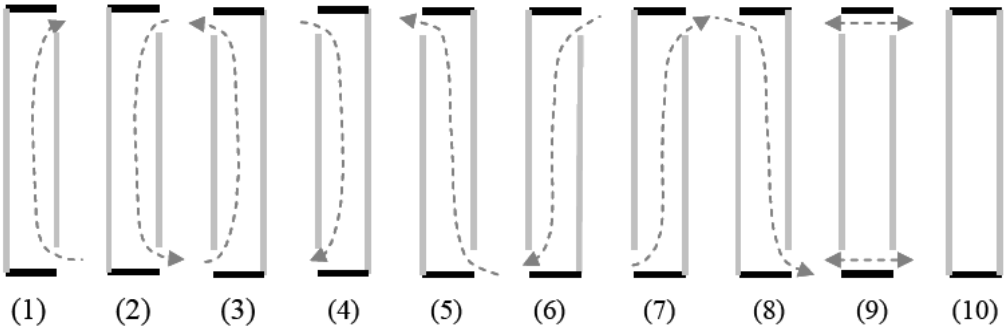

Figure 2-3. Ten air flow regimes (louver slats not drawn for clarity), Park, et al. (2003).

In the modes 1-2 the modelling of air flow has been explained in another article, but *"it is based on a conventional 1-dimensional formulation utilizing momentum and energy conservation. By combining the momentum equation and the total flow resistance parameter, the mean air velocity in the cavity is solved algebraically, where it depends on the cavity depth and length, indoor air*

temperature, cavity air temperature and the form loss factor". More details can be found in the original paper (Park, et al., 2003).

In the modes 3-4 the overall velocity (wind) pressure is expressed by a modified Bernoulli equation. The power law equation describes the relationship between the flow rate and the pressure difference. Sherman, (1992), suggests the relationship between the air flow caused by combined wind and buoyancy and the authors of the model derive a final expression to calculate mean velocity in the cavity.

In the modes 5-8, the diagonal flow is modelled. The total pressure difference also includes a static pressure difference caused by (de)pressurization of an interior space and the air flow is described by the power law equation.

The modes 9-10 were not included in model.

Takemasa, et al. (2004)

The intention of developing this model was to calculate the year-round performance of the DSF. The process of the DSF modelling and of the DSF simulation is roughly described, but the interesting fact is that the model was developed on a basis of a large set of experiments which show a strong correlation between the incident solar radiation and the temperature difference in DSF and the external environment as can be seen in Figure 2-4 and Figure 2-5:

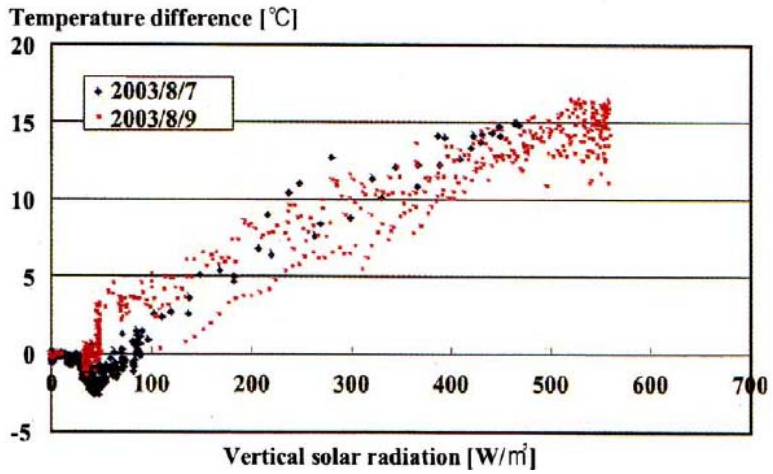

Figure 2-4. Correlation between vertical solar radiation and temperature difference in Summer, (Takemasa, et al., 2004).

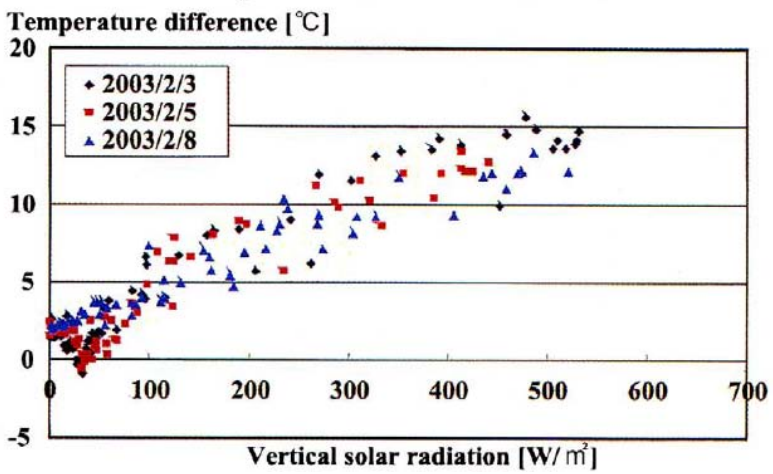

Figure 2-5. Correlation between vertical solar radiation and temperature difference in Winter, (Takemasa, et al., 2004).

According to the article (Takemasa, et al., 2004): *"The building incorporates a hybrid ventilation system (natural ventilation integrated with air-conditioning system)… The inner wall of the facade has windows that can be opened… In order to promote utilization of natural ventilation, the system incorporates a sophisticated automatic control strategy that takes into account outdoor conditions such as air temperature, humidity and wind velocity. The inner air intake openings can be opened to 5 openings angles including 'completely closed' and 'completely open' according to the outside conditions".*

The control strategy applied during the measurements has not been explained in the article and it is not possible to assess the changes in the air flow rate during the experiments (see Figure 2-4 and Figure 2-5) but it is reasonable to expect constant or slightly varying air flows for these Figures.

According to the authors, *"the temperature difference between the inside and the outside of the DSF is independent of the outside temperature, but dependent on the vertical solar radiation transmitted…"*

The starting point in the model are known boundary conditions such as the outside air temperature and the incident solar radiation. Thus from Figure 2-4 and Figure 2-5 the air temperature in the cavity of the DSF can be estimated. By interpolation the exhaust air temperature is found and it is possible to calculate the air change rate.

The DSF is vertically subdivided into four sections. The surface heat balance for each section is set up and solved and the final value of the DSF air temperature is calculated.

2.2.3 DISCUSSION OF NETWORK MODELS

The introduced network models have a varying complexity of nodal connections which depend on the author's decision about the elements governing the physics of DSF (i.e. flow element, thermal element, optical element). When these elements are distinguished then the technique for estimation of their impact has to be defined and expressed in the model by the author. As mentioned before, authors may neglect some of the elements or use very rough approaches, while some of the elements are more thoroughly investigated. In this way the structure of the model becomes unbalanced and weak. The beneficial side of this situation is that single studies of elements already exist and work is needed to integrate them into one product (model). A significant contribution to the list of three-elements-integrated-models was made by Saelens, (2002), who came up with the model where the impact of all elements is fairly estimated; in addition, he revised the available approaches for dealing with separate elements and documented the reasons for the chosen techniques.

Such models, as described by Faggembauu, et al. (2003), Di Maio and van Paassen, (2000), Lehar and Glickman, (2004), and others, are also remarkable for the attempt to integrate different physical elements of DSF physics.

It is possible to define various modes of the double-facade functioning; some of them may involve HVAC systems. A mode of DSF functioning and a contribution of HVAC systems are essential for estimation of heat and mass transfer processes through the cavity space. Consequently, a mode and an application of HVAC must be included into the model by means of nodes and internodal connections. This fact increases the complexity of the predictions as the modelling of 'stand alone DSF' has not yet succeeded and the integration of the DSF with the whole building is even more complex. There are some models that integrate the DSF with the building systems (see Stec and van Paassen, 2003, Takemasa, et al. 2004, Park, et al. 2003, and others).

The network model typically describes the bulk temperatures, velocities, etc. in the zones. The term 'zone' is associated with the whole room (or even a few rooms). In this case the DSF is treated as one zone and the accuracy of the predictions appears to be unacceptably low. In the case when the predictions are performed with the CFD software tool, then, as mentioned earlier,

the distribution of velocity, temperature and energy dissipation is calculated for every single grid in a room, and as a consequence, the approach is regarded as too accurate for the design needs. To overcome the lack of accuracy in the network method and 'overaccuracy' in CFD modelling the technique of coupling the models was introduced by Manz, (2004), Manz, et al. (2004), Hensen, et al., (2002), Beausoleil- Morrison, et al. (2001), Beausoleil-Morrison, (2001) as explained in the above sections.

However, another tendency in DSF modelling exists. These are the models developed on the basis of the traditional network approach which has been highly evaluated for the modelling of conventional buildings and systems. The successful part of the model (related to the conventional part of the building) is kept unchanged and solved by the traditional network approach, while the model of the DSF zone has been improved. Different procedures for DSF zone enhancement can be seen between models developed by Saelens, (2002), Grabe, (2002), Ciampi, et al. (2003), etc. It is performed in a way that the DSF is represented by a few nodes instead of one and as a result solved with a better accuracy. The number of nodes and their distribution in the DSF may vary, but the approach stays the same: an additional number of nodes is introduced for improvement in accuracy of DSF simulation by means of the network method.

In the literature this approach is often regarded as the most promising for the DSF simulations for pre-design stage. The illustration of this technique corresponds to the case (e) in Figure 2-6. Saelens, (2002), performed an investigation of an accuracy change with stepwise enhancement of the network model. The diagram, depicted in the Figure 2-6, represents the stepwise change in the network models starting from the simplest case (a) – a single zone model.

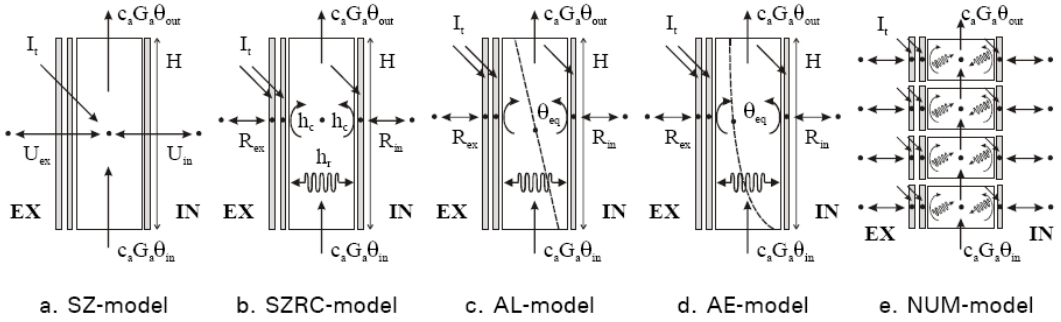

Figure 2-6. Diagram of the different models with raised shading device, (Saelens, 2002).

According to the author:

- *"(SZ) The first model is a single zone model in which each cavity is represented by a single node. Radiation and convection in the cavity are combined. The heat transfer through the cavity surfaces is described by a single U-factor. The solar radiation is inserted in the air node and the cavity surface temperatures are not calculated.*
- *(SZRC) As a first improvement, radiation and convection in the cavity are treated separately. In addition to the heat balance for the air nodes, a heat balance for each cavity layer is written. The absorbed solar energy is inserted in the cavity layers and is function of the angle of incidence. It is calculated for each pane with the embedded technique.*
- *(AL) A further improvement consists of accounting for the temperature gradient along the height of the cavity. In order to allow an analytical solution, a temperature profile has to be chosen. As a first, easy choice, a linear temperature gradient is assumed.*
- *(AE) A theoretical study of the temperature distribution in a ventilated cavity shows that the temperature profile is exponential. Consequently, an exponential temperature gradient is assumed as a further improvement for the analytical model.*
- *(NUM) The outline of the numerical model which is based on a cell centered finite volume method. As improvement over the other models, the radiation heat transfer in the cavity is treated more correctly and shadowing is taken into account.*

In order to allow a correct comparison, the convective heat transfer coefficient as calculated by the numerical model is implemented in the models which separate convection and radiation."

These five cases can be useful as a scale to estimate the complexity of any network model, especially when it is necessary to characterize a model in a few words instead of listing all applied techniques and approaches. In order to make the scaling as practical as possible, the definition for the above models (SZ, SZRC, AL, AE and NUM) has to be simplified. In this way, every case would be able to cover wider modelling ranges.

This chapter includes Table 2-1, which provides an overview on DSF modelling approaches. A major part of the reviewed articles includes information on simplifications used during the modelling. The physical processes covered by the optical element, the heat transfer element and the flow element exist independently of whether the author of the model identifies them or not. However, it is up to the author to decide which elements in the model are to be simplified or to be neglected. Often the scientific papers include records of particular difficulties and consequences for taken decisions. These facts can be essential and will be investigated in the following sections:

- Heat transfer
- Air flow
- Optical and solar properties

However, some information overlaps because the physical processes are interconnected.

Author/year	Nodal-structure	Optical element	Thermal element		Air flow element	Exp. studies
		Optical and solar properties	Long wave radiation	Convection		
Cho, et al. (1995)	DSF is described by bulk temperature	Not described	The ray tracing method to calculate overall thermal characteristics.	The external and internal convective coefficients from Lockmanhekin (1975)	No air motion	no
Tanimoto and Kimura (1997)	More than one node in the DSF zone	The absorbed solar radiation is expressed through the incident solar radiation and through the absorption property of the surface	The long wave radiation within the cavity space is expressed through the linearized radiative heat transfer coefficient and nodal temperatures. The long wave radiation with exterior and interior environment has not been described	Convective coefficients are not described but the text supposes their discussion during the research. The accumulation of heat in the constructions is included	The air flow induced by the exhaust fan and stack effect. In the first case the air flow is known, and in the other it is calculated from the results of iterations by temperature	yes
Todorovic and Marik (1998)	DSF is described by bulk temperature	$i_t = ik$ i_t - transmitted solar radiation i – incident solar radiation k- transmittance coef.	$q_{LW} = \varepsilon AC\ \phi \Delta T$ A - area φ – temperature coefficient ΔT - temperatures of exchanging surfaces	Convection coefficients are undefined	The air flow has to be known	yes
Haddad and Elmahdy (1998)	More than one node in the DSF zone	Not described	Calculated as a sum of emitted energy and reflected part of the incident energy	Fully developed laminar flow. The Nusselt number is calculated from empirical relationships provided by author	Mass flow is accepted accordingly to ventilation requirements. Air flow modelled acc. the references specified by author	no
Di Maio and van Paassen (2000)	One bulk segment is of the height of one story	$q = iA_1A_2A_3A_4$ $A_{1\text{-}4}$ - solar radiation factors i -solar radiation on surface	$q = \alpha_{LW} A(T_1 - T_2)$ α_{LW}- long wave radiation heat transfer coefficient, which is undefined A- area	Convective coefficient described by equation: $\alpha = (-7.52\ d + 8.68)v - -0.448\ d + 0.542$ d- width of cavity, v- velocity	The air flow through DSF is calculated from the total pressure differences between the inlet and outlet openings, which is caused by buoyancy and wind forces and flow resistance coefficients. The wind force is calculated for the high-raise buildings by application of wind pressure coefficients calculated acc. Chandra and Swami, (1994), and the stack effect acc. Liddament, (1996)	no
van Passen and Stec (2001)	More than 1 node in the DSF zone	Not described	Not described	Heat balance is written for each node in each layer. Convective heat transfer coefficient is calculated using an expression, specified by author	The air flow through DSF is calculated from the total pressure differences between the inlet and outlet openings, which is caused by buoyancy and wind forces. The wind force is calculated for the high-raise buildings, by application of wind pressure coefficients calculated acc. Chandra and Swami, (1994)	no

Author/year	Nodal-structure	Optical element	Thermal element		Air flow element	Exp. studies
		Optical and solar properties	Long wave radiation	Convection		
Saelens (2002)	More than one node in the DSF zone	Edwards' method	Calculated as for external and internal environment. The approaches are specified by author	The convective coefficient inside the cavity depends on type of flow. The external and internal convective coefficients are specified by author	The naturally and mechanically ventilated cavity. In the first case the air flow is calculated from the buoyancy and wind forces	yes
Grabe (2002)	The temperature varies between two point: 1. the inlet 2. the outlet	Not described	Approximated by radiative heat exchange factor (for two parallel planes with infinite expansion), which is averaged by the height of DSF	Convective coefficients are treated separately for the internal and external shafts. These are calculated for free convection for vertical panes (specified by author)	Transformed Bernoulli equation, the basic steps of transformations explained in the article. Friction factors for mechanical and natural ventilation are different	yes
Balocco (2002)	More than one node in the DSF zone	Not described	Not described	The convective heat transfer coefficient is calculated for the turbulent flow, the approach for calculations is specified by author	Velocity in the cavity is calculated as for the solar chimney where the friction factor is calculated. Approach is specified by author	no
Faggembauu et al. (2003)	More than one node in the DSF zone	References for calculation of the diffuse radiation are available. Transmitted solar radiation is calculated by Iterative Net Heat Radiation Algorithm. the reference is available	Radiation heat exchange with internal environment is calculated as for the net heat transfer between two infinite opaque parallel plates. Radiation heat exchange with external environment is calculated as the heat exchange with the sky. Reference for calculation of sky temperature is available. Radiation heat exchange with the ground - calculated with the help of view factor.	Free/Forced convection External convective coefficient is calculated as a function of wind velocity and direction . The reference is available (Rohsenow, 1985). Internal convective coefficient is calculated for natural convection, the reference is available.	Calculated for the buoyancy forces. No wind considered	yes
van Dijk and Henk Oversloot (2003)	This model is slightly related to the DSF modelling and there is not enough information on this model					
Park, et al. (2003)	Bulk temperature	Calculated acc. Rheault, 1989	Not described	Six different convective heat transfer coefficients which are estimated acc. references provided by author	10 different models are applied: inside circulation; outside circulation diagonal flow. The air flow is solved differently for different cases	no
Takemasa et al. (2004)	There are four sections with bulk temperatures	Not described	Not described	Temperature is calculated from the experimentally obtained figures	Hybrid ventilation. The DSF is integrated with the building	yes

Table 2-1. The overview of the available models for prediction of DSF performance.

Heat transfer

In the beginning it is necessary to call attention to the fact that: *"Global heat transfer coefficients, such as overall heat transfer coefficient (U-value) and the solar heat gain coefficient (g-value) are commonly studied to determine the thermal behaviour of the facades. Standard coefficients assume steady state and one directional heat flow and this cannot be directly applied to ventilated facades"* (Faggembauu, et al., 2003).

Saelens, (2002), came to the same conclusion: *"the use of standard energy performance indicators such as U-factor and g-value is shown to be unsuitable to assess the overall energy performance of multiple skin facades"*, besides *"a comparison of numerical model with models of lower complexity revealed that not separating radiation and convection in the cavity is unacceptable simplification".*

However, U-value and g-value are inevitable inputs in the majority of thermal building simulation tools. g-value expresses the amount of solar radiation, which is transmitted to the room through the fenestration plus amount of solar radiation absorbed by glass and then re-transmitted towards the interior mainly by means of convection and radiation.

In this case the convective and radiative surface heat transfer coefficients are considered to be characteristic for a building. However, these differ a lot for DSF, since the surface temperature of the glazing and shading in DSF increase significantly with the height of the cavity. Thus a local g-value of the glazing may differ a lot, as well as actual area averaged g-value of glazing, compared to its characteristic g-value, normally provided by a producer.

The convective heat transfer contribution to the g-value is also important, since air velocities in DSF cavity are normally higher than the ones in a conventional room. The surface temperatures of the glazing/shading can also become relatively high. Finally, the convective and radiative heat transfer contribution to the actual g-value is not straight forward to estimate. The g-value is actually varying in time and depends not only on angle of incidence, but also on surface temperatures and mass flow rates. Surface heat transfer is also included into the U-value characteristic and therefore the same limitations are valid if it is necessary to estimate an actual U-value of the DSF constructions.

The first dilemmas appear when the heat transfer coefficients are separated and the convective heat transfer coefficient is to be estimated, as argued in Mei, et al. (2003): "*The convective heat transfer coefficients within the gap are far from straightforward to estimate. This is because, in reality, the heat transfer processes involve a combination of forced and natural convection, laminar and turbulent flow and, certainly in the entrance region, simultaneously developing flow (in which the hydrodynamic and thermal flow profiles are both evolving).*" In addition, the necessity of appropriate modelling of diverse types of flows in one model (turbulent/laminar, free/forced), is emphasised.

Additional difficulties arise when a shading device is installed in the gap. The double skin cavity is then divided into two sections and differences in the flow regimes may appear. In this case it is necessary to estimate the convective heat transfer coefficients for each flow regime in each sub-cavity. Also, different shading devices exist, some of them allowing an exchange of air between the sub-cavities. In the case of Venetian blinds being installed as a shading device, in addition to the potential for flow between the cavities, flow disturbance at the blinds exists and further complicates the situation of estimating the convection heat transfer coefficient. It is noted in Park, et al. (2003): *"Especially the convective heat transports in the cavity occur with rotating curve louver slats in the various air flow regimes (upward or downward air flow either in the closed cavity or the open cavity). Unfortunately there is a very limited data available on these behaviours. Thus these coefficients are estimated with parameter estimation technique, based on the extensive data points obtained from the experiments".*

Venetian blinds, as a shading device, may cause many difficulties also when the radiative heat exchange is predicted, especially when they are partly or fully open. This topic will be expanded in the section of optical and solar properties.

The temperature of the inlet air and the vertical temperature profile in the DSF have been noted as important factors in the double facade simulations. According to Saelens, (2002), *"the results are the most sensitive to the uncertainty of the inlet temperature"* and "*the modelling of inlet temperature is very important for the output, especially when the shading device is raised".* The non-uniform vertical temperature distribution in the cavity is important from the heat transfer point of view, as it is the main reason for the variable heat flux through the double facade. At the same time, it is a difficult issue to simulate because the vertical temperature profile is a function of the inlet temperature, transmitted solar radiation and air flow. The last two matters are complex and will be explained in the following sections.

Air flow

In some articles experiments are performed in order to develop a numerical model for the calculation of the air flow and the temperatures inside the double skin facade cavity. Saelens, (2002), mentions that, "*most researchers provide models to simulate specific multiple-skin facade typologies. Only few models for naturally ventilated multiple-skin facades are available. Most multiple-skin facade models have been developed for mechanically ventilated types*".

In the case of mechanical ventilation, the air flow rate is normally known and the air flow element is therefore straightforward. In the case of natural ventilation, there are two components that determine the air flow through the DSF. These components are the buoyancy force and the driving pressure due to wind. Both of these components can be difficult to describe as the stack effect depends entirely on the temperature and thus on the heat transfer and optical properties. In addition, the wind force is related to the highly fluctuating ambient conditions. Furthermore, the occupants' behaviour and the conditions inside the room may be essential when the DSF is also open to the inside.

According to Hensen, et al. (2002), another difficulty in DSF modelling concerns *"the difference between the microclimate near the building and the weather data, which is usually representative of a location more or less distant from the building. These differences are most pronounced in terms of temperature, wind speed and direction, the main driving potential variables for the heat and mass transfer processes in buildings!"*

Models to predict wind speed reduction between the local wind speed and the wind speed at the meteorological measurement site are quite rough (Hensen, et al., 2002) and the wind pressure coefficients for the DSF openings are difficult to determine. Moreover, the flow resistance coefficients are complex to estimate for the naturally ventilated cavities, because the velocity profiles for the naturally ventilated cavities differ from the mechanically ventilated ones. The new resistance coefficients therefore have to be obtained.

In the article Grabe, (2002), the author points out the difficulties with modelling of the flow resistances: "*There are many factors involved, but the main problem is caused by assuming the same flow conditions for natural as those used for mechanical ventilation (using values from mechanical engineering tables). These values have been developed in the past for velocity profiles as they occur in pipes: symmetric and having the highest velocity at the centre* (see Figure 2-7).

With natural ventilation, however, the driving force is the reduction of the density due to increase of air temperature. This increase is greater near the heat sources, thus near the panes and the shading device. Further on it might be non-symmetric because of different magnitudes of the heat sources. A laminar profile might look like the one shown on" Figure 2-7.

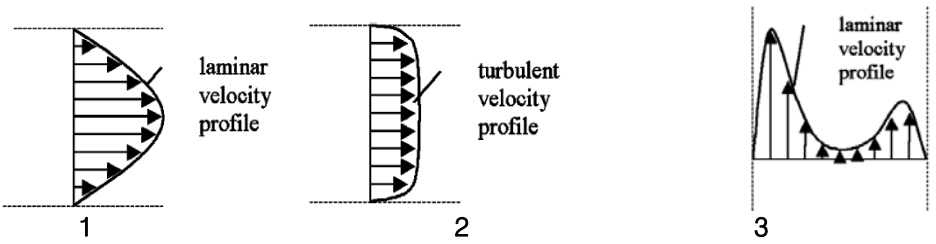

Figure 2-7. Drawing 1, 2-velocity profile for laminar and turbulent flow (pipe, mechanically ventilated). Drawing 3 - Possible laminar velocity profile for natural ventilation, (Grabe, 2002).

Hensen, et al. (2002), suggest *"to use CFD in separate studies to predict appropriate local loss factors* ξ *and friction factors for use in network methods Stringer and Janak, (2001), describe an example of such a CFD approach by predicting the aerodynamic performance of a particular double-skin facade component, at inlet grille".*

Park, et al. (2003), define challenges in prediction of performance and control of DSF systems: *"The nature of the dynamics of these systems involves complex 3D geometry where turbulent air flows and each solid and non-solid component is linked to other components by radiative and convective heat exchange",* exists *"high nonlinearity of the physical mathematical representation of the system, complicated by change of the air flow regime and thus of the mathematical representation".* In other words, the difficulties of modelling the air flow regime related not only to the type of flow, which is questionable, but also to the flow regime instability.

According to Stec and van Paassen, (2003), further research is needed for modelling of air flow in double skin facade. *"This concerns especially the following topics:*

- *The induction of the flow in the double skin facade due to the wind pressure and buoyancy effect under the real weather conditions.*
- *The air flow between the cavity and the interior of the building through the window openings in case of overpressure or underpressure is induced by a mechanical ventilation system.*
- *The influence of the construction details of double skin facade on the air flow inside"*

It is necessary to add to this list:

- The different flow regimes and the flow instability.

The statement of Stec and van Paassen, (2003), about the influence of construction details on air flow in the cavity, is also remarked by Grabe, (2002), where he defines the design parameters which have the governing role in influencing the air mass flow and temperatures in the double facade cavity space. These parameters are:

- *"The size of the upper and the lower vent of the facade;*
- *The depth of the facade and the position of the shading device in the depth of the facade gap;*
- *The material of the shading device, especially the absorption coefficient;*
- *The size of the vents of the shading device;*
- *The quality of the outer and the inner pane, especially the solar transmission factor but also the U-value and the absorption coefficient."*
-

Optical and solar properties

Very often the main difficulties related to optical and solar properties of the DSF are associated with the decision of choosing the technique for calculation. The optical properties of materials, such as transmission, reflectance and absorptance of incident solar radiation depend on:

- Wave length (spectral dependence)
- Angle of incidence
- Polarization

Knowledge is available to perform the necessary calculation of material optical properties, but the process of calculation might be time consuming, especially when the Venetian blinds are installed in the double skin cavity as stated in van Dijk and Oversloot, (2003): *"An exact description of the way solar radiation travels through the system would require a full three-dimensional calculation using the full matrix of transmission, absorption and forward and backward reflection for each angle of incidence at each component. For venetian blinds this would include the curvature of the slats and taking into account possible specularity of solar reflection at its surface".*

Manz, (2004):*"If solar radiation is not normal to the facade, it will be shielded by the frame and shading will occur on all layers, with part of the radiation being absorbed by or reflected from the frame surfaces. This results in asymmetric distribution of absorbed solar energy on the layers"* and may influence the temperature distribution in the cavity. Therefore, it is essential to be able to express the optical properties as a function of the angle of incidence and to be able to account for shadowing.

The difficulties regarding the modelling of shading devices and especially the Venetian blinds are caused by their porous structure, as listed below, following van Dijk and Oversloot, (2003). The Venetian blinds are:

- Partially transparent for solar radiation
- Partially transparent for long wave (thermal) radiation
- Have an effect of scattering when transmitting the solar radiation
- Open for the air movements between the gaps

Overall summary

The above chapter summarizes the main issues in DSF numerical modelling. It is shown that there are many particular details involved in each heat transfer element. Therefore, this work may only give an overview of the common conclusions and difficulties that are characteristic for DSF topic.

According to the reviewed literature, the DSF modelling assignment is ascertained to be very complex, but the available research results and publications are encouraging and more substantial than just a few years ago.

With regard to the future studies, following are the main aspects highlighted in the literature as important for DSF modelling:

- In general, more experimental studies are needed
- Models for prediction of naturally induced air flow require improvements
- Radiation and convection in numerical models of DSF must be at least separated
- Progress in prediction of vertical temperature gradients in DSF cavity is needed
- Predictions of flow patterns in the cavity might be helpful to resolve the question of temperature gradients in the cavity
- Reliable tools/models for estimation of convective heat transfer in cavity are needed
- Transmittance, reflectance and absorbance of glazing should be used instead of g-value. In the models, these should also be defined as a function of angle of incidence
- Models should be able to count on shadowing
- Both optical, heat transfer and air flow element require significant improvements for simulating cavities with shading devices

2.3 BUILDING SIMULATION SOFTWARE FOR DSF MODELLING

This section is based on the BBRI report by Flamant et al. (2004).

In the previous chapters, the theoretical approaches for the DSF modelling are analyzed and the difficulties associated with the modelling process are emphasized. However, attempts to model different DSF design possibilities have been made and they involve diverse building simulation software.

The age of building simulation software varies from 0 to 30 years. Software tools develop continuously, but the need for modelling of DSF constructions has appeared during recent years and has not yet reached an advanced level. The user needs a thorough knowledge of thermophysics, experience in modelling and knowledge of software abilities and limitations.

DSF modelling aspects and applicability of different building simulation software have been investigated at the Belgian Building Research Institute in December, 2004; the results are included in a report by Flamant, et al. (2004). The authors of the report recognize different options of DSF functions. They are conscious about the difficulties of modelling the ventilated DSF, especially when the air flow in a cavity is naturally driven. The issues of modelling the DSF control strategies are considered; therefore, their document comprises information on modelling of the DSF together with a whole building system. Different building simulation software has been investigated as to: the possibility to model double facade cavity, its influence on the building energy performance, possibility for the DSF control and incorporation of DSF into the building systems. The document can be helpful when the simulation tool has to be chosen. Detailed information on the modelling procedure with different software tools is provided in the report; the authors give some “tips”, which are necessary when the DSF is to be modelled, etc. The building simulation tools are described with their limitations, advantages, disadvantages and sometimes, they are rated by their user-friendliness.

The authors consider only publicly available simulation software, the ones developed by different research groups and unavailable for the majority of users are not considered. Flamant, et al. (2004) distinguish between two types of simulation software:

“Component simulation software, which are able to simulate a facade component in order to predict its thermal, energetic and visual behaviour and performances on the basis of the material properties of the component.

Building simulation software, which are able to simulate a whole building (facade included) in order to predict the thermal dynamic behaviour of the building, the indoor temperatures, the energy consumption, etc.”

The software tools described in the report are listed in the Table 2 with the classification, according to the above two definitions (Flamant, et al., 2004):

Software	Facade component	Building
WIS	X	
BISCO/TRISCO/VOLTRA	X	
CAPSOL	X	X
TRNSYS	X	X
ESP-r	X	X
TAS	X	X

Table 2-2. Simulation software considered in the report by Flamant, et al. (2004).

In order to set up the model with the correct physical processes the authors distinguish between four groups of parameters that have to be correctly represented in the model (Flamant, et al., 2004):

1. *"Outdoor climate*
2. *Model of DSF (glass and frame properties, shading device properties, air flow in DSF, etc.)*
3. *Model of building (interaction between the DSF and the building's systems)*
4. *Control strategies"*

Fulfillment of the requirements for each group would provide a user with the *"ideal"* model (the best possible to achieve), (Flamant, et al., 2004).

Regarding the outdoor climate, authors set the necessary input parameters. The exact requirements vary from program to program, but may include:

- Outdoor air temperature
- Sky temperature
- Surroundings temperature
- Wind speed
- Wind direction
- Humidity
- Incident solar radiation on a vertical surface/horizontal surface/normal to surface
- Incident solar radiation Direct+Diffuse+Reflected (by the ground)
- Spectral data of incident solar radiation
- Angle of incidence

Regarding the DSF these factors are found to be essential and necessary to model as accurate as possible (Flamant, et al., 2004):

- Heat exchange process around the shading device and the glass panes
- Air flow in the cavity due to buoyancy and wind effects

Issues of concern in the modelling of the facade element are combined in Table 2-3 by the authors (Flamant, et al., 2004):

FACADE LAYERS		*Comments*
Glass layers		
- Optical properties	Spectral? Angular dependent? Optical properties different for direct, diffuse and reflected (incident) solar radiation?	
- Thermal properties	Function of the temperature?	
Shading device		
- Type of shading device	Modelling of any type of shading device? (roller blind, Venetian blind with orientable slats, etc.) Overhang?	
- Optical properties	Spectral? Angular dependent?	
- Position of shading device in the cavity	Attached to the internal or external glass skins? Placed in center of the cavity?	
- Control	Can the shading device be controlled?	Pull down or roll up the blind according to the sunshine level, temperature, etc.
Frame		
- Modelling	Possible?	
- Thermal properties	Can ventilation air pass through the frame? Thermal properties function of the air flow rate passing through the frame? Possibility to set an inlet temperature (air entering the ventilated cavity) different to the exterior or interior temperature?	For certain applications, it is important that the frame of the ventilated double facade can be modelled. The heat transmission through the frame can represent a non-negligible part of the total heat transmission losses through the complete facade. Air entering the ventilated cavity can be heated and cooled down due to contact with the bounding surfaces and heating due to solar radiation. The inlet temperature in the cavity influences both the transmission losses and the enthalpy change of the air flowing through the cavity.
Cavity subdivision		
- Vertical	Vertical subdivision?	The number of zones into which the facade must be divided is not straightforward. This vertical subdivision is needed to take into account the temperature profile in the cavity.
- Horizontal	Horizontal subdivision?	Fictive vertical walls can be simulated? (in some programs it is needed to model fictive vertical walls to represent the shading device rolled up)

HEAT TRANSFER		
Convective heat transfer in the cavity		
- Forced convection	Convective heat transfer coefficient: - must it be given (fixed value?) Possibility to modify the value of the coefficient during the simulation (in function of some inputs)? - is calculated from some parameters? (flow regime, air flow rate, temperature difference, etc.)	
- Natural convection	Possibility to model natural ventilation in the cavity? (naturally ventilated facades)	See also "Air flow modelling" (see below)
Radiative heat transfer		
- In the cavity	Radiation and convection treated separately? Radiation heat transfer coefficient is a function of the temperature?	
- Exterior radiation heat transfer	Calculated from sky temperature and environment temperature?	
- View factor	Correct determination of the view factor between facing panes?	
Short wave radiation		
- All panes	Inter-reflections between the glass panes and the shading device?	
- Venetian blind	Inter-reflections between the slats of the Venetian blind?	
AIR FLOW MODELLING		
- Coupling air flow modelling and thermal modelling	- Combination of a thermal and an air flow network in the same software? - Possibility to combine the software to air flow models? (other software)	
- Natural ventilation	Buoyancy effect? (stack effect) Wind effect? Air flow between the cavity and the interior of the building through the window openings?	
- Coupling facade and building	Possibility to connect the facade model with the building and its installations	

Table 2-3. Simulation of the facade component (Flamant, et al., 2004).

The concern about the lack of simulation programs that are able to model shading devices such as Venetian blinds or louvers is expressed in the report (Flamant, et al., 2004), as these are the most used shading devices in practice. Only some software tools (i.e. WIS) are able to perform the intricate modelling of the porous structure of these devices. The detailed explanation on the complexity of modelling the Venetian blinds is given in the section 1.3.3.

The other difficulty in modelling of the DSF component has also been discussed in section 1.3.3. Some of the software tools in Table 2 consider only mechanically induced flow in the cavity (Both TRNSYS and ESP-r, and possibly TAS, can model buoyancy-driven flow). As has been argued before, the convective heat transfer processes in mechanically and naturally ventilated spaces differ; therefore, the expressions for the convective heat transfer with the mechanical driving force cannot be applied when the flow is naturally driven. The flow regime in the cavity may vary with the change of thermal conditions and flow rate. Consequently, the simulation software must be able to change the value of the convective heat transmission coefficient dynamically, depending on the flow regime.

There are two functions distinguished in the building simulation software:

- Thermal function - calculates the thermal properties of the model
- Air flow function - calculates the mass flow in the modelled domain

Some software tools may incorporate only one of these functions, although they can be coupled with another software tool to calculate the air flows and temperatures together. The programs that incorporate both of the functions can have different ways for coupling of the air flow and thermal functions. In the report (Flamant, et al., 2004) these are classified as depicted in Figure 2-8:

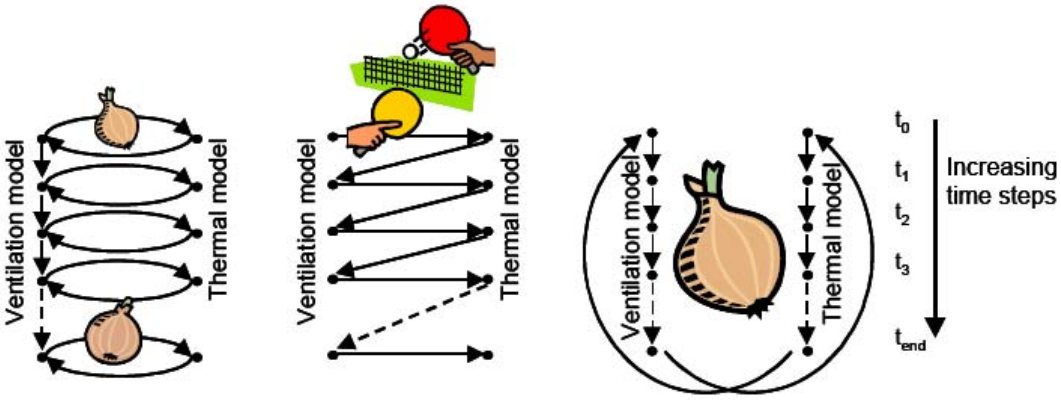

Figure 2-8. Onions, ping-pong and global onion approaches (Flamant, et al., 2004).

"The full integration approach: both ventilation model equations and thermal model equations are solved simultaneously, by incorporating both sets of equations into a single equation (e.g. ESP-r).
The onions approach: air flow rates are passed from the ventilation model to the thermal model, which calculates new air temperatures and pass them to the ventilation model, which calculates new air flow rates until convergence is reached. The procedure is then repeated for the next time step.
The ping-pong approach: air flow rates calculated in the ventilation model at time t are used as input by the thermal model to calculate new temperatures at time t. These temperatures are then used by the ventilation model to calculate new air flow rates at time t+1. This approach has as main disadvantage that it can generate substantial errors and should be used with care.

The global onion approach: the thermal model is run for the whole period. The resulting temperatures are introduced to the ventilation model, which calculates ventilation rates for the all period. These air flow rates are introduced in the thermal model to calculate new temperatures, and

so on… up to convergence of both models. This method presents a major limitation: it is not possible to implement a ventilation control strategy that is not fixed in advance"…

The simulation software assessed in the paper has been listed before in Table 2-2. A short description of the main features of different software tools is given in the following Table 2-4, which is organized with information provided in the BBRI report (Flamant, et al., 2004).

Software tool	Main characteristics for DSF modelling
WIS is developed to calculate thermal and solar characteristics of window systems	- One of the unique elements in the software tool is the combination of glazing and shading devices, with the option of free or forced circulation between both. This makes the tool particular suited to calculate the thermal and solar performance of complex windows and active facades - The shading device is considered as a scattering layer of different categories. Calculations are performed with different approaches, depending on the category (type) of shading device - WIS performs calculation of the transfer of the short wave radiation for all angles of incidence, but is unable to perform dynamic calculations - It is possible to model natural convection, caused by stack effect (wind induced convection is not covered by WIS)
BISCO/TRISCO/VOLTRA is aimed to model heat transfer of building details, able to calculate the thermal bridging effect between the components (only VOLTRA is described in the BBRI report)	- The unique feature of this software group is the potential to perform thermal calculations in combination with thermal bridging effect with the components - The solar glazing characteristics must be calculated in advance with the help of WIS software - Convective heat transfer coefficients cannot vary during a simulation - It is possible to model forced ventilation of DSF, but not the natural ventilation
CAPSOL calculates multi-zone transient heat transfer	- The characteristics of shading device have to be calculated with another software (i.e. WIS) and then it can be introduced to the CAPSOL. Solar transmission is angular-dependent, but the calculation for transmitted radiation through the cavity with the shading device may be more accurate when obtained by WIS software (WIS simulates shading device as a scattering layer). - It is possible to set up a model, where the vertical thermal stratification could be taken into account. Mechanical ventilation can be modelled as one of the control options, while natural ventilation requires coupling CAPSOL with the ventilation model. Convective heat transfer is constant during the simulation - CAPSOL is a user-friendly tool

Software tool	Main characteristics for DSF modelling
TRNSYS is developed to simulate dynamic thermal behaviour of buildings and systems	- A user can easily generate a TRNSYS model that does not exist in the standard package - When simulating thermal behaviour of a building, TRNSYS can manage air flows, but does not calculate them. In order to do that TRNSYS must be coupled with COMIS, which has been completely integrated into TRANSYS - The window model in TRNSYS uses output data from the WINDOW 5 software tool where each glazing absorbs and reflects a part of incoming solar radiation, depending on the glazing material and the incident angle - The convective heat transfer coefficient is not necessarily constant, it varies according to flow regime in the cavity - There is no detailed model for Venetian blinds that would take into account inter-reflections between the slat
ESP-r is modelling the energy and fluid flows within combined building and plant systems	- The important aspect of this tool is its ability to perform modelling in different levels of resolution (one or more zones in the building can be associated with the 3D CFD domain) - In the thermal, air flow and lightning domains all heat and mass transfer processes are solved simultaneously at each time step of simulation - It is possible to control which correlations are used for the convective heat transfer in the cavity. - Optical properties for glazing systems can be calculated with the help of WIS software - Prior to simulation, the insolation distribution is advised to be calculated via ESP-r solar tracking facility - The view factors can be calculated based on area weighting or according to the analytical solution (simple case) or by ray tracing approach - Modelling of Venetian blinds is complex
TAS is capable of thermal performance of buildings and their systems	- TAS software incorporates a module, which is capable to perform dynamic building simulation with integrated forced and natural flow, arising from wind and stack effects. - The internal convection heat transfer coefficient may vary from hour to hour - Transmission and absorption characteristics of transparent constructions depend on the angle of incidence - There is no principal difference in modelling of roller and Venetian blinds, inter-reflections between Venetian blind slats are not considered - Simplified method is used to calculate radiant heat exchange

Table 2-4. Characteristics for the DSF modelling with different software tools.

Flamant, et al. (2004) examine the simulation tools, with the particular goal of modelling the DSF. In the report, guidance and examples are given for the procedure of setting up the model. The sensitivity of the tool to some particular parameters is notified. The original paper has to be found if more information is needed on the details of modelling.

In the BBRI report (Flamant, et al., 2004) the authors have analyzed six kinds of simulation software, and according to them: *"The software TRNSYS, ESP-r and TAS are powerful transient energy simulation programs and are able to simulate a ventilated double facade, the building, the HVAC systems and strategies in a certain extent. These programs can make the coupling between thermal and air flow models. Nevertheless, all these programs face similar obstacles regarding the level of resolution necessary to model some major thermodynamic flow paths in ventilated double facades. Time and experience are required in order to use properly these quite complex software. The software CAPSOL shows less functionalities than the three previous ones but this software can be recommended for specific points of interest due to its facility of use.*

The software WIS combines a user-friendly interface with the most advanced calculations of thermal and solar properties of window and facades. The WIS algorithms are based on international (CEN, ISO) standards, but WIS also contains advanced calculation routines for components or conditions where current standards do not apply… Finally, BISCO, TRISCO and VOLTRA belong to a series of software aimed at modelling the heat transfer of building details using the energy balance technique. These programs are well adapted to calculate the interaction between the glass skins and the shading layer in combination with the thermal bridging effect of the subcomponents around the VDF (ventilated double facade) …"

This paper (Flamant, et al., 2004) does not give any recommendation of which is the most suitable tool for DSF modelling, as it depends only on the objectives for setting up the model and user's experience to work with the simulation tools.

HYPOTHESIS

Hypothesis of recirculation flow occurrence in double-skin facade cavity is developed and explained in Chapter 6. However, references to this phenomenon will be made during analysis and discussion of experimental results. Here is a short explanation to recirculation flow phenomenon is made to prepare reader for the discussions.

According to this hypothesis, recirculation flow in DSF cavity appears when the surface temperatures are high compared to fluid temperature. Then the strength of boundary layer is growing with increasing distance from the entrance plane. At some point, the mass flow rate in the boundary layer will exceed the mass flow rate of incoming air into the DSF cavity. This will cause a flow recirculation in the upper levels, as air to this plane will be drawn from the zones above to feed the development of boundary layer.

Chapter 3

FULL-SCALE EXPERIMENTS

This chapter gives a short description of outdoor test facility 'The Cube' together with an outline of the experimental set-up and experiments carried out in the fall 2006.

Attention is paid to methods for measurement of air flow in the test facility with a naturally ventilated double skin facade. These methods are described in detail and discussed. In the first method, the air flow in the cavity is estimated on the basis of six measured velocity profiles in the cavity. The second method is represented by constant injection of tracer gas.

In the end of the chapter, there is an overview of measurement accuracy and a discussion of possible errors in the experimental methods and experimental results.

3.1 AN OUTDOOR TEST FACILITY 'THE CUBE'

'The Cube' is an outdoor test facility located at the main campus of Aalborg University. It has been built in the fall of 2005 with following purposes, in the frame of IEA ECBCS ANNEX 43/SHC Task 34, Subtask E- Double Skin Facade:

- detailed investigations of DSF performance
- development of empirical test cases for validation
- further improvements of various building simulation software for modelling of buildings with double skin facades

Figure 3-1. '*The Cube*'.

The test facility (Figure 3-1) is designed to be flexible for a choice of the DSF operational modes, natural or mechanical flow conditions, different types of shading devices etc. Moreover, the superior control of the thermal conditions in the room adjacent to the DSF and the opening control allow to investigate the DSF both as a part of a complete ventilation system and as a separate element of building construction.

The air tightness of 'The Cube' was measured during construction, insulation and air tightening of the test facility, before and after installation of experimental set-up to ensure the tightness. The final infiltration rate was 0.3 h^{-1} at 100 Pa of underpressure. Transmission heat losses were estimated for two set points, when the difference between the air temperature in the test room and outdoors was 16 °C and 21 °C resulting in a heat loss of 0.26 W/(m^2 C). These tests have confirmed that 'The Cube' is extremely tight and well insulated.

'The Cube' consists of four domains, which are named as: Double Skin Facade, Experiment room, Instrument room and Engine room (Figure 3-2).

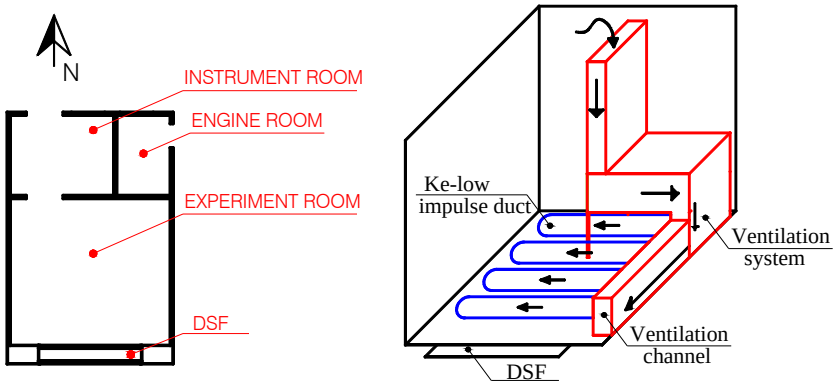

Figure 3-2. Plan of 'The Cube' (left), schema of the ventilation system in experiment room (right).

The temperature in experiment room can be kept constant, as there is a cooling unit installed in engine room and a ventilation system with a heating and cooling unit installed in experiment room (Figure 3-3). In order to avoid temperature gradients in experiment room, a recirculating piston flow with an air speed of approximately 0.2 m/s is used. This resulted in typical temperature gradient of approximately 0.02 °C/m and maximum of 0.1 °C/m. The air intake for recirculation is at the top of the room, after the intake the air passes through the preconditioning units of the ventilation system and then it is expelled at the bottom of the room through the fabric ke-low impulse ducts. Maximum power on cooling and heating unit is 10 kW and 2 kW respectively.

Figure 3-3. KE-low impulse fabric ducts in experiment room (left, centre), Ventilation system in experiment room (right).

There is approximately 40 cm layer of Rockwool insulation in the each wall. Detailed information about the construction and insulation of the test facility can be found in Kalyanova and Heiselberg (2007b). The internal dimensions of experiment room and DSF are given in Table 3-1

.

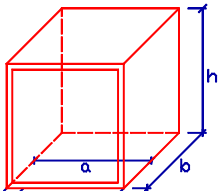

Room	a, mm	b, mm	h, mm	Volume*, m^3
DSF	3555	580	5450	11.24*
Experiment room	5168	4959	5584	143.11*

*Volume of Zone 1 and Zone 2 is calculated to the glass surfaces of the windows and NOT to the window frame or the walls

Table 3-1.Internal dimensions of 'The Cube'.

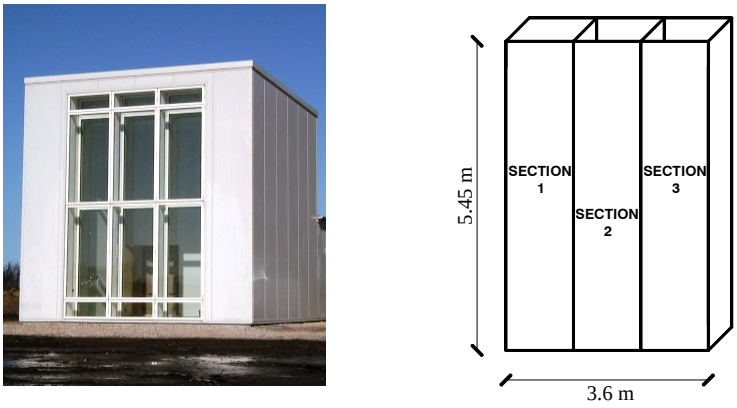

Figure 3-4. Definition of sections in DSF.

Window partitions of the double skin facade visually subdivide the DSF into three sections. The definition of the sections is given in figure and will be used in further discussions (Figure 3-4). Analogous to the definition of sections, there is a definition made for the windows in Figure 3-5.

For example:
*SOH3 – **S**mall **O**uter window, located **H**igher than the middle plane in the DSF section **3**.*
*BIL2 – Large (**B**ig) **I**nner window, located **L**ower than the middle plane in the DSF section **2**.*

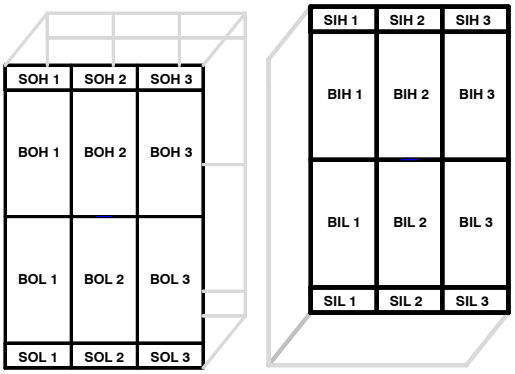

Transcription:

1st letter stands for	"B" – big "S" – small
2nd letter stands for	"O" – outside "I" – inside
3rd letter stands for	"H" –high "L" – low
Number stands for	"1,2,3"– number of DSF section

Figure 3-5. Definition of DSF windows.

Knowledge of solar radiation is crucial for the task of these experiments. However, in non-laboratory conditions the ground reflected solar radiation depends on the surrounding of the test facility and therefore it can vary a lot. For this reason, a large carpet was fixed on the ground from the side of the southern facade of 'The Cube' to achieve uniform reflection from the ground. The size of the carpet ensures a view factor between the DSF and the ground of approximately 0.5. Achieving a reasonably higher view factor would require to double-up the carpet size.

The fabric of the carpet was chosen so that it does not change reflectance property when it is wet due to its permeability and have reflectance property of approximately 0.1, close to the generally assumed reflectance property of the ground.

Absorption, reflection and transmission properties of all the surfaces in the DSF, experiment room and windows were tested at the EMPA Materials Science & Technology Laboratory. This was also the case for the ground carpet.

3.2 BOUNDARY CONDITIONS

3.2.1 WIND SPEED

Wind velocity and wind direction was measured in six points above the ground in order to build a vertical wind velocity profile. Both 2D and 3D ultrasonic anemometers were placed on the mast in the centre line of the building, 12m away from its Southern facade (Figure 3-6). The measurement frequency was 5 Hz.

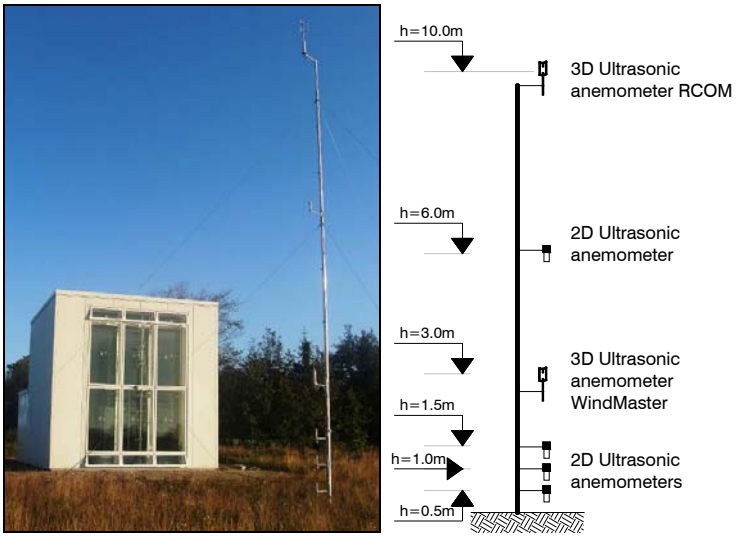

Figure 3-6. Wind profile mast (left). Positioning of equipment on the mast (right).

3.2.2 OUTDOOR AIR TEMPERATURE AND HUMIDITY

Outdoor air humidity was measured every 10 minutes, using portable COMARK data logger N2003 from Comark Instruments Inc (Figure 3-7).

Outdoor air temperature was measured using two thermocouples type K, the height of 2 m above ground. Both of the thermocouples were silver coated and the measurement took place every 60 seconds.

Figure 3-7. COMARK data logger N2003.

3.2.3 SOLAR RADIATION

For purpose of weather data assembling two pyranometers were placed horizontally on the roof of 'The Cube' (Figure 3-8). BF3 pyranometer measured global and diffuse solar irradiation on the horizontal surface. Another pyranometer, Wilhelm Lambrecht, measured only Global solar irradiation on the horizontal surface and was placed on the roof for control of BF3-readings.

Solar radiation received on the vertical surface of DSF was measured with Wilhelm Lambrecht-pyranometer. Readings from both of the devices were taken every 60 seconds.

Figure 3-8. Pyranometers on the roof of 'The Cube', Wilhelm Lambrecht pyranometer at the left and BF3 at the right.

3.2.4 MEASUREMENTS

Experiments were carried out for three modes of DSF operation these are (Figure 3-9):

- MODE 1: external air curtain mode
- MODE 2: transparent insulation mode
- MODE 3: preheating mode

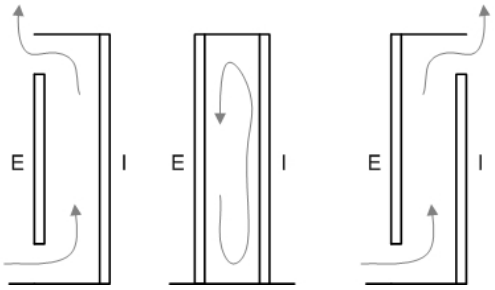

Figure 3-9. DSF operation modes during the experiments. MODE 1 (left), MODE 2 (centre), MODE 3(right).

Duration of experiments was approximately 14 days for each mode:

MODE 1	01.10.2006 – 15.10.2006
MODE 2	19.10.2006 – 06.11.2006
MODE 3	09.11.2006 – 01.12.2006

Information about the experiments is given in the next sections. It is divided into the groups, according to the matter that was measured, as following:

- Temperature
- Air flow rate in DSF
- Velocity profile in DSF
- Power supply in experiment room

3.2.4.1 Temperature

Temperature was measured with silver coated thermocouples type K. Depending on location of the sensor, temperature was registered with two frequencies: every 0.2 second and every 60 seconds. High frequencies were used for the measurement of air temperature in DSF cavity and outlet air temperatures only.

The air temperature was measured in engine room, instrument room, DSF and experiment room. Also, the ground temperature, underneath of foundation in experiment room was measured.

The air temperature in experiment room was mainly measured with bare silver coated thermocouples, which were placed at different heights in four locations in the room. Thermocouples in DSF cavity were protected from an influence of direct solar radiation by silver coated and ventilated tube, air flow through the tube was ensured by a minifan. Thermocouples were and placed in each DSF section in several heights.

Surface temperature of walls was also measured in experiment room and DSF: thermocouples were glued to surfaces with a paste of high heat transmission property.

Measurement of glazing surface temperature was performed in the centre of glazing pane for each large window section (BOL, BIL, BOH and BIH windows). The temperature was measured of:

- internal surface of inner window pane (ii)
- external surface of inner window pane (ei)
- internal surface of outer window pane (ie)

These measurements were conducted with sensors shaded from direct solar access (Figure 3-10). Continuous shading of the thermocouple sensor at the inner pain was ensured by a thin aluminium foil fixed around sensor at the external surface. As a result, the foil shaded both a sensor at the external and internal surfaces. The thermocouple at the internal surface of the outer pane was shaded in a similar way by a piece of aluminium sticky tape on the external surface of the outer pane.

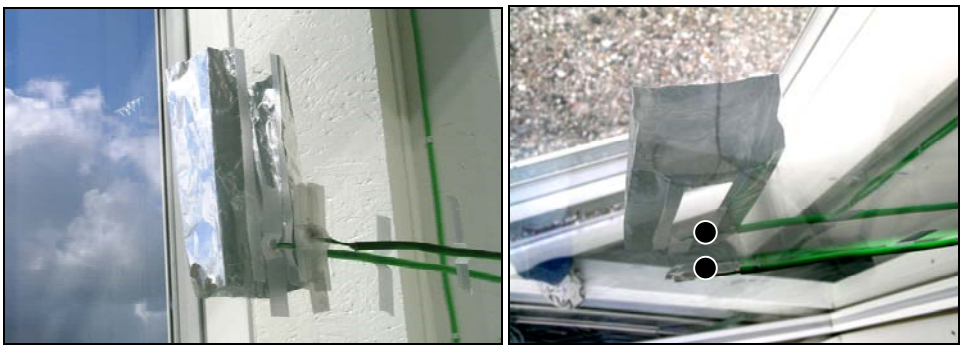

Figure 3-10. Glass surface temperature measurements. Thermocouples are shielded by silver foil.

3.2.4.2 Air flow

In the literature, there are a few methods used for estimation of the air change rate in a naturally ventilated space. The most used are the tracer gas method, method of calculating the air flow from the measured velocity profiles in an opening or calculated from the expressions for the natural ventilation or scale modelling, see (Larsen, 2006; Hitchin & Wilson, 1967; Etheridge and Sandberg, 1996), which involves measurements of air temperature, wind speed, wind direction, wind pressure coefficients on the surfaces and pressure drop across the opening.

Experimental investigation of the air flow rate requires measurement of many highly fluctuating parameters. The fluctuation frequency implies the high sampling frequency for the measurements. For example according to Larsen (2006), the wind speed has to be measured at least at the frequency of 5 Hz, otherwise peaks in the wind velocity can be lost when averaged in time. As a consequence, measurements of the air flow rate are limited to time and costs. When measured with the tracer gas method the limitations are extended to the air flow rates, as with the high air flow rate the amount of injected tracer gas will be enormous. Because of these, the investigation of the natural air flow often is carried out in the controlled environment of the wind tunnel or scale models.

This section addresses experimental set-up for measurements of the air flow rate in the DSF cavity of 'The Cube'. There were three techniques used for the air flow measurements, these are:

- Velocity profile method
- Tracer gas method
- Pressure difference method

Results from the pressure difference method are not included into this report, therefore for more information about this method see (Kalyanova and Heiselberg, 2007b; Kalyanova et al., 2007b).

Velocity profile method
This method requires a set of anemometers to measure a velocity profile in the opening, and then the shape of the determined velocity profile depends on amount of anemometers installed. At the same time, the equipment located directly in the opening can become an obstruction for the flow appearance. Thus, the method becomes a trade off between the maximum desired amount of anemometers and the minimum desired flow obstruction. Instead of placing equipment directly in the opening in the case of the double skin facade, it can be placed in the DSF cavity, where the velocity profile can be measured in a few levels instead for one.

For the double skin facade, the negative aspect of this method is explained by air flow variation, as the instantaneous air velocity in the cavity may vary from 0 to 5 m/s. This velocity range is challenging, as the equipment must be suitable for measurements of both low and higher velocities, moreover, it is necessary to be able to detect the recirculation flow appearance and follow the flow fluctuations. As explained earlier by Jensen et al. (2007), the hot-sphere anemometers have proved to be suitable for the task. These were also tested for uncertainties when measure under the direct solar radiation (section 3.3)

Tracer gas method
The measurements were completed with the constant injection method. In this method, the tracer gas is injected at a constant rate and then the concentration response is recorded (Etheridge and Sandberg, 1996). According to McWilliams (2002) the constant

injection method is more appropriate for leaky spaces where the gas would be quickly ventilated from the space, thus it is suitable for DSF. However, according to Etheridge and Sandberg (1996) and McWilliams (2002) this method is not appropriate for highly unsteady ventilation rates i.e. in a naturally ventilated DSF cavity. Thus the measurement accuracy may suffer.

Experimental set-up for air flow measurements

The velocity profile method

During experiments in 'The Cube' all of the velocity measurements were conducted in the section 2 (Figure 3-4), the velocity profiles were measured in 3-6 levels, with the various number of anemometers in different levels. Different amount of levels was used for different DSF operational modes. Levels are numbered with the Roman numbers in the Figure 3-11. All in all 46 of hot-sphere anemometers were installed in the experimental set-up (Figure 3-11), 34 of them were involved in the measurements of the velocity profiles in different levels of the DSF cavity. The measurement frequency of the hot-sphere anemometers was 10 Hz.

The tracer gas method

Carbon dioxide (CO_2) is the tracer gas used during the whole period of experiments. Carbon dioxide was released in the lower part of the double skin facade cavity, but above SOL- and SIL-openings. Even distribution of the tracer gas along DSF cavity was ensured by its injection through a perforated tube of internal diameter 3.5 mm, perforation distance 4 mm and 0.5 mm diameter of perforations. Samples of the tracer gas dilution were taken in 12 points Figure 3-12 (4 samples per section) at the top of the DSF cavity, but below SOH- openings. All samples were blended together in collector and then the concentration of the diluted tracer gas was measured by a gas analyzer BINOS.

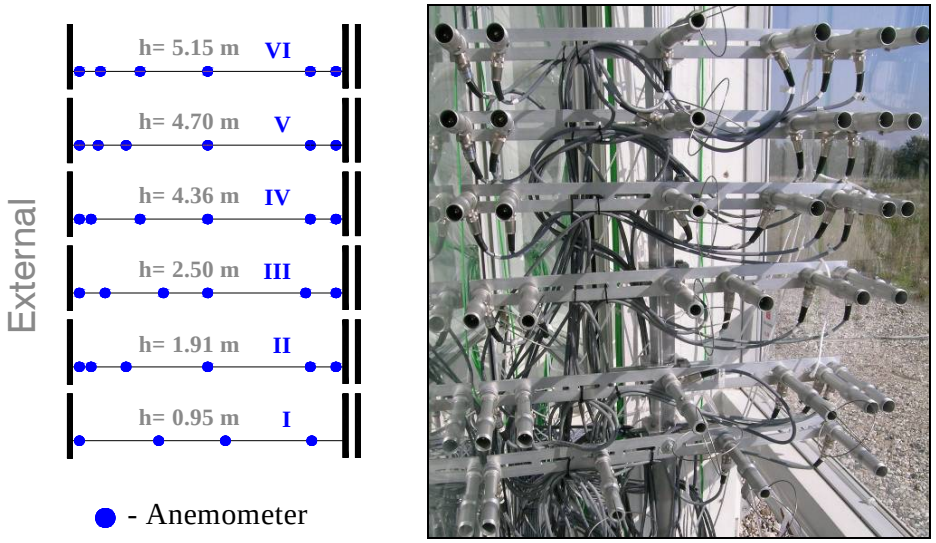

Figure 3-11. Positioning of anemometers in the DSF cavity (left). Anemometers in the DSF cavity before they were moved up to their heights (right).

Concentration of carbon dioxide in the outdoor (incoming) air was measured continuously, by a gas analyzer URAS. The Helios data logger collected the measurement data from the gas analyzers with the frequency 0.1 Hz. The constant injection method was used during the experiments and quantity of released tracer gas was kept constant (3-5 l/min).

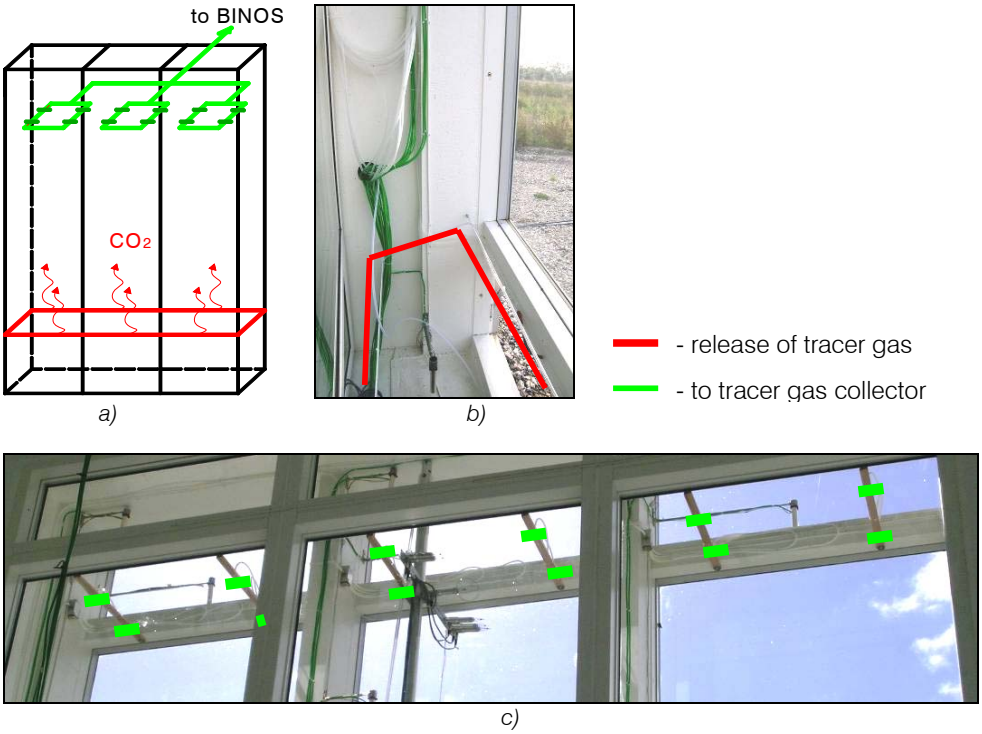

Figure 3-12. a) Experimental set-up for the tracer gas method. b) Positioning of the perforated tube for the release of the tracer gas at the bottom of DSF cavity. c) Positioning of the air intakes for samples of tracer gas polluted air, at the top of DSF cavity.

3.2.4.3 Power supply in experiment room

One of the main targets of this experimental work was to accurately estimate solar gains to the room adjacent to the double skin facade. Solar gains to the adjacent room can be used as a measure of DSF performance. Accuracy of these measurements is assured by constant air temperature in experiment room. There was no regulation of window openings used and no shading devices installed, building is very well insulated and air tight. The air tightness of the building and the transmission heat losses are known, in addition to it all boundary conditions were measured.

Cooling load

Water was used in the cooling unit of the ventilation system. With the purpose to avoid condensation on the surface of the cooling unit the minimum water temperature was set to 12 °C, this resulted in a large area of cooling surface and size of whole system.

A difference between supply and return water temperature from the cooling unit and the mass flow rate of water were measured and collected by Helios data logger at a frequency 0.1 Hz.

Heating load

The heating unit in the ventilation system was rarely activated, as in the most of cases an additional heating load was created by a fan of running ventilation system in experiment room ensured an additional load. Moreover, some equipment had to be installed in experiment room and resulted in additional loads. For keeping a track of all loads to experiment room, including the heating unit, all equipment in the room was connected to a wattmeter D5255S from producer Norma. Readings from the wattmeter were assembled at a frequency 0.1 Hz by a data logger Helios.

3.3 MEASUREMENT ACCURACY

The experimental work described in this chapter consists of measurements conducted for a number of parameters. The results of this work will be used in the empirical validation of building simulation software and therefore the measurement accuracy is crucial for further application of the results.

Real measurements can never be made under perfect conditions, therefore uncertainties and errors will always be present. Talking about the accuracy of the experimental results one should always distinguish between:

- accuracy of measuring instruments
- accuracy of experimental methods
- errors in the data processing
- errors in the experimental set-up and measurement conditions and procedures
- uncertainty in reporting characteristics and properties of test facility

Uncertainties in reporting properties of constructions in the experimental set-up become a problem for empirical validation, as difficulty of undertaking experiments and specifying an appropriate model may lead to large uncertainties when model predictions are compared with measured data (Strachan, 1993).

Here only the uncertainties related to the experimental methods are discussed and also the accuracy of the instruments is reported. Presence of errors in the experimental set-up is possible, however all known to author limitations and errors regarding the experimental set-up and test facility are mentioned in this or in the following chapters, even more detailed information can be found in the report by Kalyanova and Heiselberg (2007b).

3.3.1 ACCURACY OF INSTRUMENTS

Prior to the measurements the accuracy of all measurement equipment was checked. All of the instruments and sensors were calibrated for the suitable measurement conditions to reduce measurement uncertainty.

Temperature

Thermocouples type K (Chromel/Alumel) with the junction of approximately 2.5 mm in the diameter were used in the experimental set-up. Thermocouples were calibrated in four points: 10, 20 35 and 55 ^{o}C. Accordingly, the maximum error for the temperature measurements in the interval between 10 and 55 ^{o}C was ±0.07 ^{o}C and ±0.14 ^{o}C correspondingly for HELIOS and HBM data logger.

Solar radiation

Primary to the installation all of the pyranometers were calibrated in reference with CM21, which is calibrated in sun simulator and corrected by Kipp&Zonen B.V.

In the table below, the maximum errors prior to calibration are given. The errors are high, but these appeared to happen for the low angles of incidence.

Equipment	*Max error:*
BF3 (total)	6%
BF3(diffuse)	10%
Wilhelm Lambercht (horizontal)	3%
Wilhelm Lambercht (vertical)	5%
CM11	0.01%

Table 3-2. Maximal error of pyranometers in the experimental set-up before the calibration.

Wind speed and wind direction

The 3D ultrasonic anemometers were RCOM Research R3, type 1210+1189 PCA and WindMaster, type 1086M from Gill producer and had range from 0 to 30 m/s and from 0 to 50 m/s correspondingly. Both of 3D anemometers had an accuracy ±1 % of velocity reading and ±3° for the wind direction.

The 2D anemometers were from FT Technologies Ltd., type FT702 of range from 0 to 30 m/s. Their accuracy was ±4 % of reading for the velocity measurement and ±3° for the wind direction, prior to calibration.

Cooling/Heating load in experiment room

Water was used in the cooling unit of the ventilation system. The difference between the supply and return water temperature from the cooling unit in experiment room was measured using one thermocouple type K with a maximum uncertainty of 0.1 °C. The mass flow of the water supplied to the cooling unit was measured with a water flow meter MULTICAL from Kamstrup, which measures in a range from 0 to 1 kg/s and calibrated to an uncertainty of ±0.1 % of the reading.

To keep a track of all loads to experiment room, including the heating unit, all equipment in the room was connected to a wattmeter. The accuracy of the device was 0.1 % of the reading (2.6 kW).

Hot sphere anemometers

All in all, 46 hot-sphere anemometers were used for the measurements. The anemometers were from IFS system from Dantec. All of anemometers were calibrated in a wind tunnel for the upwards flow direction in the range 0-5m/s and had an accuracy of ±0.05 m/s.

Tracer gas measurement

Concentration of Carbon Dioxide (CO_2) tracer gas was measured by a gas analyzer BINOS and URAS. Concentration of carbon dioxide in the outdoor (incoming) air was measured continuously, by a gas analyzer URAS. Both of the devices were preliminary calibrated and had an accuracy of 10 ppm.

During the experiments the gas analyzers were located in experiment room in order to avoid any kind of the ambient temperature variations which are harmful for the measurement accuracy.

3.3.2 MEASUREMENT METHODS

In the experimental studies, there are four experimental methods deserving special attention for uncertainty considerations. These are:

- Measurement of air temperature under direct solar radiation
- Measurement of air velocity with the hot sphere anemometers under direct solar radiation
- Tracer gas method with constant injection of CO_2 for assessment of the air change rate in the DSF cavity
- Velocity profile method for assessment of the air change rate in the DSF cavity

All described measurement methods have sources of error and compared to laboratory conditions have relatively large uncertainties. Although all these measurement methods are difficult to use under such dynamic air flow conditions, their results show reasonable agreement and can be used for experimental validation of numerical models of natural ventilation air flow.

Measurements of air temperature under direct solar radiation

The presence of direct solar radiation is an essential element for the facade operation, but it can heavily affect measurements of air temperature and may lead to errors of high magnitude using bare thermocouples and even adopting shielding devices. An accurate air temperature measurement is crucial for prediction, evaluation and control of the dynamic performance of the facade, as a significant part of the complete ventilation system (Kalyanova, et al. 2007a).

Various techniques to shield thermocouples from direct irradiance were tested preliminary to the experiments, in order to achieve an accurate and reliable way to measure the air temperature reducing the error caused by solar radiation. It was found that silver coated thermocouples shielded with a silver coated tube and ventilated by a fan can provide reliable measurements of the air temperature under direct exposure to solar radiation. This technique was then used in the experimental set-up. For more information see Kalyanova et al. (2007a)

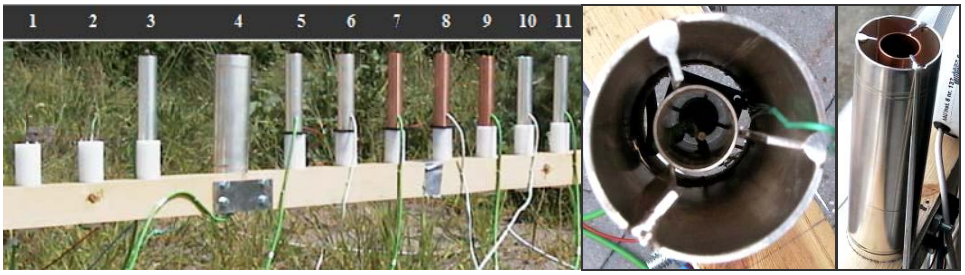

a) b) c)

Figure 3-13.a) Experimental set-up for testing techniques for measurement of air temperature under solar exposure. b) Thermocouple coated with silver and shielded with two silver coated tubes (photo from above). c) Visualization of double shielding, Kalyanova et al. (2007a).

It is not possible to estimate the accuracy of this method, as there is no reference to a true air temperature under the solar exposure exists.

Measurements of air velocity under direct solar radiation

Temperature compensation is the working principle of the hot-sphere anemometer. It is designed with two spheres: the heated and unheated one. The unheated, so called 'cold' sphere measures the temperature of the flow, while the heated 'hot' sphere measures convection at the surface of the heated sensor. The air speed is determined as a result of compensation between readings from the 'cold' and 'hot' sphere. Accordingly, an accurate measurement of the air temperature with the 'cold' sphere is crucial for the acceptable temperature compensation and thus for the reliable measurement of the air speed.

The hot-sphere anemometer are exposed to sun when measuring in the double facade cavity, the 'cold' and 'hot' spheres heated by solar radiation and, as a result, the sensor's ability to compensate for temperature become doubtful. The following experiments were performed in order to evaluate influence of solar radiation on performance of hot-sphere anemometer measuring the upward and downward flow (Jensen et al., 2007).
The experiments took place in the isothermal conditions in the laboratory. A hot-sphere anemometer was located in the jet wind tunnel, effect of solar radiation was imitated by a strong lamp, producing 800 W/m^2 of radiative heat flux). These test confirmed that the hot-spheres are not sensitive to solar radiation.

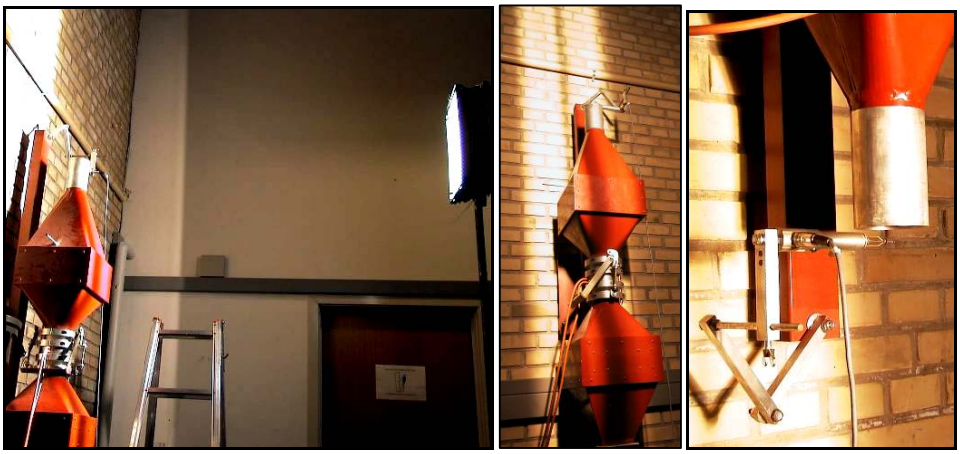

Figure 3-14. Hot-sphere anemometer in the jet-wind tunnel lit with the lamp imitating solar radiation (Jensen et al., 2007).

Tracer gas method with constant injection of CO_2

This method requires the minimum amount of measurements and equipment, but it is characterized with frequent difficulties to obtain uniform concentration of the tracer gas, disturbances from the wind wash-out effects and finally with the time delay of signal caused by the time constant of gas analyzer (Kalyanova et al., 2007b).

According to McWilliams J. (2002) the tracer gas theory assumes that tracer gas concentration is constant throughout the measured zone. For the tracer gas method an error in determined air flow is expected in the range of 5-10 %, what greatly depends on the tracer gas mixing with air in the DSF cavity.

In the tracer gas method, the main errors can appear when the tracer gas is not well mixed with the entrance air, in case of wind wash-out effects, reversed flow and/or the recirculation flow appearance. With wind washout or flow reversal the tracer gas is removed from the DSF cavity and, finally, some measurement points can be characterized with the air flow rate approximating the infinity.

Wind washout effect is explained as an additional flow pattern that occurs in DSF cavity and takes place in horizontal plane. The main cause for its appearance is found in differences of wind pressure generated on the same surface. As a consequence, DSF openings on the same plane and on same height will have different wind pressure coefficients and the wind washout will take place.

Comparing the characteristics of the errors, it is necessary to note that the appearance of reverse flow is periodical (week buoyant forces, $c_p^{top} > c_p^{bot}$) and these periods are relatively easy to point out. Wind wash-out effect is the same phenomena as the reverse flow, but its occurrence is more random and originated from the highly fluctuating wind nature.

Looking upon the bad mixing, it should be mentioned that it is not possible to evaluate the impact of this error, although a lot of effort was made during the experimental work to avoid it. In the experimental set-up the tracer gas was injected into the DSF cavity through a perforated tube. The flow regime in the DSF cavity was turbulent and highly fluctuating, therefore good mixing of air and tracer gas was expected. Though, the measurement procedure was periodically disturbed by the wind washouts or flow reversal, causing removal of tracer gas from the cavity.

Velocity profile method

The velocity profiles were measured only in the central section 2 in the cavity. Accordingly, one of the significant limitations in this method is the assumption of equal flow conditions in all three section of DSF cavity, which is not necessarily true in practice.

This method is also sensitive to the number of velocity sensors and their location in the plane, as poor approximation in the velocity profile will result in inferior accuracy. For better estimation of the velocity profile, knowledge about the flow conditions and flow patters is needed.

Another limitation related to this method is *the boundary layer flow*, which, as will be demonstrated in section 5.5 , can result in overestimation of the air flow rate in the cavity, both in days with the strong solar radiation or at night time. And, accordingly, in the periods when the boundary flow at the surfaces of the DSF cavity is relatively strong, the overestimation of mass flow rate will take place.

3.3.3 LIMITATIONS OF EXPERIMENTAL SET-UP

Any experimental set-up will always have some limitations. These could be caused by equipment that may disturb the measurements, difficulties to attain certain conditions, wrong positioning of measurement equipment, etc. In this section, the main limitations of experimental set-up in 'The Cube' will be explained.

Measurement of air temperature in the cavity

Correct positioning of equipment can have a crucial role in any experimental set-up. It is well-known that in DSF cavity there will always be a horizontal temperature gradient between the external and internal skin of the facade. This temperature gradient is caused by boundary layer flow at the surfaces. Air temperature in the boundary layer is significantly different from the temperature in inviscid flow. Thus positioning of temperature sensors in the field of the boundary layer will lead to a wrong measurement.

Due to a limited number of measurement points for evaluation of horizontal temperature profile, it is not confirmed whether the temperature measurement to place in the boundary layer or not.

There was a multiple number of cables placed on the floor of the cavity, these were of black colour and might have resulted in increased temperatures at the surface.

Estimation of cooling/heating load in experiment room

Other limitations of the experimental set-up involve estimation of solar gains to experiment room.

In Figure 3-3, positioning of ke-low impulse ducts in experiment room is illustrated. The ducts are of white colour, therefore a large part of direct solar radiation approaching the ducts is reflected. Without the ducts, a major part of solar radiation would reach a concrete floor and would be absorbed. In the test facility, though, solar radiation absorbed by the ducts is almost immediately transferred to air by convection.

Air of different than the ambient air temperature is expelled trough ke-low impulse ducts. This results in different floor surface temperature underneath of the ducts. Finally, the weight of the ventilation system, located in experiment room is approximately 750 kg, which acts as an additional thermal mass in the room.

Chapter 4

EMPIRICAL VALIDATION OF THERMAL BUILDING SIMULATION SOFTWARE

Empirical validation of building simulation software was conducted within the IEA SHC Task 34 /ECBCS Annex 43. Results of this work were described in Annex 34/43 report (Kalyanova and Heiselberg, 2008). This report was the main background and source of information for this Chapter 4.

Results of simulations included in this chapter were carried out by many people using various thermal building simulation tools. The author would like to acknowledge their work presented in this chapter:

Clemens Felsmann	*Technical University of Dresden (TUD)* *Germany* *(program TRNSYS-TUD)*
Paul Strachan	*Energy Systems Research Unit (ESRU)* *Dept. of Mechanical Eng.* *University of Strathclyde* *Glasgow, Scotland* *(program ESP-r)*
Aad Wijsman	*VABI Software BV* *Delft* *Netherlands* *(program VA114)*
Harris Poirazis *Bengt Hellström*	*Division of Energy and Building Design* *Department of Architecture and Built Environment* *Lund Institute of Technology (LTH), Sweden* *(program IDA)*

BSim simulations were completed by the author.

4.1 FOREWORD

The double-skin facade solutions are still being proposed and built as an attractive, innovative and energy efficient solution. Nowadays, different design tools are used for assessment of thermal and energy performance of DSF buildings. The results of these simulations are used, for further arguments for or against DSF application. These design tools are well-suited for performance assessment of conventional buildings, but according to the literature review (Chapter 2) they might not work for DSF. In the Chapter 2, it is explained that many mathematical models have not yet been empirically validated for application with DSF; many of these tools require an expert knowledge to perform the simulations. As a consequence, it is impossible to argue on the topic of DSF if accuracy of simulations is uncertain.

There is a lack of systematic literature or guidelines on how to model DSF and what are the most suitable tools to use. Most of this is caused by lack of empirical validations.

To address this problem, an empirical validation of building models with DSF, simulated with various building simulation tools was carried out in the framework of IEA SHC Task 34 /ECBCS Annex 43 "Testing and Validation of Building Energy Simulation Tools". In the following chapter, the background and the results from these empirical validations will be presented and discussed based on Annex 34/43 report (Kalyanova and Heiselberg, 2008).

Results of the empirical exercises are compared between several building energy simulation programs and experiments. The following is the list of organizations who participated in the exercises and the simulation programs they used to perform the simulations.

Organization		Program
VABI	VABI Software BV Delft The Netherlands	VA114
ESRU	Dept. of Mechanical Eng. University of Strathclyde Glasgow Scotland	ESP-r
TUD	Technical University of Dresden (TUD) Germany	TRNSYS-TUD
LTH	Division of Energy and Building Design Department of Architecture and Built Environment Lund Institute of Technology (LTH) Sweden	IDA
AAU	Dept. of Civil Engineering Aalborg University Denmark	BSim

Table 4-1. Organizations who participated in IEA Annex 34/43 Subtask E.

The empirical validation was conducted on the basis of empirical data gathered as described in Chapter 3 collected in the fall 2006 in the full-scale outdoor test facility at the Aalborg University, 'The Cube'.

4.2 BACKGROUND FOR EMPIRICAL VALIDATION

Test cases for the empirical validation procedure in detail are explained in the empirical test case specification by Kalyanova and Heiselberg (2007a). The geometry and the definition of the constructions, their properties in the specification are given according to the actual geometry and properties of the outdoor test facility 'The Cube'.

In the empirical specification, parameters such as air tightness, optical properties of the constructions, discharge coefficient of the openings etc. are defined according to the results of additional sets of measurements, which are explained in Kalyanova and Heiselberg (2007b).

There are two different test cases defined in the empirical test case specification. These are:

MODE1. External air curtain mode. Top and bottom openings open to the outside. The DSF function is to remove the surplus solar heat gains by means of natural cooling. Temperature conditions and air flow conditions in the DSF was examined together with the magnitude of natural driving forces.

MODE2. Transparent insulation mode. All openings closed. There is no exchange of the zone air with the external or internal environment. The zone air temperature results from the conduction, convection and radiation heat exchange. The movement of the air in the DSF occurs due to convective flows in the cavity.

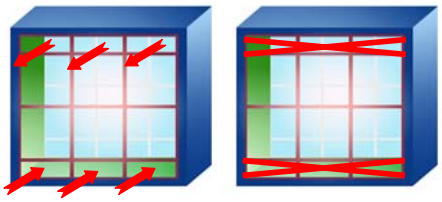

MODE 1 MODE 2

Figure 4-1. Illustration of the empirical test cases

Test case	Solar shading	Driving force			Boundary conditions		Control of opening
		Buoyancy	Wind	Mechanical	Internal–experiment room	External	
MODE 1	No	Yes	Yes	-	constant	variable	-
MODE 2	No	-	-	-	constant	variable	-

Table 4-2. Definition of the empirical test cases.

The weather data used for simulations was provided for 1-hour average and 10-minutes average time intervals. However, 10-minutes data was used only in ESP-r model. More information about the boundary conditions when simulating MODE 1 and MODE 2 can be found in Chapter 5. Parameters are given in the weather data files as following:

- External air temperature, °C
- Global solar irradiation on horizontal surface, W/m^2
- Diffuse solar irradiation on horizontal surface W/m^2
- Wind direction, deg
- Wind speed, m/s
- Air relative humidity, %
- Atmospheric pressure, Pa

Besides the weather data, the ground temperature below the foundation in experiment room was specified as a boundary condition, together with the air temperature in the neighboring zones (instrument room and engine room). Vertical wind speed profile was also specified as described in Chapter 5.

4.3 ADDITIONAL STUDIES

It is necessary to mention that the empirical validation of building simulation software within the IEA SHC Task 34 /ECBCS Annex 43 "Testing and Validation of Building Energy Simulation Tools" is not a short time exercise. On the contrary, it was an iterative process where the test case specification, models and their output were frequently adjusted according to the lessons learned from the intermediate simulations, analysis of the experimental data and comparative evaluation of the results.

Prior to the empirical validation, a set of comparative test cases was defined and completed, where performance of different models was compared against each other. The results from the comparative studies demonstrated significant differences between predictions from different models. Nearly the same conclusion was obtained with the first results of empirical case studies, which will be presented later in the chapter.

Still, the diagnosis of reasons for contradiction between the experimental data and simulation results was not easy, due to the complexity of the dynamic DSF-system and limitations in accuracy of the experimental data.

There was a need for a step back and repetition of some simulations under the simplified conditions. First, the optical/thermal properties of the glazing were double-checked and corrected if necessary. Next, a number of additional test cases was specified for the detailed diagnosis purposes:

1. Steady-state case. This test case was defined in order to find reasons for disagreements between the measured and simulated night time heating loads. The cause was found in the thermal bridge losses in the experimental test facility. These were quantified according to available experimental data of the heat losses in the test facility. Then all of the models were adjusted identically to count for these losses. Results of the adjustments are illustrated in the Figure 4-2, where the deviation between the programs and the experimental data became rather low (20W) compared to earlier results (250W).

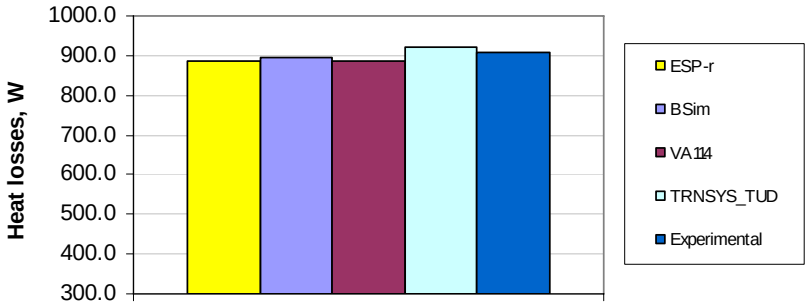

Figure 4-2. Total heat losses from the experiment room in SS models, modified to count on thermal bridges. (Kalyanova and Heiselberg, 2008).

2. No-solar case. In the earlier simulations, it was observed that the results of simulations were very sensitive to solar radiation intensity. Significantly different degree of correspondence was seen for the periods with none or low solar radiation in contrast to the periods with strong solar radiation (Figure 4-3). In

order to perform the diagnosis, the dynamic simulations were simplified by removing the impact of solar radiation and defining the 'no-solar case', where the global and diffuse solar radiation in the weather file were set to zero. As a result of this simplification, it was demonstrated that the thermal models in the software being tested have reasonably good agreement (Figure 4-4). And, as long as the DSF functions as a conventional facade without solar exposure, its performance can also be evaluated using the conventional tools.

The most significant deviations between the models in the 'no-solar' case were observed only for the surface temperatures of the glazing, for the surfaces. The differences in the surface temperatures are explained by the differences in calculation of the convective/radiative heat transfer, which is further investigated in Chapter 6.

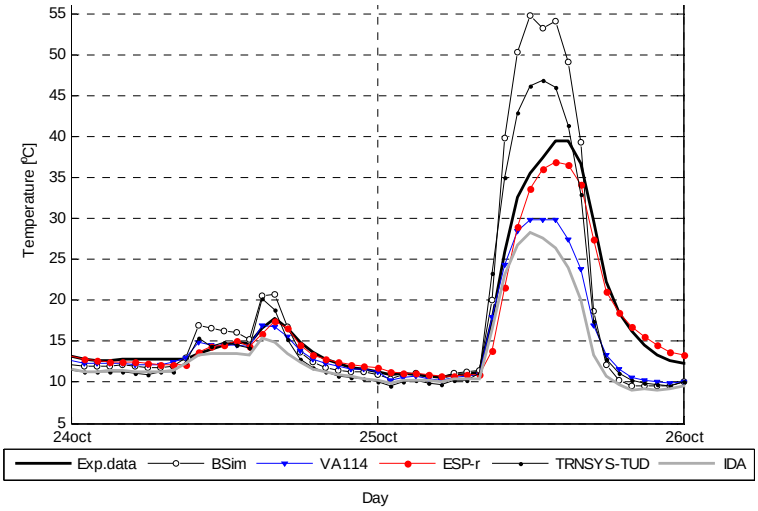

Figure 4-3. Air temperature in the experiment room in the earlier simulations for MODE 2. (Kalyanova and Heiselberg, 2008).

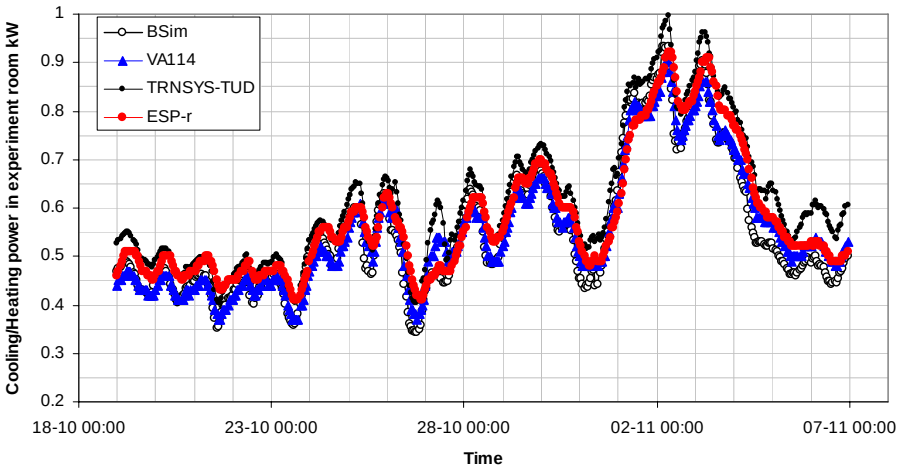

Figure 4-4. Cooling/Heating power in experiment room in 'no-solar' case for MODE 2. (Kalyanova and Heiselberg, 2008)

3. Sensitivity study of impact from surface film coefficients. More details about the results of this study can be found in Kalyanova and Heiselberg (2008). Different (combined and split, fixed and variable) surface coefficients were applied in one of VA114 model by Aad Wijsman and ESP-r model by Paul Strachan, for more detail see Table 4-3. It is necessary to mention that case 4 and 4a are principally different, as in case 4a the internal film coefficients are fixed only in experiment room and vary in the DSF, while in case 4 – all of the internal film coefficients were fixed.

   These sensitivity studies demonstrated the importance of assumptions made towards the longwave and convective heat transfer with reference to MODE 2. Some examples can be seen from Figure 4-5 and Figure 4-6. Following observations have been made from these studies:

   - The internal convective heat transfer is of great importance
   - The external convective heat transfer is of minor importance
   - Internal longwave radiation heat exchange might be important (most likely due to longwave radiation exchange in DSF)
   - External longwave radiation heat transfer is of great importance
   - The magnitude of changes in the results is huge for the peak cooling load, air temperature and surface temperatures when different assumptions are applied (combined/split treatment of surface heat transfer fixed/variable surface film coefficients)

Case	Convection		Radiation		Combined		Radiation ΔT		Model
	Int	Ext	Int	Ext	Int	Ext	Surf-surf using view factors	Surf-air	
1	vary	vary	vary	vary			yes		ESP-r for 'no-solar' case and MODE 2
2a	3.0	18	pc*	pc*			yes		VA114 for MODE 2
2b	3.0	12	pc*	pc*			yes		VA114 for MODE 2
2c	2.0	18	pc*	pc*			yes		VA114 for MODE 2
2d	2.0	12	pc*	pc*			yes		VA114 for MODE 2
4					8	23		yes	VA114 for MODE 2
4a					7.7**	25		yes	ESP-r for 'no-solar' case and MODE 2
5	vary		vary			25	yes (int)	yes (ext)	ESP-r for 'no-solar' case and MODE 2

* pc - for VA114 models, coefficient for long-wave radiation means, that its value is precalculated, based on view factors, emissivity and surface temperature.

** Internal surface film coefficients were fixed only for the surfaces in the experimental room.

Table 4-3. Test cases for the sensitivity studies of surface film coefficients. (Kalyanova and Heiselberg, 2008)

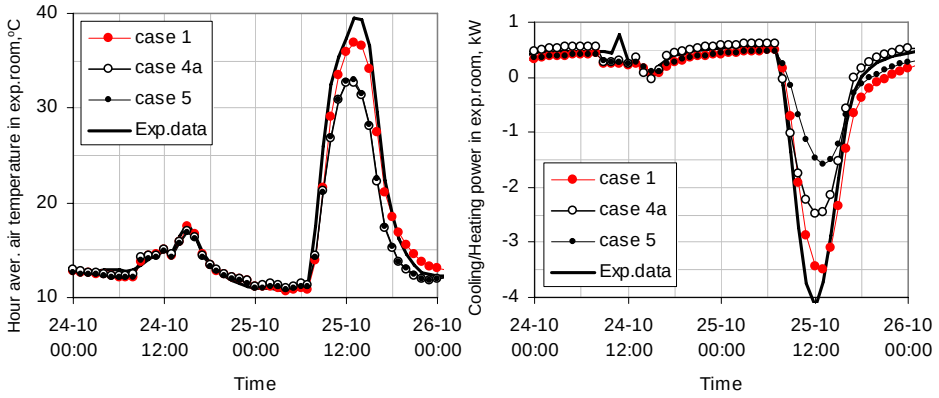

Figure 4-5. MODE 2 simulated with ESP-r. Sensitivity study cases 1, 4a, 5. (Kalyanova and Heiselberg, 2008)

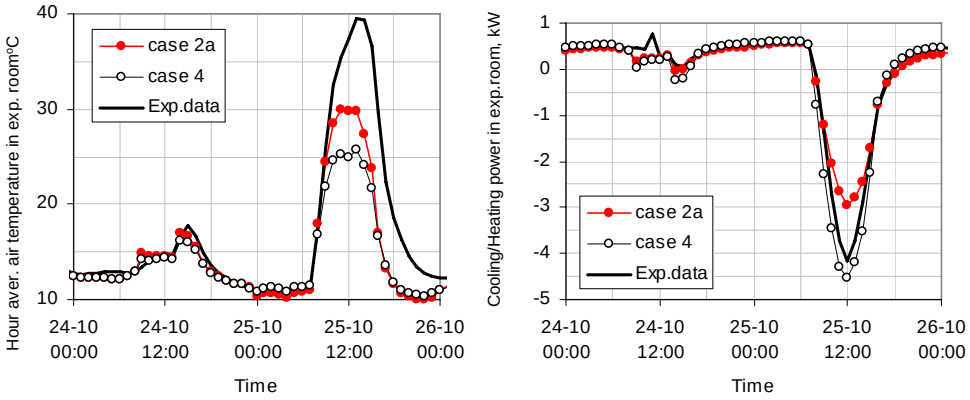

Figure 4-6. MODE 2 simulated with VA114. Sensitivity study cases 2a and 4. (Kalyanova and Heiselberg, 2008)

Finally, it was concluded that the assumptions towards the surface heat transfer in the model are crucial for simulation of buildings with double-skin facade. It is necessary to stress that the assumptions must be considered for two levels of detail when modelling a surface heat transfer:

- Separate or combined treatment of surface film transfer
- Fixed or variable surface film coefficients

D. Saelens (2002) reached a similar conclusion, as explained in Chapter 2. According to Saelens, not separating radiation and convection in the cavity is unacceptable simplification.

More attention might be needed when modelling internal convective heat transfer and longwave radiation heat exchange. Errors may appear in calculations for peak loads of solar radiation if using fixed combined surface film coefficients.

It is also necessary to point out that the best performance, in regard to experimental results, is achieved for a model using split variable surface film coefficients, while the other models may perform well, but only for a limited number of parameters.

The overall summary of these studies show the directions for further improvements. More studies are necessary if the guidelines for modelling of DSF should to be prepared.

4.4 MODELS IN THE EMPIRICAL VALIDATION

In this section, the main assumptions for the models and modelling principles for the test cases are compared and summarized. The models were set-up in the different building simulation programs by different users. Accordingly, different limitations and assumptions are present in these models. This is due to the differences between the programs and also due to the human factor, which involves different opinions, experience, and preferences. These differences, however, were minimized by definition of the empirical test case specification (Kalyanova and Heiselberg, 2007a).

Specified test cases (Kalyanova and Heiselberg, 2007a), in real life, involve interaction of various heat and mass transfer processes. These may require activation of various software applications in order to model the processes properly. And normally, these applications and their limitations have some significant differences when compared across the simulation tools.

For this reason, the requirements for the modelling were untied. The design of the models was allowed according to the capability of the simulating software and user's decision, but as close as possible to the specification. Detailed modeller reports are available as a part of the final report (Kalyanova and Heiselberg, 2008).

4.4.1 GEOMETRY AND THERMAL PROPERTIES OF CONSTRUCTIONS

According to the modeller reports, all of the models were set-up with nearly the same overall geometry and thermal properties of the constructions. Good agreement in definition of thermal properties in the specification and in the models was verified via the steady state case studies (see section 4.3), which resulted in good agreement between the measurements and predictions.

A geometrical issue that can have a significant impact on calculation of transmitted solar radiation in the models, is the assumption made towards the geometry of windows in the model. The geometry of the DSF in 'The Cube' is complex: there are 9 windows, containing transparent part (glazing) and opaque part (window frame). The modellers made their assumptions regarding simplification of the geometry: the areas of the window frame and glazing were kept according to the specification, but the geometry definition has been changed (Figure 4-7). Since the solar path during the day is calculated in all of the models, the distribution of shadow and the distribution of the direct solar radiation in all of the models will be different from the actual empirical case and, sometimes, can be overestimated.

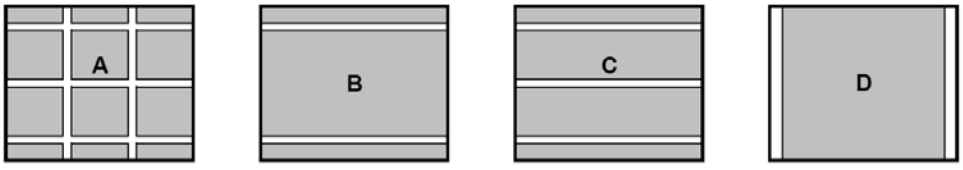

Figure 4-7. Schematics of assumptions made towards the geometry in the models. A - actual geometry in the specification. B - ESP-r model. C - BSim and TRNSYS-TUD model. D - VA114 model. (Kalyanova and Heiselberg, 2008).

The double-skin facade was modelled in ESP-r as 3 equal zones stacked on the top of each other in MODE 1. In TRNSYS-TUD, for MODE 1 and MODE 2, it was modelled as 4 stacked zones, shaped according to the size of the SOL-, BOL-, SOH- and BOH-windows (Figure 4-9). In BSim and VA114 the DSF was modelled as one zone.

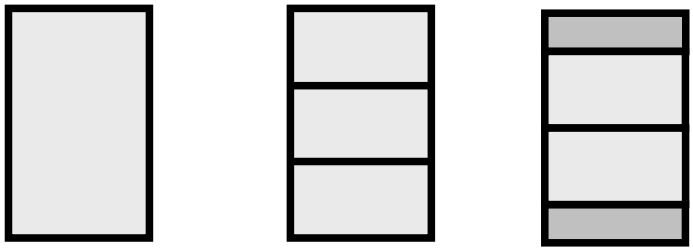

Figure 4-8. Illustration of zoning in the models. VA114 and BSim (left), ESP-r (center), TRNSYS-TUD (right). (Kalyanova and Heiselberg, 2008).

4.4.2 TRANSMISSION OF SOLAR RADIATION

Modellers completed their simulations with Perez model (1990 or 1987) and circum solar radiation treated as diffuse. The choice of Perez model was primarily made on basis of previous experience in modelling of solar radiation.

Spectral properties of the glazing are available in the empirical specification together with the results of WIS calculations, where the properties of the glazing are given as a function of angle of incidence. Still, different level of detailing is possible when setting up a window model using diverse simulation tools. A number of programs allow manual definition of function of angle of incidence. In the latter case, the modellers have used optical properties as a function of angle of incidence as specified (ESP-r and TRNSYS-TUD). Regarding VA114 and BSim the g-value for 45° and 90° angle of incidence, correspondingly, is used as an input in the model. Then, a default function is applied by the program to calculate the g-value, depending on angle of incidence.

In Figure 4-9 solar transmission property of glazing in the models is compared. Good agreement is seen between the optical properties used in the models. Small deviations are only present for VA114 and BSim model when describing solar transmission property of the external window at the large angles of incidence, which is of minor importance.

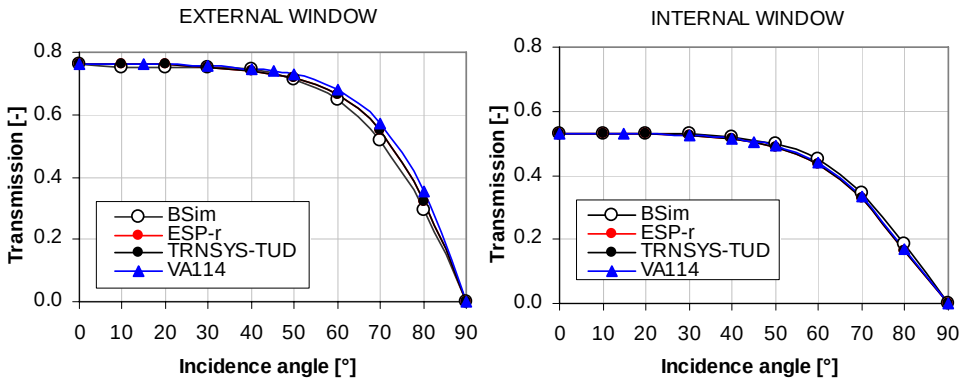

Figure 4-9. Transmission of direct solar radiation. External window (left). Internal window (right). (Kalyanova and Heiselberg, 2008).

Since various software tools treat the diffuse and direct solar radiation separately when calculating the transmission or distribution of solar radiation, different calculation

procedures are used. These procedures depend on whether the solar radiation is treated as diffuse or direct. In all of the models except for TRNSYS-TUD the direct solar radiation was treated as direct after the first bounce (with the external layer of fenestration) and after the second bounce (with the internal layer of fenestration). In TRNSYS-TUD model the direct solar radiation is treated as diffuse after the second bounce. The diffuse solar radiation is treated as diffuse in all of the models.

Summary of solar calculations in the models is given by Table 4-4. According to the table, in the ESP-r model, the transmission of the diffuse solar through the external window will be approximately 9% and 3% higher than those calculated correspondingly by BSim and VA114.

Property	BSim	VA114	ESP-r	TRNSYS-TUD
Transmission of direct solar radiation into DSF	f(α)*	f(α)*	f(α)	f(α)
Transmission of direct solar radiation into DSF	f(α)*	f(α)*	f(α)	f(α)
Transmission of diffuse solar radiation into DSF	f(60°)	f(58°)	f(51°)	f(const)

* - default function of incidence is used
α - an incidence angle

Table 4-4. Assumptions for solar transmission in the models. (Kalyanova and Heiselberg, 2008).

Modelling of such properties as ground reflectivity and longwave emissivity is almost identical for all of the models. However, a serious limitation applies for BSim, as all of solar radiation striking the internal surface is fully absorbed, leading to overestimation of solar gains in the zones and finally to overestimation of energy use for cooling.

4.4.3 SURFACE HEAT TRANSFER

No matter the operational strategy of the DSF, the air temperature in the gap is the result of the solar radiation absorbed by glazing and/or shading device. Since, the air temperature in the DSF cavity is the consequence of convective heat transfer between the heated surfaces of glass and air. The floor or ceiling and side walls of the DSF rarely have any importance. As in a real life, the weight of their areas is very small compared to the area of fenestration and shading.

The convective heat transfer is relatively easy to estimate for the mechanically induced flow motion compared to the naturally driven flow, where the convection heat transfer depends on size, shape, orientation, flow regime, temperature etc. The importance of the assumptions made towards the surface heat transfer coefficients was investigated by Paul Strachan and Aad Wijsman in Kalyanova and Heiselberg (2008), mentioned earlier in section 4.3 . It was found that the assumptions made towards the surface heat transfer coefficients are very important. Similar findings are also available in the literature (Chapter 2). In the literature, the difficulties in modelling convective heat transfer in DSF are also explained due to questionable type of flow and flow regime instability in the cavity.

Below is the table of summary of the surface heat transfer coefficients used in models.

Software	BSim	VA114	ESP-r	TRNSYS-TUD
External heat transfer coefficient				
Convection	if $v_w \leq 5$ m/s $h = 5.82 + 3.96 v_w$ else $\alpha = \frac{7.68 \cdot v}{\sqrt{v_w}}$	18 W/(m²K)	$\alpha = 2.8 + 3 \cdot v_w$ V_w -local wind speed, for which there are relationships with the climate wind speed and the difference between the surface azimuth and wind direction	25 W/(m²K) - set acc. to modeller opinion
Radiation (components)	sky, ground	sky, ground	sky, ground	sky, ground
Internal heat transfer coefficient				
Convection	for vertical surfaces: $if\ \Delta T \leq 9.5/L^3$ $\alpha = 1.42\left(\frac{\Delta T}{L}\right)^{0.25}$ $if\ \Delta T > 9.5/L^3$ $\alpha = 1.31(\Delta T)^{0.33}$	3 W/(m²K)	Buoyancy correlations of Alamdari and Hammond (1983) (Clarke, 1985) $h_c = \left\{\left(a \cdot \left(\frac{\Delta T}{d}\right)^p\right)^m + \left(b(\Delta T)^q\right)^m\right\}^{\frac{1}{m}}$ a,d,p,m,b,q – coefficients (see reference)	4.4W/(m²K), except 3W/(m²K) for ceiling and floor (set acc. to modellers opinion)
Radiation	Linearized coefficients based on surface emissivity and view factors	Linearized coefficients based on surface emissivity and view factors	Linearized coefficients based on surface emissivity and view factors	Nonlinear treatment of radiation heat exchange

Table 4-5. Convection and radiation heat exchange at the surface. (Kalyanova and Heiselberg, 2008).

4.4.4 AIR (MASS) FLOW MODELS

Depending on outdoor conditions and the double skin facade functioning mode the air flow rate in a ventilated cavity can have significant variation in order of magnitude and in occurrence of wind wash out effect or flow reversal. Contradictory, in a traditionally ventilated domain the minimum air change rate is specified in requirements for the indoor air quality, while maximum is normally restricted by the energy savings considerations or comfort conditions. In view of that, the great variations in the magnitude of the air flow rate are identified as the distinctive element of the cavity flow. The variation of the flow magnitude may result in variation of the flow regimes and will further intricate the situation.

The commonly used models for calculation of the natural air flow rates are:

- The network pressure model – is based on continuity equations to determine pressures in different zones of the network and then the air flow rates are determined on the basis of different relationships (orifice, power-law etc.)
- The loop pressure equation model – is a method where the pressure loop equations are written for the whole air path loop and the air flow rate is determined on the basis of those equations.
- The experimental method is using empirical relationships for the determination of the air flow rates depending on temperature, wind speed, pressure difference coefficients and the discharge coefficient.

The pressure network and the pressure loop method are very similar. Moreover, both of these methods can apply the orifice and the power-law relationships for determination of the air flow rate on the basis of pressure difference. However, an application of one or another relationship is a sensitive matter, as the classic orifice equation is more suitable for large openings and fully developed turbulent flow. Meanwhile the power-law equation is more flexible and can be adjusted to different conditions and opening sizes via the exponent *n* and coefficient *C*.

Equation 4-1

$$\Delta P = \frac{\rho V^2}{2 \cdot c_D \cdot A^2}$$ Orifice equation

Equation 4-2

$$\Delta P = \left(\frac{V}{C} \right)^{\frac{1}{n}}$$ Power-law equation

ΔP - pressure difference across the opening
ρ - air density
V - volume flow
c_D - discharge coefficient
A - opening area
n, C - exponent and flow coefficient

In the experimental method, the transient character of the wind is simplified and a relationship as shown below used for the calculation of air flow rates.

Equation 4-3

$$V = \left| \frac{c_v}{|c_v|} \cdot (c_v \cdot V_{10})^2 + \frac{\Delta T}{|\Delta T|} \cdot (c_t \cdot |\Delta T|)^2 \right|^{1/2}$$

Equation 4-4

$$c_t = \sum_{j=1}^{n} c_{D,j} \cdot A_j \cdot \left(\frac{2 \cdot (H_o - H_j) \cdot g}{T_i} \right)^{1/2}$$

Equation 4-5

$$c_v = 0.03 \cdot A$$

V - volume flow
c_v, c_t - coefficient for the wind force and buoyancy correspondingly
V_{10} - the reference wind velocity at the height 10m
ΔT - temperature difference between two environments
n - number of openings
j - opening number
c_D - the discharge coefficient
A_j - area of the opening 'j'
H_o - height of the neutral plan
H_j - height of the opening 'j'
g - gravity force

The size and the discharge coefficients for the double-facade openings were specified in specification (Kalyanova and Heiselberg, 2007a). The discharge coefficients were measured in the laboratory conditions for all openings, as explained in Kalyanova and Heiselberg (2007b).

The wind pressure coefficients were specified on basis of measurements and CFD studies by Matthew Peter Straw (Straw, 2000) for a building of nearly the same shape as 'The Cube'. The pressure coefficients were specified both for the top and for the bottom openings of the DSF. These were used in the ESP-r and TRNSYS-TUD models, while in VA114 due to the same orientation of the openings the Δc_p is modelled as zero. Here, it can be argued that for the openings on the same surface, the wind pressure component is fairly week and the wind turbulence can become more significant. From all of the models only VA114 model includes the impact from the wind turbulence on the magnitude of mass flow in the cavity. Meanwhile BSim is the only model that uses the experimental method for prediction of air flow in the cavity. In that model the Δc_p also equals zero, but the impact of wind pressure is included by application of c_v-coefficient.

Software		BSim	VA114	ESP-r	TRNSYS-TUD
Influencing parameters in the flow model	wind force	x	x	x	x
	wind fluctuations	-	x	-	-
	buoyancy	x	x	x	x
Air flow model*		experimental	network	network	network
Pressure-Air flow relationship used			power-law	orifice	power-law
Discharge coefficient		as in spec. 0.65/0.72	0.61	as in spec. 0.65/0.72	0.65
Pressure difference coefficients		different from spec, $\Delta c_p = 0$, but wind impact is included by application of c_v-coefficient	$\Delta c_p = 0$	as in spec	as in spec
* None uses the loop equations					

Table 4-6. Comparison of air flow models used in the empirical models. (Kalyanova and Heiselberg, 2008).

Besides the parameters included into the table above the reduction of wind speed to the local terrain next to the building can have some degree of influence on the calculations of the wind pressure magnitude and influence of the wind turbulence for the air flow calculations. Table 4-7 provides a comparison of the wind speed reduction relationships used in different models and it demonstrates that the models use almost the same wind reduction relationship in the simulations.

Software:	BSim	VA114	ESP-r	TRNSYS-TUD
Reduction factor to the reference wind velocity at the height of 10m:	0.922	0.922	0.922	0.84

Table 4-7. Reduction factor to the reference wind velocity at the height of 10m in different models. (Kalyanova and Heiselberg, 2008).

4.5 RESULTS FROM THE EMPIRICAL VALIDATION

4.5.1 FOREWORD

Results of the empirical validation are reliant with the quality and accuracy in the experimental data. The measurement accuracy is considered in section 3.3 and will be further discussed together with results of simulations.

In the empirical report (Kalyanova and Heiselberg, 2008) several parameters were compared in order to evaluate the overall performance of the models. These parameters are:

- Air temperature in the DSF cavity
- Cooling/heating power in the experiment room
- Mass flow rate in the cavity

Little attention was paid to the surface temperatures in the cavity and in the experiment room, since these are entirely dependent on the surface film coefficients and may even become misleading. Results of simulations were plotted together with the empirical results. To support these studies results from a simple statistical analysis are also available in Kalyanova and Heiselberg (2008) and repeated in this report. The definition of the statistical parameters is given in Table 4-8.

Minimum	MIN	$Xmin=Min(X_t)$
Maximum	MAX	$Xmax=Max(X_t)$
Average	MEAN	$\overline{X} = \sum_{t=1}^{n} \frac{X_t}{n}$
Difference	DT	$D_t=X_t - M_t$
Difference 5%	DT95	*5% percentile* (D_t)
Difference 95%	DT5	*95% percentile* (D_t)
Average Difference	MEANDT	$\overline{D} = \sum_{t=1}^{n} \frac{D_t}{n}$
Absolute Average Difference	ABMEANDT	$\left\|\overline{D}\right\| = \sum_{t=1}^{n} \left\|\frac{D_t}{n}\right\|$
Root Mean Square Difference	RSQMEANDT	$\sqrt{D^2} = \sqrt{\sum_{t=1}^{n} \frac{D_t^2}{n}}$
Standard Error	STDERR	$\sigma = \sqrt{\frac{1}{n}\sum_{t=1}^{n}(D_t - \overline{D})}$

Where
X_t - predicted value at hour t
M - measured value at hour t
n - total hours in period of comparison

Table 4-8. Definition of the statistical parameters. (Kalyanova and Heiselberg, 2008).

In this report, the results of simulations will be presented on basis of two days: one day with strong solar radiation and one day with rather thick cloud cover of the sky and therefore weak solar radiation, which mainly consists of the diffuse component. Plots for the complete period can be found in are included in report by Kalyanova and Heiselberg (2008).

4.5.2 BOUNDARY CONDITIONS

First, it is necessary to look at modelling of boundary conditions in different models, in order to be able to compare between the results of simulations. The boundary conditions are the solar altitude, solar radiation striking on the double skin facade surface (direct, diffuse and total), solar radiation transmitted into the DSF and into the adjacent experiment room, air temperature in the neighbouring zones, etc. These were closely investigated in the empirical report (Kalyanova and Heiselberg, 2008) and only the main results are highlighted in this chapter.

In the empirical report, it is shown that modelling of the boundary conditions were consistent for all models when compare the data from MODE 1 and MODE 2, therefore only the results from MODE 2 will be included in this report.

Solar altitude

Calculation of the solar height in the empirical report (Kalyanova and Heiselberg, 2008) is available only for three programs: VA114, TRNSYS-TUD and ESP-r. Some minor differences in calculation of solar height are characteristic for TRNSYS-TUD, which are slightly higher (Figure 4-10). Still, the instance of sunset and sunrise in TRNSYS-TUD model is calculated the same as for VA114 and ESP-r. In BSim model, the solar height is reported only at the end of hourly interval, which was also compared with the other results and confirmed a good agreement between the models.

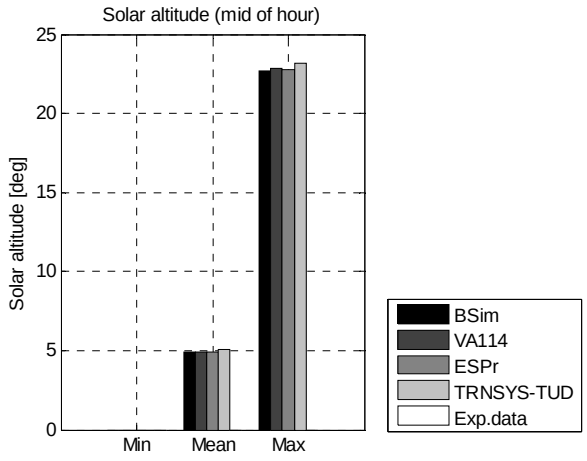

Figure 4-10. Solar altitude. MODE 2. (Kalyanova and Heiselberg, 2008).

Direct, diffuse and total solar radiation

Generally, good agreement is seen between the models when calculate the direct solar radiation striking the external surface of DSF (Figure 4-11): the deviation of the mean values is nearly negligible, while the deviation of max values between the programmes is about ±10 W/m^2.

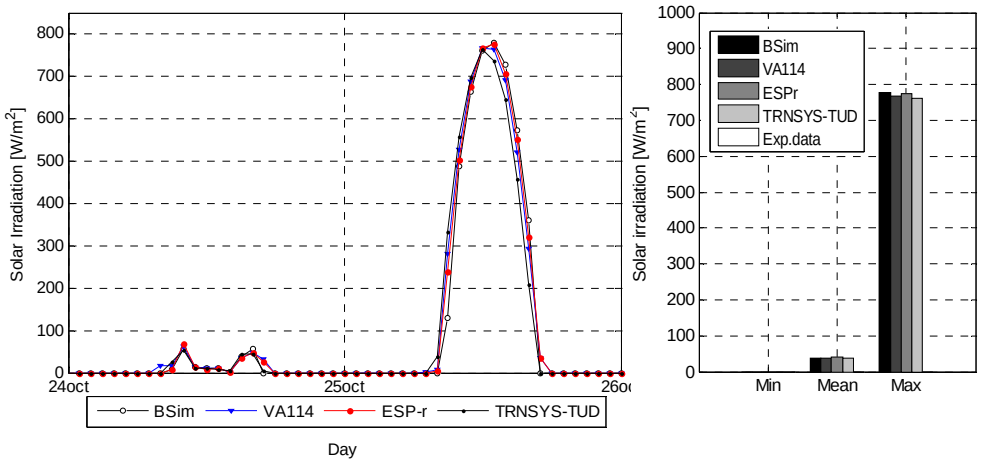

Direct solar irradiation on ext window surface	BSim	VA114	ESP-r	TRNSYS-TUD
MIN, W/m^2	0	0	0	0
MAX, W/m^2	779	767	775	762
MEAN, W/m^2	37	39	40	38

Figure 4-11. Direct solar irradiation on the external window surface. MODE 2. (Kalyanova and Heiselberg, 2008).

Calculations of the diffuse solar radiation are also in agreement when the mean values are concerned (Figure 4-12). Meanwhile, the maximum values are somewhat more different, probably due to high variation of cloud distribution in the sky.

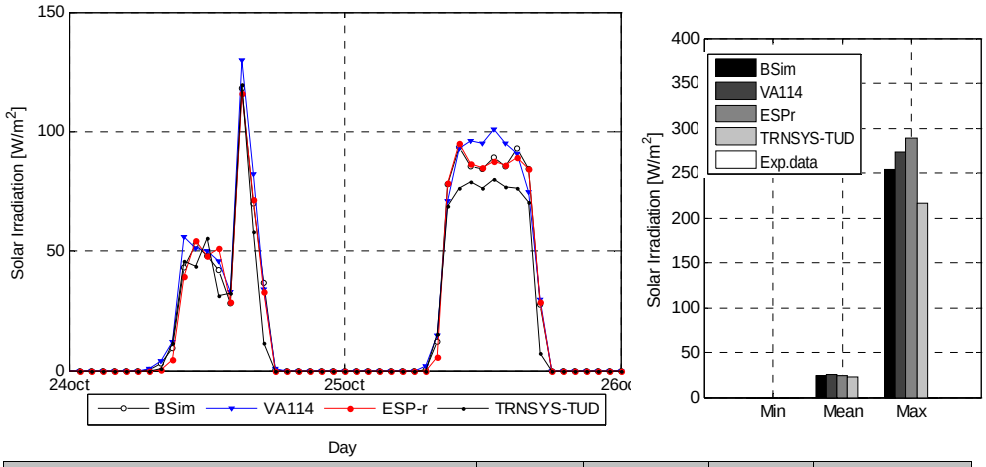

Diffuse solar rad. on the ext. DSF surface	BSim	VA114	ESP-r	TRNSYS-TUD
MIN, W/m^2	0	0	0	0
MAX, W/m^2	254	274	290	217
MEAN, W/m^2	24	25	24	22

Figure 4-12. Diffuse solar radiation on the external DSF surface. MODE 2. (Kalyanova and Heiselberg, 2008).

The deviations in calculation of direct and diffuse solar radiation striking the vertical surface of DSF are then reflected on the values for total solar radiation. In general, the programs agree well on calculation of the total solar radiation on the external window surface when comparing the mean values. TRNSYS-TUD has the widest spread of error when compare against experimental data, as DT5=50 W/m^2 and DT95=-33 W/m^2, which is less in the other models. Comparing the maximal values the experimental data seems to be slightly lower and the disagreements are more pronounced (Figure 4-13).

Regarding the experimental data in the empirical report (Kalyanova and Heiselberg, 2008), it is mentioned that the total solar irradiation was measured, but there is no access to the direct and diffuse components on the vertical surface of the DSF. At the same time, the ground reflection in the models had a fixed value, which can differ from the true experimental conditions, as only 0.5 of the DSF view factor was covered with ground carpet (section 3.1). Moreover, the measurement accuracy can also have an impact, especially because of frequent rain drops on the pyranometer.

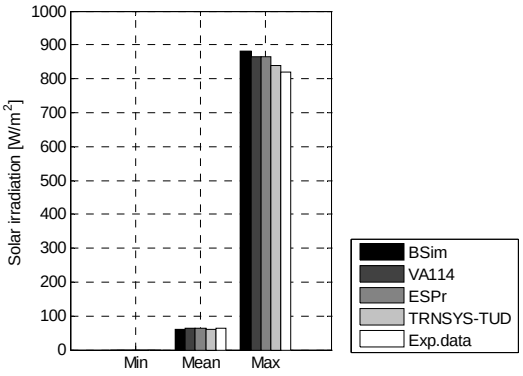

Total solar rad. on ext window surface	BSim	VA114	ESP-r	TRNSYS-TUD	Exp.
MIN, W/m^2	0	0	0	0	0
MAX, W/m^2	882	866	864	838	821
MEAN, W/m^2	61	64	63	61	65
DT95, W/m^2	-4	0	-7	-33	
DT5, W/m^2	44	45	44	50	
MEANDT, W/m^2	5	7	6	3	
ABMEANDT, W/m^2	8	9	9	11	
RSQMEANDT, W/m^2	21	19	21	27	
STDERR, W/m^2	20	18	20	27	

Figure 4-13. Total solar radiation on the external DSF surface. MODE 2. (Kalyanova and Heiselberg, 2008).

Solar radiation transmitted into the DSF cavity and the experiment room (first order of solar transmission)

Similar to calculations of the total solar radiation on the external surface of the DSF, the transmission of solar radiation into the DSF and experiment room had a good correspondence of the mean values. Still, deviations that are more significant were observed when comparing the maximum values. These are more or less consistent with the calculations of the total incident solar radiation on the facade and also with solar radiation transmitted into the experiment room.

The transmission/absorption property of the glazing was modelled almost identically. Therefore, the main reasons for disagreements in the maximum values are, first of all

traced, from the differences in calculation of the incident solar radiation on the double-skin facade.

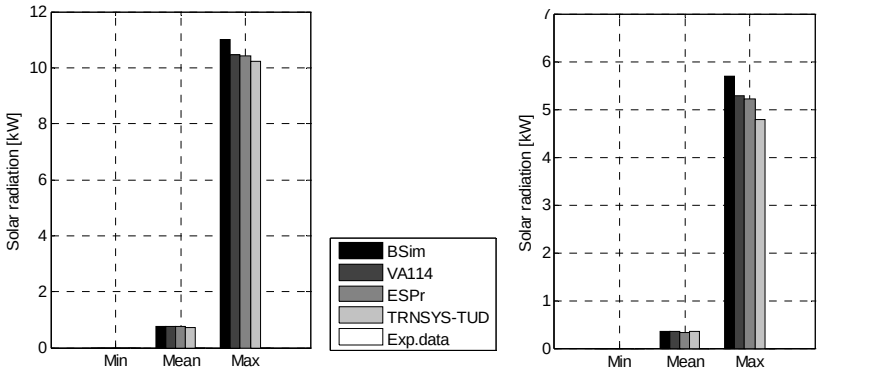

Transmitted into the DSF

Transmitted into the experiment room

Solar rad. transmitted into the DSF	BSim	VA114	ESP-r	TRNSYS-TUD
MIN, kW	0	0	0	0
MAX, kW	11.02	10.45	10.42	10.21
MEAN, kW	0.74	0.75	0.74	0.71
Solar rad. transmitted into the exp.room	BSim	VA114	ESP-r	TRNSYS-TUD
MIN, kW	0	0	0	0
MAX, kW	5.70	5.29	5.22	4.78
MEAN, kW	0.34	0.34	0.33	0.35

Figure 4-14. Solar radiation transmitted from outside into the DSF cavity (left) and from the DSF cavity into the experiment room (right)- first order of solar transmission. MODE 2 (Kalyanova and Heiselberg, 2008).

Summary

One of the most essential measures for validation of simulation programs for buildings with the double skin facade is their ability to predict air temperature and air flow in the double facade cavity. The accuracy of these predictions is then reflected in the cooling/heating power in a neighbouring zone – experiment room. Cooling/heating power in that zone is the main characteristic of the double-skin facade performance. As a result, DSF is also the consequence for the thermal performance of the whole building. Therefore, the differences in the boundary conditions, such as solar radiation incident on the DSF surface, can be crucial. Glazing area of the double skin facade windows at the outer skin is 16.158 m^2 and the differences in predictions of solar irradiation of $\pm 100 W/m^2$ will result in ± 1.6 kW difference in received solar radiation on the glazing surface.

For the defined empirical test case, MODE 2, solar altitude was verified in the first place in the empirical report (Kalyanova and Heiselberg, 2008). In the further investigations of the direct and diffuse solar irradiation, a degree of deviations in the maximum values was observed. The deviations are then traced through all of the results. These, probably, are the reason for differences in solar loads to DSF cavity and experiment room.

By any means, calculation of the incident, transmitted and distributed solar radiation is not the focus of these empirical exercises. However, the results of these calculations are the tool and the quality measure for completing the exercises. These were evaluated as being of sufficient accuracy.

4.5.3 MODE 2 RESULTS

It is clear that solar radiation has a great impact on the air temperature in the cavity. In Figure 4-15, the air temperature in the cavity is shown for two days with different solar radiation intensity. All models fit well with the experiments in a cloudy day and have a spread of 10-20 °C in a clear day. It is remarkable that ESP-r agrees also well with the dynamics of the air temperature measured in the cavity (also lowest STDERR), especially in the afternoons, while all of the other models show remarkable temperature drop. This is probably caused by the differences in modelling of the time constant in the zone or the fact that ESP-r uses 10-min weather data as an input, while 1-hour data used in other models.

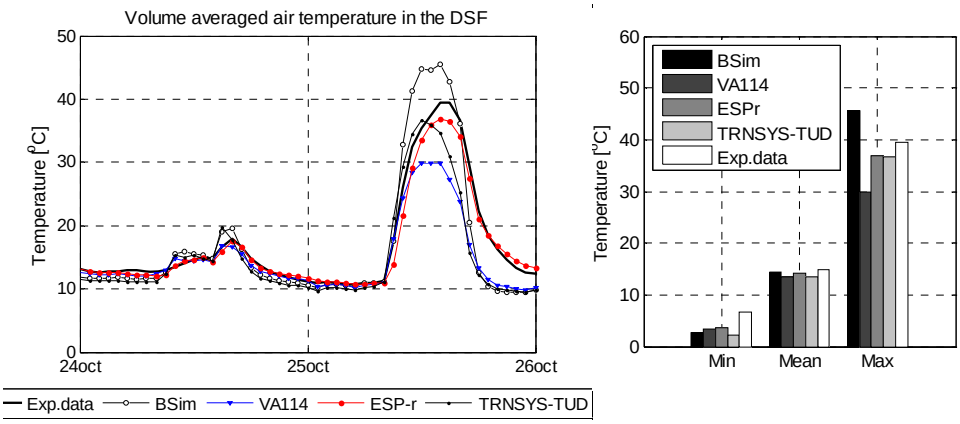

Volume averaged air temperature in zone 1	BSim	VA114	ESP-r	TRNSYS-TUD	Exp.
MIN, °C	2.72	3.32	3.55	2.23	6.73
MAX, °C	45.49	29.91	36.92	36.74	39.48
MEAN, °C	14.35	13.49	14.14	13.54	14.96
DT95, °C	-2.95	-5.21	-2.55	-4.26	
DT5, °C	5.15	0.61	0.98	3.01	
MEANDT, °C	-0.17	-0.92	-0.51	-0.90	
ABMEANDT, °C	1.57	1.13	0.82	1.78	
RSQMEANDT, °C	2.58	2.34	1.42	2.64	
STDERR, °C	2.58	2.16	1.32	2.49	

Figure 4-15. Volume averaged air temperature in the double facade cavity. MODE 2. (Kalyanova and Heiselberg, 2008).

Again, looking at the plots of power supply in the experiment room (Figure 4-16), it is obvious that most of the models underestimate the cooling power in the zone (positive MEANDT), especially during peak loads. It is characteristic that BSim predicts the highest cooling power, what is consistent with overestimation of the air temperature in the DSF cavity, and due to the fact that all solar radiation approaching the internal surfaces in the model is assumed to be fully absorbed. For the other models, underestimation of cooling loads is also consistent with underestimation air temperature in the cavity. For example for in TRNSYS-TUD model, solar radiation transmitted to experiment room is significantly lower than in other models. However, calculation of cooling power seems to be independent of that.

Since the agreement between the measurements and simulations is poor only for the periods of peak loads, the performance of the models on average level (mean values)

seems satisfying. However, this is not enough when assessing the performance of the dynamic models.

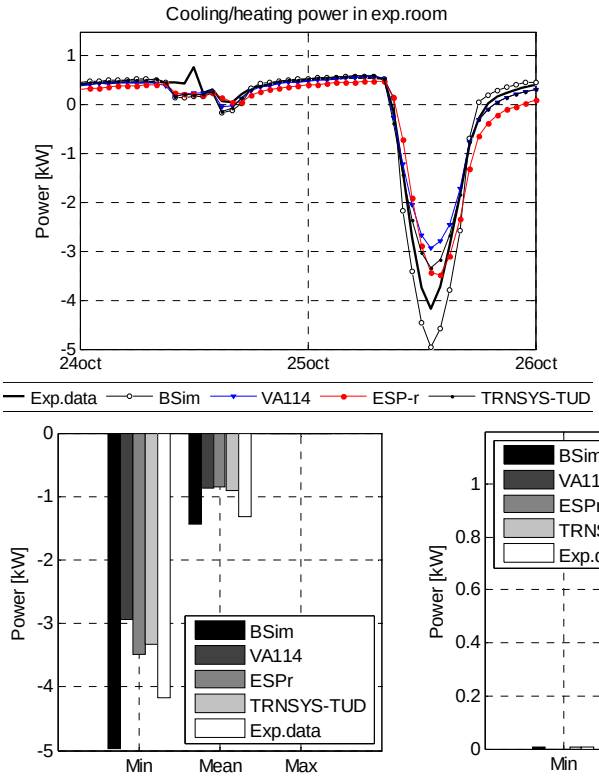

Cooling power in experiment room	BSim	VA114	ESP-r	TRNSYS-TUD	Exp.
MIN, kW	-4.97	-2.94	-3.49	-3.33	-4.18
MAX, kW	-0.02	0.00	0.00	-0.02	0.00
MEAN, kW	-1.44	-0.88	-0.86	-0.91	-1.33
DT95, kW	-0.92	-0.15	-0.49	-0.32	
DT5, kW	0.14	1.17	1.16	0.83	
MEANDT, kW	-0.45	0.32	0.26	0.13	
ABMEANDT, kW	0.47	0.37	0.43	0.27	
RSQMEANDT, kW	0.56	0.54	0.55	0.37	
STDERR, kW	0.35	0.44	0.49	0.35	
Heating power in experiment room	BSim	VA114	ESP-r	TRNSYS-TUD	Exp.
MIN, kW	0.01	0.00	0.00	0.01	0.01
MAX, kW	0.90	0.81	0.76	0.88	0.89
MEAN, kW	0.44	0.39	0.33	0.43	0.44
DT95, kW	-0.13	-0.13	-0.29	-0.15	
DT5, kW	0.12	0.03	0.04	0.08	
MEANDT, kW	0.00	-0.06	-0.12	-0.03	
ABMEANDT, kW	0.06	0.07	0.13	0.06	
RSQMEANDT, kW	0.09	0.09	0.16	0.09	
STDERR, kW	0.09	0.07	0.10	0.08	

Figure 4-16. Cooling/heating power in the experiment room. MODE 2. (Kalyanova and Heiselberg, 2008).

Earlier, in section 4.3 it was demonstrated that the surface heat transfer coefficients could have a significant influence on the results. Thus, another agreement between

experiments and simulations can be expected if the convective heat transfer in the cavity is modelled differently.

In general, results from TRNSYS-TUD and ESP-r models perform best in the MODE 2 when calculation of DSF air temperature and cooling/heating power in experiment room are evaluated.

The night time periods demonstrate good agreement in the heating loads. This indicates that the models were set-up according to the empirical specification and the thermal performance of the models is in a good agreement with the experimental data. The minor deviations are probably caused by differences in the surface film coefficients. However, these thermal models fail when the DSF is exposed to solar radiation.

To facilitate the improvements in performance of the models when simulating a double-skin facade in the mode of thermal insulation (MODE 2), it is necessary to predict air temperature distribution in DSF cavity correctly. Until now, predictions of air temperature in DSF are sufficient only for periods without any significant solar loads.

For that reason, in the report by Kalyanova and Heiselberg (2008) it is argued that application of separated variable surface film coefficients could be considered, in order to obtain predictions that are more realistic during peak loads of solar radiation. This, especially, involves the radiation surface film coefficients and internal convective film coefficients. However, it is necessary to have some guidelines in order to decide on which convection heat transfer correlation should be used.

Another issue here is that results from all models, in this report, consider thermal zone as one node of certain properties. With regard to the zone air temperature, it is assumed that the zone air is fully mixed and has a uniform temperature, represented by a node in the middle of the zone. In this case, the actual and simulated heat transfer through the internal and external skin of the DSF is different, as no temperature gradients in the cavity are considered.

To overcome this limitation the DSF cavity was modelled as a few zones stacked on the top of each other in TRNSYS-TUD, this could be a reason why TRNSYS-TUD predicts nearly same cooling power as ESP-r does, while solar gains in experiment room in TRNSYS-TUD are significantly lower.

Splitting the cavity into a number of zones still requires an application of appropriate surface film coefficients. The natural convection and the dynamic conditions are still, however, a challenge in the field of building physics and it is still difficult to decide on which film coefficients to use.

If the DSF cavity is modelled as one thermal zone then the zone air temperature must be representative for the temperature gradient occurring in the double-facade cavity. This requires a possibility for estimation or prior knowledge of vertical temperature gradient in the cavity.

4.5.4 MODE 1 RESULTS

In this test case, MODE 1, the external air curtain mode, the heat transfer processes in the DSF cavity are closely related with the naturally induced mass flow rates.

In view of fact that the air flow rate in a double skin facade cavity is rather high compared to the temperature difference between the air in the cavity and outdoor, it is essential to

perform the empirical validation of the air temperature predictions in the models via *the temperature raise in the cavity compared to the outdoor air temperature*. It is necessary to mention that an error in prediction of air temperature in the range of 1 degree Celsius can mean hundreds of watts of error in energy balance.

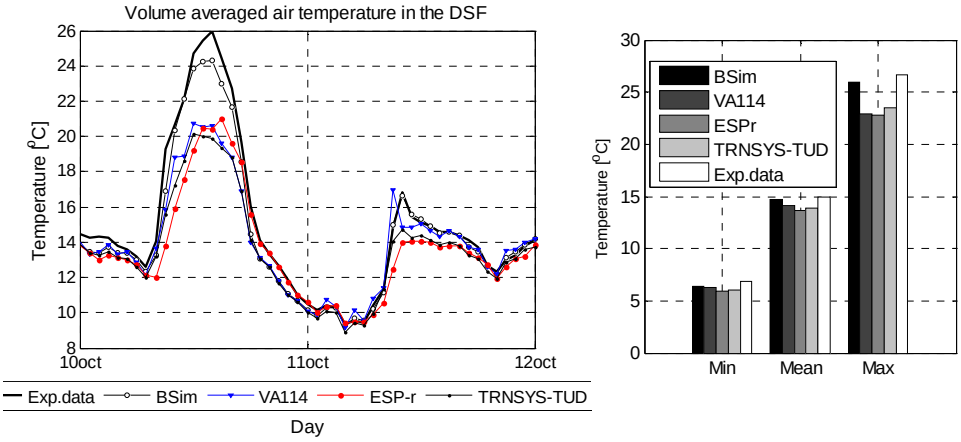

Figure 4-17. Air temperature in the DSF cavity. MODE 1. (Kalyanova and Heiselberg, 2008).

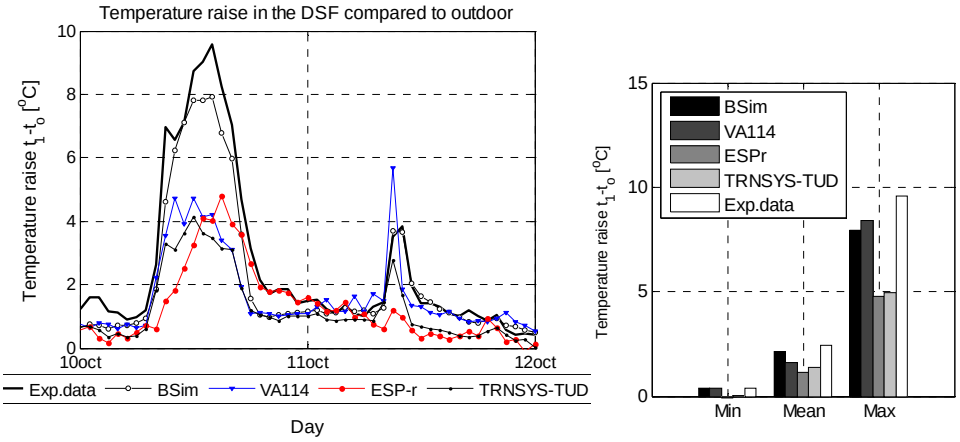

Temperature raise in the DSF compared to the outdoor air temperature	BSim	VA114	ESP-r	TRNSYS-TUD	Exp.
MIN, °C	0.37	0.36	-0.08	0.02	0.40
MAX, °C	7.93	8.39	4.79	4.97	9.59
MEAN, °C	2.17	1.63	1.12	1.36	2.43
DT95, °C	-1.10	-3.63	-4.46	-3.60	
DT5, °C	1.15	0.30	-0.13	-0.04	
MEANDT, °C	-0.24	-0.80	-1.31	-1.07	
ABMEANDT, °C	0.55	0.89	1.31	1.10	
RSQMEANDT, °C	0.71	1.39	1.86	1.52	
STDERR, °C	0.67	1.14	1.33	1.09	

Figure 4-18. Temperature raise in the DSF cavity compared to the outdoor air temperature. MODE 1. (Kalyanova and Heiselberg, 2008).

It is obvious from the Figure 4-18, that all of the models underestimate the air temperature in the cavity, all of MEANDT values are negative. The absolute mean error varies between 0.5 and 1 °C, that corresponds to energy transport with the mass flow of approximately 0.2-0.3 kW, when the mass flow is 1000 kg/h.

Certainly, the accuracy of the measurements become even more important here, since the range of temperature variation is small.

For MODE 2, it was seen that using variable convective heat transfer coefficient ESP-r model was more successful to calculate the air temperatures in the cavity zone. In the present MODE 1, however, this is not the case. This time, the plot of the results differs a lot: ESP-r predictions are similar to the other models.

Is this caused by the change in the flow regime and thus convection heat transfer in the cavity?

Both in BSim and ESP-r model variable convective heat transfer coefficients were used, nevertheless BSim and ESP-r are considerably different, as different assumptions in definition of dynamic convective film coefficients were used.

Empirical validation of naturally induced mass flow rates in the DSF cavity is one of the most difficult assignments. This is because the air flow occurred in naturally ventilated spaces is very intricate and extremely difficult to measure. The stochastic nature of wind and, as a consequence, non-uniform and dynamic flow conditions in combination with the assisting or opposing buoyancy force cause the main difficulties. In Chapter 3, the measurement procedure using the velocity profile method and tracer gas method are explained and discussed. There, it is also argued that no preferences can be given to results from one or another method, as both of them have sources of error and compared to laboratory conditions have relatively large uncertainties. Though, both of these methods provide results of reasonable agreement.

For the better visualization of the results, these plots are divided into three periods, with the scale that is suitable for each period. A plot with a complete measurement period is given in Figure 4-19 and Figure 4-21.

Related statistical data are not included into this report, as their application requires a flawless set of experimental data. Therefore, the main discussion will have to take place upon the plots of simulated and measured mass flow rates.

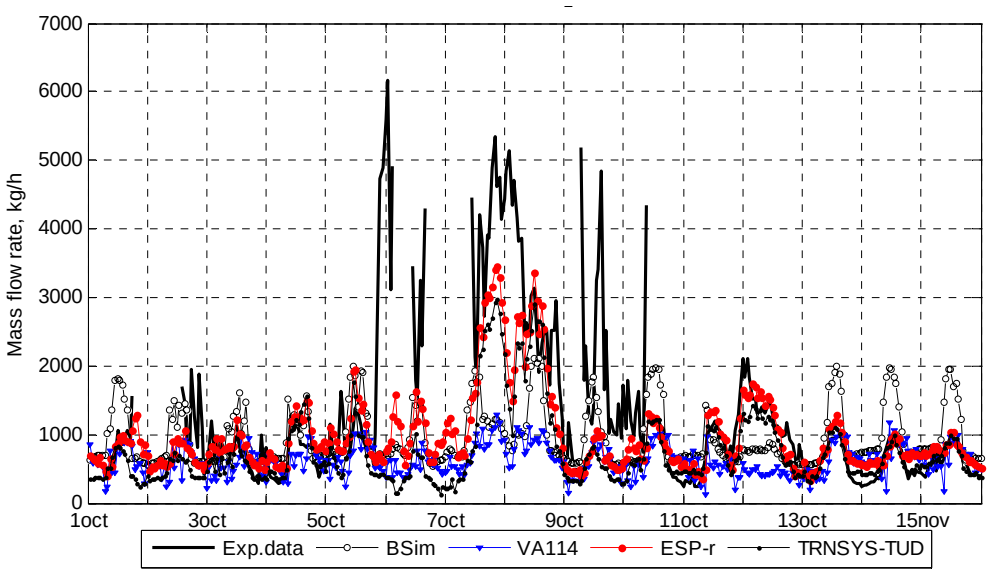

Figure 4-19. Hour averaged mass flow rate in the DSF cavity, measured with the tracer gas method. MODE 1. (Kalyanova and Heiselberg, 2008).

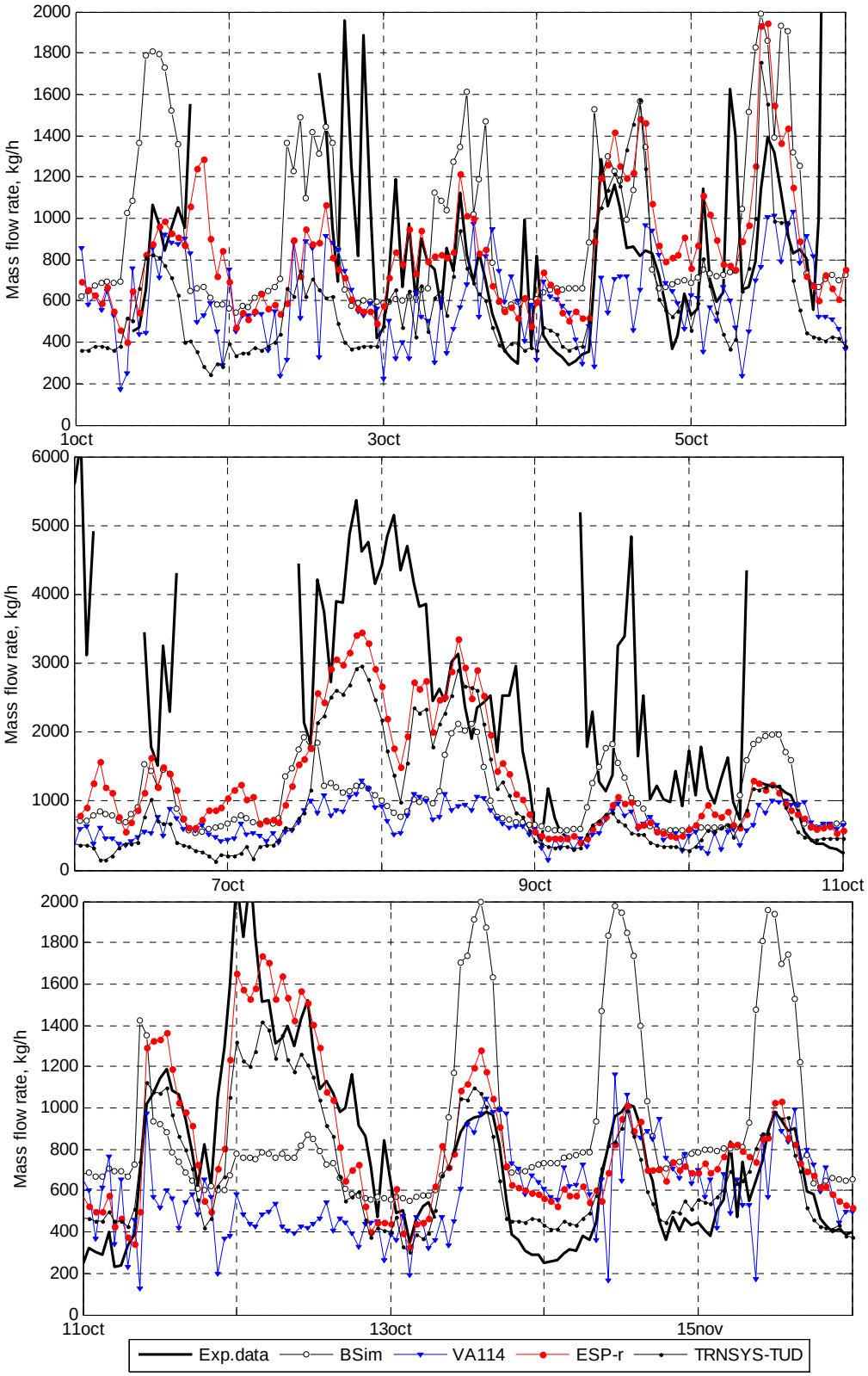

Figure 4-20. Hour averaged mass flow rate in the DSF cavity, measured with the tracer gas method: period 1, period 2, and period 3 in MODE 1. (Kalyanova and Heiselberg, 2008).

In section 3.3 , characteristics of possible errors in both experimental methods are described. With regard to tracer gas method it is noted that the appearance of the reverse flow is periodical (South wind direction). These periods are relatively easy to observe in the plots of the experimental results for tracer gas method, as they are present when the air change rate is extremely high. The wind wash-out effect is also a wind generated phenomena, but its impact on measurement results is more uncertain. Finally, there is a third phenomenon that may take place in the DSF cavity; this is so called recirculating flow. Occurrence of this phenomenon is described in detail in section 6.2 , where its appearance is explained by increasing strength of the boundary layer flow.

Errors possible in velocity profile method are also discussed in section 3.3 . The most significant error for this method is an impact of boundary layer flow in the cavity. This is because in days with strong solar radiation and also at night the boundary layer flow can result in overestimation of air velocity in the cavity and thus in overestimation of air flow. This error is not possible to quantify and it is not obvious between experimental results.

The overall discussion of the air flow measurements is available in section 3.3 .

Results corresponding to the first two periods in the tracer gas method (Figure 4-20) are very difficult to evaluate. Both the results of simulations and experimental results seem to be very fluctuating and random, while in the third period it is easy to distinguish between periods with the higher/lower solar irradiation, etc. It is likely that the haphazard air flow rate in the DSF cavity during the first to periods is caused by often variation in the wind directions between the South-East and South-West. Moreover during the second period was experienced high wind speed above 6m/s. More stable wind direction, relatively low wind velocity (below 6 m/s), cooler outdoor temperature and less changeable solar radiation have resulted in a more clear simulation results in the third period. Though some of the measurements are lacking for this period.

The night time ventilation of the DSF is mainly driven by wind, therefore the correspondence of the experimental results with the simulations in the night time periods in the Figure 4-20, tells about proper estimation of the pressure difference coefficients in the empirical specification.

There is an agreement seen between experimentally and analytically estimated mass flow rate in the cavity, in conditions of pure buoyancy using the experimentally estimated discharge coefficients (section 5.5). This provides some level of confidence in the discharge coefficients determined experimentally in a wind tunnel (Kalyanova and Heiselberg, 2007b).

The night and day periods are less distinguished in VA114 model. This is partly due to the model, which includes the impact of wind fluctuations on air flow rate in the cavity. At the same time this model does not include direct influence of the wind forces, as Δc_p. In VA114 the mass flow rate is calculated based on air temperature in the zone at the end of the previous time step, which causes calculation of somewhat more fluctuating mass flow rate.

BSim often overestimates the air flow rate, both during the day and night time, but during the period of strong wind speed the air flow is underestimated, caused by the simplified empirical air flow model.

Similar to the tracer gas method results of the velocity profile method are subdivided in three periods, see Figure 4-22. The results are presented for the velocity profile measured at the height of 1.91 m. The reason for that is explained in section 5.5 . For the velocity

profile method there is a better agreement between experimental results and calculations, although the order of error is still in the range of 500 kg/h.

Simulation and measurement of naturally induced flow rates is extremely difficult. Therefore, the similarities in the shapes between the measurements and simulations for TRNSYS-TUD and ESP-r model show a great potential possibly due to the fact that both of these programs take into the consideration the pressure difference coefficients for each opening. Thus, it is important to use appropriate pressure difference coefficients for each opening separately when modelling naturally induced flow.

Still, the evaluation of the results against the empirical data is difficult, as there are two sets of the results available. Finally, the estimation of the accuracy of these two methods is still the weak point in the validation procedure. There is also a strong disagreement between the predictions by different models.

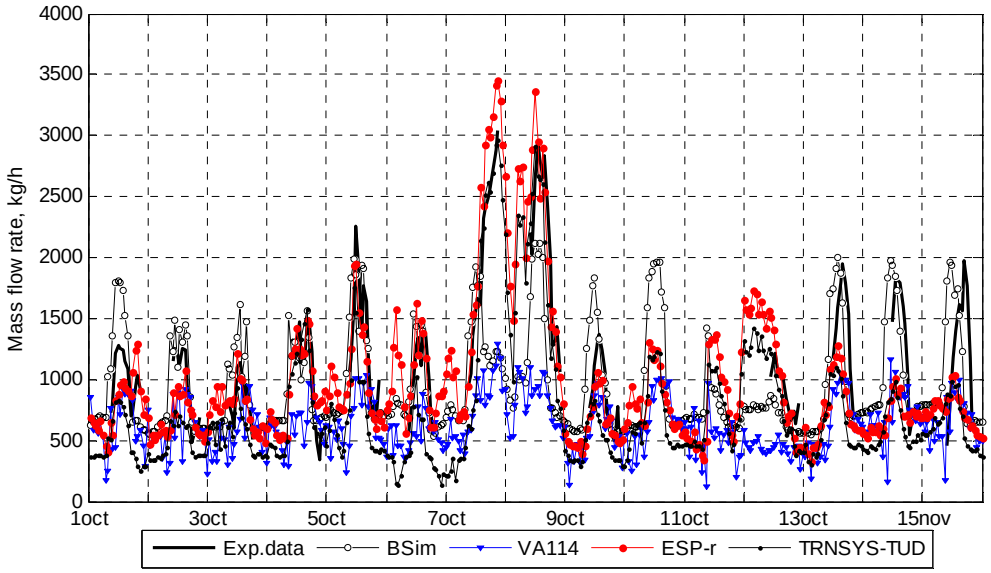

Figure 4-21. Hour averaged mass flow rate in the DSF cavity, measured with the velocity profile method at h=1.91m. MODE 1. (Kalyanova and Heiselberg, 2008).

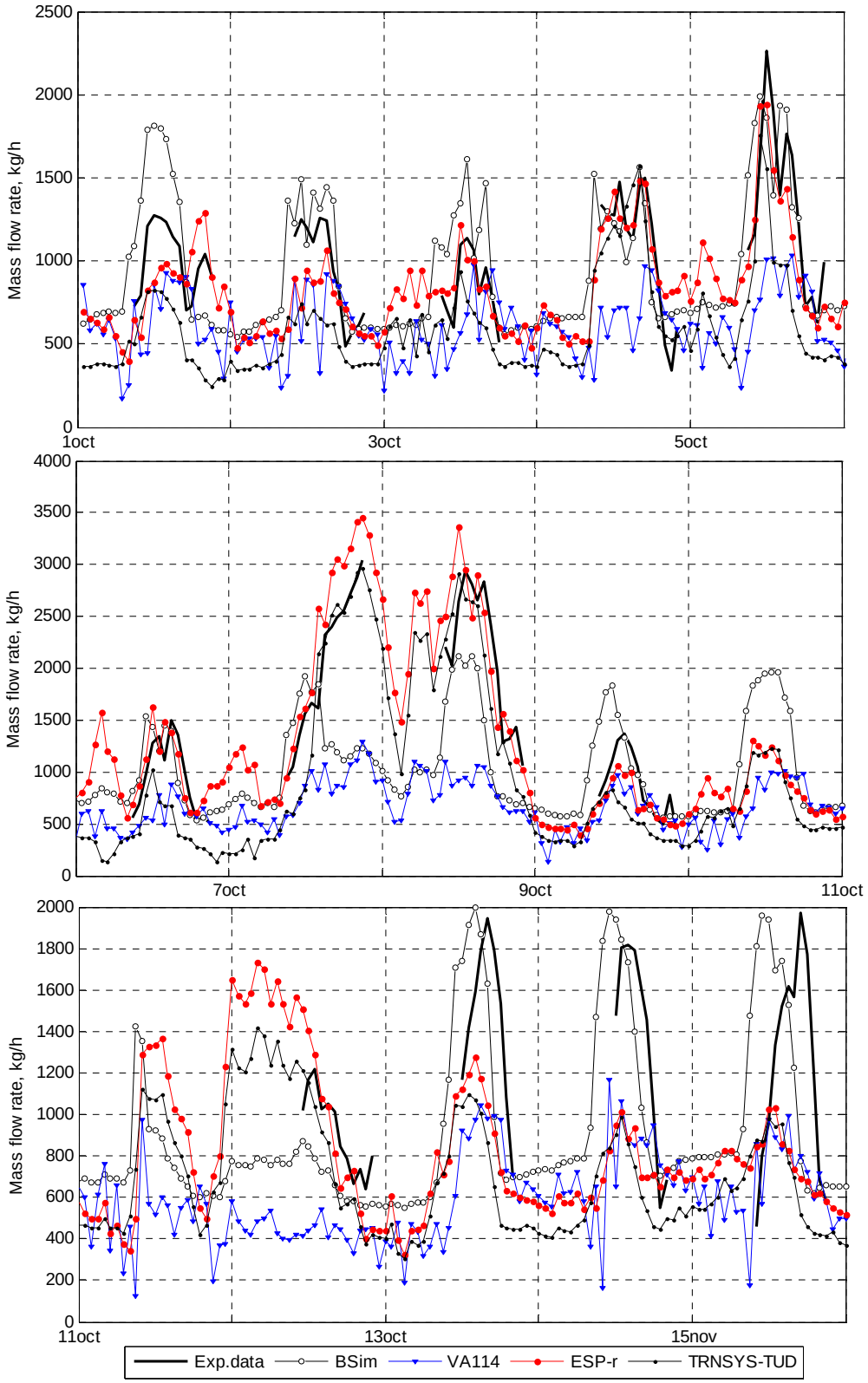

Figure 4-22. Hour averaged mass flow rate in the DSF cavity, measured with the velocity profile method at h=1.91 m : period 1, period 2, and period 3 in MODE 1. (Kalyanova and Heiselberg, 2008).

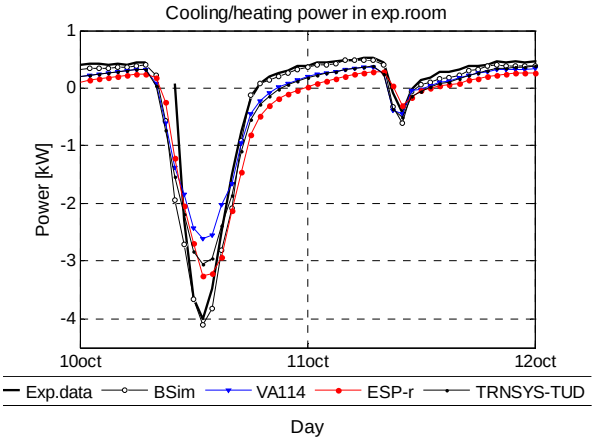

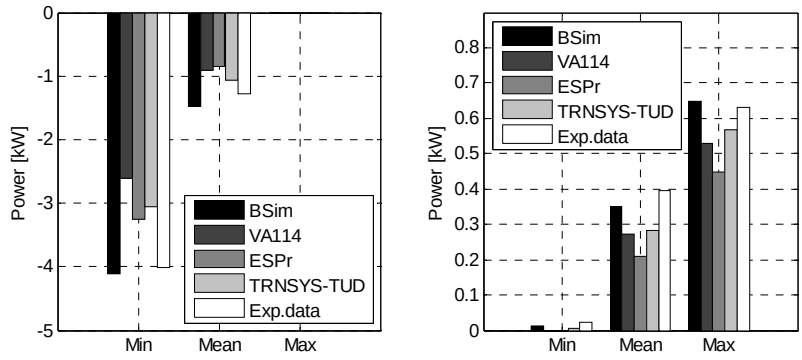

Cooling power in the exp.room	BSim	VA114	ESP-r	TRNSYS-TUD	Exp.
MIN, kW	-4.12	-2.61	-3.25	-3.06	-4.00
MAX, kW	-0.01	0.00	0.00	0.00	-0.01
MEAN, kW	-1.47	-0.91	-0.86	-1.07	-1.28
DT95, kW	-0.58	-0.28	-0.61	-0.41	
DT5, kW	0.02	1.03	0.91	0.65	
MEANDT, kW	-0.24	0.19	0.12	-0.03	
ABMEANDT, kW	0.25	0.33	0.40	0.29	
RSQMEANDT, kW	0.30	0.46	0.47	0.34	
STDERR, kW	0.18	0.42	0.46	0.34	
Heating power in the exp.room	BSim	VA114	ESP-r	TRNSYS-TUD	Exp.
MIN, kW	0.01	0.00	0.00	0.01	0.02
MAX, kW	0.65	0.53	0.45	0.57	0.63
MEAN, kW	0.35	0.27	0.21	0.28	0.40
DT95, kW	-0.13	-0.26	-0.37	-0.26	
DT5, kW	0.03	-0.06	-0.09	-0.02	
MEANDT, kW	-0.05	-0.15	-0.23	-0.14	
ABMEANDT, kW	0.06	0.15	0.23	0.14	
RSQMEANDT, kW	0.07	0.16	0.24	0.16	
STDERR, kW	0.04	0.06	0.09	0.07	

Figure 4-23. Cooling/heating power in the experiment room. MODE 1. (Kalyanova and Heiselberg, 2008).

The cooling power in the experiment room is mainly underestimated by all models. Moreover cooling power appears to be underestimated when the air temperature in cavity is underestimated too.

4.5.5 SUMMARY

The deviations between the measured and simulated *cooling/heating power in* the experiment room are obvious. Most of the models underestimate the cooling loads to the zone especially in days with intensive solar irradiation, while at night the agreement became acceptable after the modifications of models where the impact of thermal bridges was quantified.

Underestimated cooling power and thus underestimated heat flux through the interior skin of DSF can most likely be explained by:

- underestimation of air temperature in the DSF cavity
- underestimation of solar gains to DSF and/or experiment room
- limitations of the experimental set-up and errors in modelling of time constant in experiment room

Limitations of experimental set-up

Limitations of the experimental set-up have already been discussed earlier in section 3.3 . These limitations were incorporated in some of the models. In ESP-r model, an additional layer of insulation was attached to the floor surface to model reduction in accumulation of solar gains. In addition to that, thermal mass in experiment room was represented as additional surfaces inside the room. The ventilation system has a stated mass of 750 kg, it was assumed that 375 kg is "accessible" to the room air (Strachan, 2007).

In VA114 model, 90% of solar gains to experiment room were modelled as convective gains in order to model effect from ke-low impulse ducts on the floor in experiment room.

In TRNSYS-TUD the emissivity of floor in experiment room was reduced to model the effect from ke-low impulse ducts on the floor in experiment room.

Solar gains to DSF and/or experiment room

The importance of angular-dependent solar properties and ability to count on shadowing in DSF models is mentioned in the literature review (Chapter 2).

As described in section 4.4.2 all models use angular dependent properties of glazing. These models are also able to count on shadowing. Prior to this empirical validation exercise, all window models except for BSim were successfully validated within other subtasks of Annex 43 Task 34. BSim model was not validated.

In view of that, it is believed that modelling of transmission and distribution of solar radiation in DSF and experiment room is reasonable in MODE 2. When the cavity is ventilated (MODE 1), the question is not only about the amount of received solar radiation, but also about amount of solar gains removed from the cavity with the natural air flow.

Finally, according to the results, underestimation of cooling power in the experiment room gives an impression of being fully dependent on air temperature in the cavity and not the solar radiation received in the room.

Air temperature in the cavity

Air flow rate, flow regime, convective and radiative heat transfer have an impact on resulting air temperature in the cavity. To be successfully validated a model has to demonstrate consistency of predictions for all parameters. All of the parameters for one model should have certain agreement with the experimental data. For the moment, none of the models appeared to be consistent enough when compare results of simulations with the experimental data.

In section 4.5.3 , it is argued that in MODE 2, air temperature in the cavity is sensitive to solar gains and convective/radiative heat transfer. Differences in predicted air temperature in the cavity together with differences in transmitted solar radiation to the zones result in differences of peak cooling power in experiment room.

In MODE 1, the difficulties with simulation of cooling power during day time are also a consequence of greater deviations in predicted air temperature in the cavity, which is interconnected with the natural driving forces and mass flow rate in the cavity and solar gains removed with the cavity air.

With regard to naturally induced air flow in the cavity, the similarities in the shapes between the measurements and simulations for TRNSYS-TUD and ESP-r model show a great potential. This is probably due to the fact that both of these programs take into the consideration the pressure difference coefficients for each opening. It is then reasonable to expect that prediction of mass flow rate in the cavity will certainly improve when thermal model works without the flaws: with appropriate calculations of the air temperature and vertical temperature gradient in the cavity under the strong solar radiation.

Improvement of thermal model requires more knowledge within the convective and flow regimes in the cavity. A dynamic model for estimation of convective heat transfer in DSF would be beneficial, as application of combined film coefficients appeared to be inappropriate and application of fixed film coefficients does not prove to be satisfactory. Until now, none of the models account for recirculation flow in the cavity. Considering the consequences that recirculation flow in cavity may have on the temperature gradient in the cavity and also on the total mass flow rate, it is necessary to think of a mathematical model that is able to incorporate the effect from recirculation flow.

The disagreements between the models and experiments allow indicating a problem, while further research is needed to solve these problems. The results of this empirical validation are regarded as an argument for further search for the improvements, as most of the results do not allow deriving any solid conclusions, and only designate the directions to follow in search for the improvements.

Chapter 5

ANALYSIS OF EXPERIMENTAL RESULTS

In this chapter results of experimental studies in 'The Cube' are presented. First of all, a discussion of boundary conditions for the measurements takes place. Results of temperature measurements which include air temperature in the double-skin facade cavity, surface temperatures of the glazing, temperature gradients etc. are reported and discussed. Investigation of naturally induced air flow in the DSF cavity is carried out in section 5.5

Briefly, results of air flow measurements in mechanically ventilated cavity are discussed in section 5.6 . Finally, cooling and heating power in experiment room and general performance of DSF is investigated.

5.1 GENERAL

In Kalyanova and Heiselberg (2007b) and Chapter 3, the experimental test facility is characterized as an entire system of certain properties (the heat transmission, air tightness, properties of the constructions, geographical site location, etc.). These characteristics could be identified as 'passive' experimental boundary conditions, and the 'active' conditions would be the climatic parameters at the local site of the test facility and thermal conditions in the adjacent zones of the experiment room.

Before the experimental results are further discussed, it is convenient to begin with an overview of the 'active' boundary conditions for the experimental results, which is given in section 5.2 - 5.3 . Then, the experimental results are introduced in the next following sections.

5.2 MODELS OF WIND SPEED PROFILES

Wind phenomenon is known for its complexity, it depends on multiple numbers of parameters such as earth rotation, temperature differences between oceans and land, polar and tropical air, geographical location and landscape. Mainly the meteorological sciences are dealing with wind and wind influencing parameters. There are a number of scales to describe the climatic models in meteorology: global, regional, local and microclimate scale. Building design is primarily related to local and microclimate scale, where the local scale model describes how the local wind (climate) is affected by geography and urbanization, while the microclimate scale model relates to the parameters of local district planning and architecture that could be essential for the wind flow (Awbi, 2003).

The natural wind speed varies in time and space, the character of its variation is highly random and the wind flow is highly turbulent. At the same time, the wind speed is one of the main contributors to the natural ventilation flow.

The change of the mean wind velocity depending on height and intervening terrain is expressed through the mean wind speed profile. Once the mean wind speed profile is identified and if it is based on a wide spectrum of wind velocities and wind directions with a substantial number of measurement points then the wind profile turns to be one of the characteristics of the local cite and can represent the 'passive' boundary conditions. However, this is not valid for the experiments described in this chapter, as the duration of wind measurements was not enough to build up the wind profile independent from the wind direction, as it will be demonstrated in the next sections.

In this chapter, the commonly used models to build a vertical wind velocity profile are described and the mean vertical wind speed profile is built for all wind directions and microclimate scale of the test facility.

5.2.1 POWER LAW MODEL 1

Power law based models represent empirical expressions developed for mean vertical wind velocity profile. These models are more suitable for predictions of wind velocity in the upper regions, as their application for the lower regions is of inferior quality.

An approximate correlation that accounts for height difference and intervening terrain is suggested in AIVC (1996):

Equation 5-1

$$V(h) = V_{ref} \cdot k \cdot h^{\alpha}$$

$V(h)$ - wind speed at height h
V_{ref} - wind speed measured in open country at a standard height 10 m
h - height above the ground
α, k - constants dependent on terrain

Terrain Coefficient	k	α
open flat country	0.68	0.17
country with scattered wind breaks	0.52	0.20
urban	0.35	0.25
city	0.21	0.33

Table 5-1.Terrain coefficients for power law model 1.

5.2.2 POWER LAW MODEL 2

Estimation of a local wind speed, considering type of local terrain and height difference, is defined according to ASHRAE (2001):

Equation 5-2

$$V(h) = V_{ref}\left(\frac{\delta_{met}}{h_{ref}}\right)^{\alpha_{met}} \cdot \left(\frac{h}{\delta}\right)^{\alpha}$$

δ - wind boundary layer for a local terrain
α - local building terrain coefficient
δ_{met} - wind boundary layer for the meteorological station
α_{met} - terrain coefficient for the meteorological station
V_{ref} - wind velocity at the reference height (at the meteorological station)
h_{ref} - reference height (normally 10 m)

Wind boundary layer and building terrain are determined from the table below (ASHRAE, 2001):

Terrain category	Description	α	Layer thickness δ, ft
1	Large city centres, in which at least 50% of buildings are higher than 15 m, over a distance of at least 0.8 km or 10 times the structure upwind, whichever is greater	0.33	460
2	Urban and suburban areas, wooded areas or other terrain with numerous closely spaced obstructions having the size of single-family dwellings or larger, over a distance of at least 0.8 km or 10 times the structure upwind, whichever is greater	0.22	370
3	Open terrain with scattered obstructions having heights generally less than 10 m, including flat open country typical of meteorological station surroundings	0.14	270
4	Flat, unobstructed areas, exposed to wind flowing over water for at least 1.5 km, over a distance of 460 m or 10 times the height of the structure inland, whichever is greater	0.10	210

Table 5-2.Terrain coefficients for power model 2.

5.2.3 LOGARITHMIC LAW MODEL

The logarithmic law model is the mathematical description of the atmospheric boundary layer known from aerodynamics. It is more complicated than the power law model, but provides results of a better quality than the power law model does.

General expression for the logarithmical wind velocity profile is (Allard, 1998):

Equation 5-3

$$V(h) = \frac{V_*}{K} \cdot \ln\left(\frac{h}{h_o}\right)$$

V(h) - wind speed at height h
h - height above the ground
V_* - friction velocity
K - von Karman's constant
h_o - roughness height

The logarithmic profile law is only valid for homogeneous and stationary flow under neutral conditions. The reference velocity cannot be deduced for a reference height of 10 meters in too rough terrain. It is not valid in the wake of a building and close to a building at the windward side (AIVC, 1994).

Von Karman's constant is approximately 0.4, the values of V_* and h_o are obtained experimentally, according to an experimental results. The roughness height can be estimated as in Allard (1998):

Terrain description	h_o
Sea, snow, sand	0.0005
Sea with very strong wind	0.005
Short grass	0.01
Cultivated open fields	0.05
High plants, open country	0.10
Country side and spread habitat	0.25
Peripheral urban zone	0.50
Mean city centre, forest	1.00
Metropolitan centre, tropical forest	4.00

Table 5-3. Terrain coefficient for logarithmic model.

5.2.4 DETERMINATION OF VERTICAL WIND VELOCITY PROFILE FOR LOCAL MICROCLIMATE OF 'THE CUBE'

The wind profile models described in the previous sections involve different parameters, which result in the different shapes of a general wind speed profile. Moreover, the level of resolution and definition of the terrain parameters in the reference literature differs a lot. As a consequence, it becomes meaningless to compare the shapes of the profile in different models (Figure 5-1).

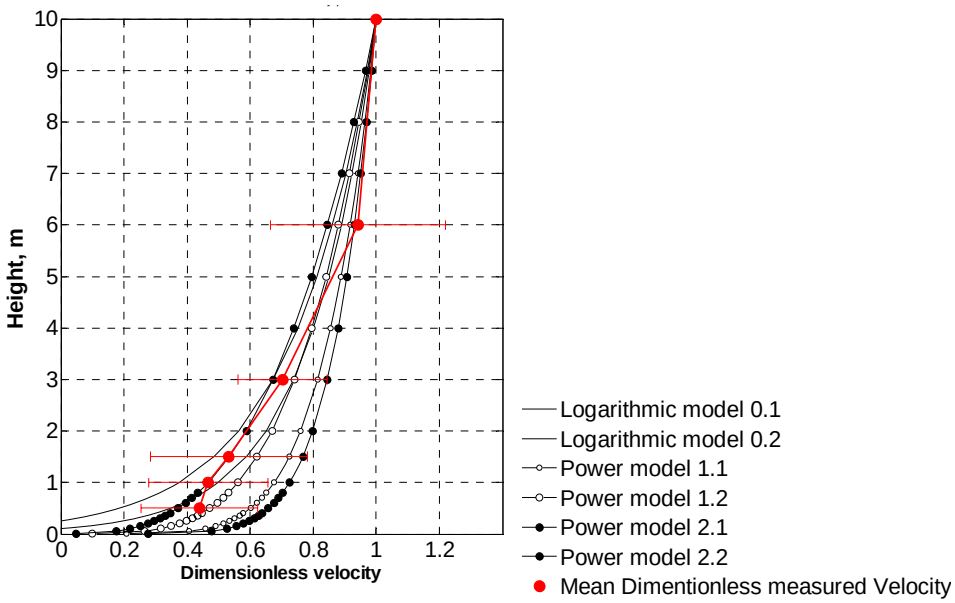

*Logarithmic model 0.1	– for high plants in an open country
Logarithmic model 0.2	– for country side and spread habitat
Power Model 1.1	– for an open flat country
Power Model 1.2	– for urban country
Power Model 2.1	– for an open terrain with scattered obstructions
Power Model 2.2	– for large city centres

Figure 5-1. Comparison of measured dimensionless wind speed profile with the mathematical models.

Experimental data for the vertical wind speed profile covers a measurement period from the 1st of June, till 1st of January (2007). This period includes various wind directions and wind speeds, see Figure 5-3. The wind rose is build for the wind speeds and wind directions measured at the height 10m above the ground.

The experimental data obtained for the wind speed measured at the height 0.5m was not included into the estimation of the mean vertical wind speed profile. The reason for that was a risk of measurement errors caused by close positioning of anemometer to the ground surface, and it is likely that the measured wind speed was overestimated due to increased turbulence at the ground.

The dimensionless wind profile, which is obtained experimentally for the local microclimate at 'The Cube', is described by a mathematical model in form of Equation 5-3. This equation represents the logarithmic model, where the roughness height is set to 0.16 (Equation 5-4). The form of the mathematical model and the model constants were estimated on the basis of the least square method, however the interrelation of the friction

velocity, V_*, and roughness height, h_o, has set the main constrains to their definition and the shape of the wind speed profile (Figure 5-2).

Equation 5-4

$$V(h) = \frac{V_*}{K} \cdot \ln\left(\frac{h}{0.16}\right)$$

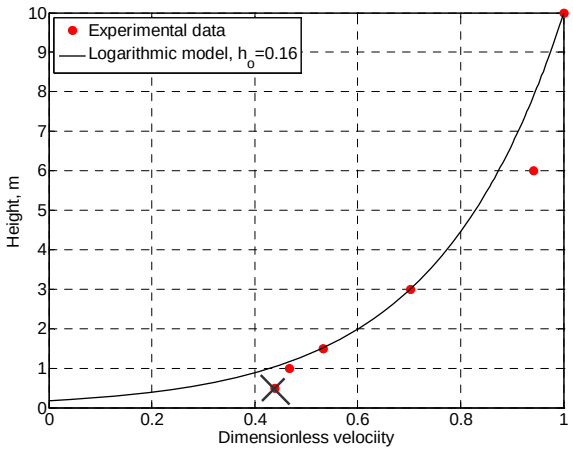

Figure 5-2. Plot of the measured dimensionless wind speed profile, for the reference velocity at the height 10 m above the ground.

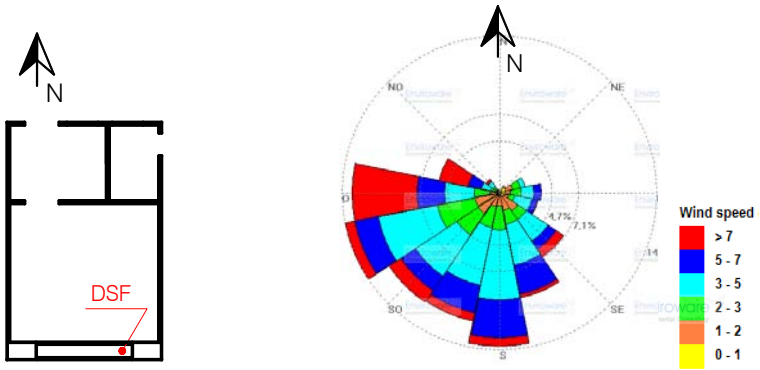

Figure 5-3. Wind rose for the period of wind speed measurements.

An impact of a wind direction on the shape of the wind speed profile is investigated. Originally, the eight sectors of wind direction with the corresponding wind speed were identified from the set of experimental data. The definition of the sectors is given in Table 5-4. A comparison of wind profiles for the dominating and less dominating direction is given below in Figure 5-4.

Sector	Wind direction, °*	Number of data points
1	1-45	36
2	46-90	494
3	91-135	1263
4	136-180	2094
5	181-225	2666
6	226-270	3019
7	271-315	1464
8	316-360	189

* Direction is given in degrees from North

Table 5-4. Definition of sectors for wind direction.

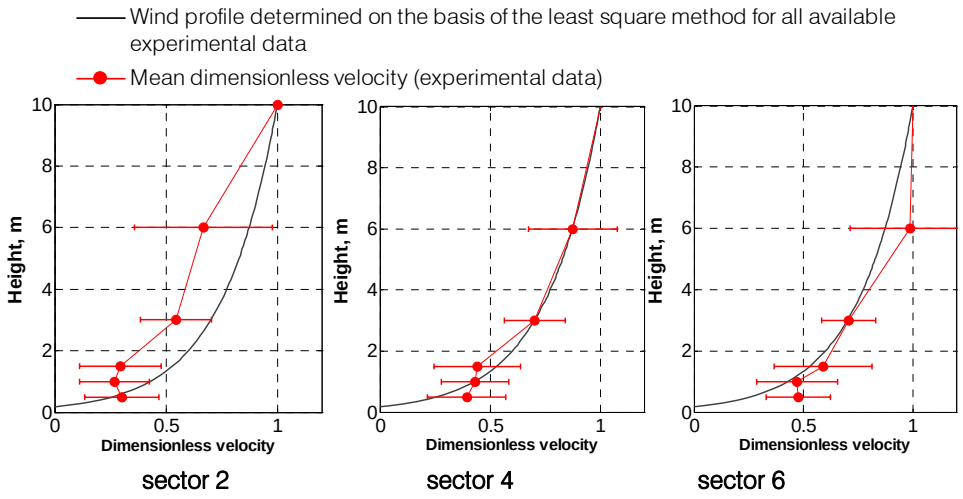

Figure 5-4. Wind profile in sector 2, 4, 6.

From the experimental results, it is obvious that the shape of the wind profile is different for the different wind speed directions (Figure 5-4). At the same time, the distribution of the data points between the 8 sectors of wind directions is highly uneven, it varies between 36 and 3019 data points per sector. Consequently, it is uncertain whether the wind profile changes due to the local landscape or due to the lack of experimental data.

5.3 CLIMATE AND THERMAL CONDITIONS IN EXPERIMENTAL ROOM

The experimental data is available for the test cases in the period from October to December 2006. In Denmark, this period of a year is characterized by a contrast in the day-time and night-time air temperature. Besides, in autumn the day-time outdoor air temperature is relatively law while the solar irradiation stays relatively strong. And finally, the weather conditions and the length of a day in October and December differ a lot.

For that reason, this section is meant to give an idea about the conditions characteristic for each test mode and the range of variation in weather conditions, while the plots of the climate data can be found in appendix. Periods with lack of climate data were replaced by data purchased from Danish Meteorological Institute.

In the Table 5-5 the climatic boundary conditions are divided into three groups, corresponding to each test mode.

MODE		Outdoor air temperature °C	Wind speed m/s	Diffuse solar irradiation W/m²	Total solar irradiation on horizontal W/m²
MODE 1	MIN	4.3	0.1	0	0
	MEAN	12.5	3.6	91*	175*
	MAX	19.5	14	302	554
	STD	2.8	2.5	64*	143*
MODE 2	MIN	-2.6	0	0	0
	MEAN	9.6	5.2	58*	89*
	MAX	17.1	20.8	261	372
	STD	4	3.7	46*	87*
MODE 3	MIN	0.4	0.55	0	0
	MEAN	7.5	5.2	36*	51*
	MAX	14.1	12.3	188	341
	STD	2.4	2.3	34*	57*

* Mean and standard deviation for solar irradiation is given only for the periods with sun.
Table 5-5. Statistical analysis of climate data for MODE 1, MODE 2 and MODE 3.

5.3.1 THERMAL CONDITIONS IN EXPERIMENT ROOM

Since the power supply in the experiment room were critical for completing of the empirical validation of the building simulation software in the Annex 34/43, subtask E, these were measured during the experiments. However, an accurate application of these results requires knowledge of the volume averaged air temperature in the experiment room. Moreover, the temperature variation was unacceptable. Thus, the air temperature was kept constant at approximately 22 °C.

In this section, the presence of vertical temperature gradients in the experiment room is analyzed together with the amplitude in air temperature variations.

The air temperature in the experiment room was measured with silver coated thermocouples placed on 4 stands in the experiment room. The thermocouple shielded from the solar radiation and ventilated by a minifan was located in the middle of the room. One of the stands 3 or 4 was always in the shadow of the side wall and the

thermocouples were not exposed to solar radiation, while stand 1, stand 2 and shielded-ventilated thermocouple were always exposed to solar radiation if there was any.

According to the temperature plots, the largest peaks of the temperature variation are observed in all ventilation modes for the stand 1 as it is located most away from the KE-low impulse ducts. In MODE 3 (supply ventilation mode, mechanical forces), the temperature variations are also large for stand 3 and 4, as they are located closer to the supply openings.

As an example, the measured air temperature during one day is plotted as a function of height in Figure 5-7. The figure also includes air temperature measured by shielded and ventilated thermocouple for comparison. According to the figure, night-time is characterized by a good correspondence of measured air temperature by all sensors, including the shielded and ventilated thermocouple. At day-time, air temperature measured on stands 2, 3 and 4 demonstrates differences between the readings at the different heights of approximately 0.5-1.5 °C, while readings from the shielded thermocouple do not change when compared to night time measurement.

Closer look at the readings from the shielded and ventilated thermocouple leads to an observation: according to the shielded and ventilated thermocouple, the air temperature kept by ventilation system was relatively constant, while bare thermocouple shows a swing in the periods with the direct solar access to the sensors (Kalyanova et al., 2007).

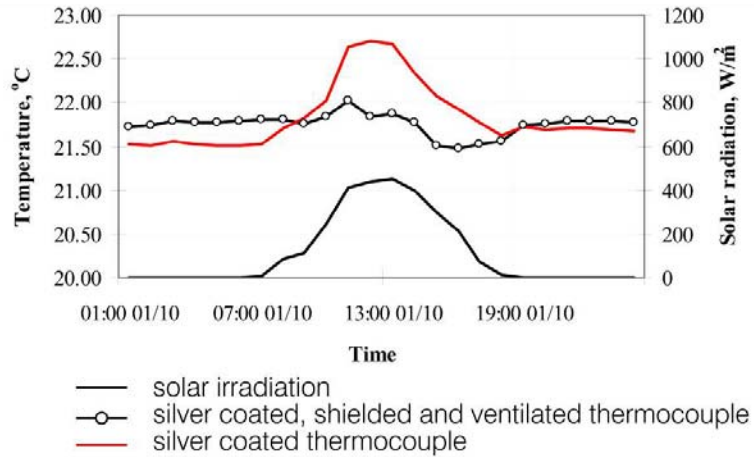

Figure 5-5.Results of application shielding technique from test case 2 and 5. (Kalyanova et al., 2007).

Due to lack of shielded and ventilated thermocouples in the other locations in the experiment room it is difficult to conclude on temperature gradients in the room. However the above figure demonstrates relative stability of air temperature in the room even under the load of solar radiation.

Temperature gradients in the experiment room are plotted in dimensionless form, in Figure 5-6, where the dimensionless temperature relates to temperature measured by the shielded and ventilated thermocouple:

Equation 5-5

$$t_{\dim} = \frac{t}{t_{fan}}$$

t_{dim} - dimensionless air temperature (in the experiment room), °C
t - temperature at a certain height, °C
t_{fan} - air temperature in the experiment room measured by silver coated thermocouple, shielded with a silver coated tube and ventilated by a minifan, °C

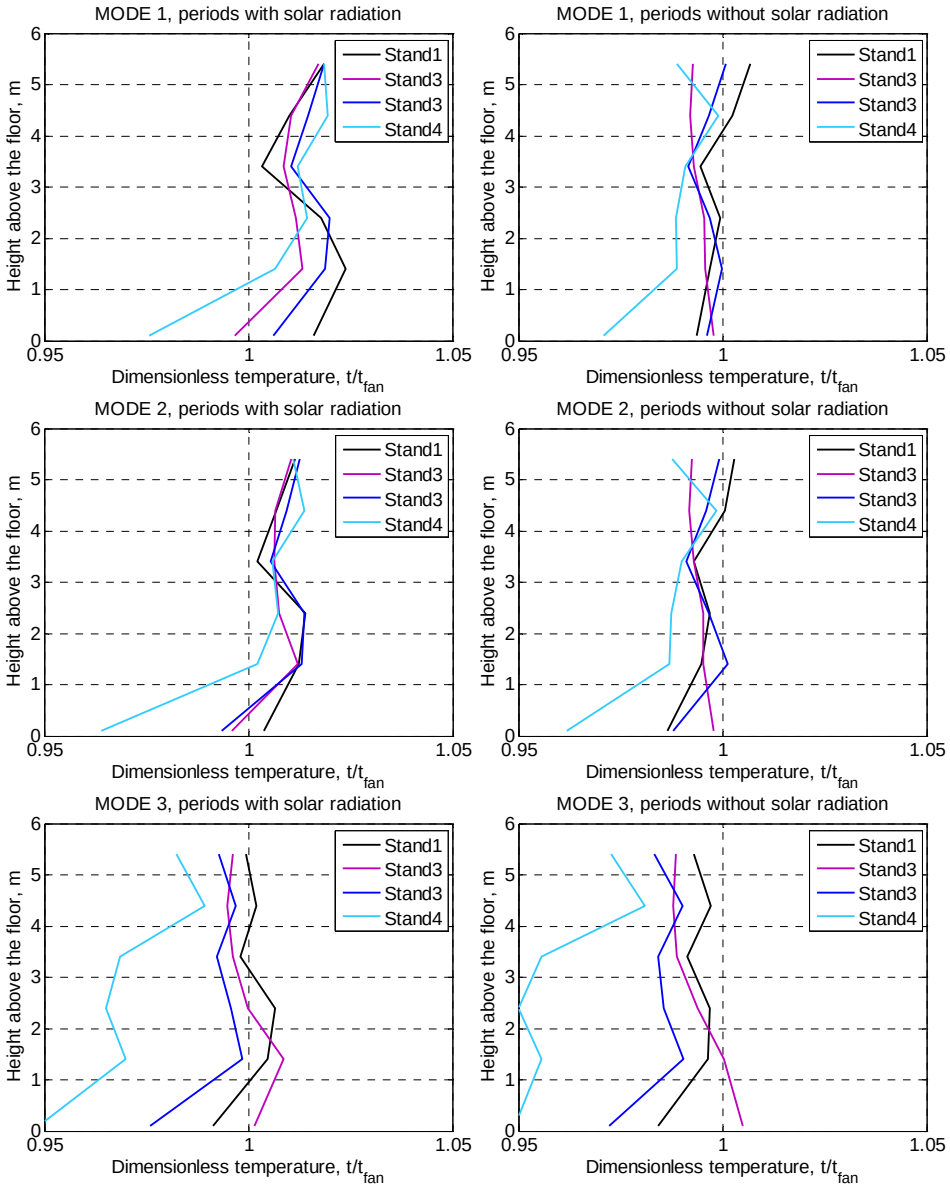

Figure 5-6. Measured dimensionless temperature gradient in the experiment room.

From the above figures the mean maximum gradient can be expressed as 6% of the temperature readings by shielded and ventilated thermocouple (6% corresponds to approximately 1.3 oC). This data has been statistically analyzed and the results are given in the Table 5-6. Although, some of the sensors could have been exposed to sun and may have lead to overestimation of the temperature in certain locations of the experiment room, the temperature gradients still appear to be relatively small.

Parameter	MODE 1	MODE 2	MODE 3
MIN, °C	21.13	20.97	20.05
Mean, °C	21.75	21.82	21.61
*MAX, °C	23.97	27.40	23.38
STD, °C	0.16	0.31	0.10

*Maximum values were obtained due to the external disturbances and must not be taken into consideration.

Table 5-6. Statistical analysis of the air temperature measured with shielded and ventilated thermocouple in the experiment room.

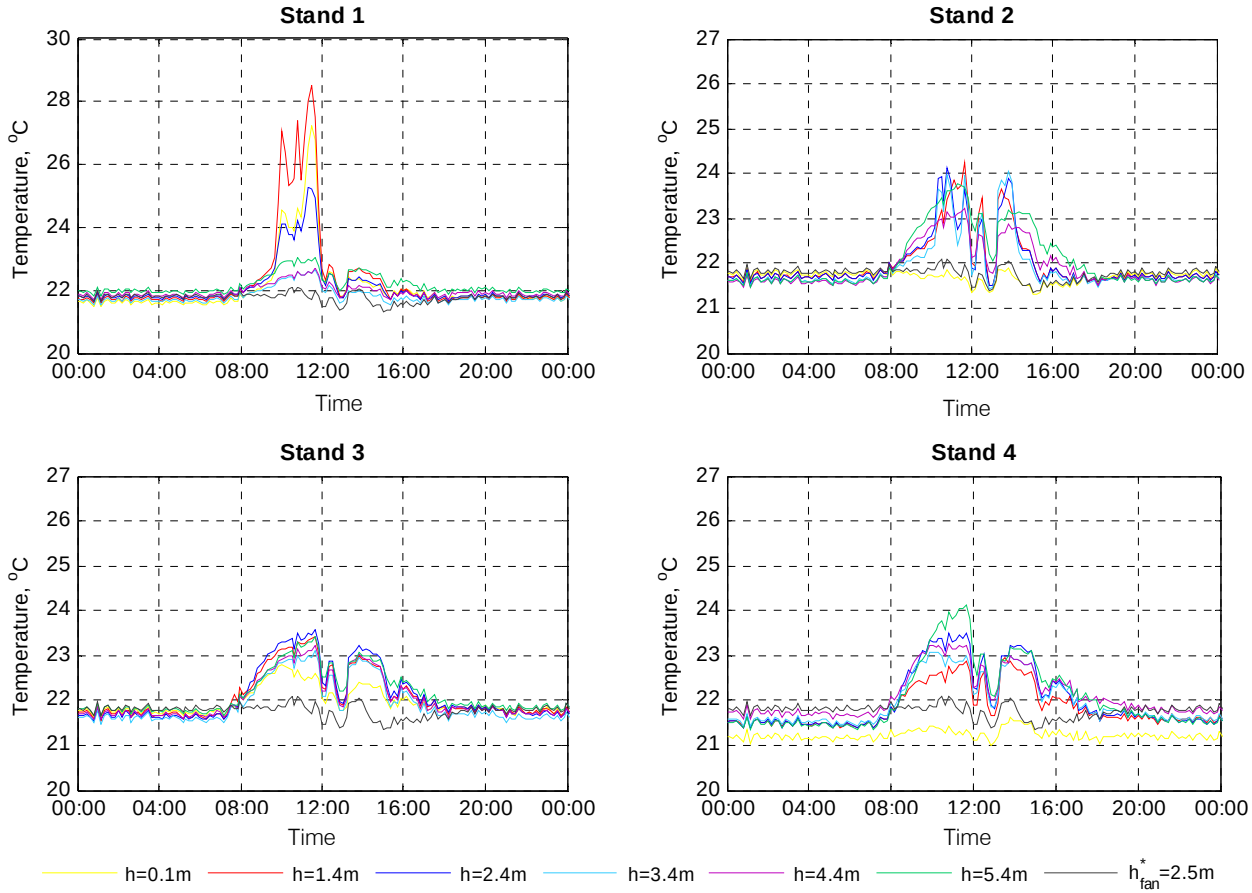

* Fan – is silver shielded and ventilated thermocouple

Figure 5-7. Air temperature measured in the experiment room on the Stand 1-4 on October, 5th.

5.4 TEMPERATURES IN DSF

When talking about the temperatures in the double-skin facade, there are normally a few groups of thermal parameters to consider, these are:

- The vertical temperature gradient in the cavity – this is a specific parameter that primarily tells about the combination of solar radiation that was prohibited from further penetration into the adjacent room and the strength of the buoyancy driving force in the cavity.
- The volume averaged air temperature in the cavity or the dimensionless volume averaged air temperature in the cavity that designates the general state of the double-skin facade cavity and its general performance.
- The raise of the air temperature when leaving the DSF cavity compared to the indoor and outdoor air temperature expresses its preheating efficiency and thus the overall performance of the DSF.
- The vertical temperature gradient of a shading device surface located in the cavity (if there is any) and the area weighted temperature of the surface reflect the combination of an amount of the prohibited solar radiation to the adjacent room and its amount removed by the cavity air.
- The vertical temperature gradient and the area weighted temperature of the glazed surfaces, which also reflect the amount of the prohibited solar radiation, similar to the surface temperature of the shading device. Moreover, the surface temperature of the inner pane of the internal window *(ii*) is an important contributor to the comfort criteria, such as an operative air temperature in the adjacent room and therefore this temperature reflects the DSF performance for the comfort point of view.

The parameters mentioned above represent the list of overall parameters that are used in the design and simulation of the DSF performance. Anyhow, this list can be expanded to any specific need.

Horizontal temperature gradients between the sections of the DSF cavity were investigated, these prove that there is no or only insignificant horizontal gradients existed between the sections during the measurements. Results of these investigations are not included into this report. Horizontal temperature gradient between outdoor skin and inner skin is not discussed in this thesis due to the lack of experimental data.

In this section, the experimental results for three operational modes of the DSF cavity will be illustrated and discussed. Most of the results will be reported using the groups of parameters mentioned in the list above. However, all experiments were completed without shading devices and no experimental data with application of shading devices is available.

5.4.1 VERTICAL TEMPERATURE GRADIENT IN DSF CAVITY

The dimensionless air temperature was used to investigate the vertical temperature gradients in the DSF cavity. The definition of it is given in Equation 5-6:

Equation 5-6

$$t_{\dim} = \frac{t - t_o}{t_i - t_o}$$

t - temperature in a certain point, °C
t_o - outdoor air temperature, °C
t_i - indoor air temperature (in the experiment room), °C

Here, the vertical temperature profiles are discussed only for MODE 1 and MODE 3, as in MODE 2 the DSF functions similar to a conventional window and it can be satisfying enough to deal with the volume averaged air temperature.

As explained in Kalyanova and Heiselberg (2007b), the air temperature in the DSF was measured in three sections at three different heights in section 1 and 3 and at six different heights in section 2.

For all sections, the measurements at the bottom of the cavity were at height 0.1m. Looking upon the dimensionless profiles (Figure 5-8) it is possible to observe that the air temperature measured at the bottom of the DSF is relatively high. This is one of limitations of experimental set-up, as the air to the thermal sensor was taken through the shielding tube in direction from floor to ceiling. Meanwhile, the distance between the shielding tubes and the floor was short and the floor surface was covered with a thick layer of black cables. As a consequence, the air approaching the thermal sensor was already heated up. Thus, the reader is asked to keep in mind that the slope of actual temperature gradient at the heights between 0.1 and 1.5 meter can differ from those illustrated in the following figures.

Even though the horizontal temperature gradients were not observed during the measurements, the differences in the shapes of the temperature profiles between the sections of the DSF cavity exist. The differences are characteristic for the profiles in sections 1 and 3 compared to the section 2. It is obvious that due to larger number of measurement points in section 2, shape of temperature profile in this section is more defined. Accordingly, temperature profiles from section 1 and 3 cannot be used in further studies, except for verification or comparison of thermal conditions between the sections.

Dimensionless temperature profiles of the mean values in Figure 5-8 are plotted for the whole set of the experimental data (•), for the periods with solar radiation (o), without solar radiation (*) and for the periods with solar radiation higher than mean (▲).

Prior to further examination of the temperature profiles it is worthy to have a look at the flow conditions in MODE 1 and MODE 3. The air flow rate in the latter case is mechanically driven and in an ideal situation, the flow motion is constant, well established and one directional. On the contrary, the air flow magnitude and flow direction in MODE 1 may vary a lot due to the scatter character of the natural wind and varying weather conditions. More to the point, the inlet/outlet openings during the experiments in MODE 1 were not controlled.

It is difficult to perform a general comparison of the temperature profiles between the modes, as solar radiation intensity in these two modes was essentially different. However, the shape of the temperature profile for MODE 3 is more defined and clear compared with MODE 1. During the experiments in MODE 1, the occurrences of reverse flow, wind washout effect and recirculation flow were experienced and most likely, these factors had an influence on temperature distribution.

There is no doubt that the temperature raise in the DSF cavity is highly correlated to solar radiation intensity, however this correlation is not direct, as it involves many other factors discussed in the section 5.4.2 . However, for MODE 1 that is characterised by high air change rates (above 50 h^{-1}) the increase of air temperature in DSF is evident when compare temperature gradients in periods with high (▲) and rather low (o) solar radiation intensity.

In the literature survey (section 6.2) it is explained that appearance of recirculation happens when solar radiation is strong. Recirculation can cause deformation of vertical temperature profile so, that maximum air temperature appears not at the top of the cavity. A similar to described shape of vertical temperature profile in the cavity is seen in Figure 5-8, MODE 1 for $I_s > I_{sm}$. This can be an indication of recirculation flow or a measurement error, caused by influence of wind washout effect.

In the later studies, it will be explained that wind washout effects depend on wind direction and its occurrence is explained by differences in pressure coefficients in-between SOL-openings or in-between SOH-openings. An additional examination of vertical temperature gradients in the cavity was carried out. The objective of this study was to investigate whether the reduction of air temperature in the cavity at h=5.5 m compared to air temperature at h=4.5 m is characteristic for certain wind directions. This would mean that the reduction of temperature is caused by wind washout and not by recirculation flow.

However, it appeared that the shape of vertical temperature profile for strong solar radiation is independent of wind direction.

When comparing the same plots for MODE 3, the impact of the solar radiation intensity gives the impression of being smaller, but this is partly because of fairly low solar irradiation for the whole period of measurements in MODE 3.

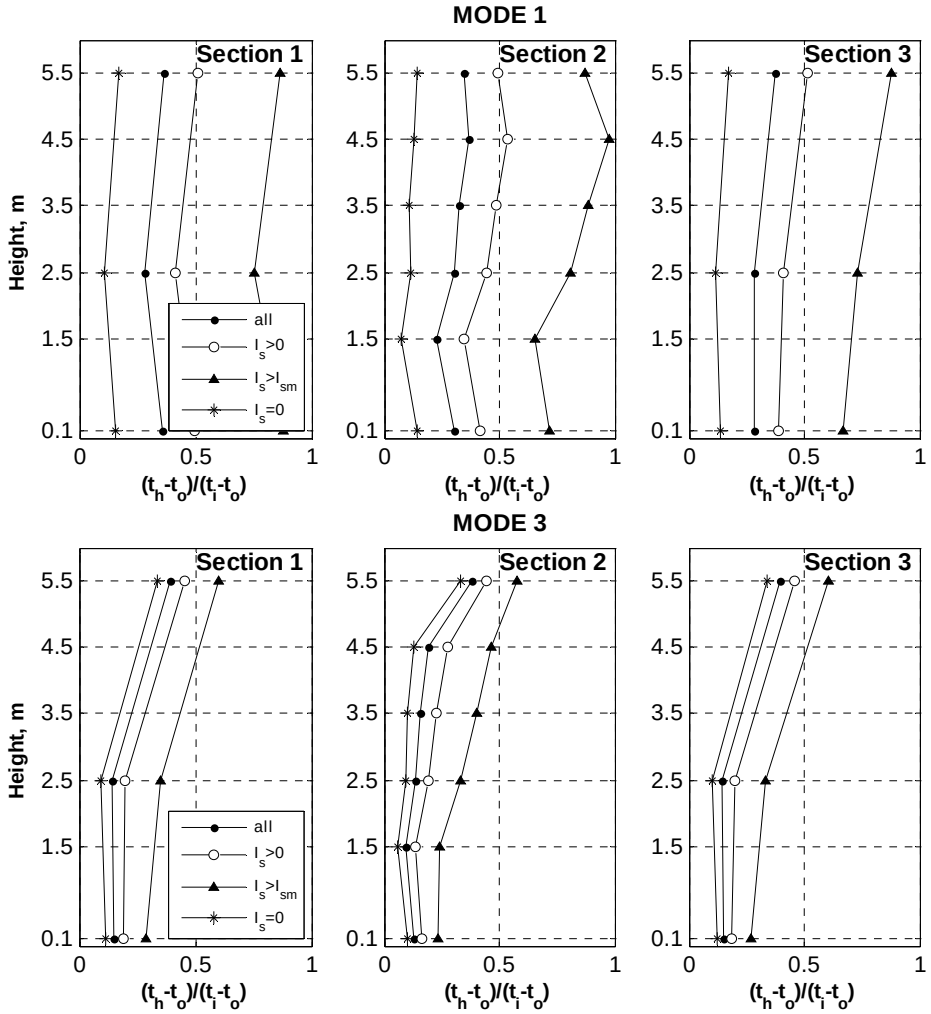

all – complete set of experimental data
$I_s>0$ - corresponds to the period with solar radiation
$I_s=0$ - corresponds to the period without solar radiation
$I_s>I_{sm}$ - corresponds to the period with solar radiation higher than mean

Figure 5-8. Dimensionless vertical temperature profile in MODE 1 and MODE 3.

5.4.2 VOLUME AVERAGED AIR TEMPERATURE IN DSF CAVITY

The air temperature in the double-skin facade cavity is related to absorbed solar radiation and the combination of the driving forces. With application of solar shading device in the cavity, the stack effect will increase, due to an additional amount of solar radiation captured in the cavity.

MODE 1

In the external air curtain mode, the mean volume averaged air temperature in the DSF cavity was 14.2 °C, for the periods with solar radiation it was 16.2 °C, while for the periods with solar radiation higher than mean it was 19.8 °C and for the night time periods it was 12.2 °C. The mean outdoor air temperature for the whole period of measurements was 12.5 °C.

When a double-skin facade cavity is naturally ventilated, the air temperature in the cavity is linked with the horizontal temperature gradients (convective flows at the surfaces) and the vertical temperature gradient that represents the strength of the buoyancy driving force. The wind speed, wind direction, pressure difference coefficients, etc. stand for the driving force generated by wind.

The direct correlation between air temperature and air flow rate in the cavity can be found if the buoyancy force is dominating. This will be investigated in the section 5.5 . In meantime, the relationship between the dimensionless air temperature in the cavity and solar radiation intensity is illustrated in Figure 5-9.

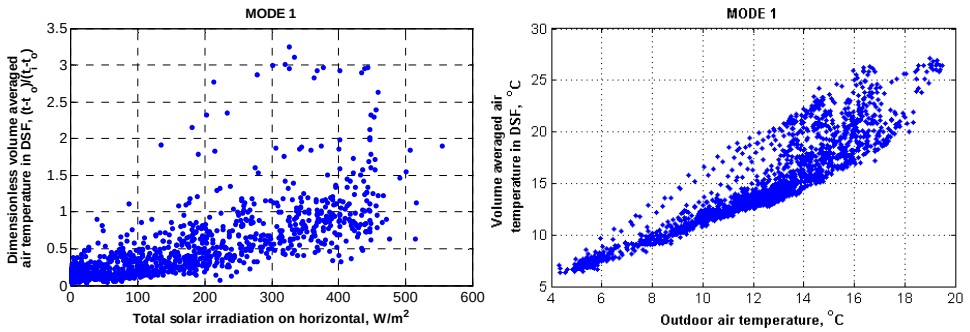

Figure 5-9. Volume averaged dimensionless air temperature in DSF cavity as a function of solar intensity (left). Volume averaged air temperature in DSF cavity as a function of outdoor air temperature (right).

In fact, the air temperature and thus the air flow in the DSF cavity does not depend on the amount of incident solar radiation, but on the amount of solar radiation that was absorbed by glazing and shading. This, however, depends on the form of incident solar radiation (direct or diffuse) and on the solar incidence angle.

Both the ratio of direct/diffuse solar radiation and the incidence angle vary in time and therefore the incident solar radiation cannot be directly linked to the air temperature, as there is no linear correlation between the incident and absorbed solar radiation. Also, the time constant of the DSF can have an impact. Then Figure 5-9 can only give an idea of solar conditions during the experiments and about DSF performance via the dimensionless air temperature.

Air temperature in DSF cavity as a function of outdoor air temperature is given in Figure 5-9. The results in the figure are different from results of earlier research because in present case the air temperature in the cavity is strongly correlated with the outdoor air temperature and not so sensitive to solar radiation intensity. Even for periods with intense solar radiation, the correlation between outdoor air temperature and air temperature in the cavity is still present. This is due to extremely high air flow rates and generally low solar radiation intensity.

MODE 2

Thermal buffer mode. When a double-skin facade is not ventilated, the air temperature in the cavity is mainly linked to the absorbed solar radiation. During the experiments in 'The Cube', the mean air temperature in the cavity was 14.9 °C, for the corresponding incident mean total solar irradiation 89 W/m^2 and outdoor air temperature 9.6 °C. Considering the periods with and without solar radiation, following mean temperatures were measured in the cavity 18.1 °C and 13.0 °C correspondingly.

Similar to MODE 1, Figure 5-10 demonstrates there is a strong correlation between the outdoor and cavity air temperatures. This is due to many cloudy days during measurement period. The correlation is uneven during the periods when there were some significant solar gains. All of it is also a reason why there is no correlation to be seen between the air temperature in cavity and solar radiation intensity. However the effect of thermal capacity is seen for periods of heating up and cooling down.

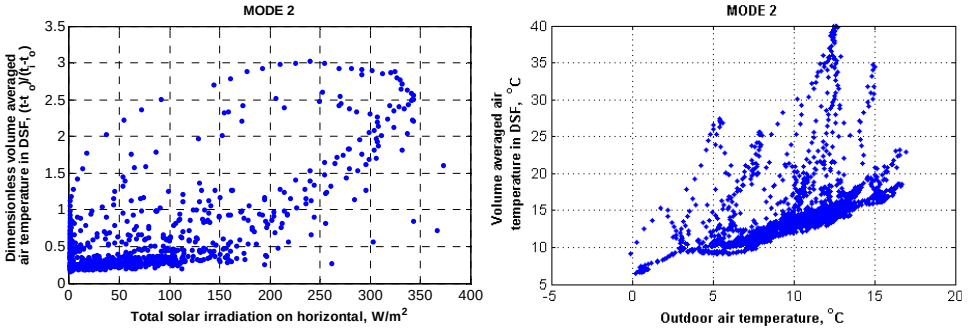

Figure 5-10. Volume averaged dimensionless air temperature in the DSF cavity as a function of solar intensity (left). Volume averaged air temperature in DSF cavity as a function of outdoor air temperature (right).

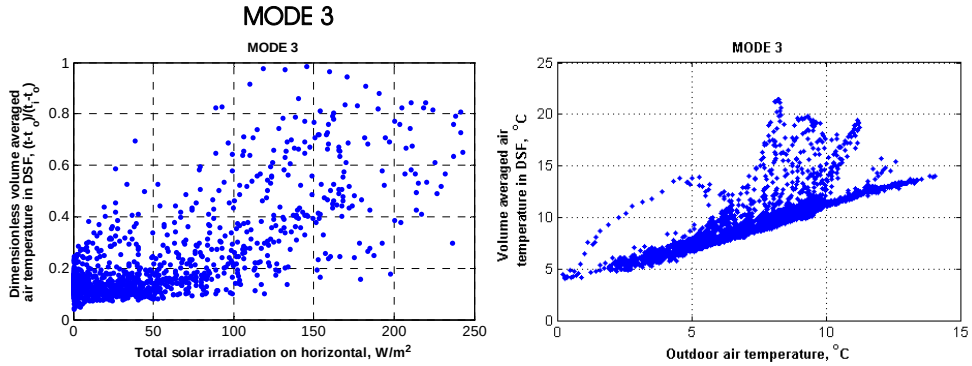

Figure 5-11. Volume averaged dimensionless air temperature in the DSF cavity as a function of solar intensity (left). Volume averaged air temperature in DSF cavity as a function of outdoor air temperature (right).

Preheating mode. When the mechanical forces are introduced to generate an air change rate in the cavity, the air temperature is closely related to the air flow rate and absorbed solar radiation. Since the cavity was mechanically ventilated and air flow rate was kept constant during the experiments, the absorbed solar radiation is the most important for the air temperature in the cavity.

The mean air temperature in the cavity during the preheating mode was 9.6 °C. In periods with solar radiation, the air temperature in the cavity was 10.5 °C. The mean outdoor air temperature for the whole period of measurements was 7.5 °C.

The air flow rate generated by the ventilation system was 143m^3/h, however, in section 5.6 it will be demonstrated that there were some periods when natural driving forces were dominating above the mechanical force.

These measurements were performed for the coolest season, with very limited solar radiation intensity. As a consequence, there is no or little correlation between cavity air temperature and solar radiation, but instead for cavity and outdoor air temperatures are

closely related for the most of the time. Only for periods with intensive solar radiation the correlation between outdoor and cavity air temperature disappears.

5.4.2.2 Surface temperature of glazing

The distribution of surface temperatures of the glazing is investigated via the dimensionless temperature. The dimensionless temperature was already introduced in the Equation 5-6, where *t,* defined as a temperature in a certain point. Though, in this section *t,* corresponds to measured glass surface temperatures in different locations.

The surface temperature of glazing was measured for three surfaces of the double-skin facade (*ei, ie, ii*) see Chapter 3.

Initially, the deviations between the DSF sections in measured surface temperatures were investigated and no differences were observed. Minor deviations were found when comparing the surface temperature profiles for two windows in the same section (for example BH2 and BH5).

Following Figure 5-12 illustrates the dimensionless temperature profiles plotted for the whole set of the experimental data (•), for the periods with solar radiation (o), without solar radiation (*) and for the periods with solar radiation higher than mean (▲).

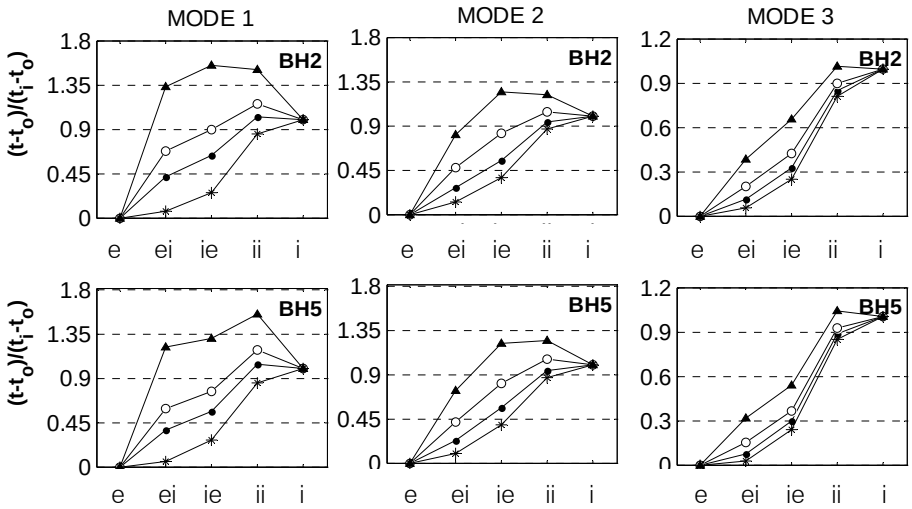

- for the whole set of the experimental data (•), for the periods with solar radiation (o), without solar radiation (*) and for periods with solar radiation higher than mean (▲).

- external ('e'), external window, facing the DSF cavity ('ei'), inside window facing the DSF cavity('ie'), inside window facing the experiment room ('ii'), indoor/experiment room ('i').

Figure 5-12. Dimensionless glass surface temperature profiles for MODE 1, MODE 2, MODE 3.

Looking upon the results in Figure 5-12, it is notable that in periods with solar radiation the ei-, ie- and ii- surface temperatures are relatively high, especially for MODE 1, which is characterized with the higher solar intensity. First of all, it means that a large part of solar radiation has not been removed with the cavity air and further on, this leads to an increased cooling demand in the adjacent room and poorer comfort level due to high temperature of the ii-surfaces.

The concern about the accuracy of the glass surface measurements was expressed earlier. However, considering the results for the periods without solar radiation (*), in

Figure 5-12, the raise of the external glass surface temperature (*ei*) is almost negligible compared to the outdoor air temperature at night. This is reasonable due to the relatively high heat transmission property of that glazing. This indicates that good contact was achieved between the sensor and the glass.

Glass surface temperature increases significantly compared to the outdoor air temperature in periods with present solar radiation, due to the absorbed solar radiation in periods with solar radiation (o) and (▲).

5.4.3 SUMMARY

Efficiency of DSF to preheat ventilation air (MODE 3) or to remove surplus solar gains (MODE 1) was not discussed in the previous sections. This is because no opening control was used and therefore the operation of DSF was not optimal for evaluation the efficiency. Instead, the main focus was set on investigation of DSF thermal performance using the dimensionless temperatures.

Unfortunately, monitoring of DSF performance in all modes took place in a period with very limited number of hours of intensive solar radiation. Consequently, thermal performance of DSF was not explored entirely. A slope of vertical temperature gradient in the experimental data is relatively small compared to published experimental results (Saelens, 2002). On contrary to publications (Takemasa et al. 2004; Marszal and Thomas, 2008) air temperature in the cavity in present experiments has stronger correlation with outdoor air temperature then with solar radiation intensity. Still, the vertical temperature gradient in the cavity occurred to be sensitive to solar radiation intensity.

In MODE 3 the maximum temperatures were measured at the top of the cavity. While in MODE 1, the maximum temperature in the cavity appears at height 4.5 m and not at the top of the cavity. It was argued that this might be due to wind washout effect. Otherwise, it might be an indication of recirculation flow appearance. An investigation of vertical temperature gradient in the cavity with regard to wind direction proved that temperature gradient in the cavity is independent from wind direction and the theory of wind washout influence does not apply.

Measurements of glass surface temperature indicate that surface temperate is sensitive to solar radiation. For periods with high solar intensity in MODE 1 the dimensionless surface temperature of inner (ie) and outer skin (ie) exceeds value of 1, and surface temperatures in the cavity are very high. Thus, a large part of solar radiation has not been removed with the cavity air and further on, this leads to an increased cooling demand in the adjacent room and poorer comfort level due to high temperature of the ii-surfaces. These high surface temperatures will result in a strong boundary layer flow, which is further discussed in Chapter 6.

5.5 MASS FLOW RATE IN DSF CAVITY, MODE1

The mass flow rate in the DSF cavity was measured using different methods, which principle is explained in the section 3.2.4.2 . Here the results of these measurements are discussed.

Besides the information about the mass flow in the DSF cavity, conduction of experiments using these measurement methods has contributed to knowledge about the flow conditions, flow pattern in the DSF cavity, convection at the surfaces, about the reverse flow and wind washout effect and many other issues that are normally difficult to deal with both in modelling and experiments. The above-mentioned issues will, among other things be discussed in this and following chapters.

5.5.1 EXPERIMENTAL RESULTS

The natural driving forces were responsible for the air flow in the cavity in the external air curtain mode, whilst the influence of the driving forces was limited by the opening size, shape and pressure losses in the DSF cavity.

Considering the combination of the wind forces and the buoyancy force, it is necessary to bear in mind that one of them can dominate over the other. In case of wind dominated forces, the behavior of the instant air flow in the cavity attains a scatter character, similar to wind behavior, due to the wind washout effects, wind pulsation and flow reversal occurrences. Whereas in the case of buoyancy domination, the *total* air flow in the cavity behaves steadier, since the temperature variation depends on solar irradiation and often is evened out. In that case occurrence of recirculation flow can cause disturbances.

First of all, it is necessary to mention that the mass flow rate in the tracer gas method was calculated for the atmospheric pressure, outdoor air humidity and volume averaged air temperature in the DSF cavity. Using the velocity profile method, the velocity profile was measured in 6 levels of the DSF cavity, and then the mass flow rate for each of these profiles was calculated on the basis of the atmospheric pressure, outdoor air humidity and air temperature in the DSF cavity at the height corresponding to the height of the velocity profile measurement. In the Figure 5-13, the mass flow rate for the velocity profile method is given as a mean value for all 6 levels.

The mass flow rate reported in this and all of the following chapters is calculated as a 10 minutes averaged value of 10 seconds scanning interval.

The measurement of the natural mass flow rate is very difficult and although the accuracy of the equipment is rather good, different measurement errors may appear and as a consequence the disagreement between the tracer gas method and velocity profile method is evident from the Figure 5-13.

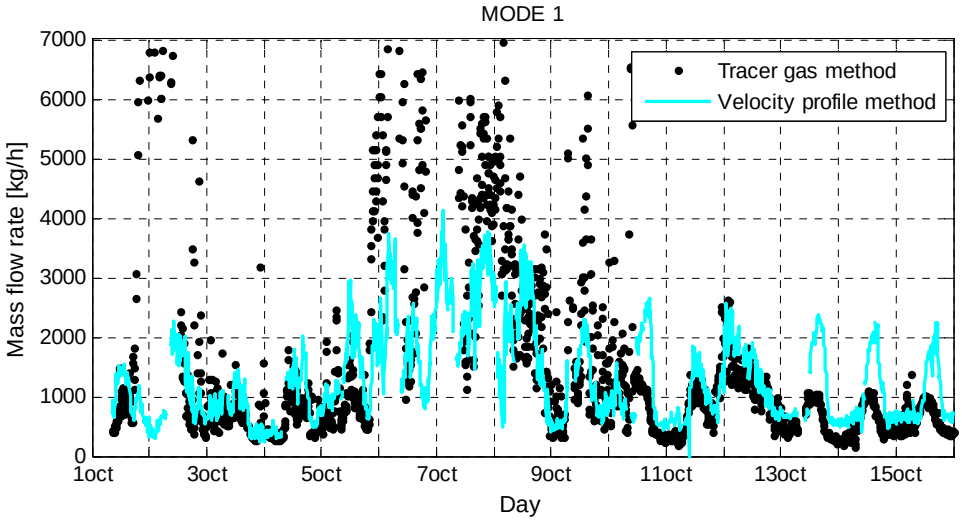

Figure 5-13. Mass flow rate in the DSF cavity, measured with the tracer gas and the velocity profile methods. MODE 1.

5.5.2 EFFECT OF NATURAL DRIVING FORCES

The stack effect, known also as a buoyancy force, is the force that generates the flow motion between two or more zones with different air densities due to the differences in temperatures and/or moister content.

It is common to assume that air flow in naturally ventilated cavities is buoyancy driven in summer, especially if a solar shading device is lowered in the cavity space. The solar radiation is then captured by the shading device, which emits radiation in all directions and also releases it to the surrounding air by convection. Finally the strength of the stack effect increases.

The kinetic energy of the wind changes into the potential energy (pressure) when it meets the obstacles. The windward surfaces are submitted to positive and leeward surfaces to negative pressure. Natural ventilation by wind is the air exchange between zones, caused by wind-induced pressure differences on the building facades that propagate into the interior of the building (Heiselberg, 2005). The distribution of wind pressure on the building is described with the pressure difference coefficients c_p.

Figure 5-14 and Figure 5-16 illustrates the different impacts of the driving forces on the mass flow rate in the cavity. The wind force is expressed by means of the wind speed and the buoyancy force by means of the dimensionless air temperature in the cavity. Furthermore, the dimensionless air temperature results for the night time period ($I_s=0$) and the period with the relatively strong solar radiation ($I_s>I_{sm}$) are split.

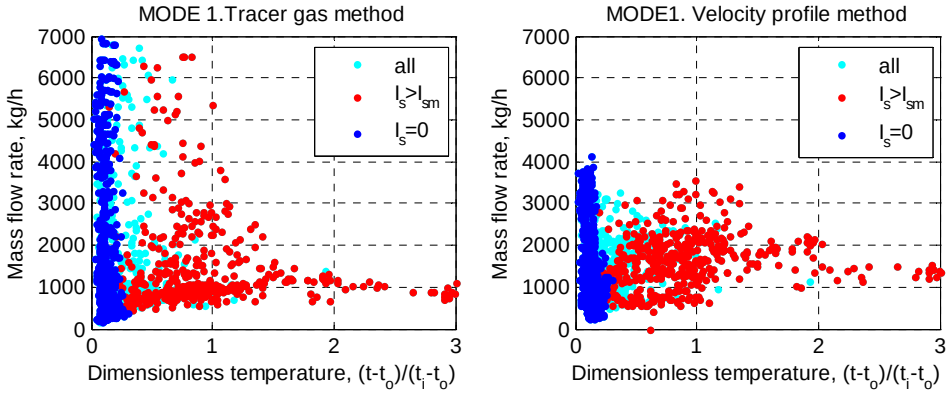

Figure 5-14. Correlation between dimensionless air temperature in the DSF cavity and mass flow rate in the cavity. MODE 1.

In the tracer gas method, it is obvious that the empirical results include measurement errors, primarily caused by the flow reversal or bad mixing, while in the velocity profile method, the measurement errors cannot be observed directly.

Looking upon the plots in Figure 5-14, it is evident that even for higher air temperatures in the cavity, it is still difficult to observe correlation between the mass flow in the cavity and air temperature.

In case of pure buoyancy, the mass flow rate in the DSF can be calculated if the discharge coefficients are exact. In report by Kalyanova and Heiselberg (2007b), these are estimated as 0.65 and 0.72 for the bottom and top opening correspondingly. The mass flow rate for conditions of pure buoyancy are estimated in correspondence with experimental conditions and illustrated in Figure 5-15. It is remarkable that the manual calculations are in good agreement with the lowest mass flow rates obtained experimentally. Still, the foremost part of experimental data available is located above the analytically obtained values for the buoyancy originated flow.

Another interesting matter to be pointed out is the choice of the discharge coefficients for the calculations in Figure 5-15. Correspondence between estimated and experimentally obtained data gives some level of confidence in achieving correct results using the discharge coefficients obtained experimentally in a wind tunnel.

When considering Figure 5-15(left), one may suspect that resistance of openings in the cavity is too high. This is due to the scale of the left plot in the figure. Looking upon Figure 5-15 (right), it is seen that except for a few points the mass flow rate in the cavity increases with increase of dimensionless temperature.

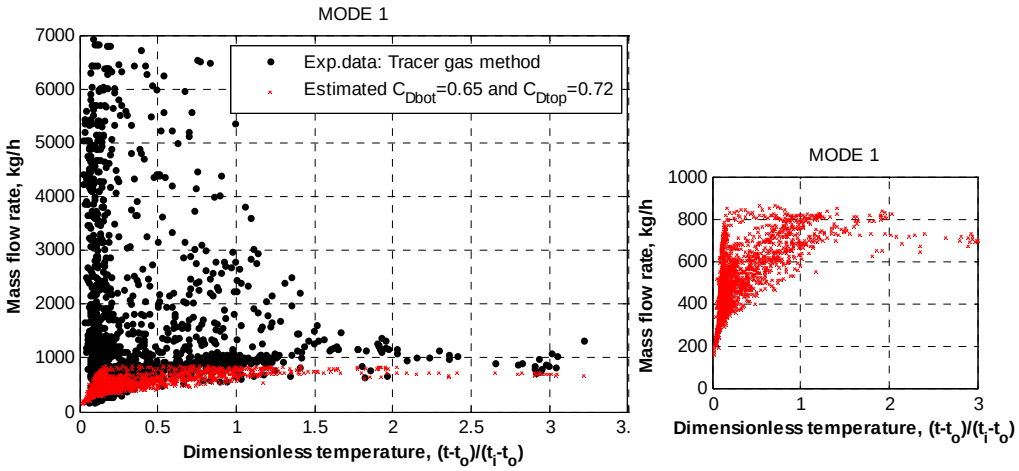

Figure 5-15. Estimated mass flow rate in the DSF cavity for pure buoyancy natural ventilation. MODE 1.

In both sets of the experimental results (tracer gas and the velocity profile methods) the high mass flow rates are characterized by a higher wind speed (Figure 5-16).

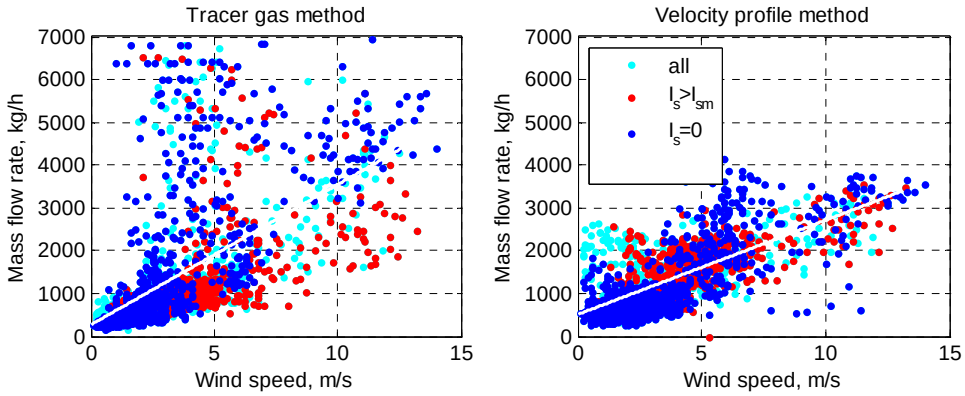

Figure 5-16. Correlation between mass flow rate in the in the DSF cavity and wind speed. MODE 1.

The only conclusion can be drawn, that the greater part of the experimental data is available for the wind dominated natural ventilation or a combination of wind and buoyant forces. However, as demonstrated in Figure 5-15, it doesn't mean that there were no periods with the buoyancy dominated natural ventilation.

Further, in order to investigate strength of the buoyancy and strength of the wind driving forces separately, the mass flow rate is plotted as a function of wind speed and dimensionless air temperature in the DSF cavity in Figure 5-17 and Figure 5-18. The dimensionless air temperature in these figures is divided into three groups in order to identify conditions for buoyancy dominated natural ventilation in the empirical results:

- Negative dimensionless temperature, $t_{dim}<0$
- Moderate temperature difference between indoor and outdoor, $0\leq t_{dim}<0.8$
- Relatively high temperature difference between indoor and outdoor, $t_{dim}>0.8$

From Figure 5-17 it is seen that for the low wind speed (0-2m/s) and high dimensionless temperatures ($t_{dim}>0.8$) mass flow rate in the cavity is relatively constant. For moderate wind speed (2-3 m/s), more experimental errors are present. However the range of the

mean flow rate for the high dimensionless temperature is almost the same as for the low wind speed (apx. 900 kg/h). Moreover, the mass flow rate is nearly constant and thus independent from the wind speed. In the last plot, with the higher range of wind velocities (4-14 m/s) the mass flow rate has a scatter character and no consistency of the results can be observed.

A similar situation is observed for the velocity profile method (Figure 5-18), but it is still different, especially looking upon the spread of the flow rates for $t_{dim} \geq 0.8$ and wind speed 0-4 m/s. Meanwhile, for the wind speed above 4m/s, there is a clearer dependency between the mass flow rate and wind speed, which isn't seen in tracer gas method plots.

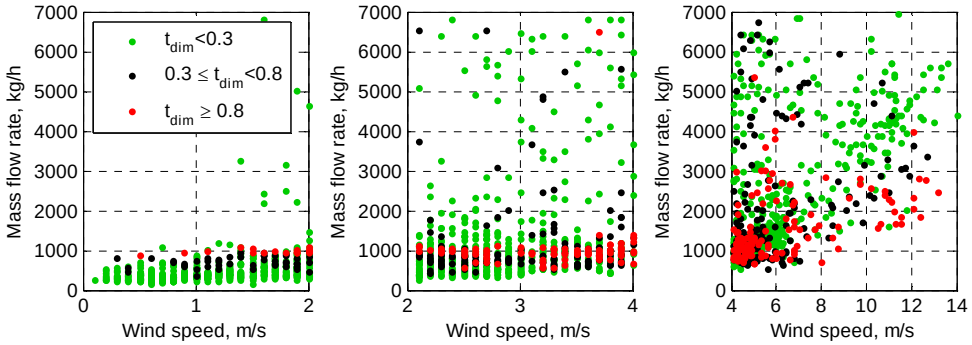

Figure 5-17. Effect of wind speed and air temperature on mass flow rate in DSF. Tracer gas method. MODE 1.

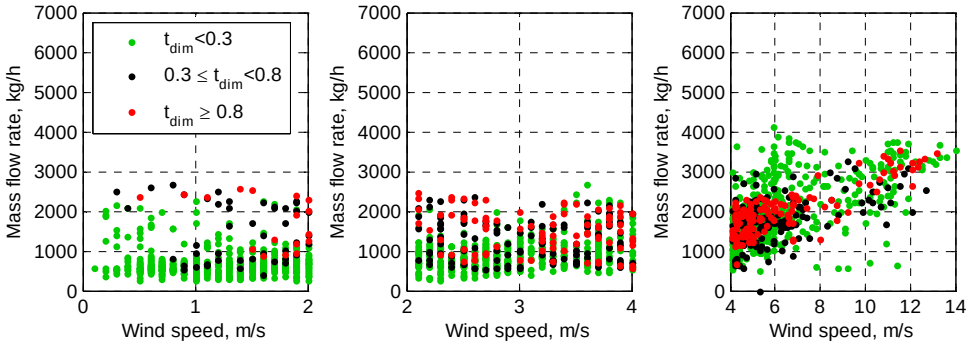

Figure 5-18. Effect of wind speed and air temperature on mass flow rate in DSF. Velocity profile method. MODE 1.

To outline Figure 5-17, it is necessary to draw attention to the fact that mass flow rate, plotted with the red spots ($t_{dim} \geq 0.8$) stays constant with the wind speed up to 4m/s. Consequently these are the results obtained for the buoyancy dominated natural ventilation, while for wind speed above 4m/s, the driving force in the cavity was resulting from wind forces or combined forces. And the greater part of the experimental data is available for wind dominated or combined natural ventilation.

A similar observation was made by Larsen (2006) when measured air flow rate through an opening in a wind-tunnel (single-sided natural ventilation). With increase of wind speed up to 5 m/s effect of buoyant forces on the air flow rate through the opening was estimated as close to none-existing.

This outline, however, causes two disagreements. First one is an existing general assumption about the buoyancy driven natural ventilation in DSF. This disagreement, in the first place, is caused by lack of a shading device in the DSF cavity, which normally

functions as an additional heat source in the cavity and correspondingly helps to generate higher vertical temperature gradients.

The second disagreement is the occurrence of the wind dominated or combined natural ventilation for the external air curtain mode in the double-skin facade (natural ventilation principle in this mode is categorized as single-sided natural ventilation on different levels) and the DSF openings are subjected to nearly the same wind generated pressure ($\Delta c_p \approx 0$).

Taking into account the significance of the wind forces in the experimental data attention is paid to the pressure coefficients c_p in the following section.

In Figure 5-19 it is demonstrated that the major part of the measurement errors is characteristic for approximately Southern wind direction (apx.180°, wind is towards the DSF). The South wind directions are also characterized by $\Delta c_p \approx 0$, thus the main reason for these measurement errors was probably the instability, when the smallest change in the wind pressure at the top or bottom opening could reverse flow or cause multiple wash-outs.

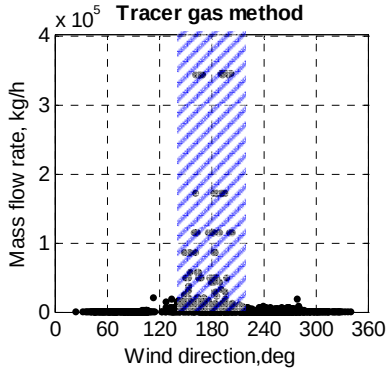

Figure 5-19. Effect of South wind direction on the mass flow rate in the DSF cavity. Tracer gas method. MODE 1.

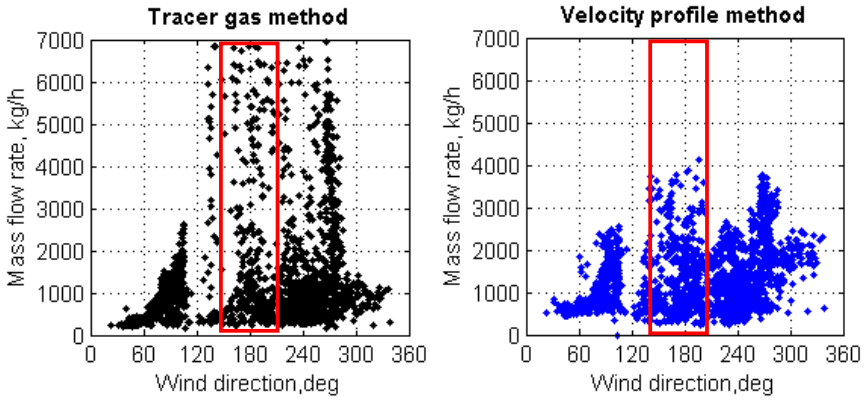

Figure 5-20. Effect of wind direction on mass flow rate in the DSF cavity. Tracer gas method (left). Velocity profile method (right). MODE 1.

From Figure 5-20 it is seen that air flow increases with Southern wind directions for both of measurement methods. This indicates that not only the measurement errors take place for these wind directions, and the flow rate for Southern wind directions, in fact increases.

This, however, causes a contradiction with the commonly used theory of the wind pressure coefficients for estimation of wind generated natural driving forces, as for $\Delta c_p \approx 0$ the wind forces in practice become disregarded.

Meanwhile, increase of mass flow rate is seen in left and right Figure 5-20 for 90 and 270 degrees of wind direction. In Figure 5-21 these wind directions are characterized with the maximal differences in pressure coefficients between the openings (Δc_p). This is one more indication of properly chosen wind pressure coefficients for the test facility, but also an indication of reasonable measurement results of naturally induced air flow in the cavity.

Wind pressure coefficient C_p

The wind pressure coefficients were not measured during the experiments, however the experimental data is available for a building of the same external geometry as 'The Cube', located in an open flat country, in Straw (2000) and Richards et al. (2001). In this literature the plots are available for the C_p-values measured in a number of points along a vertical central line of the building (illustration by the blue line in the Figure 5-21 (left), for different wind directions.

The C_p-values for the corresponding height of the openings in 'The Cube' were extracted from the plots in these publications and the missing points were taken from the results of CFD simulation in Straw (2000). In Figure 5-21 it is assumed that the C_p-values for all tree top openings of the DSF cavity are always identical. The same is valid for the bottom openings.

- *– location that was used to extract the C_p-value for the top (SOH) and the bottom(SOL) openings in the DSF*
- *- location of the measurements of pressure difference coefficient*

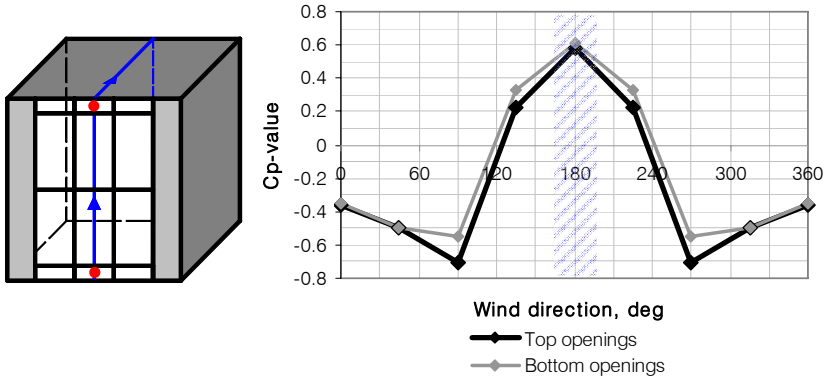

Figure 5-21. Left- location of the measurements of pressure difference coefficients at Silsoe research institute (Straw, 2000). Right- c_p values for the South facade of 'The Cube' for different wind directions, extracted from Straw (2000) and Richards et al. (2001).

Figure 5-21, again demonstrates small differences between pressure coefficients on the same surface $\Delta c_p^{max} = 0.16$. Still, the c_p-values have a significant impact on the total mass flow rate in the cavity, as earlier it was argued that the majority of the measurement data is available for the wind dominated or combined natural ventilation. For that reason it is necessary to keep in mind that the choice of proper pressure difference coefficients when modelling the DSF performance is extremely important. Moreover, underestimation of the flow rates in the DSF cavity may take place for the wind directions towards the facade openings, as explained in section Error! Reference source not found..

Buildings with a DSF are commonly built as multistory high raise buildings, and therefore the distribution of pressure difference coefficients along the surface can be significantly different from the ones in 'The Cube' partly due to larger surface areas, different shape and partly due to the differences in wind profiles.

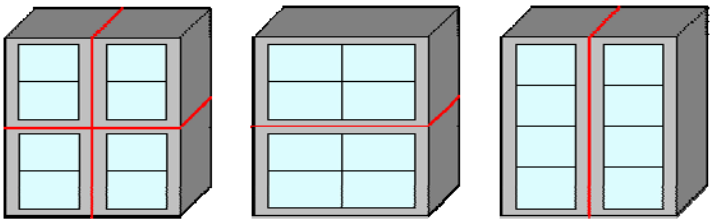

Figure 5-22. The key partitioning principles of the DSF cavity: box type (left), corridor type (centre) and shaft type (right).

Generally, the distribution of the c_p-values on the surface of any building depends on location of the wind stagnation point (C_p=1), from which the parallel flow along the building surfaces is originated, Figure 5-23, Sandberg (2005). Nevertheless in the DSF building, the location of the stagnation point in combination with the partitioning principle of the double skin facade (Figure 5-22) can cause significantly different Δc_p in the different 'boxes', 'corridors' and 'shafts'. Thus the air flow in different compartments of DSF will be different, even if they have the same orientation.

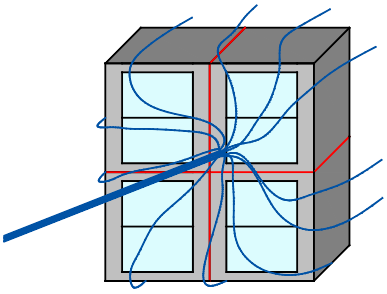

Figure 5-23. Illustration of the stagnation point flow.

For the empirical validation of building simulation software in MODE 1, the pressure difference coefficients were used as in Figure 5-21. The night time ventilation of the cavity was wind driven. Results of the simulations demonstrate that most of the software tools were able predict the night time air change rate using the specified c_p-values and the results of simulations are in a good correspondence with the experimental results (section 4.5.3). Accordingly, the choice of the c_p-values was reasonably accurate.

5.5.3 MASS FLOW RATE IN THE VELOCITY PROFILE METHOD

In the section 6.2 , it is explained that the boundary layer flow in the DSF cavity can be very strong and the deformation of the velocity profile can take place. Accordingly, the overestimation of mass flow rate can occur when using the velocity profile method, due to increased velocities in the boundary layer and the recirculation flow appearance.

The boundary layer thickness increases with the distance from the entrance plane and with increase of surface temperature. During the measurements, some the velocity sensors were placed near window panes (section 3.2.4.2) that is in the field of the boundary layer flow. Since the velocity profiles in the DSF cavity were measured at six different heights, the error due to the buoyancy in the boundary layer will increase with height of the velocity profile measurement. This is investigated in the Figure 5-24.

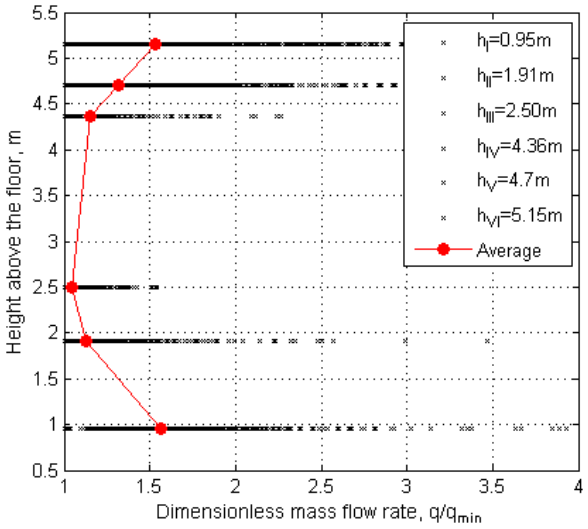

Figure 5-24. Dimensionless mass flow rate in the DSF cavity, measured at the different heights, using the velocity profile method.

In Figure 5-24, the mass flow rate in the cavity is dimensionless, where the value of 1 corresponds to the minimum air flow rate measured with one, out of six velocity profiles.

The figure demonstrates that actually the mass flow rate at the bottom of the cavity is not minimal. This is due to the bending of the jet when entering the cavity and wind wash-out effects. The dimensionless mass flow rate at the height of 2.5 m is close to 1. This is due to close location of measurement equipment to the window frame, which destroys the boundary layer flow and the shape of the velocity profile (Figure 5-25). Again, after passing the window frame at height 2.5 m, the development of the boundary layer should begin, as it is seen in Figure 5-24 for height 4.36 m and further up to 5.15 m.

As a consequence, in order to minimize the influence of the boundary flow, the mass flow rate in the DSF cavity should be calculated on the basis of the velocity profile at the height where the air flow is measured to be minimal and thus at height 2.5 m. However, at this height, there is a lack of measurement data and therefore measurements on height 1.91m will be used instead.

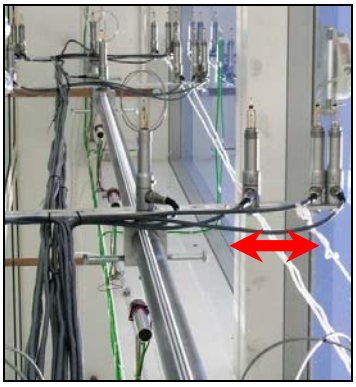

Figure 5-25. Distance from the glass pane to the edge of the frame in the DSFcavity. View from the bottom of the cavity towards the ceiling.

Comparison of the experimental results obtained with the tracer gas and velocity profile method is done in Figure 5-26, for the velocity profile measured at the height 1.91 m. Previously the mass flow rate, measured with the velocity profile was reported as a mean value for all six measurement heights (Figure 5-13).

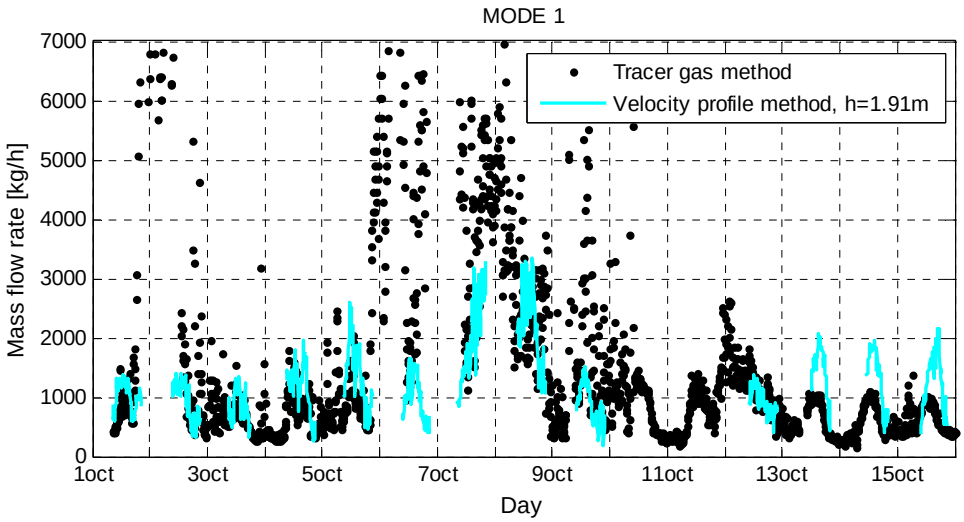

*The mass flow rate measured with the velocity profile method is plotted for the velocity profile measured at 1.91m height.

Figure 5-26. Mass flow rate in the DSF cavity, measured with the tracer gas and the velocity profile (h=1.91 m) methods.

From the figure, it can be seen that from the 11th of October, the velocity profile method again predicts higher mass flow rates in the cavity during the daytime. For the night time periods the mass flow rate for the velocity profile method at the height 1.91 m is unavailable, as well as for many other periods. Thus the evaluation of the simulation results upon the experimental data is difficult.

Finally, considering the potential impact of the boundary layer flow on the accuracy of the velocity profile method for deducting mass flow rate in the cavity, it is recommended to use the tracer gas method, as more simple and reliable one. In case if the velocity profile is to be used for future measurements, caution must be paid to:

- The number of velocity sensors in a plane, for accurate approximation of the velocity profile
- Positioning of the velocity sensors in relation to the surrounding surfaces
- Measurement of the velocity profile closer to the entrance pane, where the impact of the boundary flow is minimal
- May be allocating some obstacles to destroy the boundary layer flow

5.5.4 SUMMARY

In this chapter, results of full-scale measurements of naturally induced air flow in DSF cavity are examined.

These results were obtained with the tracer gas method and velocity profile method. Both of them have sources of error and compared to laboratory conditions have relatively large uncertainties. Still, reasonable agreement is seen between the results.

On contrary to literature, it is found that the mass flow rate in DSF cavity was wind driven for the most of time. This observation is a contradiction to common assumption of buoyancy driven flow in the cavity. Only for the moderate wind speed (below 4 m/s) the air flow was dominated by buoyancy, similar to findings made by Larsen (2006) for single-sided ventilation.

Along, it must be mentioned that pressure difference coefficients were found in the literature (section 5.5.2). When analyzing influence of wind direction on flow rate in the cavity, it is noticed that for wind directions which correspond to maximum Δc_p, measured mass flow also increased. This is, in some way, confirms reliability of experimental data.

Measured air change rate in the DSF cavity is enormous even with small differences in pressure coefficients between the openings. Aforesaid that natural ventilation in the cavity is dominated by wind. Accordingly, accurate estimation of pressure and discharge coefficients is essential for prediction of DSF performance with naturally ventilated cavity.

Using different schemas for compartmentalization of DSF cavity in high-raise buildings will normally result in situation when the mass flow rate is significantly different between the compartments, as it will highly depend on location of stagnation point on building surface.

Mass flow rate induced by buoyant forces in cavity is analytically estimated using experimentally obtained discharge coefficients for the DSF openings. Analytical and experimental results are in good agreement. This indicates use of appropriate discharge coefficients in this work.

Mass flow rate in the cavity estimated using the velocity profile method is significantly different when measured on different heights in DSF cavity. Moreover, it is increasing with height. This is argued to be due to strong boundary layer at the surfaces in the double-skin facade cavity causing recirculation flow. The recirculation is explained as buoyant forces in the boundary layer which become dominant over the bulk flow in the cavity, this is explained in detail in Chapter 6. However, no clear evidences for flow reversal are available, as wind washout can have a similar effect on measurement results.

In the earlier sections it is also argued that only one velocity sensor for estimation of the air flow rate in the cavity is unacceptable simplification, as the velocity profile varies a lot across the cavity.

Significant improvement of measurement results would be achieved with proper visualization technique for flow pattern in the cavity. This would allow verifying the presence of recirculation flow, impact from wind washout effect and conditions for its appearance. It is also necessary to use for identification of the best position to supply tracer gas and locations where it is best to measure the dilution of it. Finally, it would be possible to evaluate mixing of tracer gas with incoming air using visualization. However, most of visualization techniques are incompatible with solar exposure.

5.6 MASS FLOW RATE IN DSF CAVITY, MODE 3

Contrary to MODE 1, in MODE 3 the air flow in the DSF was originated from the mechanical driving force. A fan extracted air from the DSF cavity through the experiment room. The extracted mass flow rate was kept constant and measured with an orifice, the velocity profile method and the tracer gas method.

The volume flow extracted by the fan was 143 m^3/h, which is then translated into the mass flow rate according to the local conditions. Despite the fact that the mass rate extracted by fan was constant, experimental results demonstrate that the natural driving forces were still involved.

First of all, it is necessary to mention that the mass flow rate in the tracer gas method was calculated for the atmospheric pressure, outdoor air humidity and volume averaged air temperature in the DSF cavity. Using the velocity profile method, the velocity profile was measured in 3 levels of the DSF cavity, and the mass flow rate for each of these profiles was calculated. In Figure 5-27, the mass flow rate for the velocity profile method is given as a mean value for all 3 levels.

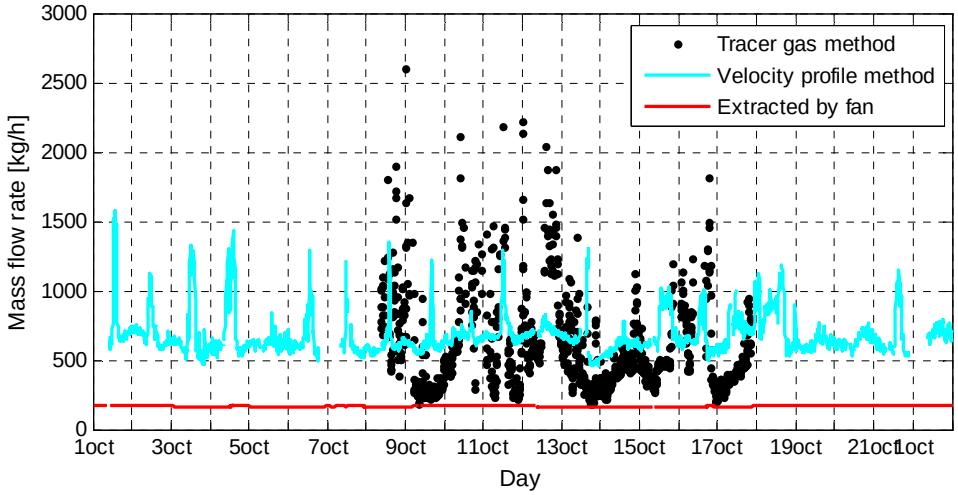

Figure 5-27. Mass flow rate in the DSF cavity estimated with the tracer gas method and the velocity profile method. MODE 3.

From Figure 5-27 it is obvious that either the measured mass flow rate is inaccurate or the natural driving forces were still involved. Only for the short time intervals the flow rate obtained with the tracer gas method is in the same range as the flow rate extracted by fan (17 November, 19 November, etc).

As can be seen in the Figure 5-28 for the Southern wind directions and relatively high wind speed, the mass flow rate in the cavity is increased. This indicates the impact of natural driving forces.

The experimental data obtained with the tracer gas method is also more reliable in MODE 3, as the occurrence of the total flow reversal is very unlikely in this case. Figure 5-28 one more time denotes the impact of the wind forces and although the orifice must have ensured high pressure losses in the duct system, the experimental data is proving the opposite. This is also possible, if the exhaust fan was not connected tightly with the duct system.

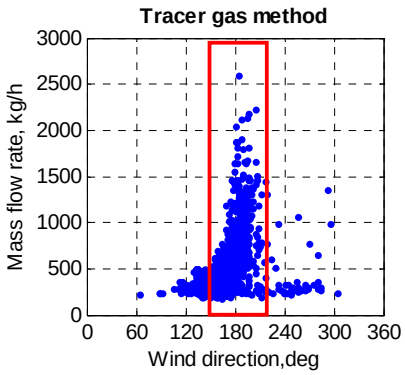

Figure 5-28. Effect of wind direction on mass flow rate in the DSF cavity. Tracer gas method. MODE3.

Experimental results obtained for this mode cannot be regarded as accurate and therefore they will not be discussed further.

5.7 COOLING/HEATING POWER IN EXPERIMENT ROOM

Power supply to experiment room is an overall parameter that represents thermal and energy performance of double-skin facade. Figure 5-29 illustrates a correlation between cooling/heating power to experiment room and solar radiation intensity for all three measurement modes.

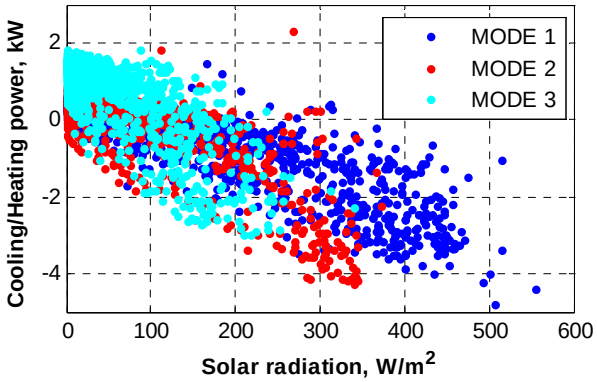

Figure 5-29. Cooling/Heating power to experiment room as a function of global solar radiation.

It is reasonable that for naturally ventilated cavity (MODE 1), a significant part of solar gains is removed together with cavity air. As a result, cooling power will be minimal compared to MODE 2 and MODE 3. MODE 3 (preheating mode) is sensitive to solar radiation intensity, as all solar gains captured by cavity are being delivered to experiment room. IN that perspective MODE 2 is similar with MODE 3. This is confirmed in Figure 5-29, where the slope for MODE 1 is less then for MODE 2 and MODE 3.

It is also seen that need for cooling arises even at very low solar radiation intensity. Thus using a proper shading devise will be inevitable when designing a double-skin facade building.

In Figure 5-30, a 24 hour period with strong solar radiation is shown for each mode of DSF operation. In each plot power supply to experiment room almost immediately follows the peaks of solar radiation and storage ability of experiment room doesn't seem to have any influence.

Changes of the air temperature in the cavity are more slow and in MODE 1 follow the shape of outdoor air temperature due to high air change rate. Anyhow, the shift between plots of solar loads and air temperature in the cavity corresponds to approximately 1-2 hours. This is probably a reason for the delay effect seen earlier in Figure 5-9 - Figure 5-11 and heat storage capacity in the cavity is somewhat higher then expected.

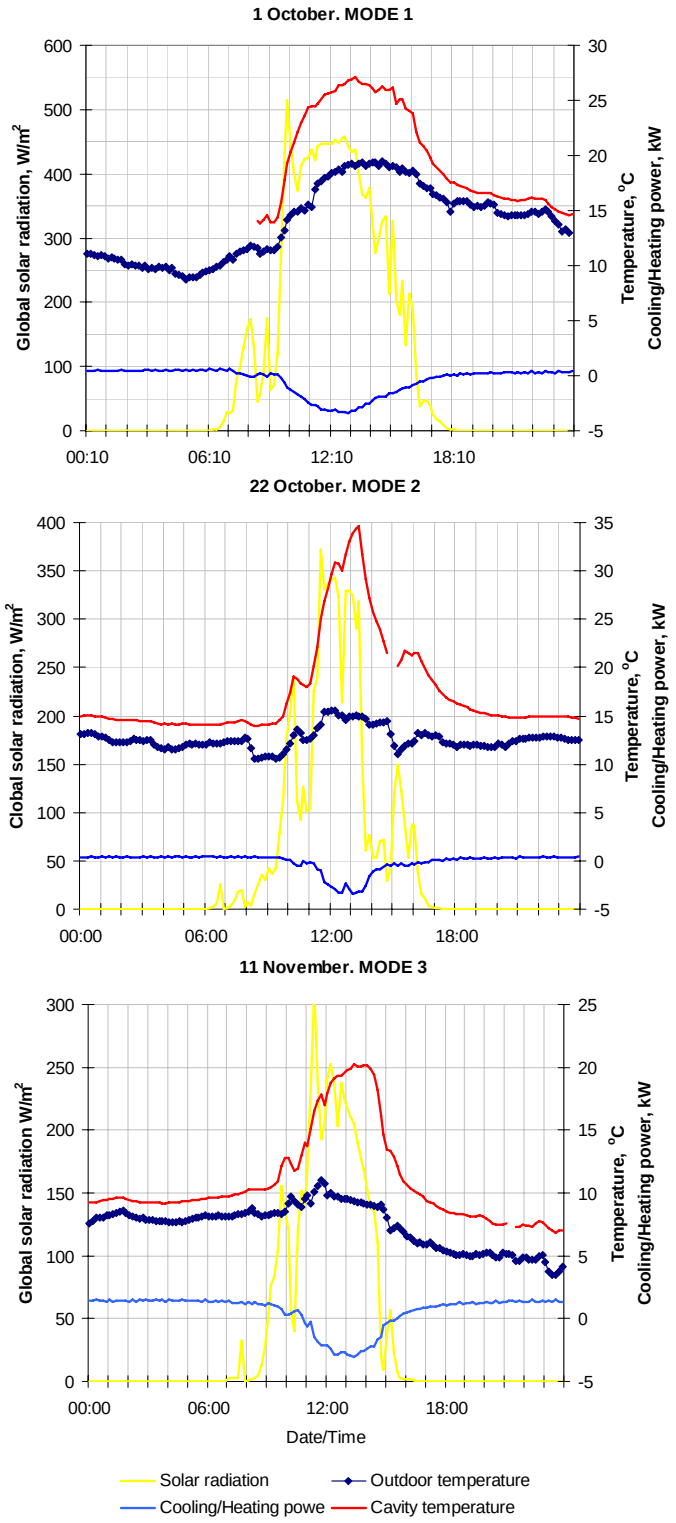

Figure 5-30. Comparison of 24-hour DSF performance for different modes.

Chapter 6

CONVECTION AND FLOW REGIME

In this chapter convective and flow regimes that take place in DSF cavity are investigated. It is argued that flow regime in the DSF cavity is foremost undeveloped turbulent and the double-skin facade cavity in 'The Cube' acts as a wide channel. Analysis of the results show that in most of cases natural convection is dominating above forced convection in the cavity.

Measured velocity profiles in the DSF cavity are investigated on subject of recirculation flow appearance. Finally, a hypothesis, describing in detail phenomenon of recirculation flow is developed and explained. Further development of the hypothesis is supported with a detailed literature study of the subject and some calculations, which indicate consistency of the experimental results with the hypothesis.

6.1 CONVECTION, FLOW REGIME - THEORY AND MEASUREMENTS

6.1.1 DIMENSIONLESS NUMBERS

The dimensionless numbers are used to characterize and classify the heat transfer problems. Here the dimensionless numbers relevant to the DSF fluid flow are defined.

Reynolds number, Re_l, is interpreted as the ratio of interia to viscous forces in a region of characteristic dimension (Incropera et al., 2006).

Equation 6-1

$$\mathrm{Re}_l = \frac{\rho \cdot V \cdot l}{\mu} = \frac{V \cdot l}{\upsilon}$$

Grashof number, Gr_l, is a measure of the ratio of the buoyancy forces to the viscous forces acting on a fluid element (Incropera et al., 2006).

Equation 6-2

$$Gr_l = \frac{g \cdot \beta \cdot (T_s - T_\infty) \cdot l^3}{\upsilon^2}$$

Transition between laminar and turbulent flow regime in a free convection boundary layer depends on the relative magnitude of the buoyancy and viscous forces in the fluid. It is customary to correlate its occurrence in terms of the Rayleigh number, Ra_l, which is the product of Grashof and Prandtl numbers (Incropera et al., 2006):

Equation 6-3

$$Ra_l = Gr_l \cdot \mathrm{Pr}$$

Where the Prandtl number, *Pr*, is a grouping of the properties of the fluid:

Equation 6-4

$$\mathrm{Pr} = \frac{c_p \cdot \mu}{k}$$

Nusselt number, Nu_l, may be interpreted as the dimensionless temperature gradient at the surface, and it provides a measure of the convection heat transfer occurring at the surface (Incropera et al., 2006).

Equation 6-5

$$Nu_l = \frac{\alpha \cdot l}{k}$$

Where,

ρ - fluid density, kg/m^3
V - average velocity of the fluid, m/s
μ - dynamic viscosity, N.s/m^2
υ - kinematic viscosity of the fluid, m^2/s
g - gravitational acceleration, m^2/s
β - coefficient of volumetric expansion, 1/k

T_s, T_∞ - temperature of the surface and fluid, K
α - convective heat transfer coefficients, W/m^{2}K
k - thermal conductivity of the fluid, W/mK
c_p - specific heat at constant pressure, J/kgK
l - characteristic length

The characteristic length l, is usually the hydraulic diameter, height or width of the domain where the flow motion occurs. For the double-skin facade cavity, the characteristic length is normally the height of the cavity, H. However, sometimes, the reference will be made to the hydraulic diameter, D_h, and depth of the cavity, L.

6.1.2 WIDE AND NARROW CAVITIES

Ideally, the convective heat transfer in a double skin facade cavity can be represented as the convection between two vertical, infinitely wide heated surfaces. For exceptionally wide cavities, the convective heat transfer can be idealized to a vertical infinitely long heated surface, where the impact from another surface is negligible.

The distinction is made between narrow and wide channels (Saelens, 2002):

Equation 6-6

$$L/H > Ra_H^{-1/4} \quad \text{or} \quad L/H > Ra_L^{-1}$$

For the dimensions of the double-skin facade cavity in 'The Cube', L/H is equal to 0.1 and the resulting aspect ratio of the facade is 10. In literature, cavities of such aspect ratio are regarded as wide.

The surface temperatures of the glazing were different for the internal (ie) and external (ei) window panes, and the results of Equation 6-6 for both of the surfaces are illustrated in Figure 6-1. According to the figure, the DSF cavity acts as a wide cavity, looking both upon ie- and ei-glass surfaces.

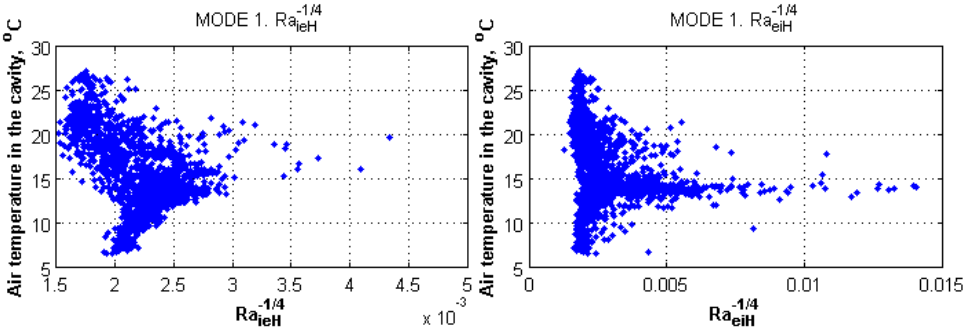

Figure 6-1. The results for the Equation 6-6 to distinguish between narrow and wide cavity for the conditions in MODE 1 in 'The Cube'.

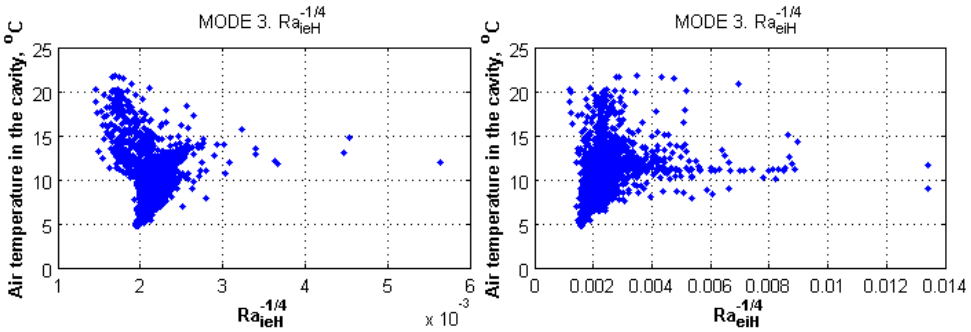

Figure 6-2. The results for the Equation 6-6 to distinguish between narrow and wide cavity for the conditions in MODE 3 in 'The Cube'.

6.1.3 CONVECTION REGIME

The Reynolds number characterises the flow condition for forced convection flows, while Grashof number has a similar role for the free convection flows. Grashof and Reynolds numbers are also applied to identify the convection regime (Incropera, et al., 2007):

Equation 6-7

$\frac{Gr_l}{\mathrm{Re}_l^2} << 1$ forced convection

$\frac{Gr_l}{\mathrm{Re}_l^2} >> 1$ free (natural) convection

$\frac{Gr_l}{\mathrm{Re}_l^2} \approx 1$ mixed convection

In the literature, it has already been distinguished between the convection regimes:

- Free (natural) convection - is when the body force acts on a fluid in which there are density gradients (Incropera, et al., 2007).
- Forced convection – is when fluid flow is originated from an external force
- Mixed convection accounts for the buoyancy effects on forced flows or the forced flow effects on buoyant flows (Armaly, et.al. 1987)

In the DSF cavity, both free and forced convection may take place. The differentiation of the convective flow regimes in the cavity can be done via estimation of the strength of the boundary layer flow compared to the bulk flow, see Equation 6-7. Even though the free convection flows are normally smaller than those associated with forced convection, the free convection can become comparable with the forced convection caused by ventilation flow rates, when the surface temperatures in a double skin facade are high.

Considering MODE 1 as an ideal case, the development of the boundary layer flow will start at the bottom of the cavity, where the bulk flow is strong and the convection is forced. Further up, the strength of the boundary layer flow can improve, but not enough to dominate over the main flow, the interference of forced and natural convective mechanism might take place, which typically results in mixed-convection regime. With further development of the boundary layer, the mixed convection regime might transform into free convection regime. So, in theory, all three convection regimes can take place in the DSF cavity.

In MODE 2 only free convection takes place. In MODE 3, forced convection is expected due to the external fan force. However when the mechanical flow rates are small and the buoyancy forces are comparable with the fan forces, it is possible to have coexistence of both, resulting in mixed convection flow regime or even the free convection.

The Grashof number for the experimental data in MODE 1 and MODE 3 is calculated separately for the external window and internal window panes in the DSF cavity (ei and ie). T_∞ is the temperature of the free stream, but for the wide channel flow, this is identified as the temperature of the fluid.

The negative values of Gr_H/Re_H^2 –ratio are caused by the fluid temperature higher than the surface temperature of the glazing. This will normally mean the downward convective flow at the surface.

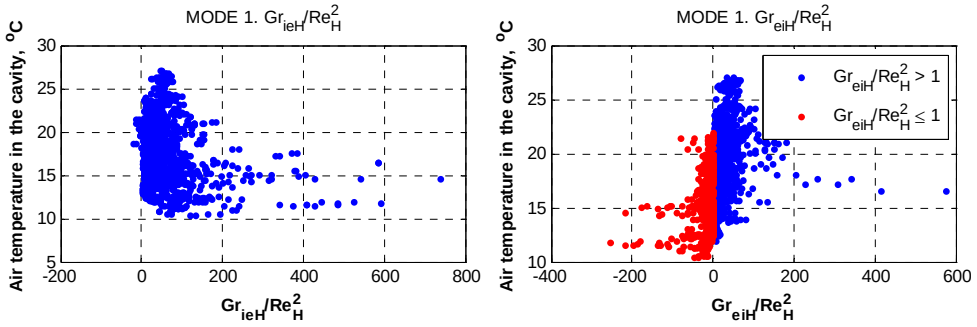

Figure 6-3. Identification of convection regime in MODE 1 according to Equation 6-7.

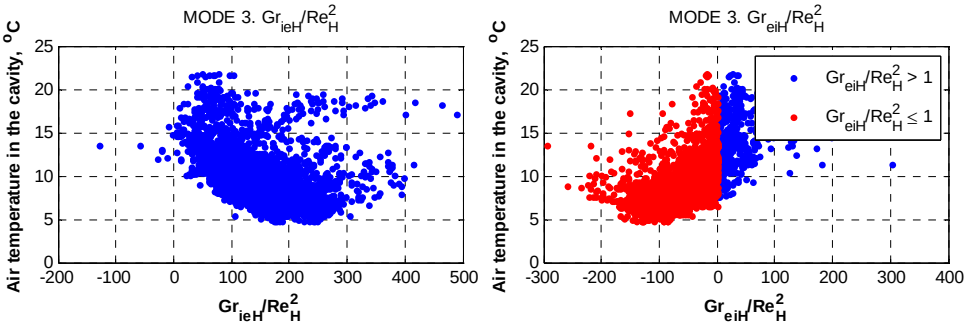

Figure 6-4. Identification of convection regime in MODE 3 according to Equation 6-7.

In MODE 3 (Figure 6-4) convection regime at the ie-surface appears to be dominated by buoyancy and in that way identifies free convection regime. Though, all convection regimes may possibly take place at ie-surface in MODE 3 and at ie- and ei-surfaces in MODE 1 (Figure 6-3). Both for MODE 1 and for MODE 3 the boundary conditions vary a lot during a day and during the whole measurement period. This explains why different convection regimes are seen in the experimental data set.

Another relevant matter here is the distribution of local Gr_H/Re_H^2 - ratio as a function of height in the double-facade cavity. Due to very wide range of Gr_H/Re_H^2 - ratio in the experimental data set working with the mean values was found inappropriate. The experimental data set was subdivided into three groups according to the *mean* value of Gr_H/Re_H^2 for ie- and ei-surfaces separately:

- $Gr_H/Re_H^2 < 0.9$
- $0.9 \leq Gr_H/Re_H^2 \leq 10$
- $Gr_H/Re_H^2 > 10$

The only reason for this separation is the scale of the plots in Figure 6-5 and Figure 6-6.

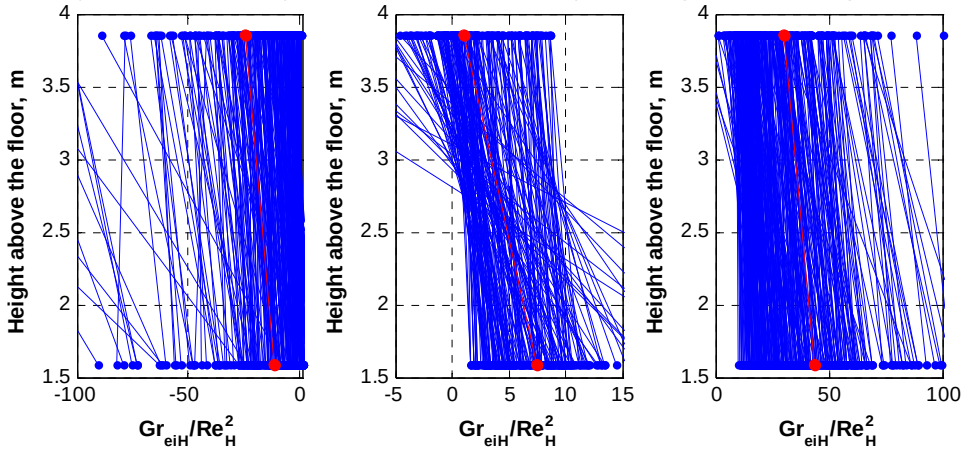

Red line – illustrates mean values for corresponding plot

Figure 6-5. Vertical distribution of Gr_H/Re_H^2 in the DSF cavity for ei-surface. MODE 1.

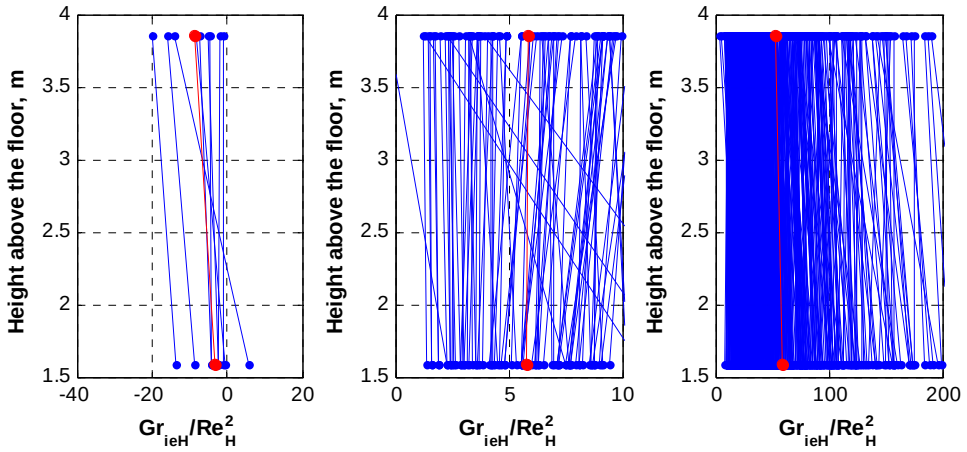

Red line – illustrates mean values for corresponding plot

Figure 6-6. Vertical distribution of Gr_H/Re_H^2 in the DSF cavity for ie-surface. MODE 1.

The above plots of vertical distribution of Gr_H/Re_H^2 - ratio in the DSF cavity are based on surface temperature measurements at only two heights, therefore connecting these points with a line is a rather rough approximation.

It is interesting that Gr_H/Re_H^2 - ratio is independent of height for ie-surface (Figure 6-6), while Gr_H/Re_H^2 ratio reduction with height is seen for ei-surface (Figure 6-5). It is still difficult to conclude on that due to the lack of experimental data, as this might be an experimental error, wind washout effect or an indication of changes in the convective heat transfer at the upper levels of the cavity. At last, it can be an indication of recirculation flow that is characterised with increase of turbulence in the recirculation area.

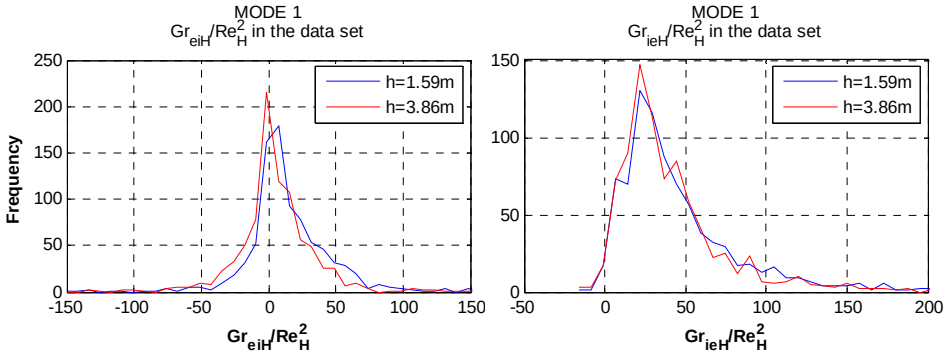

Figure 6-7. Frequency distribution of Gr_H/Re_H^2 –ratio in the data set. MODE 1.

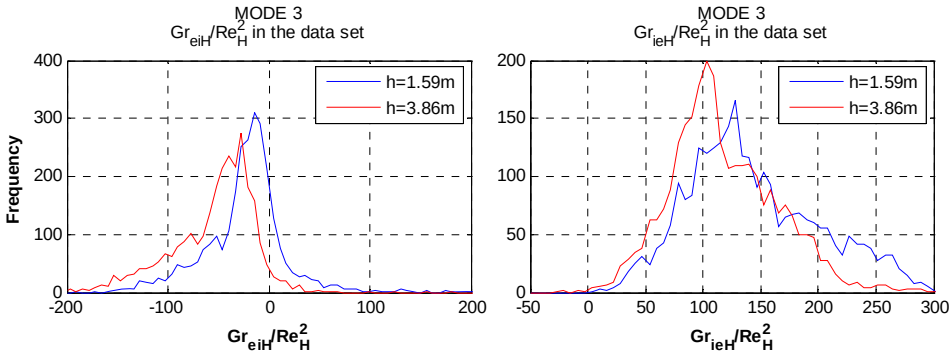

Figure 6-8. Frequency distribution of Gr_H/Re_H^2 –ratio in the data set. MODE 3.

From the frequency charts (Figure 6-7, Figure 6-8) it is seen that the majority of data in MODE 1 and MODE 3 belongs to the range of mixed or free convection. Discussed earlier change of convective regime cannot be identified from the data set, as it requires detailed measurements of surface temperatures in the cavity.

6.1.4 FLOW REGIME

When dealing with any convection problem, the significance of flow conditions is always discussed. There is a distinction made between turbulent and laminar flow regime.

- Turbulent flow is very irregular. It is characterized by random, three-dimensional motion of large parcels of fluid
- Laminar flow is characterized as smoothed flow with parallel streamlines of fluid flow
- Transition flow is when the conversion from laminar to turbulent regime takes place.

The transition between laminar and turbulent flow is found depending on the convection regime, constrains to the boundary layer development (internal/external flow) and vertical/horizontal flow direction. For wide cavities, the transition to turbulent in a free convection boundary layer is distinguished as for free convection on a vertical plate. According to Incropera, et al. (2007) the transition to turbulent flow is correlated in terms of Rayleigh number and the critical Rayleigh number is:

Equation 6-8

$$Ra_H \approx 10^9$$

For circumstances with forced convection on a plate the transition point is defined as following (Saelens, 2002):

Equation 6-9

$$2 \cdot 10^4 < \mathrm{Re}_H < 10^6$$

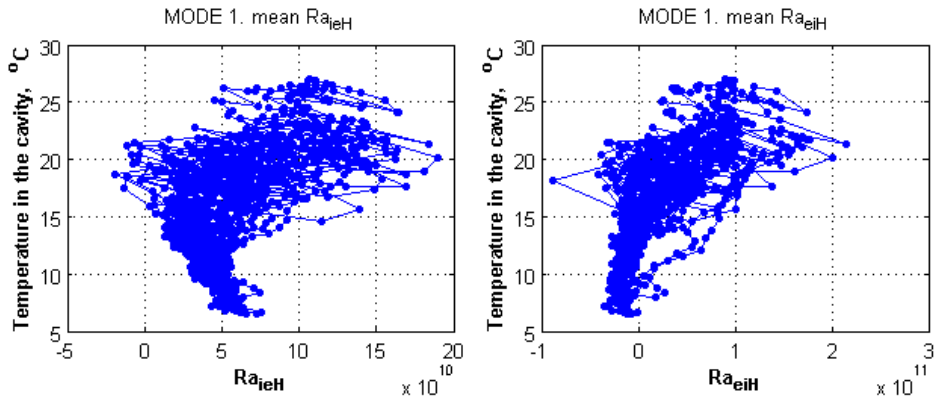

Figure 6-9. Mean Rayleigh number for ie-surface (left) and for ei-surface (right), in MODE 1.

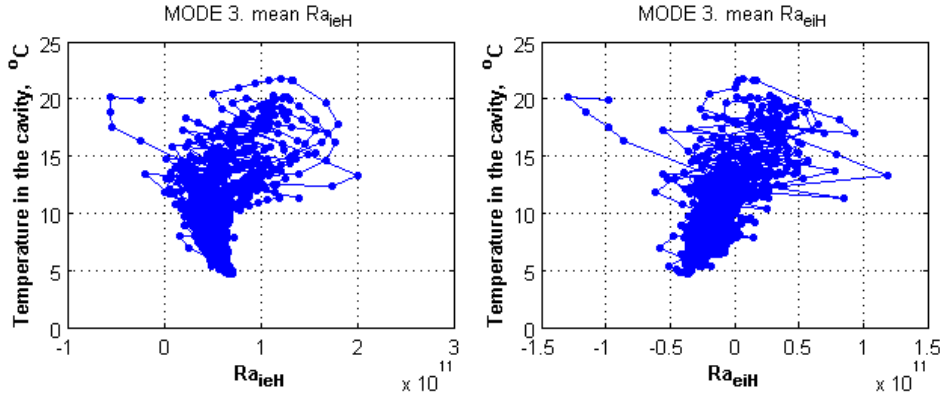

Figure 6-10. Mean Rayleigh number for ie-surface (left) and for ei-surface (right), in MODE 3.

According to experimental studies in Lloyd et al. (1972), for free convection at the vertical plate, the transition to turbulent regime first occurs at Rayleigh number of approximately 2×10^{11}. It is also argued that Rayleigh number may not be a unique criterion for that. Rather, there may be a separate dependence on the Prandtl and Schmidt number.

In the numerical studies of the convective heat transfer at a vertical plate in free, forced and mixed convective regime, the onset of the turbulent motion is assumed to happen for conditions given in Equation 6-10.

Equation 6-10

$$Ra > 10^9 \quad \text{and} \quad Re > 10^4$$

In view of fact that for the majority of the experimental results, free or mixed convection takes place, then the Rayleigh number (Equation 6-8), is the main parameter for assessment of the flow regime in the cavity. Though, considering the uncertainties about the convective regime in the cavity, it is wise to use a general expression, Equation 6-10.

Both equations lead to the conclusion of turbulent or in transition to turbulent flow regime in the DSF cavity. However, the shape of the velocity profile (section 6.3) does not confirm the occurrence of fully developed turbulent flow and therefore the flow regime in the cavity is assumed to be undeveloped turbulent flow (section 6.4.1)

In the section 6.2.2 it is also argued for the flow regime undeveloped turbulent.

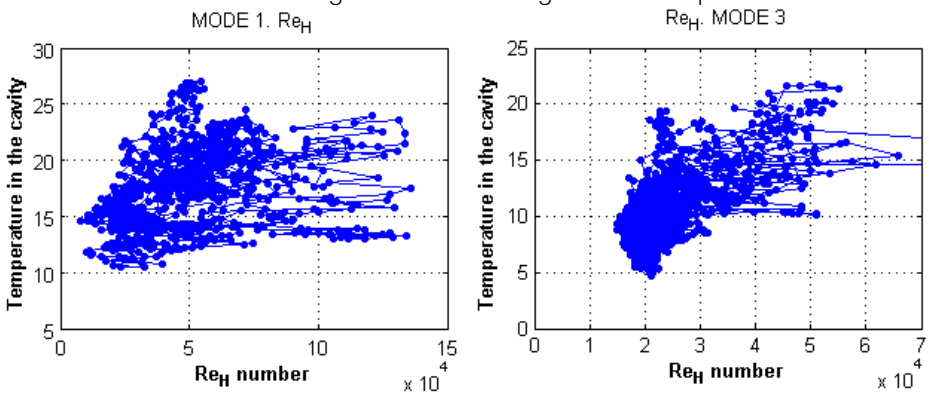

Equation 6-11. Reynolds number in the DSF cavity in MODE 1 (left) and MODE 3 (right).

6.2 RECIRCULATION FLOW

6.2.1 HYPOTHESIS

Consider a fluid flow between two heated, infinitely wide, vertical surfaces. When air enters the cavity and makes contact with the surface, the boundary layer develops due to the viscous effects, its thickness increases with increasing distance from the entrance until the boundary layers merge and the flow regime turns to fully developed. Regard this case as a reference.

Now, consider the following case when the entrance flow is low, the cavity is wide and the surface temperatures are high. Then the boundary layer development in the cavity will start as in the reference case (Figure 6-11, 1). The thickness of the boundary layer will increase with increasing distance from the entrance plane. Due to the relatively high surface temperature and buoyant forces in the boundary layer, the air speed in the layer can actually exceed the air velocity in the inviscid flow (Figure 6-11, 2). According to the mass balance, the development of the boundary layer can only occur at the expense of the inviscid flow. Subsequently the velocity in the inviscid flow region decreases due to a velocity increase in the inviscid flow, Figure 6-11, 2. The same applies for mass flow. It increases in the boundary layer on expense of mass flow in inviscid flow.

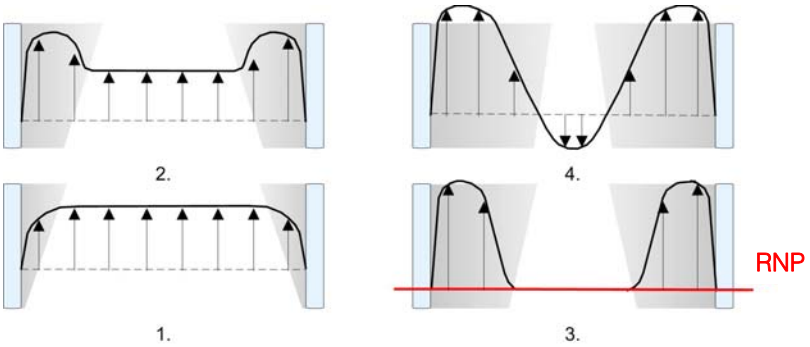

Figure 6-11. Illustration of possible velocity profiles in a DSF cavity. 1-Channel flow. 2-Plane with a strong boundary layer flow. 3- Recirculation neutral plane (RNP). 4. Plane with a recirculation flow.

Further development of the boundary layer may first reach the circumstance when the boundary layer mass flow is equal to the mass flow entering the cavity. The plane where it happens is referred as a *Recirculation Neutral Plane (RNP)* (Figure 6-11, 3), which is different from the neutral plane in a natural ventilation theory. According to the mass balance the mass flow rate of the inviscid flow in the neutral plane is zero.

Formation of the boundary above the neutral plane will lead to the boundary layer flow exceeding the flow rate entering the cavity and, as a consequence, the air to this plane will be drawn from the zones above, causing the recirculation flow in the centre-line of the cavity (Figure 6-11, 4, Figure 6-12).

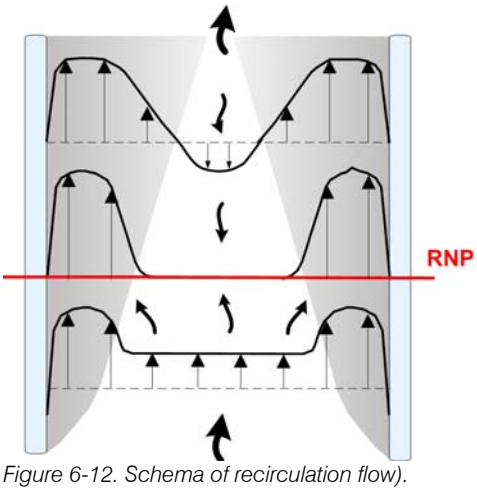

Figure 6-12. Schema of recirculation flow).

In theory, the appearance of recirculation flow in the upper zones of the DSF cavity mean also that there are zones with increased air velocities and that there is a mixing of air from the inviscid and boundary layer flow. On the whole, this should lead to increased convective heat exchange with the surfaces (due to higher velocity), higher temperature gradients in the cavity and finally increased buoyant forces of natural ventilation.

Appearance of recirculation flow is most probable for periods when solar radiation is strong and the pressure difference across the openings is small (MODE 1). As a result, total mass flow rate induced by natural forces will be low and insufficient for healthy development of boundary layer. This would be a case when buoyancy and wind force oppose each other or if the wind force is weak. If flow is mechanically driven, then low air change rate together with strong solar radiation will lead to recirculation flow.

Regarding the convective flow regimes, flow in a naturally ventilated DSF cavity can represent a combination of free, mixed or forced convection. In the bottom of the cavity, where the boundary layer flow is weak, forced or mixed convection will take place. Later on, with the development of strength of the boundary layer, free convection attains control over the system, causing the recirculation flow appearances.

Until now, none of experimental results contain direct evidences of presence of recirculation flow. There have been a few indications, but these are not enough to confirm the hypothesis. In view of that, further investigations were carried out and described in the following chapters.

6.2.2 LITERATURE SURVEY WITH FOCUS ON RECIRCULATION FLOW

This literature review targets a very narrow subject in the field of convective heat transfer prepared for a topic of convective heat transfer with recirculation flow in a vertical, wide cavity.

There is some irregularity present:

- The cavity is considered to be wide and therefore in a regular case the convective heat transfer at the surfaces of the cavity is considered as for separate, infinitely long vertical surfaces. At the same, as explained earlier, in section 6.2.1 , the presence of these two surfaces can still limit the volume of incoming flow for the healthy development of the boundary layer. Finally, the deduction of the convective heat transfer as for a wide cavity, in many

circumstances become inappropriate. Meanwhile, the flow in DSF cavity cannot be regarded as confined internal flow, as those is normally associated with fully developed flow.

- The other issue is the possibility for coexistence of more than one convective flow regimes in the DSF cavity: forced convection at the entrance region, mixed convection and then the appearance of recirculation flow, is a symptom for dominating natural convection.

This literature review is focused on the experimental studies of the free, forced, and mixed convection heat transfer in a vertical channel, to investigate the circumstances for the flow reversal. However, only a limited amount of publications is available, as most of the literature is dealing with the fully developed flow in a channel and laminar flow.

Earlier, in the numerical investigations of the convective heat transfer in a channel (Aung and Worku, 1986; Morton et al., 1989) occurrence of the recirculation flow was already described. However, the experiments focused on this phenomenon were first conducted by Gau, Yih and Aung (Gau et al., 1990). The experiments were carried out for a vertical channel with one wall insulated and the opposite wall uniformly heated, with the Gr/Re^2 ratio up to 50 and $Re=600$. Though, the flow reversal was documented only for the buoyancy opposed flow in a channel.

Later on, another range of Gr/Re^2 was experimentally investigated for a vertical channel (Gau et al., 1992 a,b), a vertical divergent channel (Gau et al., 1996) and a vertical convergent channel (Huang et al., 1995). Zhang and Dutta performed numerical studies of mixed convection in an asymmetrically heated channel (Zhang and Dutta, 1998). Cheng and Yang studied numerically the developing fluid flow and heat transfer of mixed convection in a vertical parallel-plate channel with fin arrays (Cheng 1994). All of these later studies confirmed the recirculation flow appearance.

According to Gau et al. (1992a), the flow reversal is triggered when the buoyancy force becomes so large that local natural convection starts to dominate the flow process and the total flow rate, generated by an external force is not enough for the healthy development of the boundary layer. As a consequence, a field with minimum pressure is created in the channel that causes the flow reversal.

It is also pointed out by the authors that the occurrence of flow reversal depends on the ratio Gr/Re^2, *Re-, Pr*-number and the aspect ratio of the channel. The same conclusion was also derived in Cheng et al. (2000) and Zhang and Dutta (1998).

The concept of mixed convection is based on coexistence of two convective regimes. Consider free convection development in a vertical channel: in the entrance region, its effect is almost negligible, while the forced convection is strong. As explained in the section 6.2.1 , for increasing distance from the entrance region, the density gradients become more significant, until the moment when free convection becomes dominant. In the article (Gau, et al., 1992a) it is explained that when the free convection begins to dominate and the critical value, with the local Grashof number, Gr^*/Re, is reached then recirculation flow will occur.

Observations of the flow reversal (Gau, et al., 1992a) reveal that increasing the buoyancy parameter Gr/Re^2 has the effect of causing the heated buoyant flow to move more rapidly, which leads to a deeper penetration of the recirculation flow and a wider recirculation region. An opposite effect was seen with increase of Re-number, which pushes the recirculation flow to move downstream (to the top of the channel) and can make the recirculating region wider. In general, the shape of the recirculation flow is

described as V-form and the flow reversal occurrence is observed for a relatively high Gr/Re^2- ratio.

According to another set of observations for 3°-convergent channel (Huang, et al., 1995) and 3°- divergent channel (Gau et al., 1996), the recirculation flow occurs at the cooler surface, of the channel and tends to move upwards if the buoyancy parameter is small. An interesting observation was made for a divergent channel (smaller opening at the entrance), as the recirculation flow, actually, enters the channel from the outside at the top.

A noteworthy finding was made by the authors when describing the recirculation flow behaviour that was not discussed in the past: the V-shaped recirculation flow is not steady, but instead, it grows and collapses in a periodic manner. The mechanism responsible for this is the counterflow motion between the heated buoyant flow and the recirculation flow that makes flow unstable, three-dimensional and turbulent. Flow reversal and instability in mixed laminar vertical tube flow was also studied numerically by Nguyen and co-workers (Nguyen et al., 2004). The authors have studied both the opposed and assisted buoyancy cases and have found that the flow stays stable and unique up to a critical level of Grashof number. The authors opinion is that beyond this level the flow experiences the transition to turbulent.

Speaking about the free, forced and mixed convection flow regime in the literature, rarely, the distinction is made between the convective regimes. Although the studies of the flow reversal phenomenon are frequently described as the mixed convection, most of the articles agree on the fact that one or another force is dominating, depending on which part of the channel is being scrutinized. In Gau et al. (1992a) the following assumption is made towards the convection regime: the natural convection process in the channel at and beyond the separation point can be viewed as a natural convection along the plate, which starts developing from the entrance of the channel. This assumption is based on the fact that the recirculation takes place only if the natural convection dominates.

Finally, the authors conclude that the V-shaped recirculation can enhance the heat transfer process, due to increased turbulence in the recirculation flow region (Gau et al., 1992a,b). Similar conclusion has been made by Zhang and Dutta (1998), who argue that the significant enhancement of heat transfer has been achieved due to the buoyancy caused irregularities.

Finally, it is necessary to ask a question: how do the findings in the literature overlap with the heat transfer and the flow motion in the DSF cavity? Can we explain the behaviour of the DSF flow using the literature?

The experimental results available from Gau et al., (1992a,b) involve a channel with the aspect ratio 15, which is thinner than the dimensions of DSF cavity, with an aspect ratio of 10.

The Gr/Re^2-ratio is investigated between 0.7 and 95 with the Reynolds number in the range between 600 and 2200 (Gau et al., 1992b). Experimental data for the higher Gr/Re^2-ratio is also available (Gau et al., 1992a), but this was achieved by reducing the entrance velocity, which has led to reduction of Reynolds number ($Gr/Re^2=120$ and $Re=514$; $Gr/Re^2=210$ and $Re=400$).

Obviously, the aspect ratio of the DSF cavity is significantly smaller, while the level of turbulence in MODE 1 is considerably higher ($Re\approx5\cdot10^5$) when compared with the published results. Nevertheless, Gr/Re^2 –ratio stays high even with the high Reynolds number. It is not possible to argue that the decrease of the aspect ratio and the increase

of the flow rate in the cavity may lead to the recirculation, unless empirical or numerical investigations are available.

Unique study of this matter has been carried out by Zöllner, et al. (2002), where the turbulent mixed convection flows had been studied in a double-skin facade with different aspect ratios: 13, 6.7, 4.4. In this work, the impact of the wind pressure effect has been eliminated and the flow rates were originated only by stack effect. Analogous to the study of Gau et al., 1996, the authors have noted an appearance of highly circulating flow in the cavity, with the recirculation flow at the external facade of the cavity (at the cooler surface). However, it must be mentioned that the authors explain the flow reversal by the high flow resistance of inlet/outlet grating. High resistance of the grating results in a smaller flow rates in the cavity and, as a consequence, there appears a lack of flow for the healthy development of the boundary layer.

All of the articles reviewed in this chapter until now (except for Zöllner et al., 2002) focus on natural convection for laminar flows. According to the literature study by Habib and co-workers (Habib et al., 2002), only a few studies reported velocity profiles for natural convection turbulent flows and all of these studies were carried out numerically. In order to contribute to understanding of turbulent natural convection in vertical channels authors (Habib et al., 2002) have performed a row of experimental investigations for symmetrically and asymmetrically heated vertical channel. For the symmetrically heated channel the aspect ratio was approximately 3 and the surface temperature was 20°C above the ambient temperature. In these experiments, the velocity profiles were measured with Laser Doppler Velocimetry System for the Rayleigh number of $4.0*10^6$ for the symmetrical flow and appearance of the recirculation flow was observed at the end of the channel.

One of numerical studies for the turbulent flows was carried out in 2004 by Francisco Marcondes and co-workers (Marcondes et al., 2006) for parallel, convergent and divergent open-ended channels. The authors have also found that for high values of Rayleigh number, a recirculation region was observed close to the outlet of the channel when the buoyancy effect increases. These results were obtained for the aspect ratio of approximately 11, which is significantly different from the aspect ratio studied in Habib et al. (2002) and similar to the dimensions of DSF cavity. However, the recirculation phenomena was observed for $Pr=5$ and $Ra_L=10^7$, what corresponds to $Ra_H=15*10^9$.

In 2007, there were two studies published of temperature and velocity field characteristics of turbulent natural convection in a vertical parallel-plate channel with asymmetric heating by Yilmaz, Gilchrist and Fraser (Yilmaz and Gilchrist, 2007 and Yilmaz and Fraser, 2007). The numerical and experimental results of these studies showed that for the studied conditions the flow reversal has not been detected, however the velocity profile was continuously skewed towards the heated surface.

Recently turbulent natural convection flow was studied experimentally in a converging channel by Ayinde (Ayinde, 2008) and clearly revealed presence of recirculation flow.

Literature available about laminar flow conditions, especially regarding the flow reversal, is more complete then for turbulent flow. Therefore the insight gained into the flow reversal phenomena for laminar flows is also valuable when considering turbulent flow. This is so particularly due to the similarities seen between for laminar and turbulent flow regime with regard to flow reversal in the above literature study:

- Flow reversal appears with increasing Grashof number
- Flow reversal takes place in the end of the channel
- Flow reversal takes place at the cooler surface of the channel

Aspect ratio of the channel, Reynolds number and Prandtl number has an influence on flow reversal phenomenon, but due to the lack of experimental and numerical studies it is not appropriate to conclude on that.

The above literature indicates that the appearance of the recirculation or so-called recirculation flow in the DSF cavity is not an assumption, but a possibility both for laminar and for turbulent flow regime. Then again, most of the works considered in this literature study did not focus on the flow reversal phenomena itself. The conditions for its appearance have not been studied as well as its' consequences for the heat transfer and for the vertical temperature gradients in the cavity. These consequences have an exceptional importance for the DSF performance and approaches for modelling double facade cavity.

Some of the experiments conducted at 'The Cube' include measurements of the velocity profiles in the DSF cavity. These will be further examined in section 6.3 and will disclose whether there is any identification of flow recirculation occurrences available in the experimental data.

6.3 VELOCITY PROFILE, MODE 1

It was already illustrated that with application of the velocity profile method for the measurement of the mass flow rate in the cavity, the measured flow rate increases with the distance from the entrance pane. From the mass balance, the increase of the measured flow rate is possible when the flow that crosses the plane is two-directional. Now, the velocity profiles in the DSF cavity are analyzed on the subject of two-directional flow.

The shape of the velocity profile in a channel flow differs between the fully developed flow regime or entrance region, between laminar or turbulent flow. The presence of two-directional flow will cause the deformation of the velocity profile in that plane and its shape will not be characteristic for a particular flow regime.

The hot-sphere anemometers used for measurement of the velocity profile do not distinguish the flow direction and therefore the velocity profiles are built for one-directional flow. In Figure 6-13 the velocity profiles are dimensionless and as in the Figure 5-24, value of 1 corresponds to the minimum area averaged velocity in one, out of six measured velocity profiles:

Equation 6-12

$$V_{\dim} = \frac{V}{V^*_{\min}}$$

V_{dim} - dimensionless velocity
V - measured velocity in a point
V^*_{min} - minimum area averaged velocity in all six measurement planes

Examination of the mean dimensionless velocity profiles built for the whole set of experimental data may lead to an erroneous conclusion, seeing that the surface temperature of the external window pane at night is low, and the buoyancy forces in the boundary layer at the surface can be weak or even work against the main flow. Thus inclusion of this effect into the mean value is meaningless and must be avoided.

In view of that, the mean dimensionless profile is built for three conditions, defined according to ratio Gr/Re^2:

Equation 6-13

$$\frac{Gr_H^{ie}}{\mathrm{Re}_H^2} \le 10$$

Equation 6-14

$$10 < \frac{Gr_H^{ie}}{\mathrm{Re}_H^2} < 100$$

Equation 6-15

$$\frac{Gr_H^{ie}}{\mathrm{Re}_H^2} \ge 100$$

Gr_H^{ie} - Grashof number, calculated for the characteristic length H and included as an average for the whole volume.

Re_H^2 - Reynolds number, calculated for the characteristic length H and minimal mass flow rate

Llooking upon Gr_l/Re_l^2 the differentiation is made between low, high and intermediate *k*, where, $k = Gr_H/Re_H^2$ and its low, high or intermediate values are defined by conditions in Equation 6-13, Equation 6-14, Equation 6-15 and the results of this differentiation is available in the Figure 6-13.

Equation 6-16

$$k = Gr_H^{ie} \Big/ \mathrm{Re}_H^2$$

It was explained earlier, that the shape of the velocity *Profile I* is most probably defected due to the bending of incoming air. Further on, the shape of *Profile II* confirms the development of the boundary layers at the glass surfaces, when $k>100$. Yet here the velocity in the boundary layer is comparable with the air velocity in the inviscid flow. In fact, both the *Profile I* and the *Profile II* are relatively close to the inlet opening, hence they are still in the flow field where the effect of natural convection is still small.

In the velocity *Profile III*, for $k>50$, the air velocity at the glass surface of the internal window is similar to *Profile II*, but it is obviously different at the surface of external window. Also the area averaged air velocity in this profile is approximately equals to 1. All of it is due to the window frame at the external window, which functions as an obstruction to further development of the boundary layer at ei-surface.

The depth of the DSF cavity is 56 cm, thus the development of boundary layer at the internal window surface in *Profile III* went undisturbed by the frame-obstacle. As a result, higher velocities were measured at the internal window surface in *Profile IV,* apx. 2.4 for $k>100$. Here the dimensionless velocities in the inviscid flow are approximately equal to 1 or smaller than 1. Meanwhile for the low and intermediate k, the dimensionless velocity is approximate to 1 and demonstrates weak boundary layer.

The shape of the velocity *Profile V* is out of the ordinary. Mean dimensionless air velocity, near the glass pane of the internal window exceeds 3.5 for $k>100$, while at the external window surface it is significantly smaller, also compared to the other profiles. Assuming that the velocity measured at the internal window is the velocity in the boundary layer, it is reasonable to presume that the mass flow rate in the boundary layer exceeds the incoming flow rate and that the growth of the boundary layer at this level happens along with the recirculation flow. Then the recirculation flow causes the deformation of the velocity profile, especially closer to the outer pane.

It is difficult to conclude on the velocity *Profile VI*, but it is probable that either the recirculation flow at the level *V*, has been established and dominates the left part of the *Profile VI* with the recirculation flow (next to the external window) or either the boundary layer at the internal window surface has grown up to the width of the cavity.

Both profile V and VI could have been influenced by wind washout.

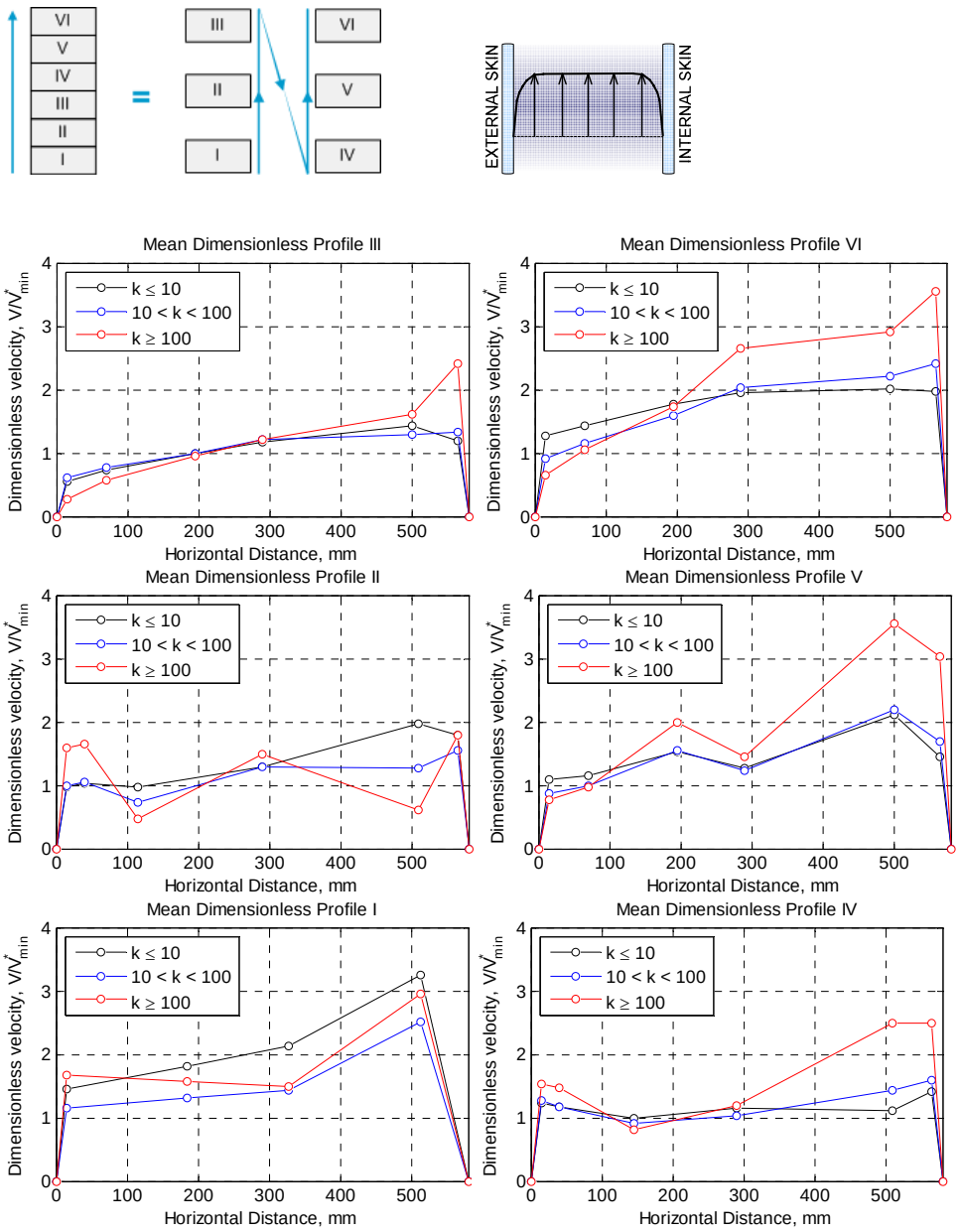

Figure 6-13. Mean dimensionless velocity profile at six different heights: h_I=0.95 m, h_{II}=1.91 m, h_{III}=2.5 m, h_{IV}=4.36 m, h_V=4.7 m, h_{VI}=5.15 m.

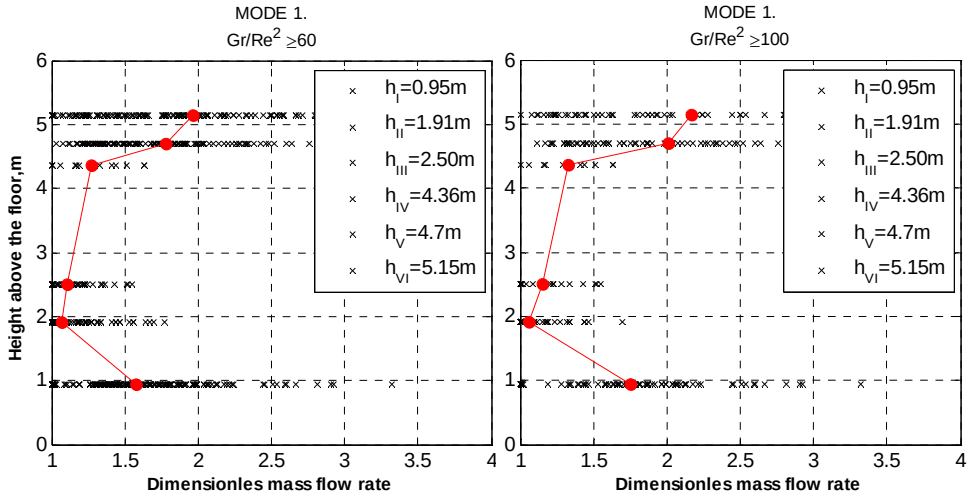

Figure 6-14. Dimensionless mass flow rate in the DSF cavity, measured at the different heights, using the velocity profile method.

Seeing that the velocity profile can be classified according to Gr/Re^2 ratio it is good interesting to repeat the same procedure for the dimensionless mass flow rate presented in earlier chapters (Figure 6-14).

From Figure 6-14 it is clearly seen that for high Gr/Re^2 ratio the mass flow rate increases significantly for the heights above 1.91 m. This supports findings made above when investigated velocity profiles in the cavity. This is also confirms a possibility of recirculation flow appearance.

Another relevant issue to the shape of the velocity profile in the DSF cavity is the measurement of the mass flow rate in a cavity using only one velocity sensor. In view of variation in the shape of velocity profile and velocity magnitude, measurement in only one point is unacceptable simplification. Moreover, the number of measurement points within the velocity profile and also the measurement frequency are very essential for accuracy.

The hot-sphere anemometers do not determine the flow direction and the estimation of the air mass flow rate in the cavity is suitable only if there are no changes in flow direction within the profile, as appearance of the recirculation flow, which is not possible to determine is damaging for the accuracy of estimated mass flow rate in the DSF cavity.

An additional point to mention is the lack of method for visualization of the flow pattern in the DSF cavity. This is a serious draw back for the experiments, as the preliminary visualization tests would enhance positioning of velocity measuring equipment as well as they would help to determine better locations of the tracer gas injections and finally would serve for improvement of the measurements accuracy.

6.4 BOUNDARY LAYER, MODE 1

Eckert and Jackson (Eckert and Jackson, 1951) were probably between first who attempted to analyze turbulent boundary layer flow. Eckert and Jackson have studied conditions for a flat surface with constant temperature difference between the surface and environment. Their analysis of boundary layer is based on integral formulation, where the focus is set on the boundary layer movement as a whole, instead of looking at movement of every particle in detail (Heiselberg, 1990).

Although their assumptions were not very accurate from a theoretical point of view, their approach was still used by Heiselberg (Heiselberg, 1990) who argued that the error caused by these assumptions is rather acceptable if the expression is used for engineering applications i.e. when calculating the downdraught from a window. Moreover, it is possible to generalize the expression developed by Eckert and Jackson so that it can be easily used.

Following is the solution derived by Eckert and Jackson (Heiselberg, 1990), which is valid for the constant temperature difference between the surface and environment.

Equation 6-17

$$v_1 = 1.186 \cdot \frac{\upsilon}{y} \cdot Gr_y^{\frac{1}{2}} \cdot \left[1 + 0.494 \cdot \mathrm{Pr}^{\frac{2}{3}}\right]^{-\frac{1}{2}}$$

Equation 6-18

$$\delta = 0.566 \cdot y \cdot Gr_y^{-\frac{1}{10}} \cdot \mathrm{Pr}^{-\frac{8}{15}} \cdot \left[1 + 0.494 \cdot \mathrm{Pr}^{\frac{2}{3}}\right]^{\frac{1}{10}}$$

Maximum velocity in the boundary layer is found by differentiation of the velocity profile assumed for the boundary layer (Heiselberg, 1990):

Equation 6-19

$$v_x = 0.537 \cdot v_1$$

Volume flow in the boundary layer is calculated by integration of the velocity profile assumed for the boundary layer (Heiselberg, 1990):

Equation 6-20

$$M = \int_0^{\delta} v \cdot dx = \int_0^1 1.86 \cdot v_x \cdot \eta^{\frac{1}{7}} \cdot (1-\eta)^4 \cdot \delta \cdot d\eta = 0.272 \cdot v_x \cdot \delta \qquad \left[\frac{m^3/s}{m}\right]$$

Following is the definition for the film temperature that can be used to decide on the material properties in the above equations:

Equation 6-21

$$t_{film} = \frac{1}{2}(t_s + t_\infty)$$

v_1 - velocity in the boundary layer, m/s
υ - kinematic viscosity, m^2/s
y - vertical distance, m
x - horizontal distance, m
δ - thickness of boundary layer, m

v_x - maximum velocity in the boundary layer, m/s
M - volume flow in the boundary layer, $m^3/(s.m)$
η - dimensionless distance (x/δ)
t_{film} - film temperature, °C
t_∞ - temperature of the surface and fluid, °C
t_s - surface temperature, °C

First of all, using the Equation 6-18 it is possible to estimate the thickness of the boundary layer in the DSF facade cavity for different conditions. And, by this means, it is possible to recognize whether the flow is fully developed or not.

Secondly, frequently discussed in this report phenomena of flow reversal can now be scrutinized using the theory developed in section 6.2.2 concerning conditions for its occurrence.

6.4.1 THICKNESS OF BOUNDARY LAYER IN DSF

In the Chapter 3, it is explained that the glass surface temperature in the DSF cavity was measured in the centre of glass pane for each BIH, BOH, BIL and BOL window. This corresponds to the measurements on ie-surface and ei-surface at the height 1.59 m and 3.86 m for each surface. Earlier it was shown that the surface temperature of the glazing was identical for all windows in the same plane, measured on the same height. Therefore, only one value representing all BIH, all BOH etc. windows is used as:

- ie-surface, h=1.59m
- ie-surface, h=3.86m
- ei-surface, h=1.59m
- ei-surface, h=3.89m

Using the experimental data, the thickness of the boundary layer is calculated for ie- and ei-surfaces at corresponding heights. The results are illustrated in Figure 6-15.

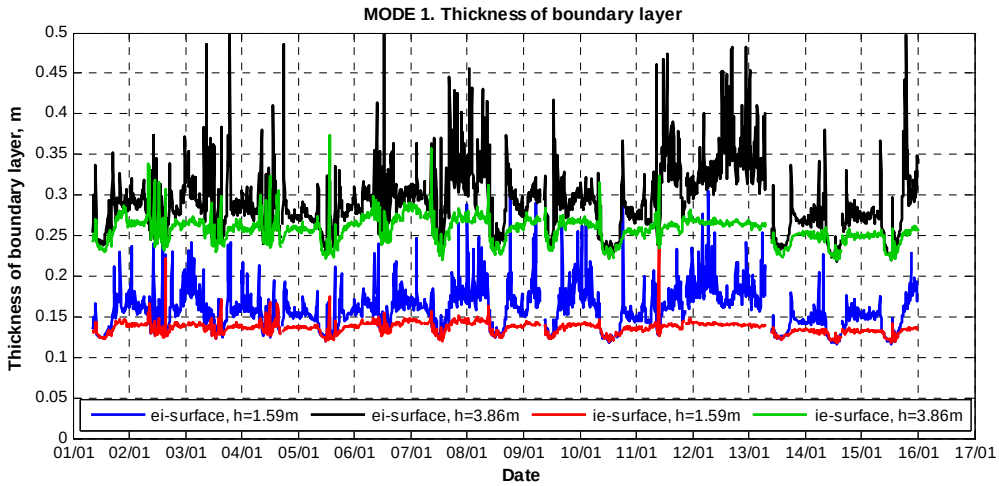

Figure 6-15. Analytically estimated thickness of boundary layer in the DSF cavity. MODE 1.

Analytical estimation of the boundary layer thickness demonstrates that:

- There are significant fluctuations of the boundary layer thickness, especially in the middle of day. This is probably caused by self-regulating principle of natural ventilation: with temperature increase, naturally induced flow through the cavity increases too, causing the temperature drop in the cavity and also of the cavity surfaces.
- The fluctuations of the boundary layer thickness are much more pronounced for the ei-surface. It must be noted that external windows of double facade cavity are single glazed. Therefore the temperature of ei-surface must be more sensitive to the temperature variations in external environment and also to the convective heat transfer at the ee-surface.
- Thickness of the boundary layer increases with height, which is expected.
- At the height 1.59 m above the floor, the thickness of boundary layer for the ie- and ei-surfaces is 0.14 m and 0.18 m correspondingly. The internal depth of the DSF cavity in 'The Cube' is 58 cm, thus at the height 1.59 m the boundaries from ie- and ei-surfaces have not merged yet, and the flow is still undeveloped.
- For the measurements at the upper level in the cavity – 3.86 m, it seems that the boundary layers are about to meet. In that case, the flow will become fully developed turbulent above that level in the cavity. However, this is still uncertain.

6.4.2 VELOCITY PROFILE IN THE BOUNDARY LAYER

Experimental data obtained for the velocity profile in the DSF cavity is available. Using the assumptions regarding the velocity profile in the boundary layer (Equation 6-20) it is relevant to examine how does the analytically obtained velocity profile in the boundary layer suits with the measured velocity profiles in the cavity.

From the available data it is possible to calculate the velocity profile in the DSF boundary layer at two heights: 1.59 m and 3.86 m above the floor, while the nearest measured velocity profiles to compare with were measured at the height 1.91 m and 4.36 m above the floor.

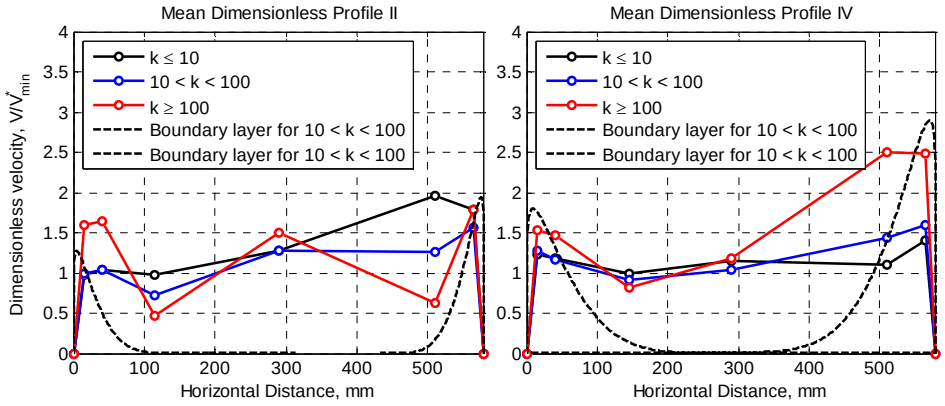

Definition of k is given by Equation 6-16
h_{II}=1.91 m, h_{IV}=4.36 m

Figure 6-16. Analytically estimated velocity profiles of boundary layers in the cavity in comparison with measured velocity profiles in the cavity. 10<k<100. MODE 1.

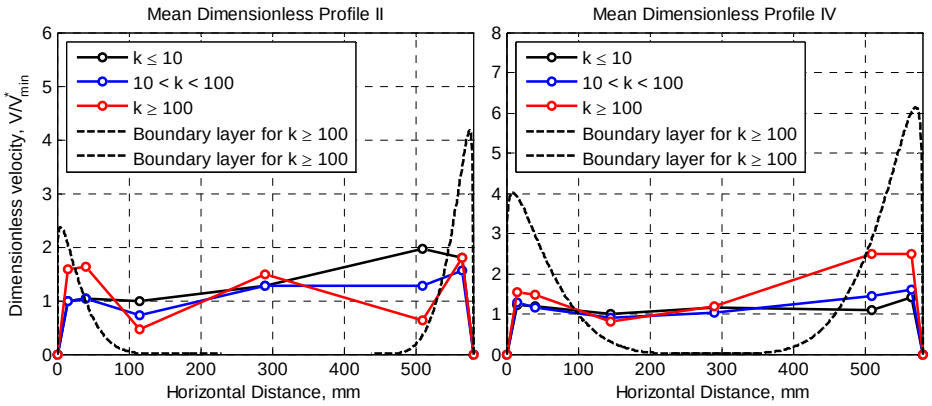

Definition of k is given by Equation 6-16
h_{II}=1.91m, h_{IV}=4.36m

Figure 6-17. Analytically estimated velocity profiles of boundary layers in the cavity in comparison with measured velocity profiles in the cavity. k≥100. MODE 1.

In Figure 6-16, calculated velocity profiles in the boundary layers of ei- and ie-surfaces are plotted together with the measured velocity profiles in the cavity. In this figure, the experimental data is sorted so, that earlier defined parameter *k* (Equation 6-16) is in the range from 10 to 100. This range corresponds to buoyancy assisting flow (*k>10*), but not dominating (*k<100*).

In the experimental data, however, it is impossible to distinguish whether the air velocity was measured in the boundary layer or not. Also, the lack of measurement points in each profile does not allow any reliable approximation of the velocity profiles, as the maximum velocity in the boundary layer might not have been captured. Therefore, the plots in Figure 6-16 and Figure 6-17 are very uncertain to derive any conclusions upon them.

From these figures, it is seen that measured and calculated velocity profiles are of the same velocity range. This is reasonably good, as the method used for calculations is developed for a flat plate and not for a channel flow with reasonably high free stream velocity instead of zero.

6.4.3 MASS FLOW IN BOUNDARY LAYER IN DSF

The mass flow rate in the boundary layer was calculated for the same surfaces and at the same heights as thickness of boundary layer in section 6.4.1 . The results of these calculations are compared with the mass flow rate obtained empirically using the velocity profile method and tracer gas method.

In view of the arguments mentioned earlier (section 6.3), the mass flow rate measured for profile II at the height 1.91 m is estimated to provide the most realistic estimation of mass flow rate using the velocity profile method.

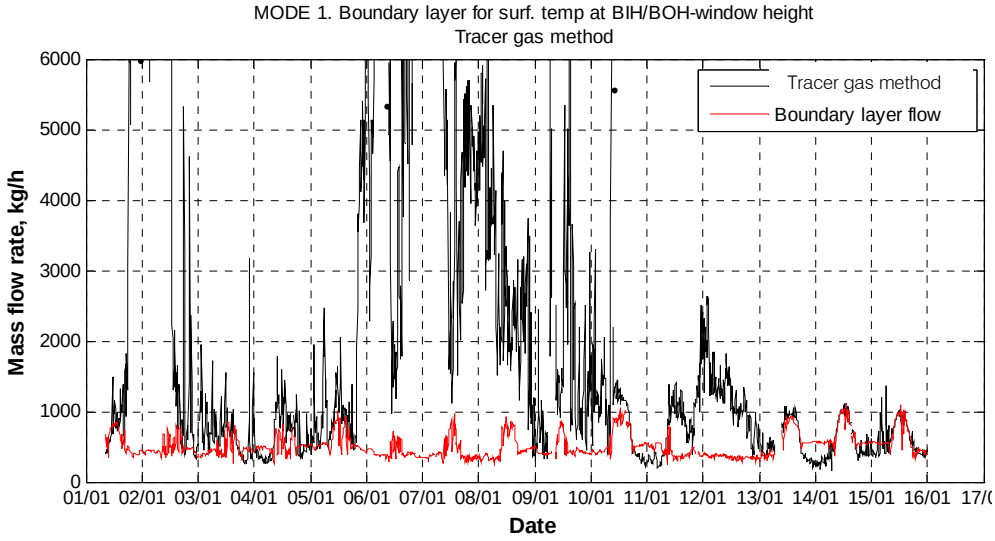

Figure 6-18. Mass flow rate in the boundary layer in the DSF cavity compared to the mass flow rate measured with the tracer gas method. MODE 1.

The question of the most accurate data set of measured mass flow rate in the cavity was already raised in the previous chapters. However, it was not possible to answer this question. Therefore, it is impossible to make any conclusion upon Figure 6-18 and Figure 6-19.

On the other hand, using the tracer gas method the errors are normally found in overestimation of the flow rate. This is explained by wind wash-out effects and bad mixing. For these particular measurements in the DSF cavity – the same behaviour applies for the velocity profile method. Thus choosing the minimum value from both of the methods could be beneficial for further assessment of the results.

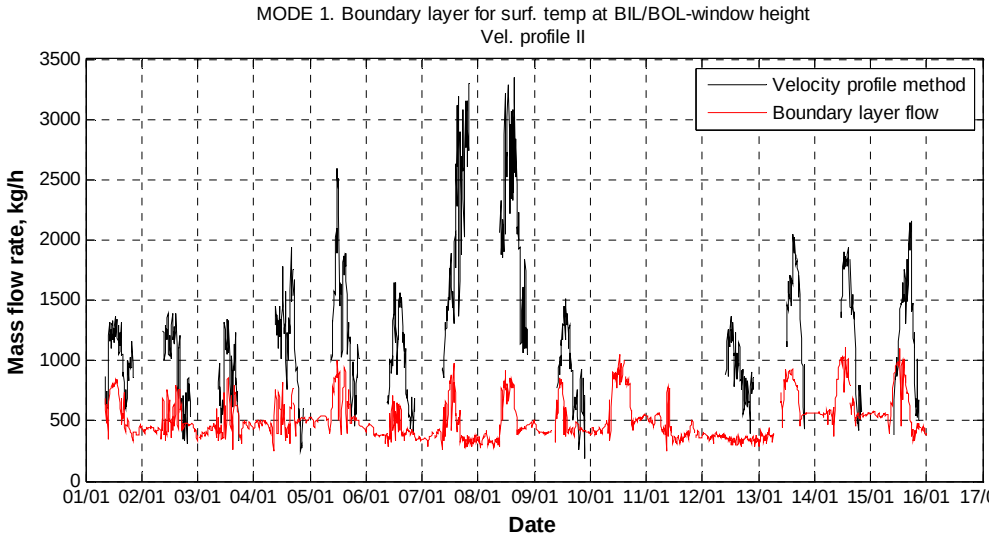

Figure 6-19. Mass flow rate in the boundary layer in the DSF cavity compared to the mass flow rate measured with the velocity profile method for Profile II at height 1.91m. MODE 1.

Looking upon Figure 6-18 and Figure 6-19, and using the argument from the previous paragraph it is seen that the mass flow rate in the boundary layer in the middle of the day is often in the range or even higher than the total mass flow measured in the cavity. What

corresponds well with the theory developed in section 6.2 . These results one more time indicate a possibility for appearance of flow recirculation. However, one would expect much higher mass flow rates in the boundary layer to explain significant deviations between mass flow rates measured using the velocity profile and the tracer gas method. This has not been confirmed, but it is necessary to mention that the mass flow rate in the boundary layer was calculated for the height h=3.86m, which is much below the expected height for flow recirculation.

6.4.4 SUMMARY

In the present chapter, the conditions in the double-facade cavity were examined using the dimensionless numbers. But besides that, the main issues in flow recirculation occurrences in a double-facade cavity are explained in section 6.2 .

Often, in the field of engineering, a rule of thumb is used to identify whether the cavity acts a wide or narrow cavity: if the aspect ratio (*H*/*L*) equals or above 10, then the cavity is wide. In section 6.1.2 , more thorough investigation of wide/narrow cavity issue is reported. And, using the experimental data, it is illustrated that indeed the cavity in 'The Cube' acts as a wide cavity.

Due to the significant variations of the boundary conditions throughout a day and also throughout the whole period of measurements, the distribution of Gr_H/Re_H^2 –ratio appeared to be in a very wide range if look at the whole measurement period. To obtain a quantitative estimation of Gr_H/Re_H^2 relationship in the cavity the frequency distributions plot were used. According to those, most of the experimental data belongs to the range of free or mixed convection. However, distinguishing of these convection regimes is a challenging task.

Because of the lack of experimental data, the assumption of change of the convection regimes within the cavity (in vertical direction) was not confirmed.

Looking upon Rayleigh number in the section 6.1.4 , it was concluded that the flow in the DSF cavity is turbulent or in transition to turbulent. However, the shape of the velocity profile (section 6.3) does not confirm the occurrence of fully developed turbulent flow.

In section 6.2.2 , a literature survey explains the experimental and numerical studies of the free, forced, and mixed convection heat transfer in a vertical channel by different researchers. Only a limited amount of publications is available, as most of the literature is dealing with fully developed flow and laminar flow regime.

As a result of literature study it was concluded that the appearance of the return or so-called recirculation flow in the DSF cavity is not an assumption, but a possibility both for laminar and for turbulent flow regime. Then again, most of the works considered in this literature study did not focus on the flow reversal phenomena itself. The conditions for its appearance have not been studied as well as its' consequences for the heat transfer and for the vertical temperature gradients in the cavity. However, these consequences have an exceptional importance for the DSF performance and approaches for modelling double facade cavity.

A closer look to the velocity profiles at the different heights in the DSF cavity shoved the very first indication of flow recirculation in the upper part of the cavity. These indications were found for conditions of strong buoyancy forces, represented by Gr_H/Re_H^2 –ratio above 60, but these were even more pronounced for Gr_H/Re_H^2 –ratio above 100.

Next, the thickness, velocity and mass flow in the boundary layer of the DSF cavity were calculated using the Eckert and Jackson approach (Eckert and Jackson, 1951; Heiselberg,1990). For the height 3.89m above the floor, the total thickness of the boundary layers at ie- and ei-surfaces appeared to be comparable with the cavity depth (58 cm). Accordingly the flow regime in the cavity is most probably in transition to turbulent, as the shape of velocity profiles in the cavity do not confirm appearance of fully turbulent flow.

The velocity profile of the boundary layer, assumed in the calculations was compared with the measured velocity profiles in the cavity in section 6.4.2 . The measured and calculated velocities appeared to be in the same range. Though, any further conclusions would require advanced experimental data.

Finally the mass flow rate calculated for the boundary layer flow appeared to be comparable with the measured mass flow rate in the cavity, what according to the theory developed in section 6.2.1 also indicates appearance of the recirculating flow. Some other indications of recirculation flow were seen in:

- Vertical temperature gradient in DSF cavity
- Vertical distribution of Gr_H/Re_H^2
- Velocity profiles in DSF cavity

In section 6.2.1 it is assumed that appearance of recirculation flow is most probable for periods with strong solar radiation and weak wind forces (low air change). Considering earlier indications of flow reversal in the vertical temperature profiles and dimensionless mass flow rate, it is possible to choose a time-interval in the experimental data set to verify this assumption. Two periods were selected: 1st October 13.20-13:30 and 8th October 13:30-13:40 (Figure 6-20 and Table 6-1).

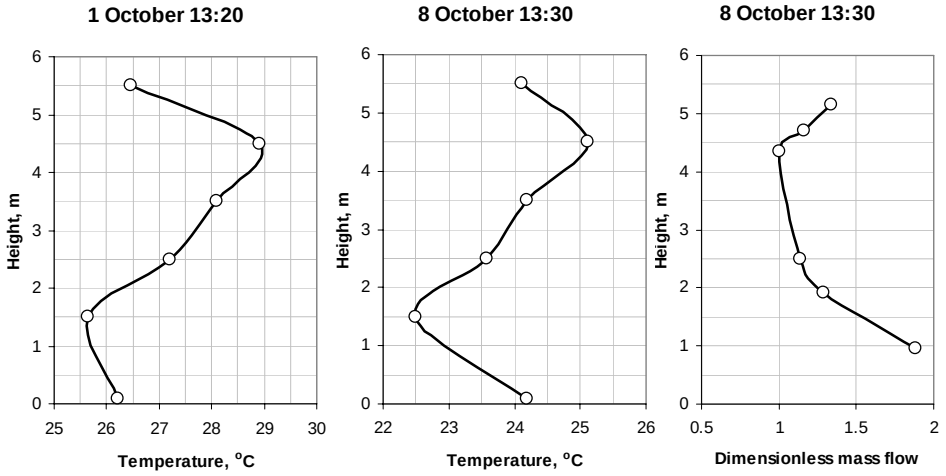

Figure 6-20. Vertical temperature gradient in the cavity (left and centre). Dimensionless mass flow rate measured for 6 velocity profiles (right).

	01 October at 13:20	08 October 13:30
Outdoor air temperature, °C	18.5	16.2
Wind speed, m/s	4.9	11.3
Wind direction, deg	195	280
Global solar radiation, W/m^2	452	439
Diffuse solar radiation, W/m^2	185	169
Air flow measured with tracer gas, m^3/h	850	1690
Air flow measured with velocity profile, m^3/h	1325	2566

Table 6-1. Experimental data for Figure 6-20.

From Figure 6-20 it is seen that significant increase of mass flow rate in the cavity is measured above 4.5m height. This is also a level with the maximum air temperature measured in the cavity. Both of these observations are reasonable for wind washout effect, but also for recirculation flow occurrence. These are the periods with strong solar radiation and on 1st of October the wind speed was also moderate.

SOL-openings in MODE 1 are shown on Figure 6-21 for visual evaluation for possibilities for wind washout effect. Velocity profile I, was measured at approximately 0.5m above the upper edge of SOL-openings. The distance from the low edge of SOH-opening to velocity profile VI was apx. 0.2 m and 0.7 m to velocity profile V.

Figure 6-21. SOL-openings in MODE 1.

Another set of measurements was conducted in the same test facility for MODE 3 operation strategy, but during summer season by Marszal and Thomas (2008). Vertical temperature gradient in their results looks remarkable (Figure 6-22). Measurement results shown in the figure belong to a period with strong solar radiation intensity. Air temperature was measured almost in the centre of the cavity. According to the figure, the temperature stays constant in the upper part of the cavity when the solar radiation is strong and this is a clear indication that the temperature was measured in the core of recirculation flow.

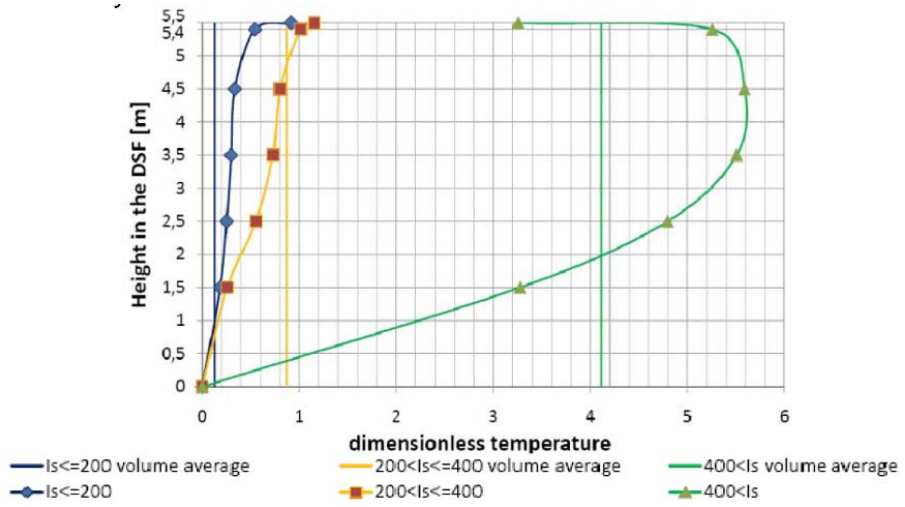

Figure 6-22. Vertical dimensionless temperature gradient in DSF cavity for MODE 3 by Marszal and Thomas (2008).

All things considered, it is concluded that there are no clear evidence for presence of recirculation flow in the experimental data, as many indications of recirculating flow could also be a measurement error. It is clear that more detailed experimental studies are needed to document appearance of this phenomenon. Besides, there are many strong arguments that do not allow disregarding of recirculation flow when assessing DSF performance in the periods of peak loads.

In the literature (Gau et al., 1992b, Zöllner, et al. 2002), it is argued that appearance of the flow reversal may lead to a significant increase of the heat transfer in the cavity, according to Zöllner, et al. (2002) this may also change the shape of the vertical temperature gradient in the cavity, where the maximum temperatures will not appear at the top of the cavity, but closer to its middle. These issues will have significant consequences for the naturally induced mass flow rate in the cavity and for the overall thermal performance of the DSF cavity.

All in all, the heat transfer in the DSF cavity during the high solar loads will differ a lot from the generally assumed one. And, in order to be able to deal with the DSF buildings, it is necessary to know exactly when the recirculation appears, what behavior it has and how, exactly, this affects the heat transfer and flow motion in the DSF.

Gau et al., (1992b) describes the appearance of the recirculation flow of highly unstable, three-dimensional, transient behavior that has never been documented before. The flow instability results from the counterflow motion and mixing of the heated buoyant flow with the V-shaped recirculating flow. This renders instability and leads to generation of eddies, vortices and fluctuation of vortices.

The fact that the flow is 3D and unstable-periodic has a great importance for the accuracy of CFD predictions and the choice of the turbulence model. Thus this information can be used as an argument to explain why there have been a lot of CFD predictions regarding the heat transfer in the double-facade cavity, but it is exceptionally rare that the CFD models can capture the flow reversal. Also, commonly used parabolic procedure in the numerical methods can be a reason for that, according to Marcondes et al. (2006) the parabolic method neglects the diffusion terms in the streamwise direction in the energy and momentum equations and then this does not allow to capture the recirculation flow.

Chapter 7

SUGGESTION FOR A NUMERICAL MODEL

In this chapter a suggestion for a new numerical model for prediction of thermal and energy performance of DSF is presented and described. The model should be able to assess the effect of recirculation flow occurrence in the cavity and the consequences that it will have for the mass and heat transfer.

Suggested model consists of two part: thermal- and mass-model. Both of the models are based on Eckert and Jonson's approach (Eckert and Jackson, 1951; Heiselberg, 1990), which is used to calculate the mass flow rate and the convective heat flux in the boundary layer.

7.1 GENERAL

In the previous chapters, it was demonstrated that recirculation flow might take place in the DSF cavity in during periods with significant solar loads. These are also the periods when prediction of thermal and energy performance of DSF cavity is difficult, as it is difficult to assess convective and radiative heat transfer in the cavity and thus the vertical temperature gradient, naturally induced flow rate and finally the heat flux through the DSF.

Appearance of recirculation flow is significant, as heat transfer in the cavity will increase with recirculation flow, and vertical temperature gradient will be different from typically assumed or calculated profile.

Being able to count on mass and heat transport via recirculation flow, will help to resolve the question of heat transfer through double-facade in periods of peak solar loads. In this chapter an attempt is made to describe the main principles for a new mass- and thermal-model, which would be able to count on recirculation flow in the DSF cavity. The background for the model was found in Eckert and Jonson's approach (Eckert and Jackson, 1951; Heiselberg, 1990) as will be described in the following chapters.

7.2 MODEL DESCRIPTION

As explained earlier, the main cause for recirculating flow in the top of double-facade cavity is the increasing flow in the boundary layer. At some point, the boundary layer flow becomes dominant and therefore defines the flow pattern in the cavity space.

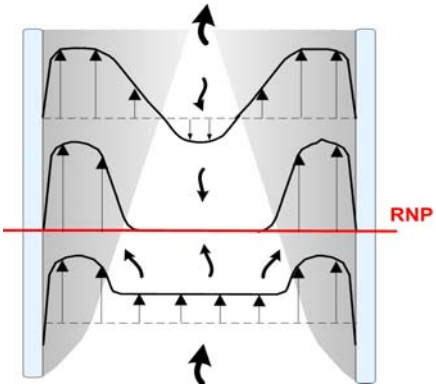

Figure 7-1. Illustration of recirculation flow in a DSF cavity.

In section 6.1.4 it was recognised that in the experimental data set, the flow was undeveloped turbulent. Also, the experimentally studied double-facade cavity acted as a wide cavity for the majority of the experiments. For these conditions, Eckert and Jonson's approach (Eckert and Jackson, 1951; Heiselberg, 1990) was applied for calculations and the strength of the boundary layer flow was confirmed.

Using the knowledge gained in Chapter 6, here, the main ideas behind the new flow model for the DSF cavity will be described.

It is assumed that the model, when completed, can be integrated with a thermal building simulation program, as a separate module that is activated only for the double-facade cavities. Because of the main principles used in the flow model, it will be impossible to integrate the flow model as a stand alone module with a thermal simulation program. Therefore, a separate thermal model should be developed to complete the module for

simulation of double facade thermal performance. The main principles, necessary for setting up thermal model are also explained in this chapter.

Assumptions for future steps should be made:

1. Air is treated as incompressible fluid
2. Flow regime in the cavity is undeveloped turbulent
3. The DSF cavity acts as a wide cavity. Thus following a rule of thumb, the model can be applied for all cavities with the aspect ratio (H/L) equal or above 10.
4. The velocity and the temperature boundary layers are of the same thickness (assumption necessary for application of Eckert and Jonson's approach (Eckert and Jackson, 1951; Heiselberg, 1990).

The thermal and the flow model are two-dimensional. The section of the double-skin facade cavity is divided into a number of layers *n* (Figure 7-2), where one layer is illustrated in detail by Figure 7-2 (right). For every layer the double facade cavity is divided into three zones, where zone 'ei'- and zone 'ie'- represent the boundary layers at the ei- and ie-surfaces correspondingly. The 'c'- zone is the core-flow, outside the boundary layer flow and zone 'o' – represents the outdoor. In further mathematical formulations following definitions will be used:

zone code + layer code

Where the zone codes – are *ei, c*, *ie, o*. And, the layer codes are numbers from *1* to *n*. For example 'ei1*'* – stands for zone ei in the layer 1 of the model.

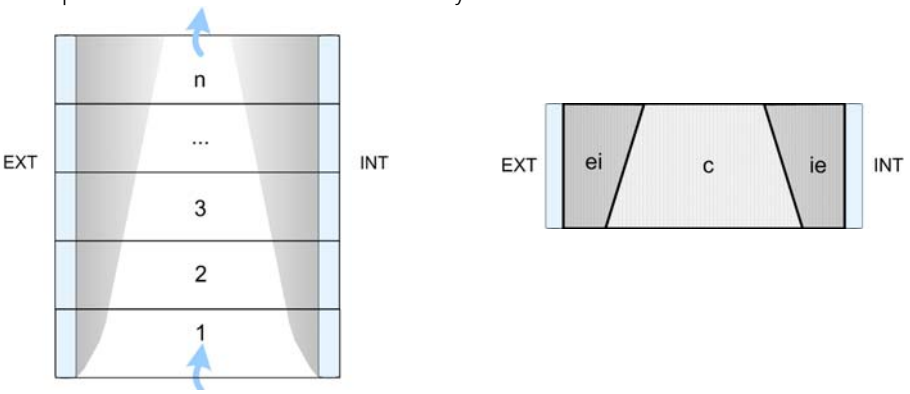

Figure 7-2. Layers in a section of DSF cavity (left). Zones in a layer of the model (right).

In the model, the stationary heat and mass balances are written for each zone and solved for every time step. The flow rates are treated as mass of air carried around in kg/s, while the zones and the layers of the model are treated as control volumes. The actual schema of DSF in the model can be seen as in Figure 7-3 (left). However, it can be further simplified, as illustrated in Figure 7-3 (right). Assumptions regarding treatment of the top layer in the model will be discussed in section 7.2.1 .

Solution process in any numerical model requires and initialization process and this can be adopted from a simulation program that the module is being integrated in. Then, an iterative process between mass and heat balances will have to take place.

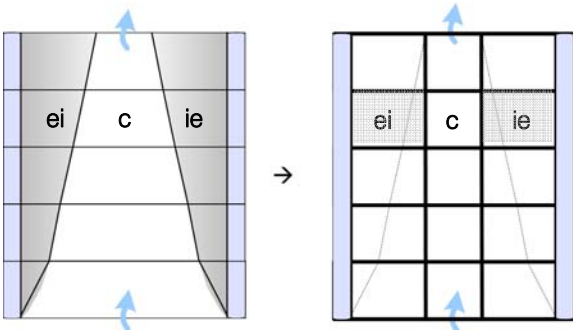

Figure 7-3. Representation of a DSF cavity in the model. Actual (left) and simplified (right).

7.2.1 FLOW MODEL

For a naturally ventilated cavity (MODE 1), the total mass flow rate in the cavity can be calculated from the pressure difference across the openings, induced by buoyancy and/or wind, as explained in the section 7.2.1.1 . For mechanically ventilated cavity (MODE 3) the total mass flow rate is known.

By means of Eckert and Jonson's approach (Eckert and Jackson, 1951; Heiselberg, 1990) the mass flow rate in the boundary layers of ei- and ie-surfaces can be assessed with reasonable accuracy until the recirculation neutral plane (RNP). The recirculation natural plane is explained in the 6.2.1 , as a plane where the mass flow of the boundary layer equals to the mass of flow entering the cavity (total mass flow rate, induced by the natural forces in case of external air curtain mode).

If the development of the boundary layer above the RNP proceeds, independently, from occurred recirculating flow then, ideally, the situation may look like in the Figure 7-4,B. However, in practice, the situation may look different due to deformation of boundary layers above RNP (Figure 7-4 A). Moreover, the mass of air removed from the boundary layer at ei-surface can differ a lot from the mass of air removed from ie-surface. Then, the recirculation flow will not take place in the centre of the cavity, but on the contrary will be formed closer to one or another surface (normally at the cooler surface), as was experienced in the experiments by Gau et al. (Gau, et al., 1992a).

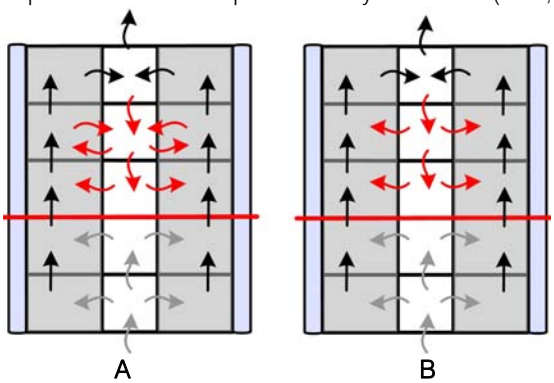

Figure 7-4.Illustration: A, - Mass flow rate distribution, if the development of boundary layer above RNP is weak. B - Mass flow rate distribution, if the development of boundary layer above RNP did not change (ideal case).

Still, the maximal velocity in the boundary layer is high and, because of surface temperatures, it will not change with appearance of recirculation flow. For most of cases, only the field of lower velocities in boundary layer (the tail of boundary layer) will be disturbed either by recirculation flow or by the main stream.

By reason of little studies available about the recirculating flow phenomena, it is difficult to consider how the boundary layer will develop above the recirculation neutral plane and what degree of error will be present in the model when use Eckert and Jonson's approach for channel flow. A question appears if flow regime in the cavity becomes fully developed, what consequences it will have on recirculation flow behaviour?

For this flow model, it is assumed that flow is undeveloped turbulent and boundary layer development is unrestricted above the neutral plane (Figure 7-4, B). A consequence of this assumption is fixing the upper end of recirculation field in the model to the last layer in the cavity.

This assumption creates some restrictions for calculation of the flow pattern and temperature gradients in the cavity. However, this is a necessary simplification for keeping the model simple. Also, according to the experimental studies published by different authors (section 6.2.2), in practice, the recirculation flow does appear at the top of vertical channels or pipes. And, since the model is purposed for a limited number of layers with certain thickness (more than 30 cm), it is realistic that the recirculation flow will be fed from the top layers and then assumption become very rational.

The mass balance is set up and solved for every zone, as for example for an arbitrary zone in Figure 7-5 and Equation 7-1.

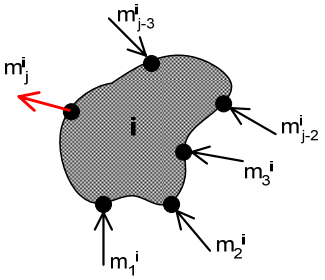

Figure 7-5. Illustration of mass balance for an arbitrary zone i.

Equation 7-1

$$\sum_{j=1}^{n} m_j^i = 0$$

The mass balance for the zones in layer *1* and *n* is given by Figure 7-6 and Equation 7-3. The mass balance for a zone is written for all incoming or outgoing fluid, which crosses the edge of the zone. The horizontal edges in the zone correspond to the horizontal planes that define the layers in the model. While, the vertical edges follow the shape of the boundary layer, as can be seen in Figure 7-3 (left).

In the following mathematical formulation, the upper index for mass flow *m*, will always mean the zone that the mass balance is formulated for and the lower index will always mean a zone, with a shared edge.

For example, $\sum_{j=1}^{n} m_j^i$ - mass balance for a zone *i*, which has shared edges with the zones j.

Finally following condition will always apply:

Equation 7-2

$$m_j^i = m_i^j$$

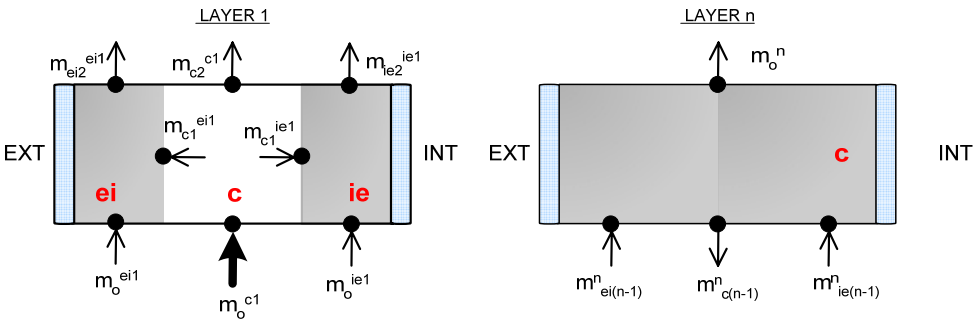

Figure 7-6. Illustration of mass balance for the zones in the DSF model, layer1 (left) and layer 'n' (right).

Equation 7-3 (for layer 1)

$$\begin{cases} m_o^{ei1} + m_{c1}^{ei1} + m_{ei2}^{ei1} = 0 \\ m_o^{c1} + m_{ei1}^{c1} + m_{ie1}^{c1} + m_{c2}^{c1} = 0 \\ m_o^{ie1} + m_{c1}^{ie1} + m_{ei2}^{ie1} = 0 \end{cases}$$

However, for the 1st layer, m_o^{ie1} and m_o^{ei1} equal zero, as no boundary layer yet developed and all of the air enters via the core-sector. For the last layer in the cavity *n*, it is assumed that all air in this layer is well mixed, than the mass balance for the whole layer can be written as in Equation 7-4:

Equation 7-4 (for layer n)

$$m_o^n + m_{c(n-1)}^n + m_{ei(n-1)}^n + m_{ie(n-1)}^n = 0$$

For a layer *(n-1)* a system of equations will look as following:

Equation 7-5 (for layer (n-1)

$$\begin{cases} m_{ei(n-2)}^{ei(n-1)} + m_{c(n-1)}^{ei(n-1)} + m_{ein}^{ei(n-1)} = 0 \\ m_{c(n-2)}^{c(n-1)} + m_{ei(n-1)}^{c(n-1)} + m_{ie(n-1)}^{c(n-1)} + m_{cn}^{c(n-1)} = 0 \\ m_{c(n-2)}^{ie(n-1)} + m_{c(n-1)}^{ie(n-1)} + m_{ein}^{ie(n-1)} = 0 \end{cases}$$

When the complete system of linear equations is formulated, it can be solved for m^c- or m_c- elements, which are in that case unknown. m_{ie}- and m_{ei} - elements can be calculated by means of Eckert and Jonson's approach (Eckert and Jackson, 1951; Heiselberg, 1990) and m_o is known in case of mechanical ventilation or calculated using the natural ventilation theory (section 7.2.1.1) for naturally induced flow.

Equation 7-6

$$M = 0.272 \cdot v_x \cdot \delta \quad \left[\frac{m^3/s}{m}\right]$$

Equation 7-7

$$\delta = 0.566 \cdot y \cdot Gr_y^{-\frac{1}{10}} \cdot \Pr^{-\frac{8}{15}} \cdot \left[1 + 0.494 \cdot \Pr^{\frac{2}{3}}\right]^{\frac{1}{10}}$$

Equation 7-8

$$v_x = 0.537 \cdot v_1$$

Equation 7-9

$$v_1 = 1.186 \cdot \frac{\upsilon}{y} \cdot Gr_y^{\frac{1}{2}} \cdot \left[1 + 0.494 \cdot \Pr^{\frac{2}{3}}\right]^{-\frac{1}{2}}$$

Equation 7-10

$$t_{film} = \frac{1}{2}\left(t_s + t_\infty\right)$$

M - volume flow in boundary layer per 1 meter of surface width at the distance y from the cavity entrance, $m^3/s/m$
v_1 - velocity in the boundary layer at the distance y from the cavity entrance, m/s
υ - kinematic viscosity, m^2/s
y - vertical distance, m
x - horizontal distance, m
δ - thickness of boundary layer at the distance y from the cavity entrance, m
v_x - maximum velocity in the boundary layer at the distance y from the cavity entrance, m/s
η - dimensionless distance (x/δ)
t_{film} - film temperature, °C
t_∞ - temperature of the surface and fluid, °C
t_s - surface temperature, °C

7.2.1.1 Natural ventilation

Natural ventilation uses the natural forces of wind or buoyancy, or a combination of those two forces. These forces applied to a building create certain pressure differences between the openings. The magnitude of these pressure differences determines the air flow through the openings to keep the system in equilibrium.

For a double-skin facade, functioning as an external air curtain, the ventilation principle is identified as *single sided ventilation on different levels*. This is because all of the openings in the double facade have the same orientation, but their elevation above the ground is different.

Buoyancy force

The buoyancy force, or so called stack effect, is due to density differences, induced either by differences in temperature or/and humidity. When the density of the indoor air is different from the density of outdoor air, the pressure difference across an opening is caused by the differences in hydrostatic pressures of indoor and outdoor air.

The height of the neutral plane above the floor, H_o is the height at which the hydrostatic pressure of the outdoor air is equal to the hydrostatic pressure of the indoor air and thus the pressure difference equals zero.

The pressure difference for an opening caused by buoyancy force at height *h* can be derived as in Equation 7-11 (Heiselberg, 2005). Then, the pressure difference across an opening above the neutral plane is negative and thus the opening functions as an outlet.

Equation 7-11

$$\Delta P_b = \rho_i \cdot g \frac{T_i - T_o}{T_o}\left(H_o - h\right)$$

ΔP_b - pressure difference across the opening at the height *h,* due to buoyancy, Pa
h - opening height, m
ρ_i - indoor air density, kg/m^3
H_o - height of the neutral plane, m
T_i - indoor air temperature, K
T_o - outdoor air temperature, K

The height of the neutral plane, H_o can be determined by iteration from Equation 7-12 (Heiselberg, 2005):

Equation 7-12

$$\sum_j^n A_j \left|H_o - h_j\right|^{1/2} \frac{H_o - h_j}{\left|H_o - h_j\right|} = 0$$

h - opening height, m
H_o - height of the neutral plane, m
A_j -area of opening *j*, m^2
j - refers to an opening (inlet or outlet)
n - total number of openings in the building

Wind pressure

When wind is passing over a building, a certain pressure is created on the surfaces of the building. These surface pressures vary a lot between the surfaces, but also across a surface. There will be an overpressure on the windward side and an underpressure on the leeward side. Thus, the air flow in the building will be driven from the opening on the windward side to an opening on the leeward side, or from an opening with higher surface pressure to an opening with the lower surface pressure around. The wind pressure on a surface is described as,

Equation 7-13

$$P_w = c_p \cdot \frac{1}{2} \cdot \rho_e \cdot V_{ref}^2$$

P_w - wind induced pressure, Pa

V_{ref} - wind speed at a reference height (roof of the building), m/s
C_p - wind pressure coefficient
ρ_e - outdoor air density, kg/m^3

The pressure difference across an opening, induced by wind is described as:

Equation 7-14

$$\Delta P_w = P_w - P_i$$

ΔP_w - pressure difference across the opening due to wind, Pa
P_i - internal pressure in the building, Pa

The internal pressure at height, H_o, can be determined by iteration from the mass balance Equation 7-17.

Combined buoyancy and wind

It is rare when the buoyancy and wind force exist alone. Normally, there will always be a combination of the wind force and buoyancy. In some cases, they will be opposing to each other and in some cases they will be assisting each other.

The total pressure difference across the opening is then found as a sum of both components:

Equation 7-15

$$\Delta P = \Delta P_w + \Delta P_b = \frac{1}{2} \cdot c_p \cdot \rho_o \cdot V_{ref}^2 - P_i + \frac{\rho_o (T_i - T_o)}{T_i} \cdot g \cdot (H_o - h)$$

Flow rate across an opening

When the pressure difference across an opening is known, then the flow rate can be calculated as following:

Equation 7-16

$$q_v = C_D \cdot A \cdot \sqrt{\frac{2\Delta P}{\rho}}$$

q_v - air flow rate, m^3/h
A - geometrical opening area, m^2
C_d - discharge coefficient
ΔP - pressure difference across the opening, Pa
ρ - air density of the air passing the opening, kg/m^3

The mass balance for a building can finally be written as in Equation 7-17 (Heiselberg, 2005):

Equation 7-17

$$\sum_{j=1}^{n} C_{d,j} A_j \rho_j \left(\frac{|\Delta P_j|}{\frac{1}{2} \rho_j} \right)^{\frac{1}{2}} \cdot \frac{\Delta P_j}{|\Delta P_j|} = 0$$

7.2.2 THERMAL MODEL

When the distribution of the mass flow rates in the DSF cavity is solved, a system of equations for thermal balance should to be formulated and solved.

There are three major heat transfer processes to consider: conduction, convection and long wave radiation. Furthermore, the mass flow rate should be included into the thermal balance as an enthalpy carrier and also the distribution of solar radiation must be known.

In this chapter the models for distribution and transmission of solar radiation, longwave radiation exchange at the external surface (ee) and also the convective heat transfer at the ee-surface and not described. These, however are included into the thermal balance.

Conduction

In the field of building thermal simulation, conduction heat transfer, is usually straight forward to estimate. It is defined according to Fourier's law of heat conduction,

Equation 7-18

$$q_c = -\lambda \frac{\Delta t}{\Delta x}$$

q_c - conduction heat flux, W/m^2
λ - thermal conductivity of the material W/(m^{o}C)
Δt - temperature difference between the nodes, ^{o}C
Δx - distance between the nodes, m

The thermal capacity in the glazing is frequently neglected as the quantity of glass is rather low compared to the amount of air that is passing through the system.

Convection

Convection is one of the most difficult issues of heat transfer, which is often referred to as Newton's Law of Cooling and in general terms is defined as,

Equation 7-19

$$q_{conv} = \alpha \cdot \Delta t$$

q_{conv} - convection heat flux, W
α - convective heat transfer coefficient, W/(m^2 ^{o}C)
Δt - temperature difference between the surface and fluid, ^{o}C

Contrary to conduction, the convective heat transfer is not always constant and it is not a material property. In fact, the assessment of this coefficient is one of the biggest challenges. Nusselt number is normally used as a measure for convective heat transfer that occurs at the surface:

Equation 7-20

$$Nu = \frac{\alpha \cdot l}{k}$$

ρ - fluid density, kg/m^3
V - average velocity of the fluid, m/s
μ - dynamic viscosity, Ns/m^2

υ - kinematic viscosity of the fluid, m^2/s
g - gravitational acceleration, m^2/s
β - coefficient of volumetric expansion, 1/k
T_s, T_∞ - temperature of the surface and fluid, K

Nusselt number is then expressed via the governing dimensionless numbers. It depends on the convective regime, flow regime dimensions of the cavity and other boundary conditions. To obtain a relationship for Nusselt number different numerical and experimental methods are normally used. However, it can be difficult to find suitable relationship that will allow accurate assessment of convective heat transfer. This is particularly difficult to do if the boundary conditions are dynamic and the convective or flow regime varies in time.

In the definition of the flow model, as described in the previous section 7.2.1 , Eckert and Jonson's approach (Eckert and Jackson, 1951; Heiselberg,1990) was used. In this approach, the assumptions regarding the thermal boundary layer were made, and in order to keep the consistency of the modelling the energy flow along the surface should be calculated according to the same approach and its assumptions:

Equation 7-21

$$q = 0.0682 \cdot \rho \cdot c_p \cdot \nu_x \cdot (t_s - t_\infty) \cdot \delta$$

q - heat flux from the surface per 1 meter of surface width at the distance *y* from the cavity entrance, W/m
y - vertical distance, m
δ - thickness of boundary layer at the distance *y* from the cavity entrance, m
ν_x - maximum velocity in the boundary layer at the distance y from the cavity entrance, m/s
t_∞ - temperature of the surface and fluid, °C
t_s - surface temperature, °C

Longwave radiation exchange

For problems, which do not involve complex geometry, the network method can be successfully used. To calculate the radiation exchange at the surface, following parameters are involved:

Equation 7-22

$$J_i = \varepsilon_i \cdot \sigma \cdot T_{si}^{\ 4} + \rho_i \cdot G_i$$

i - index for surface *i*
J - radiosity, or total radiation which leaves a surface per unit time and per unit area
G - irradiation, or total radiation incident upon a surface per unit time and per unit area
ρ - longwave radiation reflectance property of surface
α - longwave radiation absorptance property of surface
τ - longwave radiation transmittance property of surface
ε - longwave radiation emittance property of surface
σ - Stefan-Boltzmann constant ($\sigma = 5.67 \cdot 10^{-8}\ W/(m^2 \cdot K^4)$)
T_s - surface temperature in Kelvins

Equation 7-23

$$\alpha + \tau + \rho = 1$$

According to the First Law of Thermodynamics (Equation 7-23), knowing that $\tau=0$ and assuming that $\varepsilon=\alpha$, the net energy last by a surface is the difference between radiosity and irradiation:

Equation 7-24

$$\frac{q_{LWi}}{A_i} = J_i - G_i = \varepsilon_i \cdot \sigma \cdot T_i^4 + (1-\varepsilon_i) \cdot G_i - G_i$$

Substituting Equation 7-22 in Equation 7-24:

Equation 7-25

$$q_{LWi} = \frac{\sigma \cdot T_i^4 - J_i}{(1-\varepsilon_i)/(\varepsilon_i \cdot A_i)}$$

The distribution of radiation from a surface among the surfaces in enclosure is indicated by a view factor (ASHRAE., 2001). The view factors needed for assessment of the long wave radiation exchange between the surfaces in each layer of the DSF cavity can be pre-calculated before the actual simulation.

The irradiation of surface *i* is the sum of the radiation incident upon it coming from all *n* surfaces:

Equation 7-26

$$G_i = \sum_{j=1}^{n} F_{i-j} \cdot J_j$$

i,j - surface number
F_{i-j} - view factor between surfaces *i* and *j*

Different methods for calculation of view factors can be used. For example, see Holman (1976). When the view factors and surface temperatures are known, the radiosities can be calculated from energy balance formulated for each surface (Equation 7-22). Finally, the net radiant energy lost by each surface is determined from Equation 7-25..

Enthalpy flow

The mass flow rate in the cavity is the main energy carrier in the double-skin facade systems, which is defined as,

Equation 7-27

$$Q = m \cdot c_p \cdot t$$

Q - energy transport with enthalpy flow, W
m - mass flow rate, kg/s
c_p - specific heat capacity of the air, J/(kg°C)
t - air temperature, °C

Thermal balance

The temperature in each zone is represented as a bulk temperature. Then the thermal balance is solved for every zone, and at once in the whole cavity. An illustration of the heat flows in the model is given in the Figure 7-7.

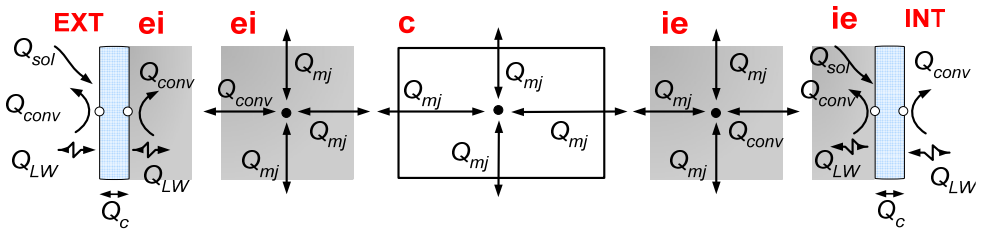

Figure 7-7. Heat flows between the zones in the DSF model.

An overall consequence of the assumptions made, earlier, regarding the boundary layer, for the thermal model is the appearance of a thermal core. The core is created by the recirculating flow. Since the recirculating flow is fed only by the air from the top layer, the recirculating flow has a constant temperature of the top layer. This was also confirmed by measurements shown in Figure 6-20.

For the practical needs, however, the air temperature of the boundary layer or core is not interesting, while the temperature gradient in the cavity is. Thus, the zone temperature for every layer can be translated into the volume averaged air temperature of the layers and thus the vertical temperature gradients in the cavity.

7.2.3 SUMMARY

In this chapter a suggestion for a model, able to count for recirculation flow occurrences in the DSF cavity has been made. The model is based on Eckert and Jonson's approach (Eckert and Jackson, 1951; Heiselberg, 1990) and consists of two parts:

- Mass model
- Thermal model

In the mass model, a simple mass balance is solved for mass flow in recalculation, according to total mass flow entering the cavity and mass flow necessary for development of boundary layer. Mass flow in the boundary layer is estimated according to Eckert and Jonson's approach, which is also used to calculate the convective heat flux in the boundary layer.

Since Eckert and Jonson's approach was developed for a flat plate with fluid velocity equal zero. This is not valid for DSF cavity and the limitations are present in the model. Moreover, some significant assumptions with regard to boundary layer development above the neutral plane have been made.

On the whole, this model is only a suggestion, which requires further development and improvement together with detailed experimental investigations in well controlled environment in a wind tunnel.

Chapter 8

CONCLUSION

In this chapter the main findings and conclusions from the work described in this thesis are summarized. At last suggestions and ideas for future work on topic of modelling and experiments of Double-Skin Facade are explained.

8.1 MAIN RESULTS ANS OUTCOME OF THIS WORK

8.1.1 LITERATURE REVIEW ON MODELLING APPROACHES

Double-Skin Facades are gaining popularity that, in fact, appears to be independent from sturdy critics of the concept in the past years. DSF buildings are being built in Europe and worldwide, DSF concept is being taught at schools of architecture and fully glazed office buildings are being favored by companies and their employees.

To bring the reduction of energy use in these buildings application of suitable tools and methods are necessary to achieve successful design solutions.

Chapter 2, the literature review reveals the main findings and difficulties experienced by scientists when attempting to model DSF thermal and energy performance. As an outcome of this review three main areas in modelling of double-skin facades are identified. These are as following: heat transfer element, optical element and flow element.

Importance and challenges of each element are discussed in detail and in conclusion, it is explained that a successful model will deal with all of these elements on an equal level to attain reliable results.

It was also recognized that there are two main topics which remain open for further development and exploration. These are the convective heat transfer in the DSF cavity and the modelling of naturally induced flow rates in the cavity. Furthermore, the lack of experimental studies and empirical validation of models has been realized.

8.1.2 EMPIRICAL VALIDATION OF MODELS

The experimental results were used for empirical validation of building simulation tools. Here it was found that the assumptions made in the models towards the surface film coefficients are curtail for DSF modelling. It was established that using fixed combined surface coefficients is not acceptable. Moreover the internal surface heat transfer coefficients are particularly important. Furthermore, a question of application of variable convective heat transfer coefficients is raised without the answer.

All in all, results of empirical validation appeared to be limited and resulted in more questions than answers. For the moment, none of the models appeared to be consistent enough when compare results of simulations with the experimental data. For the MODE 2, however, it was argued that ESP-r and TRNSYS-TUD models are reasonably close in their predictions to experimental results.

All of the models experience difficulties in predictions during the peak solar loads. Meanwhile, these are in good agreement with the experiments when solar loads are absent or low. It is seen that prediction of cooling/heating in experiment room follows the behaviour of predicted air temperature in the DSF cavity. When temperature in cavity is underestimated, then the cooling load is also underestimated. It is argued that improvements in prediction of air temperature in the cavity will resolve some of these disagreements and will contribute to more accurate calculations of natural driving forces.

Finally, it was concluded that disagreements between the models and experiments allow indicating a problem, while further research is needed to solve these problems. The results of this empirical validation are regarded as an argument for further research, as most of the results do not allow deriving any solid conclusions, and only designate the

directions to follow. Suggestions for future investigations are given in the end of the chapter.

With regard to naturally induced air flow in the cavity, the similarities in the shapes between the measurements and simulations for TRNSYS-TUD and ESP-r model show a great potential. This is due to the fact that both of these programs take into the consideration the pressure difference coefficients for each opening. Here it is concluded that application of accurate pressure difference coefficients for each opening is crucial for prediction of naturally induced flow in DSF.

8.1.3 EXPERIMENTAL RESULTS

Analysis of experimental results has lead to a number of interesting observations. Following are the observations made with regard to temperature:

- For periods with high solar intensity, the dimensionless surface temperature of glazing exceeds value of 1. It is argued that these high surface temperatures lead to appearance of strong boundary layer flow in the cavity. This was also confirmed when investigated Gr/Re^2 ratio.

- In MODE 1, the maximum temperature in the cavity appears at height 4.5 m and not at the top of the cavity. Moreover, measurements conducted by Marszal and Thomas (2008) demonstrate that for periods with strong solar radiation, vertical temperature gradient in the cavity exists only until a certain point, after that there is no temperature increase with height.

It is seen that need for cooling arises even at very low solar radiation intensity. Thus using a proper shading devise will be inevitable when designing a double-skin facade building.

Although it is difficult to measure the air flow in a naturally ventilated double facade cavity, as there is no easy method either no accurate one exists, results obtained with the velocity profile and the tracer gas method show reasonable agreement. Despite the uncertainties and errors in the results, these are essential for investigation of DSF performance and empirical validation of software tools.

Following are the main observations made with regard to air flow measurement in DSF:

- On contrary to literature, it is found that the mass flow rate in DSF cavity was wind driven for the most of time. This observation is contradictional to common assumption of buoyancy driven flow in the cavity. Only for the moderate wind speed (below 4 m/s) the air flow was dominated by buoyancy, similar to findings made by Larsen (2006) for single-sided ventilation with one opening.

- Enormous air change rates were measured in the DSF cavity. These were induced by wind even with small differences in pressure coefficients between the openings. Accordingly, accurate estimation of pressure and discharge coefficients for each opening are essential for simulation of natural air flow rate in the cavity. The same conclusion was made within empirical validation of building simulation software.

- Mass flow rate in the cavity estimated using the velocity profile method is significantly different when measured on different heights in DSF cavity. Moreover, it is increasing with height.

Measurement results carried a notion of strong boundary layer in the DSF cavity, some observations i.e. shape of vertical temperature gradient in the cavity, increasing mass flow rate when measured with velocity profile method in different heights, high surface temperatures of the glazing have lead to a hypothesis of recirculation flow appearance in the DSF cavity, which occur when mass flow in boundary layers exceeds the amount of incoming flow in the cavity.

8.1.4 RECIRCULATION FLOW

Looking upon the literature, this hypothesis was further investigated. From the literature review it was found that the appearance of recirculation flow in the DSF cavity is not an assumption, but a possibility both for laminar and for turbulent flow regime. However, most of the works considered in the literature study did not focus on the flow reversal phenomenon itself. The conditions for its appearance have not been studied as well as its' consequences for the heat transfer and for the vertical temperature gradients in the cavity. Nevertheless, these consequences have an exceptional importance for the DSF performance and approaches for modelling double facade cavity.

To verify presence of flow recirculation in the experimental data sets a number of investigations were carried out.

First of all, flow and convection regime in the DSF cavity were examined. It was found that foremost of experimental data is available for free or mixed convection regime and undeveloped turbulent flow. Along, a question of presence of all three convection regimes at the same time in the DSF cavity was raised, but due to the lack of experimental data this was not confirmed.

The velocity profiles in the DSF cavity were studied. A strong correlation between Gr_H/Re_H^2 –ratio and the shape of velocity profiles was observed, indicating either occurrence of recirculation flow or influence of wind washout effect.

Finally, the thickness, velocity and mass flow in the boundary layer of the DSF cavity were calculated using the Eckert and Jackson approach (Eckert and Jackson, 1951; Heiselberg, 1990). The mass flow rate calculated for the boundary layer flow appeared to be comparable with the measured mass flow rate in the cavity. According to the hypothesis, this indicates that it is reasonable to expect flow reversal in the cavity. Moreover, mass flow rate in the boundary layer was calculated at the lower height than the flow reversal is expected.

All things considered, it is concluded that there are no clear evidence for presence of recirculation flow in the experimental data, as many indications of recirculating flow could also be a measurement error. It is obvious that more detailed experimental studies are needed to document appearance of this phenomenon. Meanwhile, there are many strong arguments that do not allow disregarding of recirculation flow when assessing DSF performance in the periods of peak loads.

Occurrence of flow reversal may lead to a significant change of the heat transfer in the cavity and therefore will have significant consequences for temperature gradient, naturally induced mass flow rate and for the overall thermal performance of the DSF cavity. This will, normally, take place during the peak loads of solar radiation. These are also the periods when prediction of thermal and energy performance of DSF cavity is difficult.

8.1.5 SUGGESTION FOR A NEW MODEL

Being able to count on mass and heat transport via recirculation flow, will help to resolve the question of heat transfer through double-facade in periods of peak solar loads. To achieve that, the main principles for a new numerical model are explained with a need for further improvement.

The main idea behind the model is to calculate the mass of recalculation flow from the mass balance, where the total incoming flow is known or calculated from natural ventilation theory and needed mass flow in the boundary layer is calculated using the Eckert and Jackson approach (Eckert and Jackson, 1951; Heiselberg, 1990). In the thermal balance the convective heat flux is determined according to the same approach.

This model has a number of limitations, however, more information about recirculation flow behavior and its affection of boundary layer behavior are compulsory. Therefore further improvement of the model might be necessary.

8.1.6 CONCLUSION AND LIMITATIONS OF THIS WORK

Three main subjects regarding DSF performance were addressed in this work.

Experimental investigation of DSF performance was carried out to address the need for experimental studies of DSF, with attention paid to natural ventilation phenomena and measurements of naturally induced air flow in the cavity

Empirical validation of building simulation tools was conducted within IEA Annex 34/43, which results are explained and discussed in Chapter 4 of this thesis. As the request for these studies was frequently met in the literature. The results of this work confirm that this task has not been completed, and more work within empirical validation has to be done.

Finally, *convection and flow behaviour in the DSF cavity* were closely investigated and a suggestion for a new numerical model for modelling of double-skin facade is developed.

The main outcome of this work is seen in opening a discussion on issue of flow reversal in double- skin facade cavity. Moreover, a suggestion for treatment of this phenomenon in numerical models has been made. Although, the experimental investigations do not contain any clear evidences of flow reversal, future research can solve this dilemma. Recommendations for future work are given in section 8.2

The work presented in this thesis includes also some limitations. The most significant of them is the lack of studies and experiments with application of shading device in the cavity, which normally becomes a significant contributor to DSF thermal performance.

Another limitation is seen in lacking a clear message from empirical validation work.

Finally, the limitation is seen in accuracy of attained experimental data and the boundary conditions chosen for the measurements, which resulted in limited solar radiation intensity.

8.2 RECOMMENDATIONS FOR FUTURE WORK

In view of questions arose from this work following topics are recommended for future investigations:

1. Flow recirculation has not been properly documented in the present work. In the future, this can be done via detailed experimental investigations in laboratory conditions, in a wind tunnel. Here the conditions for recirculation flow appearance, its consequences for the heat transfer and boundary layer development above the recirculation neutral plane are compulsory for further studies. It is also very interesting to examine how the aspect ratio of the cavity and different surface temperatures influence the recirculation flow?

2. When occurrence of flow recirculation is documented, it is essential to examine whether Eckert and Jackson approach is adequate for application with DSF and whether their approach requires any correction. The correction might be necessary as this approach was developed for the flat plates with free stream velocity equal zero, which is not true for DSF cavities.

3. Improvements of suggested mass flow model in Chapter 7 might be needed, in view of results from above mentioned studies.

4. With regard to natural ventilation, it is interesting to investigate when the wind washout appears and what influence it has on mass and heat transfer in the DSF cavity. What are the reasons for increase of air change rate in the cavity when the wind direction is towards the openings?

5. Significant improvement of measurement results in future would be achieved with proper visualization technique for flow pattern in the cavity. This would allow verifying the presence of recirculation flow, impact from wind washout effect and conditions for its appearance. Finally, it would be possible to evaluate mixing of tracer gas with incoming air using visualization. However, most of visualization techniques are incompatible with solar exposure. Thus a new visualization tool or method is required for future work.

6. Completing the empirical validation of building simulation software is compulsory. It could be beneficial to continue with simple comparative/empirical studies, targeting investigations of one parameter at the time. More detailed sensitivity studies of the models might be necessary for exact diagnosis of the results. A simple steady state test case with presence of solar radiation might be needed with detailed heat balance for each model might be needed, etc. Also attaining more accurate empirical data would be helpful.

7. Availability of experimental results for DSF with shading device are also essential. It would be beneficial to complete these measurements for 'The Cube' test facility to be able to compare across the results.

Many recommendations has been made, however the attention must be paid to studies of DSF performance in a wind tunnel, as the full scale measurements are extremely time consuming and, often, their accuracy may suffer, as one has no control over the Nature. For the moment, there is a lot of work can be done prior to full-scale measurements.

REFERENCES

AIVC (1994) Air Infiltration and Ventilation Centre. Orme, M., Liddament, M.W. and Wilson, A. Numerical Data for Air Infiltration and Natural Ventilation Calculations. Technical Note 44, Code TN 44. 100p.

AIVC (1996). Air Infiltration and Ventilation Centre. Liddament, M. W. A Guide to Energy Efficient Ventilation, Annex V, Code GV. ISBN 0946075859

Allard, F. (1998). Natural ventilation in buildings: a design handbook. London: James & James. 356 p.

Allard, F., Ghiaus, C. and Mansouri, Y. 2003. Natural Ventilation for Health, Comfort and Energy Efficiency. ENCAC- COTEDI 2003, 21p.

Armaly, B. F., Chen, T. S. and Ramachadran, N. (1987) Correlations for laminar mixed convection on vertical, inclined and horizontal flat plates with uniform surface heat flux. Int. J. Heat Mass Transfer 30 (1987) 405–408

Arons, D.M.M., and Glicksman, L.R. (2001). Double Skin, Airflow Facades: will the Popular European Model work in the USA?, Proceedings of ICBEST 2001, International Conference on Building Envelope Systems and Technologies, Ottawa, Canada, vol. 1, 203-207.

ASHRAE (2001). ASHRAE Fundamentals, American Society of Heating, Refrigerating, and Air-Conditioning Engineers, 2001, ISBN 1- 883413-88-5

Aung, W., and Worku, G. (1986) Developing flow and flow reversal in a vertical channel with asymmetric wall temperatures. ASME Journal of Heat transfer, 1986, Vol. 108, pp. 299-304.

Awbi, H.B. Ventilation of Buildings. Air infiltration and natural ventilation (chapter 3). F&FN Spon. ISBN 0-419-15690-9.

Ayinde, T.F.(2008) Experimental investigation of turbulent natural convection flow in a converging channel. Experimental Thermal and Fluid Science, 32 (6), pp. 1204-1212.

Baker, P.H. and McEvoy, M.E. (1999) An Investigation into the Use of a Supply Air Window as a Heat Reclaim Device. Proceedings CIBSE A: Building Serv. Eng. Res. Technol. 20(3) 105-112 (1999), Great Britain.

Baker, P.H. and McEvoy, M.E. (2000) Test Cell Analysis of the Use of a Supply Air Window as a Passive Solar Component. Solar Energy, vol. 69, No. 2 , 113-130,2000, Great Britain.

Balocco, C. (2002). A Simple Model to Study Ventilated Facades Energy Performance. Energy and Buildings 34 (2002) 469-475.

Barták, M., Dunovská, T., and Hensen, J. (2001). Design Support Simulations for a Double Skin Facade. Proceedings of the 1st Int. Conf. on Renewable Energy in Buildings "Sustainable Buildings and Solar Energy 2001", pp. 126-129, Brno, 15-16 November, Brno University of Technology / Czech Academy of Sciences in Prague, Czech Republic. Web address: http://www.bwk.tue.nl/fago/hensen/publications/01_brno_dskin_design_support.pdf

Beausoleil-Morrison, I. (1999). Modelling Mixed Convection Heat Transfer at Internal Buildings Surfaces, Proceedings of Building Simulation '99, (1), 313-320, Kyoto.

Beausoleil-Morrison, I. (2001). The Adaptive Coupling of Computational Fluid Dynamics with Whole-Building Thermal Simulation, Proceedings of Building Simulation '01, (2), 1259-1266, Rio de Janeiro.

Beausoleil-Morrison, I., Clarke, J.A., Denev, J., Macdonald, I.A., Melikov, A. and Stankov, P. (2001). Further Developments in the Conflation of CFD and Building Simulation, Proceedings of Building Simulation '01, (2), 1267-1274, Rio de Janeiro.

Bredsdorff, M. (2007). 250 Aar gammelt russervindue indtager danske bygninger. Newspaper 'Ingenoeren', 17 of October, 2007. (in Danish).

CEN Report, CR1752, Ventilation for buildings - Design criteria for the indoor environment, CEN 1998

Champagne, C. (2002). Computational Fluid Dynamics and Double Skin Facades. Assignment for the Architectural Engineering Computer Labs, Pennsylvania State University, USA Web address: http://www.arche.psu.edu/courses/ae597J/Champage-Hw1.pdf

Chandra, M.V. and Swami, M.V. (1994). Correlations for pressure distribution of buildings and calculation of natural ventilation airflows. ASHRAE Transactions 94(1).

Chen, Q. (1997). Computational fluid dynamics for HVAC: successes and failures. ASHRAE Transactions, 103(1), 178-187.

Cheng, C.H. and Yang, J.J., (1994). Buoyancy-induced recirculation bubbles and heat convection of developing flow in vertical channels with fin arrays. Int. J. Heat and Fluid Flow 5, pp. 11–19.

Cheng,C.-H., Weng, C.-J. and Aung, W.(2000) Buoyancy-assisted flow reversal and convective heat transfer in entrance region of a vertical rectangular duct. Int. J. Heat Fluid Flow 21 (2000), pp. 403–411.

Cho, S.-H., Shin, K.-S. and Zaheer-Uddin, M. (1995). The Effect of Slat Angle of Windows with Venetian Blinds on Heating and Cooling Loads of Buildings in South Korea. Energy, Vol. 20, No12, pp. 1225-1236, Great Britain.

Ciampi, M., Leccese, F. and Tuoni, G. (2003). Ventilated Facades Energy Performance in Summer Cooling of Buildings. Solar Energy, vol. 75.

Clarke, J.A. (1985) Energy simulation in building design . - 2. ed. . - Oxford : Butterworth-Heinemann, 1985 . - 362 s.

Di Maio, F. and van Paassen, A.H.C. (2000). Second Skin Facade Simulation With Simulink Code. International symposium air conditioning in high rise buildings (Shanghai), s.n.,s.l.,ISBN 2-913149-07-3, cat c, Project code: 06A-V. Web address: http://www.ocp.tudelft.nl/et/Research/EnergyInBuiltEnvironment/SecondSkinFacade/DSF/publications/ACHRB_Shanghai_2000.pdf

Ding, W., Hasemi, Y. and Yamada, T. (2004). Natural Ventilation of a Double-Skin Facade with Solar Chimney. Energy and Buildings Vol. 37, No. 4, 411-418, 2005.

Djunaedy, E., Hensen, J.L.M., & Loomans, M.G.L.C. (2002). Towards a Strategy for Airflow Simulation in Building Design Center for Building & Systems TNO - TU/e. Technische Universiteit Eindhoven, the Netherlands. Web address: http://sts.bwk.tue.nl/erdj/papers/roomvent2002.pdf

Djunaedy, E., Hensen, J.L.M., & Loomans, M.G.L.C. (2003). Development of a guideline for selecting a simulation tool for airflow prediction. Proceedings of 8th International IBPSA Conference Building Simulation'03, 267-274, Netherlands

Duffie, J. and Beckman, W. (1991). Solar Engineering of Thermal Processes. John Wiley & Sons Inc., New York.

Eckert, E.R.G. and Jackson, T.W.(1951). Analysis of turbulent free-convection boundary layer on flat plate. NACA-Report 1015.

Edwards, D.K. (1977). Solar absorption by each element in an absorber-coverglass array, Solar Energy, vol. 19, pp. 401-402.

Elsner, Dittman (1992/1993). Grundlagen der Technischen Thermodynamik: Band 1 Energielehre und Stoffverhalten, 8th Edition, Akademie Verlag, Berlin, 1992/1993.

Elsner, Fischer, Huhn (1993). Grundlagen der Technischen Thermodynamik: Band 2 Wårmeubertragung, 8th Edition, Akademie Verlag, Berlin, 1993.

Erell, E, Leal, V, and Maldonado, E. (2005), Measurement of air temperature in the presence of a large radiant flux: an assessment of passively ventilated thermometer screens, Boundary-Layer Meteorology, vol. 114, pp. 205-231.

Etheridge, D, and Sandberg M. 1996. Building ventilation: theory and measurement . - Chichester : John Wiley, 1996. - 724 s.

European Standard EN 13182, Ventilation for buildings - Instrumentation requirements for air velocity measurements in ventilated spaces, CEN 2002

Faggembauu, D., Costa, M., Soria, M. and Oliva, A. (2003). Numerical Analysis of the Thermal Behavior of Ventilated Glazed Facades in Mediterranean Climates. Part I: Development and Validation of a Numerical Model. Solar Energy 75 (2003) 217-228.

Faggembauu, D., Costa, M., Soria, M. and Oliva, A. (2003). Numerical Analysis of the Thermal Behavior of Ventilated Glazed Facades in Mediterranean Climates. Part II: Applications and Analysis of Results. Solar Energy 75 (2003) 229-239.

Flamant, G., Heijmans N., Guiot E., Gratia E. and Bruyere I. (2004). Ventilated Double Facades. Determination of the energy performances of ventilated double facades by the use of simulation integrating the control aspects – Modelling aspects and assessment of the applicability of several simulation software. Final report, Belgian Building Research Institute, December, 2004.

Gan, G. (2001). Thermal transmittance of multiple glazing: computational fluid dynamics prediction. Applied Thermal Engineering. 21 (2001) 1583-1592.

Gau, C., Huang, T.M. and Aung, W. (1996) Flow and mixed convection heat transfer in a divergent heated vertical channel. ASME J. Heat Transfer 118 3, pp. 606–615.

Gau, C., Yih, K., and Aung, W.,(1990) Mixed convection heat transfer in vertically heated channels, AIAA Paper No. 90-1723

Gau, C., Yih, K.A. and Aung, W. (1992a) Reversed flow structure and heat transfer measurements for buoyancy-assisted convection in a heated vertical duct. J. Heat Transfer 114 (1992), pp. 928–935.

Gau, C., Yih, K.A. and Aung, W. (1992b) Measurements of heat transfer and flow structure in heated vertical channels. J. Thermophys. Heat Transfer 6 (1992), pp. 707–712.

Gertis, K. (1999). Sind neuere Fassadenentwickelungen bauphysikalisch sinnvoll? Teil 2: Glas-Doppelfassaden (GDF) (in German), Bauphysik, vol. 21, pp. 54-66.

Grabe, J.V. (2002). A prediction tool for the temperature field of double facades. Energy and Buildings 34 (2002) 891-899

Gratia, E. and De Herde, A. (2004). A Natural cooling strategies efficiency in an office building with a double-skin facade. Energy and Buildings, Vol. 36, No. 11, November 2004, 1139-1152.

Gratia, E. and De Herde, A. (2004). Natural Ventilation in a Double-Skin Facade. Energy and Buildings 36(2004) 137-146.

Gratia, E. and De Herde, A. (2004). Optimal Operation of a South Double-Skin Facade. Energy and Buildings 36(2004) 41-60.

Habib M.A., Said S.A.M., Ahmed S.A. and Asghar A., (2002) Velocity characteristics of turbulent natural convection in symmetrically and asymmetrically heated vertical channels, Experimental Thermal and Fluid Sciences 26, pp. 77–87.

Haddad, K.H. and Elmahdy, A.H. (1998). Comparison of the Monthly Thermal Performance of a Conventional Window and a Supply-Air Window, ASHRAE Transactions, vol. 104, Part 1 B, pp. 1261-1270.

Heiselberg, P. (2005) Natural and Hybrid Ventilation Notes, lecture notes from the PhD-course “Modelling natural and hybrid ventilation, Aalborg University.

Hensen, J.L.M. (2002). Integrated Building (and) airflow Simulation: an overview. Proceedings from the Ninth International Conference on Computing in Civil and Building Engineering, Taipei, Taiwan. Web address:http://www.bwk.tue.nl/fago/hensen/publications/ 02_icccbe_airflow.pdf

Hensen, J.L.M., Bartak, M., and Drkal, F. (2002). Modellng and simulation of double-skin facade systems. ASHRAE Transactions, vol. 108:2, American Society of Heating, Refrigerating, and Air-Conditioning Engineers, Atlanta, GA. Web address: http://www.bwk.tue.nl/fago/hensen/publications/ 0 2_ashrae_dskin. pdf

Hitchin, E. R. and Wilson, C. B. (1967) A review of experimental techniques for the investigation of natural ventilation in buildings. Building Sciences Vol. 2 ,1967, pp. 59–82.

Holman, P.J. (1991). Heat Transfer, McGraw-Hill, New York, 1991.

Holman, J. P. (1976) Heat transfer . - 4th ed . - New YorkLondon (etc.) : McGraw-Hill, 1976 . - xvii,530p

Hottel, H.C. (1954) Radiant Heat Transmission, in: McAdams, W.H. (ed.), Heat Transmission, New York: McGraw-Hill.

Huang, T. M., Gau, C., and Aung, W. (1995) Mixed Convection Flow and Heat Transfer in a Vertical Convergent Channel, Int. J. Heat Mass Transf., 38, No. 13, pp. 2445–2456

Incropera, F.P., DeWitt D.P., Bergman, T.L. and Lavine, A.S. (2007). Fundamentals of Heat and Mass Transfer, 6th Edition, ISBN: 978-0-471-45728-2, 1024 p.

Jaros, M., Charvát, P., Švorèík, P., & Gorný, R. Possibilities of CFD Simulation of Solar Heated Spaces. Brno University of Technology, Faculty of Mechanical Engineering. Institute of Power Engineering, Dept. of Thermodynamics and Environmental Engng, Brno, Czech Republic.

Jaros, M., Gorny, R., Katolicky, J. and Sedlak, J. (2002). Numerical and Experimental Investigation of the Conditions in the Double Solar Energy Facade. Proceedings: Indoor Air 2002 can’t find paper.

Jensen, R. Rl, Kalyanova, O. and Hyldgaard, C.-E.(2007) On the use of hot-sphere anemometers in a highly transient flow in a double-skin facade. I: Proceedings of Roomvent 2007 : Helsinki 13-15 June 2007. Finland : FINVAC ry, 2007.

Kalyanova, O. and Heiselberg, P. (2007). Comparative validation of building simulation software: Modelling of Double Facades: FINAL REPORT. Aalborg: Aalborg University: Department of Civil Engineering. ISSN 1901-726X DCE Technical Report No.024.

Kalyanova, O. and Heiselberg, P. (2007a). Empirical Test Case Specification: Test Cases DSF200_3 and DSF200_4 : IEA ECBCS Annex43/SHC Task 34 : Validation of Building Energy Simulation Tools. Aalborg: Aalborg University : Department of Civil Engineering. ISSN 1901-726X DCE Technical Report No.033

Kalyanova, O. and Heiselberg, P. (2007b) Experimental Set-up and Full-scale measurements in the 'Cube'. Aalborg : Aalborg University : Department of Civil Engineering,. 59 s. (DCE Technical Report; 34).

Kalyanova, O., Jensen, R.L. and Heiselberg, P.(2007b) Measurement of air flow rate in a naturally ventilated double skin facade. The International Conference on Air Distribution in Rooms, Roomvent, Helsinki, Finland. 13. - 15. juni.

Kalyanova, O., Poirazis, H., Heiselberg, P.K.(2006) Literature Review of Double Skin Facades Modelling Approaches : Report for IEA ECBCS Annex 43/SHC Task 34 Validation of Building Energy Simulation Tools. Instituttet for Bygningsteknik, Aalborg Universitet : Instituttet for Bygningsteknik, Aalborg Universitet, 2005. 34 s. Forskning: Videnskabelig rapport

Kalyanova, O., Zanghirella, F., Heiselberg, P., Perino, M., Jensen, R.L. (2007a) Measuring air temperature in glazed ventilated facades in the presence of direct solar radiation. I: Proceedings of Roomvent 2007. Finland : FINVAC ry, 2007. 10 s.

Larsen, T S. 2006. Natural Ventilation Driven by Wind and Temperature Difference. Ph.D Thesis. Aalborg : Department of Civil Engineering : Aalborg University, 2006. 140 p.

Lee, E., Selkowitz, S., Bazjanac, V., Inkarojrit, V., andKohler, C. (2002). High-Performance Commercial Building Facades. Building Technologies Program, Environmental Energy Technologies Division, Ernest Orlando Lawrence Berkeley National Laboratory (LBNL), Univer¬sity of California, Berkeley, USA (LBNL - 50502)

Li, Shang-Shiou (2001). A Protocol to Determine the Performance of South Facing Double Glass Facade System MSc Thesis in Architecture Submitted to the Faculty of the Virginia Polytechnic Institute and State University, USA. Web address: http://scholar.lib.vt.edu/theses/available/etd-04212001-152253/unrestricted/

Liddament, M.V. (1996). A guide to Energy Efficient Ventilation. Air infiltration and Ventilation Center, University of Warwick.

Lockmanhekin, M. (1975). Procedure for determining Heating and Cooling Loads for Computerized Energy Calculations - Algorithms for Building Heat Transfer Subroutines. ASHRAE, Atlanta, GA (1975).

Manz, H. (2003). Numerical Simulation of Heat Transfer by Natural Convection in Cavities of Facade Elements, Energy and Buildings, Vol. 35, 2003, 305-311.

Manz, H. (2004). Total solar energy transmittance of glass double facades with free convection, Energy and Buildings, Vol. 36, 2004, 127-136.

Manz, H. and Frank, Th. (2005). Thermal Simulation of Buildings with Double-Skin Facades. Energy and Buildings, 37 (2005) 1114-1121.

Manz, H., & Simmler, H. (2003). Experimental and numerical study of a mechanically ventilated glass double facade with integrated shad¬ing device. Proceedings of the Building Physics Conference (2003) in Belgium.

Manz, H., Schaelin, A. and Simmler, H. (2004). Airflow patterns and thermal behavior of mechanically ventilated glass double facades, Building and Environment, Vol. 39, 2004, 1023-1033.

Marcondes, F., De Souza Melo, V., Gurgel, J.M. (2006). Numerical analysis of natural convection in parallel, convergent, and divergent open-ended channels. International Journal of Numerical Methods for Heat and Fluid Flow, 16 (3), pp. 304-323.

Marcondes, F., De Souza Melo, V., Gurgel, J.M. (2006). Numerical analysis of natural convection in parallel, convergent, and divergent open-ended channels. International Journal of Numerical Methods for Heat and Fluid Flow, 16 (3), pp. 304-323.

Marszal A.J. and Thomas S.J. (2008). Modelling and Design of Double Skin Facades. Matter Thesis. Department of Civil Engineering, Aalborg University, Denmark. 90p

McWilliams J., (2002). Review of Airflow Measurement Techniques. Lawrence Berkeley National Laboratory, December 1, 2002

Mei, L., Infield, D., Eicker, U. and Fux, V. (2003). Thermal Modeling of a Building with an Integrated Ventilated PV Facade. Energy and Buildings 35(2003) 605-617.

Mills, A. (1992). Heat Transfer, Irwing

Morton, B., Ingham, D.B., Keen, D.J. and Heggs, P.J., (1989). Recirculating combined convection in laminar pipe flow. ASME J. Heat Transfer 111, pp. 106–113.

Nguyen C.T., Maiga S.E.B., Landry M., Galanis N., Roy G.(2004) Numerical investigation of flow reversal and instability in mixed laminar vertical tube flow (2004) International Journal of Thermal Sciences, 43 (8 SPEC. ISS.), pp. 797-808.

Oesterle, E., Lieb, R-D., Lutz, M., and Heusler, W. (2001). Double Skin Facades — Integrated Planning. Prestel Verlag: Munich, Germany.

Oesterle, E., Lutz, M.,Lieb, R-D., and Heusler, W. (1999). Doppelschalige Fassaden - Ganzheitliche Planung. Callwey-Verlag: Munchen, 1999.

Park, C.-S., Augenbroe, G., Sadegh, N., Thitisawat, M., and Messadi, T.(2003). Occupant Responsive Optimal Control of Smart Facade Systems. Proceedings of Building Simulation'03, August, 2003, Netherlands.

Poirazis H. (2006). Double Skin Facades for Office Buildings - Literature Review Report. Division of Energy and Building Design, Department of Construction and Architecture, Lund Institute of Technology, Lund University, Report EBD-R—04

Poirazis H. (2008). Single and Double Skin Glazed Office Buildings - Analyses of Energy Use and Indoor Climate. Division of Energy and Building Design, Department of Construction and Architecture, Lund Institute of Technology, Lund University, Report EBD-T--08/8. Web address:http://www2.ebd.lth.se/ebdhome/avd_ebd/main/personal/Project_home_page/main/home.htm

Rheault, S and Bilgen, E. (1989). Heat Transfer Analysis in an Automated Venetian Blind Window System. Journal of Solar Energy Engineering, vol. 111, No. 1, 89-95.

Richards, P.J., Hoxey R.P. and Short L.J. (2001). Wind pressures on a 6m cube. Journal of Wind Engineering and Industrial Aerodynamics, vol. 89, pp. 1153-1564.

Rohsenow, W. Hartnett, J. and Ganic, E.(1985). Handbook of Heat Transfer Applications.

McGraw-Hill.

Saelens, D. (2002). Energy Performance Assessments of Single Storey Multiple-Skin Facades. PhD thesis, Laboratory for Building Physics, Department of Civil Engineering, Catholic University of Leuven, Belgium. Web address:http://envelopes.cdi.harvard.edu/envelopes/content/resources/pdf/case_studies/PhD_Dirk_Saelens.pdf

Saelens, D., Roels, S. and Hens, H. (2003). On the Influence of the Inlet Temperature in Multiple-Skin Facade Modelling. Proceedings Building Simulation'03, 1139-1146, Netherlands.

Sandberg M. (2005). Modelling and measurements of air flow through large openings, lecture notes from Ph.D-course "Modelling Natural and Hybrid Ventilation". Aalborg University, August 2005.

SIA, (1999). Wärme- und Feuchteshutz im Hochbau, Schweizerischer Ingenieur- und Architektenverein, Z□rich, Switzerland.

Sonne, J.K, Vieira, R.K, and Rudd, A.F. (1993) Limiting solar radiation effects on outdoor air temperature measurements, ASHRAE Transactions, vol. 99 (I), pp. 231-240.

Stec, W., and van Paassen, A.H.C. (2003). Defining the Performance of the Double Skin Facade with the Use of the Simulation Model. Proceedings of Building Simulation '03, 1243-1250, Netherlands.

Stec, W., and van Paassen, A.H.C.(no date) Integration of the Double Skin Facade with the buildings, Energy in Built Environment, Energy Technol¬ogy, TU Delft, Mekelweg 2, 2628 CD, Delft, The Netherlands.

Strachan, P. (2007). ESP-r modeller report. Annex 34/43 Subtask E:Double-Skin Facade. Energy Systems Research Unit. Dept. of Mechanical Engineering. University of Strathclyde, Glasgow.

Strachan, p. (1993) Model validation using the PASSYS test cells, Building and Environment 28 (2) 1993, pp. 153–165.

Straw, M.(2000). Computation and measurement of wind induced ventilation / PhD Thesis, School of Civil Engineering, The University of Nottingham , UK .

Strigner, R.; and Janak, M. (2001). Computer simulation of ventilated double-skin facade of the metropolitan library in Brno, Proceedings 1st Int. Conf. on Renewable Energy in Buildings, Sustainable Buildings and Solar Energy 2001, Brno University of Technology/ Czech Academy of Sciences in Prague, pp. 134-137.

T.M. Huang, C. Gau and W. Aung (1995) Mixed convection flow and heat transfer in a heated vertical convergent channel, International Journal of Heat and Mass Transfer 38 (1995), pp. 2445–2456.

Takemasa, Y., Hiraoka, M., Katoh, M., Tsukamoto, H., Tanabe, M. and Tanaka, H. (2004). Performance of Hybrid Ventilation System Using Double-Skin Facade and Vertical Airshaft. KaiTRI Annual Report, vol.52, Japan. Web address: http://www.kajima.co.jp/tech/katri/technical/annualj/vol_52/pdf/52-33.pdf

Tanimoto, J.; and Kimura, K. (1997). Simulation study on an air flow window system with an integrated roll screen, Energy and Buildings, vol. 26, pp. 317 - 325.

Todorovic, B., and Maric, B. (no date) The influence of double facades on building heat losses and cooling loads. Faculty of Mechanical Engineering, Belgrade University, Belgrade, Yugoslavia. Web address:

van Dijk, D. H.A.L. and Oversloot, H.P. (2003). WIS, the European Tool to Calculate Thermal and Solar Properties of Windows and Window Components. Proceedings of Building Simulation '03, 259-266, Netherlands.Web address: http://www.ibpsa.org/PDFs/BS03%20Papers/BS03_0259_266.pdf

van Paassen, A.H.C., & Stec, W. (2001). Controlled Double Facades and HVAC. 7th world congress Clima 2000/Napoli 2001, Septem¬ber 15-18 (CD-ROM). Indoor environment technology: towards a global approach (Napels), REHVA, Brussels, 2001, p. 1-15

Walton G.N. (1989) irflow Network Models for Element-Based Building Airflow Modeling. ASHRAE Transactions: 1989, Vol.95, Part 2, pp.611-620.

Wang, F., Davies, M., Cunliffe, B. and Heath, P. (1999). The Design of Double Skin Facade: Modelling Study on some Design Parameters Affecting Indoor Thermal Conditions. Proceedings CIBSE National Conference, 1999, 540-567.

Warren, M.R., James, P.H.and Young, I.C.(1998). Handbook of Heat Transfer, 3rd Edition, Mc Graw-Hill, 1998.

Yilmaz, T., Fraser, S.M. (2007) Turbulent natural convection in a vertical parallel-plate channel with asymmetric heating. International Journal of Heat and Mass Transfer, 50 (13-14), pp. 2612-2623.

Yilmaz, T.and Gilchrist, A.(2007) Temperature and velocity field characteristics of turbulent natural convection in a vertical parallel-plate channel with asymmetric heating. Heat and Mass Transfer/Waerme- und Stoffuebertragung, 43 (7), pp. 707-719.

Zhang, X. and Dutta, S.(1988) Heat transfer analysis of buoyancy-assisted mixed convection with asymmetric heating conditions, International Journal of Heat and Mass Transfer 41 (1998), pp. 3255–3264.

Zöllner, A., Winter, E.R.F., and Viskanta, R.(2002). Experimental Studies of Combined Heat Transfer in Turbulent Mixed Convection fluid Flows in Double-Skin-Facades. International Journal of Heat and Mass Transfer 45 (2002) 4401-4408.

APPENDIX

Only plots with weather data during the experiments in MODE 1,2 and 3 are included in Appendix.

MODE 1

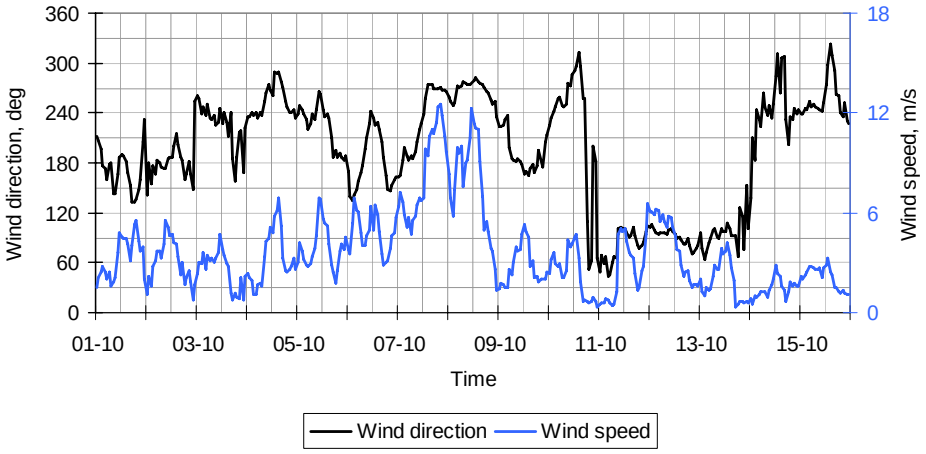
Wind direction, deg
Wind speed, m/s
Time
01-10
03-10
05-10
07-10
09-10
11-10
13-10
15-10
Wind direction
Wind speed

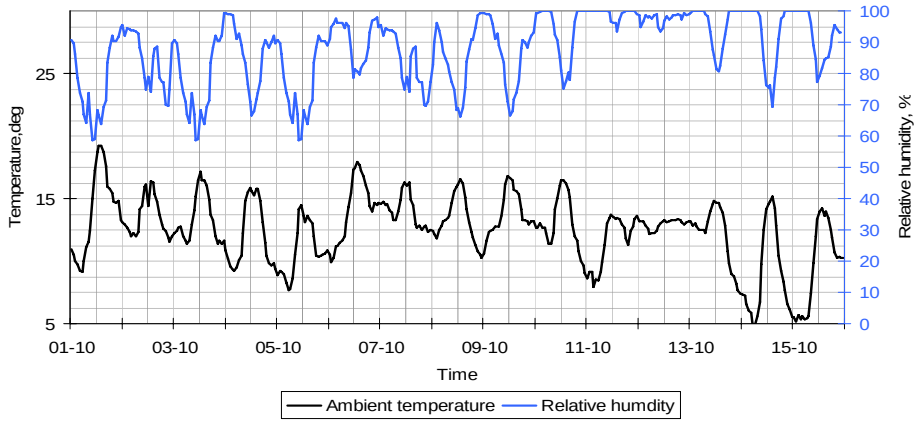
Temperature,deg
Relative humidity, %
Time
Ambient temperature
Relative humdity

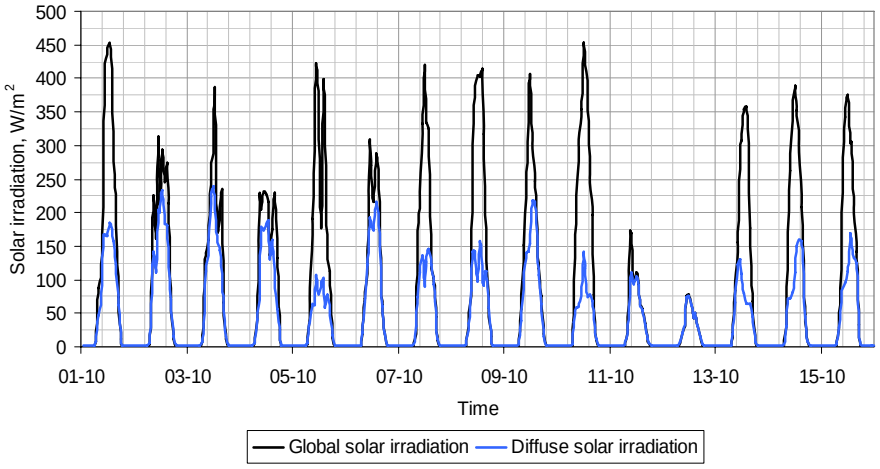
Solar irradiation, W/m2
Time
Global solar irradiation
Diffuse solar irradiation

MODE 2

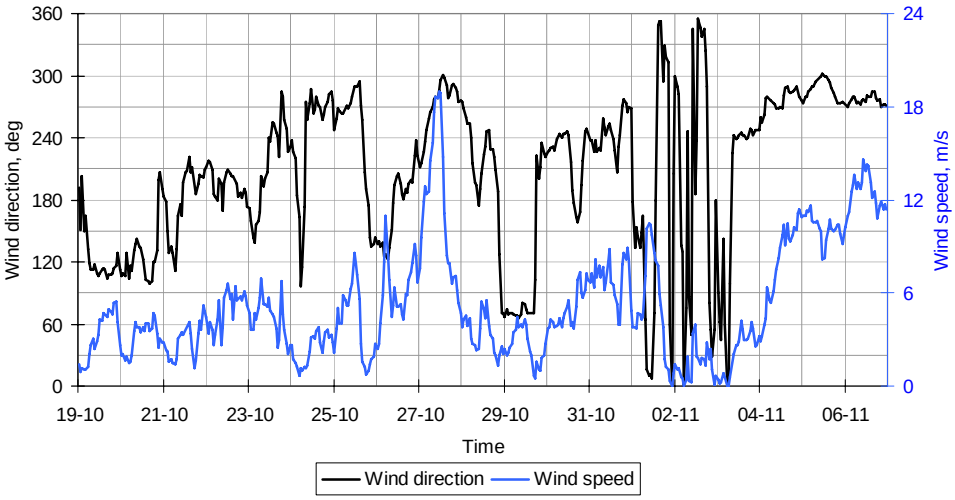
Wind direction, deg
Wind speed, m/s
Time
Wind direction
Wind speed

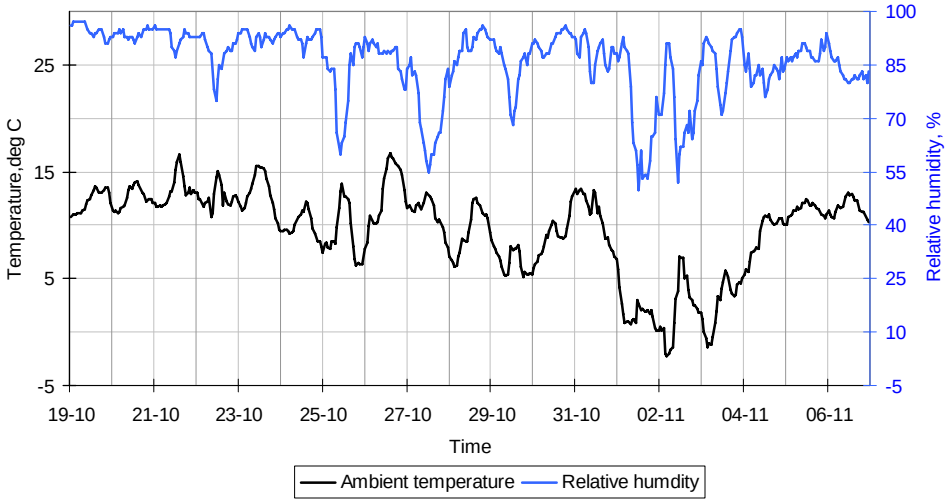
Temperature,deg C
Relative humidity, %
Time
Ambient temperature
Relative humdity

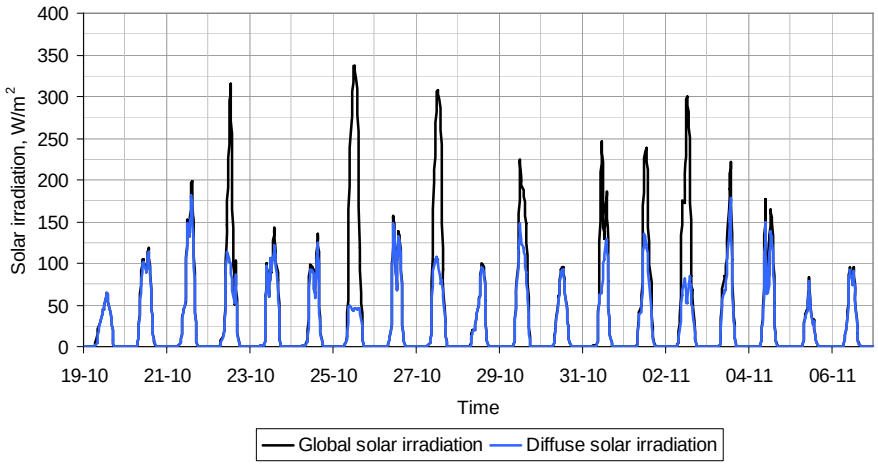
Solar irradiation, W/m2
Time
Global solar irradiation
Diffuse solar irradiation

MODE 3

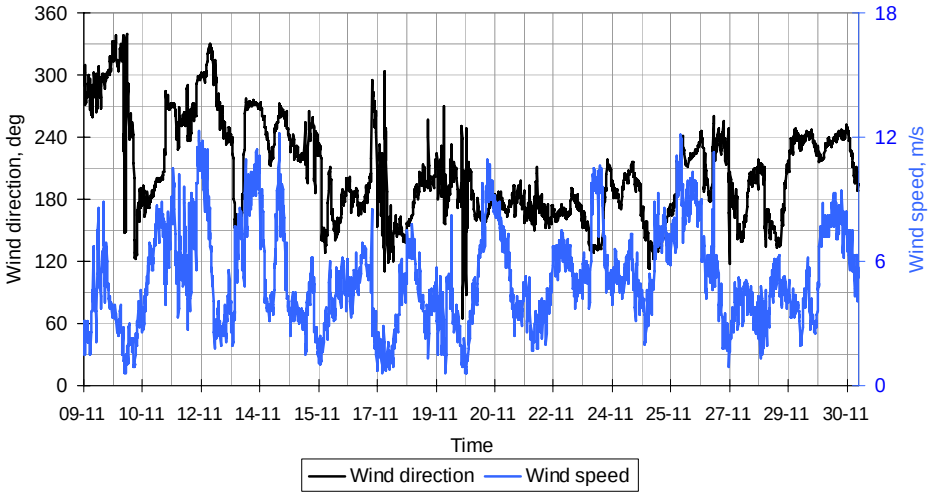
Wind direction, deg
Wind speed, m/s
360
300
240
180
120
60
0
18
12
6
0
09-11 10-11 12-11 14-11 15-11 17-11 19-11 20-11 22-11 24-11 25-11 27-11 29-11 30-11
Time
Wind direction
Wind speed

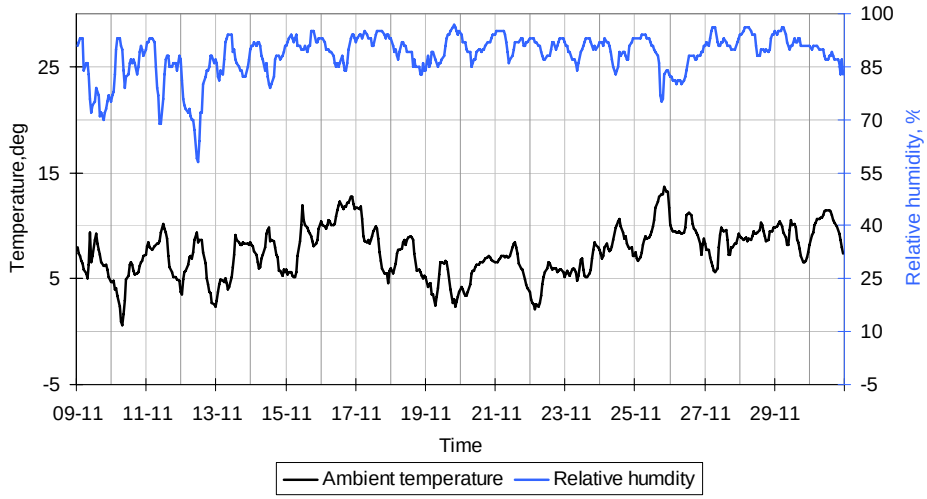
Temperature,deg
Relative humidity, %
25
15
5
-5
100
85
70
55
40
25
10
-5
09-11 11-11 13-11 15-11 17-11 19-11 21-11 23-11 25-11 27-11 29-11
Time
Ambient temperature
Relative humdity

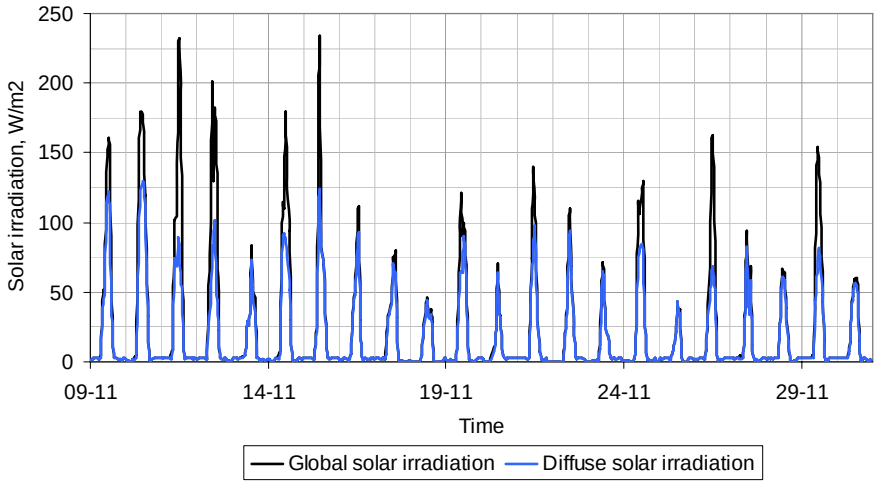
Solar irradiation, W/m2
250
200
150
100
50
0
09-11 14-11 19-11 24-11 29-11
Time
Global solar irradiation
Diffuse solar irradiation